MECHANICAL BEHAVIOUR

OF

COMPACTED DECOMPOSED GRANITE SOIL

by

IN-KEUN LEE

A thesis submitted for the degree of

Doctor of Philosophy

City University

Civil Engineering Department

September 1991

CONTENTS

List of tables

List of figures

6.2 Particle size distribution

6.3 Grading changes resulting from sieving time

6.4 Relationship between dry density and moisture content

6.5 Grading changes resulting from compaction

6.6 The effect of membrane stiffness correction (a) on the deviator stress, (b) on the stress ratio

6.7 Isotropic compression and swelling

6.8 Grading changes due to isotropic compression and swelling

6.9 Creep effects during isotropic compression

6.10 $\epsilon_v - \epsilon_a$ during isotropic compression

6.11 Typical test results (standard pressure test)

6.12 Typical test results (high pressure test)

6.13 Behaviour of the soil under the same confining stress

6.14 Behaviour of soils with same density under different confining stresses

6.15 Undrained test results (a) $q' - \epsilon_s$, (b) stress ratio and pore pressure response

6.16 Behaviour of compacted and over-consolidated samples

6.17 Grading changes during the triaxial tests

6.18 Relationship between particle crushing and pressures

6.19 The critical states in q':p' space

6.20 The critical states in v:lnp' space

6.21 Stress ratio - shear and volumetric strains

6.22 Stress-dilatancy relationships

6.23 Stress-dilatancy relationship for peak states

6.24 Stress-dilatancy of compacted and over-consolidated samples

6.25 Peak states in q':p' space

6.26 Peak states in v:lnp' space

6.27 The state parameter and the peak stress ratio (a) the initial state parameter, (b) the state parameter at peaks

6.52 Effect of flooding on the isotropically compressed soils

6.53 The effect of sample preparation on soil behaviour

6.54 Effects of flooding on the soil stiffness

6.55 Effects of flooding on the behaviour of dry samples

6.56 Stress–strain behaviour of flooded samples

6.57 Behaviour of wet compacted and later air–dried samples

6.58 Effects of flooding on the behaviour of wet compacted and later air–dried samples

Acknowledgements

The research described in this thesis was carried out at the Geotechnical Engineering Research Centre, City University, during the years of 1985-1987 and 1989-1991. The Seoul Metropolitan Government, where I have been served since 1982, very kindly granted me leave of absence for this research. The financial assistance from the Korean Government (Korean Government Long-Term Fellowship for Overseas Studies), British Council and City University (Robert Kitchin Research Scholarship) is gratefully acknowledged.

First, I would like to thank Dr Matthew Coop for his supervision. He willingly helped me whenever necessary, read the draft of this thesis to the detail and made invaluable comment on it. Without his guidance and encouragement, this research would have not been completed. Professor John Atkinson is appreciated for his guidance and provision of the facilities for this research. My thanks are also due to Mr John Evans for his supervision during the first period of the research and other members of staff and fellow students of the research centre for their advice, assistance and friendship. In addition, the technicians, headed by Mr Keith Osborne, were always very helpful to sort out any equipment difficulties.

The help of Mr Kevin Schrapel of Geomaterials Laboratory, Queen Mary and Westfield College, and Dr W J French of Geomaterials Research Services Ltd, is also acknowledged. They operated an X-ray diffractometer and provided me the mineralogy of the soil.

Finally, I have to thank my family. My parents and parents-in-law have prayed for my safety and progress and gave me moral and financial support. Being busy as a conservatory music student, Hyun-Kyung, my wife, did her best for me to concentrate on my work. My little son, Yong-Sung, also enormously helped me simply not bothering me very much.

Declaration

I grant powers of discretion to the University Librarian to allow this thesis to be copied in whole or in part without further reference to me. This permission covers only single copies made for study purposes, subject to normal conditions of acknowledgement.

Abstract

The purpose of this research was to determine the mechanical behaviour of decomposed granite soil, especially when it is used as a construction material. The soil tested was a completely weathered granite soil (grade V) taken from Seoul, Korea and was a well graded silty sand and gravel. Triaxial compression tests have been carried out on compacted samples and special attention has been given to the determination of the effects of the moisture condition on the behaviour.

The test results show that the soil conforms to the basic features of critical state soil mechanics, although particle crushing takes place during loading. A unique normal compression line, critical state line and the state boundary surface have been identified. This verifies the application of critical state soil models to the behaviour of crushable soils, which has been already revealed by the work on carbonate sands (Coop, 1990). In detail, however, the soil shows a number of unusual features.

The soil exhibits very high peak and ultimate strengths. Peak friction angles range from 39° to 51° and the ultimate friction angle is 39°. The main source of these high strengths seems to be the soil's mineral composition, in particular the high proportion of feldspars.

Particle crushing has been observed during the test. The behaviour of the soil is considerably affected by this phenomenon. The effects of particle crushing appear in a high value of the ratio λ/κ and in the location and shape of the state boundary surface. The amount of particle crushing has also been found to be dependent on the sample moisture condition as well as the maximum stress applied. Less particle crushing occurred in dry soils giving rise to a greater peak strength and higher ultimate specific volume for the dry soils. However, the ultimate strength of the soil is not affected by the moisture condition. This water sensitive behaviour has been clearly demonstrated by flooding tests.

A comparision was also made between the behaviour of compacted and truly over-consolidated samples which had been unloaded from higher stress levels. Compacted samples usually exist on the dry side of critical, however, their behaviour is different from that of the truly over-consolidated samples. Compacted samples are less stiff and do not show distinct yield points. Soils may also be densified by flooding, in which case the peak and ultimate strengths are comparable to mechanically compacted soils but the stiffness is not much improved by flooding. Samples compacted in a wet state and later air-dried show very high strengths and stiffnesses. These high strengths and stiffnesses are due to the suction between the soil particles and once flooded they follow the paths of the saturated samples.

List of symbols

The list given below includes the important symbols used in this thesis.

B	Skempton's pore pressure parameter
B_p	breakage potential
B_r	relative breakage
B_t	total breakage
D	particle size (diameter)
E'	Young's modulus in terms of effective stress
G'	elastic shear modulus
H,J	soil constants defining the Hvorslev surface
K'	elastic bulk modulus
OMC	optimum moisture content
V	volume
V_m	unit membrane penetration
c	cohesion intercept
e	void ratio
p'	mean normal effective stress
p'_e	equivalent pressure: at the point on the normal compression line at the same specific volume
p'_p	value of p' at the intersection of the normal compression line and the swelling line of an over-consolidated sample
q'	deviator stress
u	pore pressure
u_a	pore air pressure
u_w	pore water pressure
v	specific volume
v_κ	specific volume of isotropically compressed soil swelled to p'=1 kPa
v_λ	specific volume on reference section with p'=1 kPa
Γ	specific volume of soil at critical state with p'=1 kPa
Δ	large increment of ...
M	slope of critical state line on q':p' plane

N specific volume of isotropically normally compressed soil at $p'=1$ kPa

Ω common point of idealized critical state lines

$\gamma_{d\,max}$ maximum dry density

δ small increment of ...

ϵ strain

ϵ_v $\epsilon_a+2\epsilon_r$: volumetric strain for axial symmetry

ϵ_{vm} volumetric strain resulting from membrane penetration

ϵ_s $2(\epsilon_a-\epsilon_r)/3$: shear strain for axial symmetry

κ slope of swelling line (negative)

λ slope of normal compression line (negative)

ν angle of dilation

ν' Poisson's ratio

σ normal stress

τ shear stress

ϕ' friction angle

ψ state parameter

Superscripts

$'$ effective stress e.g σ', p'

^{e} elastic

^{p} plastic

Subscripts

$_a$ axial

$_f$ failure

$_p$ peak state

$_r$ radial

$_{ult}$ ultimate state

Chapter 1 Introduction

1.1 Objectives of the research

Decomposed granite soil is a type of residual soil which originates from the in situ weathering of granite. In Korea, granite is abundant and occupies around one third of the country, and decomposed granite soil is very therefore widely distributed, and is known locally as 'Masato'. The soil is visually described as a sandy or gravelly soil, but the characteristics and the behaviour are known to be quite different from those of the usual sands or gravels. For example, it has a very well graded particle size distribution, complex mineral composition, weak particle strength, and shows a decrease in shear strength with the presence of water. Due to its unusual nature, this soil is classified as a 'problem soil' or 'special soil' in Japan (Japan Society of Soil Mechanics and Foundation Engineering, 1979).

Because it is easy to acquire and to compact, the soil is often used as an earthwork fill material. Buildings and other civil engineering structures are also constructed on it. The main difficulty associated with this soil is the stability of slopes. Frequent landslides, particularly during the rainy season, have been reported in the areas formed with the soil. However, there has been little systematic research on the behaviour of the soil.

The objectives of this research are to determine the geotechnical properties of decomposed granite soil and to improve the understanding of its mechanical behaviour, especially when it is used as a construction material. These aims have been fulfilled experimentally through triaxial compression tests on compacted samples which were taken from Seoul. The test data being interpreted within the framework of critical state soil mechanics. Special attention has been given to determine the effects of the moisture condition on the behaviour.

1.2 Structure of the thesis

This thesis conforms to the typical structure of the dissertations based on experimental study. Chapter 2 presents a summary of the geology of Seoul and the formation of decomposed granite soil. Chapter 3 outlines the basic concepts of critical state soil mechanics, which will be used to analyse the laboratory test data. Current knowledge of the behaviour of decomposed granite soil is summarized in Chapter 4 and the general characteristics of residual soils, to which the soil belongs are also outlined. The triaxial apparatus used and the test procedures followed are described in Chapter 5 and the laboratory test results are presented in Chapter 6, in which the test data are also analyzed and the results are discussed. The conclusions drawn from this research are given in Chapter 7.

Chapter 2 Geology of Seoul and weathering of granites

2.1 Introduction

A discussion of the geology of Seoul and the formation of decomposed granite soil are presented in this chapter. These are necessary for a better understanding of the characteristics of the soil. Seoul city and its geology are introduced in the first two sections followed by a section on the weathering of granites which describes the weathering process, weathering profile and grades together with some weathering characeristics of Korean granites. Finally the sampling area is briefly described in Section 2.5.

2.2 General description of Seoul

Seoul, the capital city of Korea, is located at a latitude of 37°34'N and a longitude of 126°59'E and is to the west of the central region of the Korean peninsular. Seoul has become a metropolis with more than ten million residents. Geographically, Seoul is in a basin surrounded by mountains and the Han River runs westwards across the central part of the city.

The climate of Seoul is temperate and there are four distinctive seasons with great temperature changes throughout the year. The average annual temperature is 12°C with a maximum of 35°C in summer and a minimum of −15°C in winter. The average annual precipitation reaches up to 1,300 mm. However, more than 70 percent of the annual rainfall takes place during a four month period from June to September (Seoul Metropolitan Government, 1989).

2.3 Geology of Seoul

The geological map of Seoul has been published at a scale of 1:50,000 by the Korean Institute of Energy and Resources (1981,

1982). As can be seen in Figure 2.1, the main rock types are granite and banded gneiss. Alluvial deposits are found alongside the Han River and its tributaries.

The granite occupies the central and eastern part of the city. This rock is part of the Seoul granite which outcrops in the central area of the Korean peninsular as a batholith. It intruded the Precambrian basement of para-gneisses and schists during Jurassic age. It has a medium to coarse grained equigranular texture and its main mineral components are quartz, feldspars (plagioclase, orthoclase, microcline) and biotite. Due to presence of the potash feldspar (orthoclase) it shows pinkish colour. The granite is weathered up to a depth of 10m or 20m near main faults (Lee, S.G., 1987).

The banded gneiss is widely distributed in the western and southern part of the city resulting a topology of low relief. This rock is a Precambrian metasediment belonging to so-called Gyeonggi gniess complex. The rock is characterized by its alternation of bands of melanosome and leucosome. The former is mainly composed of biotite and the latter of quartz and feldspar.

Two types of dykes (acidic and quartz veins) have been intruded in many places into the granite and gniess. These may pertain to the Cretaceous age, considering the cycle of igneous activity of the Korean peninsular.

2.4 Weathering of granite

2.4.1 Weathering process

Weathering is the breakdown and alteration of minerals near the surface to produce minerals which are more in equilibrium under the new physico-chemical conditions (Ollier, 1984). Granites are weathered by physical breakdown and chemical alteration and are eventually changed to soils.

Physical weathering is the process whereby rocks are broken down without chemical change. It is caused by stress relief, thermal expansion and contraction, crystal growth (salt or ice), alternate wetting and drying and organic activity by plant roots. Their main contributions are to loosen rock masses, increase microfractures and reduce particle sizes (Mitchell, 1976). Microfractures in granites tend to be irregular in quartz grains and are cleavage controlled in feldspar and mica grains (Lee, S.G., 1987).

Chemical weathering leads to mineral alteration and the solution of rocks. In the weathering of granites, feldspars and micas are altered by the action of water while the quartz generally remains intact. At first biotite is affected and transformed to chlorite and other clay minerals, but the process is rather slow and partially weathered components often remain after the feldspars have disappeared (Lee, S.G., 1987). The weathering of biotite produces expansion of the mineral lattice which can cause microfracturing (Baynes and Dearman, 1978). The feldspars also break down to a variety clay minerals, mainly to kaolinite or sometimes to illite.

2.4.2 Factors affecting the weathering process

The type and rate of weathering is influenced by various factors such as climate, parent material, drainage, topology and vegetation. However climatic conditions, especially temperature and rainfall, are foremost, because water is essential for the weathering process and the rate of the chemical reactions generally increases with temperature. In contrast, physical weathering caused by thermal action dominates in cold regions, where chemical weathering diminishes. In relation to climatic conditons the relative importance of chemical and physical weathering can be assessed from Figure 2.2 proposed by Peltier (1950). The Seoul area, where average annual temperature and rainfall are 12°C and 1,300 mm respectively, is classified as a zone having moderate chemical weathering with frost action. However the past climate might be different from the present one and its influence on the resulting

weathered state of the rocks has to be considered.

2.4.3 Weathering profile and grades

Weathering progresses from the ground surface down, therefore the degree of weathering decreases with depth. However, weathering can also progress outwardly from cracks or joints, resulting in marked variations in the degree of weathering both vertically and laterally. The weathering profile can be devided into horizons for description and characterization, although the profile usually shows continuous change. Moye (1955) presented a classification system for weathered granites and many other systems have subsequently been proposed by a number of researchers. The weathered materials are classified by their geological or mechanical characteristics as one of the following groups: fresh (F), slighly weathered (SW), moderately weathered (MW), highly weathered (HW), completely weathered (CW) and residual soil (RS). This six fold grade system is widely accepted. A typical weathering profile and its brief explanation is presented in Figure 2.3 (Geological Society Engineering Group, 1990).

The soil and rock boundary is not clear in the weathering profile, but in engineering terms, materials of F to SW (grade I to II) tend to behave as rocks, those of CW to RS (grade V to VI) as soils. Zones of MW to HW (grade III to IV) are transitional from a rock to a soil (Dearman et al, 1978). However, the materials are often simply grouped into two categories, soil and rock, and the lower boundary of soil and rock profile is sometimes drawn at the base of HW grade (Geological Society Engineering Group, 1990).

2.4.4 Weathering of Korean granites

The weathering of Korean granite has been very well characterized by Lee, S.G. (1987). The weathering is relatively shallow compared with other countries and reaches up to a depth of 20 m in the

Jurassic coarse-grained granites and 30 m in the Cretaceous medium-grained granites. The weathering profile appears to be influenced by hydrothermal activity and chemical weathering was later superimposed. The degree of weathering generally decreases with depth and the profile shows a rather sharp transition from rock to soil. As shown in Figure 2.3, corestones are frequently developed in the granite weathering profile, however, they are not formed in Korean granite. A general weathering profile of Korean granites is shown in Figure 2.4.

2.5 Sampling area

A completely decomposed coarse-grained granite soil, typical of those encountered in Seoul, was desired for this research programme. It was obtained from a road construction site near Mt. Bulam, north-east of Seoul (Figure 2.5).

The site is situated on the southern edge of the Mt. Bulam at an altitute of 70m. On the western side the Chungrangchun river runs along the Chugaryong fault. The rock in this area is a typical Seoul biotite granite which is pinkish in colour when in a fresh state. Exfoliated domes have been developed near the peak of Mt. Bulam and the low hills are covered with weathered soil. The zone of weathering in this area has been reported to be a few centimeters thick near the peak increasing to maximum of 20 metres near the river (Lee, S.G., 1987). The specific site from which soil samples were recovered was covered with about 0.5m of residual soil and 4m of completely weathered granite soil.

Chapter 3 Basic soil mechanics theory

3.1 Introduction

The purpose of this chapter is to summerise the basic soil mechanics theory which will be used to analyse the test data presented in Chapter 6. The stress and strain parameters are defined in the first section and isotropic compression, swelling and shearing behaviour follow in Sections 3.3 and 3.4. Normalising procedures and stress-strain relationship based on elasto-plastic theory are outlined in Sections 3.5 and 3.6. Principally, triaxial compression tests on fully saturated samples are considered, however the behaviour of partially saturated soil is briefly discussed in Section 3.7, but will be covered more detail in Chapter 4.

Although it will not be fully described in this chapter, critical state soil mechanics is the basic framework chosen to understand the soil behaviour. It has been fully described by Schofield and Wroth (1968) and Atkinson and Bransby (1978). The principal feature of critical state soil models is the incorporation in the behaviour of the aspects of soil such as consolidation, yielding and failure, which are considered as substantially separate mechanisms in classical soil mechanics.

3.2 Basic parameters for the triaxial test

The state of a sample during a triaxial test may be defined by the mean normal effective stress p', deviatoric stress q' and the specific volume v.

$$p' = 1/3(\sigma_a' + 2\sigma_r') \qquad (3.1)$$

$$q' = \sigma_a' - \sigma_r' \qquad (3.2)$$

$$v = 1 + e \qquad (3.3)$$

where σ_a' is the effective axial stress, σ_r' is the effective radial

stress and e is void ratio.

Corresponding to the stress invariants p' and q' volumetric strain ϵ_v and shear strain ϵ_s are defined as

$$\epsilon_v = \epsilon_a + 2\epsilon_r \qquad (3.4)$$

$$\epsilon_s = 2/3(\epsilon_a - \epsilon_r) \qquad (3.5)$$

where ϵ_a, ϵ_r are the axial and radial strains respectively.

3.3 Isotropic compression and swelling

The normal compression line of a soil under isotropic stresses is generally idealized to be straight in v:lnp' space. Any unloading and reloading loops, known as swelling lines, are also idealised as straight lines in v:lnp' plane, as shown in Figure 3.1. Equations for the isotropic normal compression and swelling lines are respectively,

$$v = N - \lambda \ln p' \qquad (3.6)$$

$$v = v_\kappa - \kappa \ln p' \qquad (3.7)$$

where N and v_κ are specific volume of a normally consolidated soil and an overconsolidated soil at p'=1 kPa respectively. The value of v_κ depends on which swelling line the sample is on.

The isotropic normal compression line, which limits the state of an isotropically loaded soil, forms part of the state boundary surface. Elasto-plastic strains occur on the normal compression line, while the strains along the swelling lines are assumed to be elastic.

3.4 Shearing

3.4.1 Shearing and shear strength

Figure 3.2 shows typical shear stress and strain curves of dense and

loose samples. The dense sample exhibits a peak strength at P and reaches the ultimate strength at C, while the loose sample reaches the ultimate strength without a peak. Volume changes are dilative for the dense sample but compressive for the loose sample. However they show the same shear stress and void ratio at the ultimate state C under the same normal stress.

The shear strength of a soil is the maximum shear stress throughout shearing and is sometimes called peak strength to avoid confusion with other specified strengths, such as the ultimate strength or residual strength.

3.4.2 The critical state

If a soil is sheared continuously, as shown in Figure 3.2, it will eventually reach a critical state, in which deformations occur without further change of stresses or of specific volume. The critical states constitute a unique straight line in the q':p' plane and in the v:lnp' plane (Figure 3.3). These lines are described by

$$q' = Mp' \qquad (3.8)$$

$$v = \Gamma - \lambda \ln p' \qquad (3.9)$$

where M and λ are constant for a particular soil and Γ is defined as the specific volume at p'=1 kPa.

The critical state line limits all possible states at ultimate failure. It is also the reference state to explain the soil behaviour. The soil in wet side of critical (the soil is looser than the critical state) tends to contract during shearing and the soil in dry side of critical (the soil is denser than the critical state) tends to dilate.

3.4.3 Mohr–Coulomb model

Figure 3.4 shows Mohr circles for two triaxial compression tests, each at a different confining stress. The solid circles represent the peak states and the dotted circles the ultimate states. Mohr failure envelopes have been drawn for each state as a straight line. Thus the shear strength of a soil at the peak failure and the ultimate failure can be written respectively

$$\tau_p' = c_p' + \sigma_f' \tan\phi_p' \qquad (3.10)$$

$$\tau'_{ult} = \sigma_f' \tan\phi'_{ult} \qquad (3.11)$$

where σ_f' is the normal stress on the surface of failure, c_p' is the cohesion intercept and ϕ_p', ϕ'_{ult} are the angles of shearing resistance at the peak failure and the ultimate failure.

Equations 3.10 and 3.11 are known as the Mohr–Coulomb model. This model is widely used to predict the shear strength. However the volume change characteristics which are closely related to the strength of a soil are not included. Thus, although the strength parameters c_p' and ϕ_p' are assumed to be constant, they depend on the confining stress and the void ratio. The parameters also do not have physical meanings.

Hvorslev (1937) observed volume changes during shearing and stated that each failure envelope was uniquely associated with a constant water content at failure as shown in Figure 3.5. He also explained that the cohesion intercept c_p' increased exponentially with decrease of water content.

3.4.4 Stress–Dilatancy model

As discussed before, soils in the dry side of the critical show peak strength and reach the ultimate state through dilation. Any stresses greater than critical result from the dilation. The mobilised friction angle ϕ' can be expressed by the sum of two

components; ϕ'_{ult}, the friction angle at the ultimate state, and ν, the angle of dilation. The maximum friction angle at peak is reached when the angle of dilation is the greatest. Figure 3.6 shows the stress-dilatancy interpretation of the peak and ultimate states. The mobilised stress is given by

$$\tau' = \sigma_n' \tan(\phi'_{ult} + \nu) \qquad (3.12)$$

The angle of dilation also depends on the confining stress and the specific volume, as the strength parameters do in the Mohr-Coulomb model. This is explained in Figure 3.7, which shows the same test results of Figure 3.5 but interpreted in a different way. This shows failure states with the same dilation, i.e same stress ratio, but different effective normal stress. Each constant dilation contour is uniquely associated with a curve parallel to the critical state line.

There have been several stress-dilatancy equations which relate the rate of dilation, i.e the ratio of strain increments, to the stress ratio. However their theoretical background fall into one of the following two categories. One approach regards soil as particulate material and the other as a continuum.

The sliding block model and the Rowe's model belong to the former, developed by considering the sliding of the individual particles during shearing. Rowe (1962) proposed the stress-dilatancy equation in triaxial compression tests as

$$(\sigma_a'/\sigma_r') = \tan^2(45 + \phi_f'/2)\ \{1 - (d\epsilon_v/d\epsilon_a)\} \qquad (3.13)$$

where ϕ_f' varies between a lower value ϕ_u', the friction angle between the mineral particles, at pre-peak and an upper value ϕ'_{ult} at the critical state.

Taylor's model (1948) and Roscoe's equation belong to the latter category. They were developed on the basis of the energy dissipation equation. Roscoe et al (1963a) assumed that all plastic

work dissipated in friction and derived the following plastic work equation for triaxial tests.

$$(q'/p') = M - (d\epsilon_v/d\epsilon_s) \qquad (3.14)$$

This equation was employed as a flow rule when plasticity theory was applied to the soil behaviour.

3.5 Normalised soil behaviour

3.5.1 The state boundary surface

Isotropic normal compression states, critical states and peak failure states are related in q':p':v space. These relationship can be represented by a state boundary surface which limits all possible states of a particular soil. In the simpler critical state soil models this surface is also assumed to be a yield surface which separates elastic from inelastic behaviour. The existence of a unique state boundary surface is the essential feature of the critical state soil models.

The state boundary surface illustrated by Atkinson and Bransby (1978) for an isotropically compressed soil is shown in Figure 3.8. The normal compression line and the critical state line lie on the surface and limit all possible states during isotropic normal compression and for ultimate failure respectively. The curved surface joining the normal compression line and the critical state line is known as the Roscoe surface and it limits states of yielding for normally or lightly overconsolidated soil. The tension failure plane represents a condition of zero tensile stress. The surface between the critical state line and the 1:3 tension cut off is known as the Hvorslev surface and represents the states of yielding for heavily overconsolidated soil.

3.5.2 Normalising parameters

To compare the different test data and find fundamental patterns of the behaviour it is desirable to scale or normalise the data using appropriate parameters. The parameters used should be the principal factors affecting soil behaviour, such as the effective stresses and the specific volume. Normalising procedures for triaxial test data for different effective stresses and specific volumes have been described by Atkinson (1984).

Constant volume sections (p'_e), elastic wall sections (p'_p) and constant p' sections (v_λ) are usually used for normalising purposes. The parameters for these sections are defined in Figure 3.9 as follows;

$$p'_e = \exp\{(N - v)/\lambda\} \tag{3.15}$$

$$p'_p = \exp\{(N - v_\kappa)/(\lambda - \kappa)\} \quad \text{where } v_\kappa = v + \kappa \ln p' \tag{3.16}$$

$$v_\lambda = v + \lambda \ln p' \tag{3.17}$$

3.5.3 Normalised behaviour

A normalised elastic wall section is shown in Figure 3.10 (a). The normal compression line and the critical state line reduce to a single points A and B respectively. The Roscoe and Hvorslev surfaces project as a curve AB and straight line BC respectively. The normalised elastic wall section is quite similar in shape to the constant volume section but gives a normalised yield curve.

Figure 3.10 (b) shows a normalised constant p' section of the state boundary surface. The deviator stress q' is normalised with respect to p'. The normal compression line appears as a point at A for which $v_\lambda = N$ and the critical state line reduces to a point B where $v = \Gamma$ and $q'/p' = M$. The Roscoe and Hvorslev surfaces again appear as curves AB and BC.

The precise equations of the yield curves depend on the soils or

models considered. In the Cam-clay model the yield curves in the elastic wall section and constant p′ section are given respectively by

$$q'/(Mp'_p) + \ln(p'/p'_p) = 0 \qquad (3.18)$$

$$(q'/p')(\lambda - \kappa)/M - N + v_\lambda = 0 \qquad (3.19)$$

As proposed by Atkinson and Bransby (1978) the Hvorslev surface may be described in the elastic wall and constant p′ sections by

$$q' = Jp'_p + Hp'$$

$$= J \exp\{(N - v_\kappa)/(\lambda - \kappa)\} + Hp' \qquad (3.20)$$

$$q'/p' = (M - H) \exp\{(\Gamma - v_\lambda)/(\lambda - \kappa)\} + H \qquad (3.21)$$

where H is the slope and J is the intercept on the q'/p'_p axis.

Figure 3.11 shows the normalised state paths of undrained triaxial tests. Sample T1 was normally compressed and T1.5 and T5 were normally compressed and then swelled to overconsolidation ratios of 1.5 and 5 respectively. When sheared, sample T1 moves along the Roscoe surface to reach the critical state B. Sample T1.5 and T5 are inside the state boundary surface, so their initial behaviour is assumed to be elastic and their state paths are vertical until they reach the Roscoe surface and the Hvorslev surface respectively. When they reach the state boundary surface the paths move towards the critical state point as shown in the figure. In the case of drained loading the state paths of soils behaving elastically will not, in general, be vertical, except for constant p′ loading.

3.5.4 State parameter

The state parameter (Been and Jefferies, 1984) is another normalising parameter often used to interpret the behaviour of sand. The state parameter ψ is defined as the void ratio difference between the initial state and the steady state conditions at the same mean effective stress as shown in Figure 3.12. Because

practically there is little distinction between the critical and steady states, normalisation with respect to this parameter is almost same as using v_λ. Negative and positive values of ψ correspond to dry and wet side of the critical state respectively.

The concept of the state parameter is similar to critical state soil mechanics. Although the state parameter cannot describe the stress-strain behaviour in general, it can be used to characterise some key engineering features of the behaviour of sand using only one number. A high positive ψ may result in liquefaction in undrained shearing and a compressive response in drained shearing, while a negative ψ is associated with no peak shear stress in undrained shearing and dilation for drained shearing. As shown in Figure 3.13, there is a good correlation between dilation rate and the state parameter for several sands and the parameter may be used to predict the friction angle of a sand.

3.6 Stress-strain relationship

For a sample in the triaxial cell, the strain increments are related to the corresponding stress increments by

$$\delta\epsilon_s = A\,\delta q' + B\,\delta p' \qquad (3.22)$$

$$\delta\epsilon_v = C\,\delta q' + D\,\delta p' \qquad (3.23)$$

where A, B, C and D are parameters which are affected by various factors such as the characteristics of a soil, current state, stress history.

If the state of a soil remains below the state boundary surface, the soil is assumed to suffer only elastic strains. For an isotropic elastic soil, the parameters B and C are equal to zero and the parameters A and D become as follows.

$$A = 2(1+\nu')/3E' = 1/3G' \qquad (3.24)$$

$$D = 3(1-2\nu')/E' = 1/K' \qquad (3.25)$$

and $E' = 3vp'(1-2\nu')/\kappa$ (3.26)

where E' and ν' are the Young's modulus and Poisson's ratio and G' and K' are elastic moduli, known as the shear and bulk modulus.

As can be seen from the above equations, the elastic moduli are not constant but depend on the current values of v and p' as well as the values of κ and ν'. Therefore the soil behaviour, even though it is assumed to be isotropic and elastic, will not be linear.

When the state of the soil moves on the state boundary surface, the soil yields and undergoes the plastic strains. Total strain increments due to the stress increments are the sum of their elastic and plastic components i.e.

$$\delta\epsilon_s = \delta\epsilon_s^e + \delta\epsilon_s^p \quad (3.27)$$

$$\delta\epsilon_v = \delta\epsilon_v^e + \delta\epsilon_v^p \quad (3.28)$$

where scripts e and p represent elastic and plastic components.

The elastic components are given by Equations 3.24 to 3.26 and the plastic components can be calulated using the plasticity theory which has been develpoed from the behaviour of metals and includes yielding, hardening and plastic flow.

The material behaviour which involves plasticity may be idealised as one of the following models; rigid and perfectly plastic, elastic and perfectly plastic, elastic and strain hardening plastic. Only the last model will be considered here. In strain hardening models the yield surface is expanded up to the failure and the resulting plastic strain increments can be related to the stress increments by a hardening law and the ratio of the plastic strain increments and the stress ratio can be related by a flow rule. It is common to define a plastic potential such that vectors of the plastic strain increment are orthogonal to the plastic potential. If the the plastic potential and the yield surface coincide, i.e directions of the plastic strain increments coincide with the directions of the

corresponding stresses as they would for elastic behaviour, the flow rule is called associated and the normality condition holds.

If the flow rule is given by 1/F and is associated, then

$$\delta\epsilon_s^p/\delta\epsilon_v^p = F \qquad (3.29)$$

And the plastic volumetric strain increments can be related to the stress increments using the hardening parameters H and G.

$$\delta\epsilon_v^p = H\ \delta q' + G\ \delta p' \qquad (3.30)$$

From equations 3.29 and 3.30 the plastic shear strain increment is

$$\delta\epsilon_s^p = FH\ \delta q' + FG\ \delta p' \qquad (3.31)$$

The flow rule is associated, thus FG = H and the total strains can be written in the form of Equations 3.27 and 3.28 as

$$\delta\epsilon_s = (FH + 1/3G')\ \delta q' + H\ \delta p' \qquad (3.32)$$

$$\delta\epsilon_v = H\ \delta q' + (H/F + 1/K')\ \delta p' \qquad (3.33)$$

The stress-strain behaviour of a soil is non-linear so the stiffness varies with strain. Secant stiffness parameters can be used for calculations. However tangent stiffness parameters are more appropriate for the current constitutive equations which are based on elasto-plastic theory and are incremental. The tangent stiffness parameters may be normalised using current stress p' and specific volume.

3.7 Behaviour of partially saturated soils

The behaviour of partially saturated soil is also controlled by the effective stresses within soil. The relation between total stress and effective stress includes the pore water pressure u_w and pore air pressure u_a plus a parameter which is related both pressures. For

instance, the shear strength equation for partially saturated soils was proposed by Bishop et al (1960) as

$$\tau' = c' + [\sigma - u_a + \chi(u_a - u_w)] \tan\phi' \qquad (3.34)$$

where χ is soil parameter, with values between 0 and 1, depending on the degree of saturation, soil type and stress condition.

Although the parameter χ mainly depends on the degree of saturation, it is quite difficult to determine (Escario and Saez, 1986). Another shear strength equation suggested Fredlund et al (1978) is

$$\tau' = c' + (\sigma - u_a) \tan\phi' + (u_a - u_w) \tan\phi^b \qquad (3.35)$$

where ϕ^b is friction angle with respect to changes in $(u_a - u_w)$ when $(\sigma - u_a)$ is held constant.

In the above equations pore suction $(u_a - u_w)$ contributes to stiffening the soil giving it an apparent cohesion. However the strength resulting from the suction is not true strength and will diminish with saturation. Collapse by wetting a partially saturated soil under constant total stress can therefore often be explained by the loss of suction between the particles.

Chapter 4 Literature review

4.1 Introduction

This chapter presents the current knowledge associated with the behaviour of decomposed granite soil. General characteristics of residual soils, to which decomposed granite soil belongs, are introduced in the first section. This includes the definition and formation of residual soils, problems related to classification tests and some mechanical properties. In Section 4.3, the properties of decomposed granite soil are presented. The soil is very widely distributed and the properties are very much varied with location. In temperate zones soils which retain much of the original rock structure are abundant and mature residual soils are rare. It is the former which are the subject of this dissertation and these are considered greater detail. The classification of these soils, together with engineering properties, such as compaction, permeability, compressibility, strength and stress-strain behaviour have been described, discussing the effects of weathering on the properties. One of the most peculiar characteristics of decomposed granite soil, particle crushing, is discussed in Section 4.4 in detail. Most residual soils exist in a partially saturated state, showing collapse when flooded, and the behaviour of partially saturated soils, together with collapsing behaviour, is described in Section 4.5.

Some other topics, which might be part of a more general literature review, are presented elsewhere. Weathering processes and the profiles of granites are described in Chapter 2 and some items related to soil testing in Chapter 5.

4.2 Residual soils

Compared with sedimentary soils, residual soils have been almost neglected until recently. With increased development and also

frequent slope failures in areas covered with these soils, they are now receiving greater attention. Research on the residual soils is necessarily localised because the behaviour of the soils is very much affected by the weathering environment and parent rock structure. It has also been shown that some aspects of their behaviour may not conform to the conventional soil mechanics framework (Mitchell and Sitar, 1982; Vaughan, 1985 and 1988). Through the two recent international conferences on residual soils, Brasilia (1985) and Singapore (1988), several common features of the different residual soils have emerged, and some of these characteristics will be reviewed here.

4.2.1 Definition

Residual soils are defined as products of in situ weathering of rocks (Brand, 1985; Townsend, 1985), however, there is no agreement on the range of residual soils in the weathering profile. While the range is sometimes restricted to the very top layer of the profile, where original rock structure is completely destroyed (Dearman and Turk, 1985), it might be extended to the weathered zones (saprolite) which retain the original structure but can be considered to be soil-like materials (Brand and Phillipson, 1985; Geological Society, 1990). The latter interpretation is more generally accepted and will be adopted in this thesis. This includes materials of the weathering grades IV, V and VI in the profile shown in Figure 2.3. Although transported, landslide debris of weathered materials, known as colluvium, is also often categorised as residual soil for geotechnical engineering purposes (Brand, 1985).

Residual soils are found in virtually every part of the world, however, they are most widely distributed in tropical areas. For this reason, residual soils are often mistakenly known as tropical soils or laterites, which are iron-rich residual soils from the tropics which are red in colour.

4.2.2 Weathering and formation

As mentioned in Section 2.4, weathering begins at the surface of the ground and progresses downwards, thus the intensity of weathering decreases with depth. This progressive weathering process results in a sequence of material layers with different properties, known as the weathering profile (Figure 2.3). In addition to the weathering process a variety of other factors, such as parent rock, climate conditions and drainage, influence the resulting profile and its characteristics.

In temperate zones the weathering profile is rather shallow and is mainly composed of saprolite. On the other hand, deep weathering profiles and thick residual soil layers are found in tropical areas, where heavy rainfall and warm temperature produce intensive weathering.

Residual soils in the tropics are usually completely weathered and are quite different from the parent materials from which they were formed. They are usually grouped using a pedological system, which is based on the mineralogy of the clay fraction of the soils. Latosols (oxisols), andosols and vertisols are the three most distinctive residual soil types (Wesley, 1988).

Latosols, which are highly weathered reddish soils, are formed mainly on acid rocks under conditions of heavy rainfall, high temperature and good drainage. They consist of the clay minerals kaolinite and halloysite along with oxides of iron and aluminum, which may cause cementation when dried (Mitchell and Sitar, 1982). They are a very common soil type throughout the tropics and are also known as laterites, lateritic soils or red clays.

Andosols, which have a yellowish brown colour, are derived from volcanic ash and rock under conditions of heavy rainfall, moderate temperature and good drainage. They occur in volcanic areas at high altitude. They contain the clay minerals allophane and halloysite as well as iron and aluminum oxides. Allopane can alter to other

clay minerals such as kaolinite or gibbsites (Mitchell and Sitar, 1982). Thus at lower altitude, where the temperature is higher and weathering is more intensive, these materials are converted to latosols (Wesley, 1990).

Vertisols, whose colour is dark or black, are found on basic rocks under conditions of low rainfall, alternating wet and dry seasons and poor drainage. Their main clay mineral is high activity smectite. They are also known as black clays or black cotton clays and occur nearer to the edges of the tropics. Due to their good drainage conditions latosols and andosols generally show deep weathering profiles and that of vertisols is usually shallow.

4.2.3 Engineering classification

Soils may be classified into groups showing similar engineering properties (Lambe and Whitman, 1979). Conventional geotechnical classification systems, such as those defined in British and ASTM standards, are based on particle size distribution and Atterberg limits.

The engineering properties of sedimentary soils can be predicted from their grading and plasticity characteristics, which are determined easily and unambiguously. However, they seem not to be applicable to residual soils, particularly tropical soils which contain clay minerals of allopane and halloysite as the test results are very much affected by sample treatment, especially drying and remoulding before and during testing, and are far from repeatable (Mitchell and Sitar, 1982; Townsend, 1985). Drying causes alteration of the clay minerals by hydration and aggregation of the fine particles due to increased cementation. It results in remarkably lower Atterberg limits and a coarser particle size distribution. Some reported examples of the effects of drying on classification test results are summarized in Table 4.1 and illustrated on a plasticity chart in Figure 4.1. Remoulding may break the cementing bonds between clay clusters and increases

Atterberg limits and fines fraction in the particle size distribution. Table 4.2 and Figure 4.2 show the effects of remoulding on the tests. These two changes are irreversible and these effects should be considered both on the soil as used for earthworks in the field as well as for the test in the laboratory.

The classification test results vary with sample treatment and also show very wide range for each soil type, as shown in Figure 4.3. For these reasons, it is quite difficult to classify soils using conventional systems and to relate their results to any specific engineering property. In addition to these conventional systems, several alternative classification systems have been proposed for residual soils. These are reviewed by de Cavalho et al. (1985). However, none of them have been successful from the engineering point of view. For example, the weathering profile (grade) scheme, which is a type of classification system based on the parent rock and its degree of weathering, is very helpful in classifying the in situ properties of a particular formation but is not useful in comparing the properties of different formations and also does not provide any information on the composition of the soil. Wesley (1988) has suggested that this scheme might be a better system for describing weathered rock profiles than for classifying residual soils. Pedological systems are based on clay mineral composition and are the means by which soils are classified as latosols, andosols and vertisols. However, each group covers a very wide range of materials and classification is, therefore, not particularly helpful to the engineer.

There is no universally acceptable classification system for residual soils. Although conventional systems have been much criticised because they depend on pre-testing procedures, particle size distribution and Atterberg limits are often more useful than other information, such as degree of weathering or mineral composition. As pointed out by Mitchell and Sitar (1982), conventional tests might be used to identify the soils which are susceptible to property changes on drying and remoulding. For a better and more useful classification system, adequate techniques

should be introduced to the current testing procedures to avoid drying or remoulding. It may also be necessary to use weathering or pedological terms to supplement the conventional systems.

4.2.4 Engineering behaviour

Residual soils have some peculiar characteristics and these seem to be attributed to their formation process. While sedimentary soils are formed by a process of transport, deposition and consolidation, residual soils are formed by in situ weathering of rocks. In the case of the former, particles are sorted during the formation and their current state is influenced by stress history. The absence of these two factors, sorting and stress history, makes residual soils more heterogeneous and more difficult to understand within the concepts of classical soil mechanics, which have been based on sedimentary soils (Mitchell and Sitar, 1982; Vaughan, 1985, 1988).

As can be expected from the formation process, the engineering properties of residual soils are very varied. Compared with sedimentary soils, the characteristics of in situ residual soils may be summarized as follows (Mitchell and Sitar, 1982; Geological Society, 1990):

a) widely varying void ratio unconnected with stress history
b) varying mineralogy and grain strength
c) high permeability unrelated to particle size
d) presence of bonding between particles, which causes high strength and low compressibility
e) discontinuities of low strength
f) partial saturation, which may cause collapse with saturation

The mechanical behaviour of in situ residual soils depends on inter-particle bonding as well as current state. The term bonding indicates a structural component of strength and stiffness (Vaughan et al, 1988). This bonding has been also found in other natural

soils and weak rocks and soils which possess bonding have been described 'structured' by Leroueil and Vaughan (1990). Those for which the bonding has been broken down are described as 'destructured'. Bonding in saprolite is mainly inherited from the parent rock and that of mature residual soil is due to crystallization of minerals during weathering (Mitchell and Sitar, 1982).

The effects of bonding clearly appears in the oedometer test results presented by Wesley (1990), shown in Figure 4.4. He carried out tests on andosol (samples 1 and 3) and red clay (sample 2), making a comparison of the behaviour of undisturbed, remoulded and reconstituted samples. Unlike remoulded samples, whose structure has been destroyed, some undisturbed samples behave like over-consolidated soils and exhibit yield stresses. These yield stresses have been referred to as an apparent pre-consolidation pressure and are related not to stress history but to the bonding structure (Wallace, 1973). Some undisturbed samples even reach states outside of the normal compression lines which have been determined from reconstituted samples. After yield, bonding is progressively destroyed as relatively large strains occur. The effects of bonding structure seem not to appear in all residual soils, as can be seen from the results of red clay, where the effects are almost negligible.

Bonding structure also affects the shear behaviour. Figure 4.5 (a) shows two drained triaxial tests on weathered basalt (Geological Society, 1990). At the low confining stress (Test A) the soil shows a peak strength, although it is still contracting, and the maximum rate of dilation occurs much later than the peak strength. At the higher confining stresses (Test B) the soil exhibits a yield stress, at a similar level to the peak strength of Test A, and approaches the ultimate state without a peak. It is obvious that the peak strength or yield stress are a result of bonding structure rather than current state or stress history. The yield points for these tests and yield curve are shown in Figure 4.5 (b).

The behaviour of structured soils is more clearly understood through a comparison with that of the same soil in destructured state (Vaughan et al, 1988; Vaughan, 1988). Figure 4.6 shows compression curves of a bonded soil and a destructured soil. The normal compression line of the destructured soil divides void ratio-stress space into a meta-stable (structure permitted) zone and a stable zone, while the critical state line divides the stable zone into contractive and dilatant parts. A knowledge of the current states as well as the bonding strength allows the behaviour of structured soils to be estimated from the framework shown in this figure. States in the meta-stable zone are only possible for bonded structured soils. If a soil in situ reaches a meta-stable zone or moves there under engineering loading, large compressive strains may result. In the stable zones, structured soils will suffer relatively small strains. Once bonded soils lose their structure, they behave in a similar way to the destructured soil.

4.3 Decomposed granite soil

Decomposed granite soil is a type of residual soil derived from granite and is widely distributed over the world. This section deals principally with soils from temperate zones, such as Korea and Japan, where saprolite types are abundant but mature residual soils are rare.

4.3.1 General aspects

One of the most unusual features of decomposed granite soil, like other residual soils, is the variability of its properties which depend on both the parent rocks and the degree of weathering. Thus the characteristics of soils from Hong Kong, Malaysia, Japan or Korea are rather different from each other. At any location the properties also change with depth. Further variations are also observed locally from point to point due to the variations of parent rock properties and drainage conditions. After a wide-ranging

investigation of the decomposed granite soil in Hong Kong, Lumb (1962, 1965 and 1975) concluded that the degree of variation within any site was of the same order as that between different sites.

Figure 4.7 and 4.8 illustrate these variations. Figure 4.7 (a) shows the in-situ water content, porosity, densities and specific gravity of a decomposed granite soil profile in the Mt Hiei, Japan (JSSMFE,1974). The degree of weathering at the sampling point was found to gradually change with depth. Water content and porosity are decreasing but densities are increasing toward the base, i.e fresh rock, whereas specific gravity is almost constant at the value of 2.65. Figure 4.7 (b) shows the change of particle size distribution with depth in Malaysia (Komoo, 1985). It is clear that the fines content decreases and the gradings become coarser with depth. The properties of the soil change horizontally as well as vertically and Figure 4.8 (a) and (b) shows examples of the horizontal and vertical variations of particle size distribution (as of mean particle size) and void ratio (Lumb, 1962). The data are from three test pits which were only 4.5 m apart. The trends for the mean particle size and void ratio are to become coarser and smaller with depth respectively. However in each case the horizontal variations are as much as the vertical variations.

Figure 4.9 shows grading curves of decomposed granite soils from several countries. They are typically very well graded and their particles range from coarse gravel to clay size. Most of them can be classified as sandy or gravelly soils, but they sometimes contain considerable amount of fine particles.

The grading depends on the parent rock and the degree of weathering and, as weathering progresses, the grading becomes finer. Thus the soils from tropical areas, where weathering is more active, generally contain a greater fine fractions than those from temperate zones. The grading also becomes progressively finer towards the surface. Individual particles become smaller with weathering, resulting in both a decrease of the maximum and mean particle sizes and increase of the fines content. However, the shape of the

grading curve remains almost unchanged as can be seen in Figure 4.9.

Table 4.3 shows some consistency test results expressed in terms of conventional Atterberg limits. Most of them fall in the non-plastic or low plasticity range. With weathering the plasticity index tends to increase. On the plasticity chart (Figure 4.10) the results lie on or about the A-line.

As Atterberg limits tests were originally devised to index and classify fine-grained soils, difficulty arises in soils containing a significant proportion of coarse particles. For decomposed granite soils where the proportion of particles of finer than 425μm is generally small the application of conventional procedures is difficult and has little relevance to indexing the whole soil. Several methods have been introduced to accommodate the coarse particles in the measurements of consistency. Matsuo et al (1970) applied the slump test, which is usually used for concrete, and defined the flow limit (Wfl), instead of liquid limit, as the water content for a slump of 3 cm. Vaughan et al (1988) proposed an enlarged fall cone penetrometer for the liquid limit test of the soils containing coarse particles and also the standard compaction test as an alternative to the plastic limit test.

In tropical residual soils, as mentioned before, gradings and Atterberg limits are very much affected by drying and remoulding. However these effects have not been reported for the decomposed granite soils of temperate areas.

Compared with more usually encountered quartz sands or gravels, the mineralogy of decomposed granite soils is complicated. They contain quartz, feldspar and mica as primary minerals and also some clay minerals. Mineral composition varies with the parent rock and is altered by weathering. It influences the specific gravity and consistency of soils. Not having been transported, the particles are angular or subangular and their surface is generally rough. However, the particles are rather weak because of microcracks and intra-particle voids developed during weathering. As discussed

before, the feldspar grains are initially weathered and weakened. Matsuo and Nishida (1968) reported the changes of feldspar grain strength during weathering, and the results are shown in Figure 4.11. They found that the specific gravity of feldspar grains decreased with weathering and used it as a weathering index. Feldspar grain strength was measured by compressing the particles, 1.6 mm in size, with a 3 mm diameter steel rod. Although the results are rather scattered, there is a clear trend showing the particles to be rapidly weakened with weathering. This is another peculiarity of decomposed granite soil. Due to the weak particles particle degradation is caused when external loads, such as compaction, compression and shearing, is applied.

4.3.2 Compaction

Because the soils are very well graded, decomposed granite is ideal for compaction. Typical compaction curves for the soil are shown in Figure 4.12. The shape is not very much different from those of other soils. The maximum dry density ($\gamma_{d\ max}$) reported in the literature ranges from 15.5 to 18 kN/m^3 under ordinary proctor compaction and sometimes exceeds 20 kN/m^3 under the modified test. The corresponding optimum moisture content (OMC) ranges from 7 to 22 percent. Like other soils the OMC increases and $\gamma_{d\ max}$ decreases with increasing fines content.

Decomposed granite soil shows considerable particle crushing during compaction, as shown in Figure 4.13, where the amount of particle crushing has been represented by the change of specific area before and after the compaction test. Matsuo and Fukumoto (1976, 1977) carried out compaction tests on both a decomposed granite soil and a quartz river sand to determine the crushing effects. The grading of the latter had been adjusted to be similar to that of the former. The properties of the quartz river sand were assumed to be strong enough to produce the crushing-free compaction curve. Figure 4.14 illustrates the results. The solid curve represents the result for decomposed granite soil and the dotted curve those for the quartz

river sand. The arrow indicates the changes of γ_d and moisture content which result from particle crushing. Crushable decomposed granite soil shows a higher γ_d and moisture content at optimum. It seems that particle crushing increases the densification of the soil and the higher moisture content is caused by the increase of the specific surface area of the soil.

4.3.3 Permeability

Except for very clayey ones, decomposed granite soils are generally quite permeable. Some laboratory test results from Hong Kong and Japan are shown in Figure 4.15. As can be seen from the figures, permeability depends on the particle size, void ratio (density) and the structure. Smaller particle sizes and denser packing result in low permeability as expected. Data for undisturbed soil, although rather scattered, show higher permeability than those for disturbed soils, which probably results from fissures and a greater range of pore sizes. The laboratory permeability of undisturbed soils is within the range of 10^{-4} to 10^{-6} m/sec, but even higher values might be found in the field as a result of the macro-fabric of the soil.

Void ratio appears to have a much greater influence on the permeability of decomposed granite soil than other soils. For medium or fine quartz sands, whose permeabilities are in the range of 10^{-4} to 10^{-6} m/sec, values of permeability may be simply estimated using the Hazen equation, which relates permeability to particle size (Lambe and Whitman, 1979). For quartz sands permeability can be considered to be almost constant with void ratio. The variations in decomposed granite soil seem to be due to grading of the soil. In well graded soil, the pore spaces depend very much on density and are far from uniform, which is a basic assumption of the Hazen equation.

The permeabilities of compacted decomposed granite soil are very much lower than those of undisturbed ones, as shown in Figure 4.15 (b), although the void ratios of both soils are similar. This seems

to be due to particle crushing. The effects of particle crushing on permeability were estimated experimentally by Matsuo and Fukumoto (1977). These are illustrated in Figure 4.16 and were found to be considerable. The decrease of permeability as a result of particle crushing is indicated by an arrow in the figure, and was measured using a quartz river sand and decomposed granite soil as mentioned previously.

4.3.4 Compressibility

Data on the compressibility of the soil are relatively limited. An oedometer test result on an undisturbed sample is presented in Figure 4.17. The compression is progressive there being no clear yield stress and the effects of soil structure on the compression therefore seem to be minor. A normal compression line may not be determined using an ordinary oedometer, in which the maximum pressure is around 1 MPa. Recently, isotropic compression test results on these soils were reported by Murata et al. (1985) and Murata and Yasufuku (1987). They used high pressures up to 17 MPa to measure the isotropic compression and swelling properties on soils from several parts of Japan and some of the data for compacted samples are illustrated in Figure 4.18. Although the compaction energy is the same in each case, the initial void ratios are scattered for the three different soils shown. The compression behaviour is quite different for each of the three soils, however, the existence of straight normal compression lines and swelling lines in void ratio and logarithmic pressure space is clear. The range of slopes of the normal compression line, λ, is from 0.04 to 0.2 and that of swelling line, κ, is from 0.008 to 0.02. The ranges of values of λ and κ for undisturbed soils have been reported to be similar to those for disturbed ones (Murata and Yasufuku, 1987).

From the Figure 4.18 it is apparent that the compressibility is influenced by the presence of water, saturated samples being more compressible than air-dried samples. While the gradients of the normal compression lines and swelling lines of saturated and air-

dried samples are not significantly different, air-dried samples show higher void ratios than saturated ones under the same isotropic pressure, and flooding may cause collapse of the soil.

4.3.5 Strength and stress-strain behaviour

Judging from the classification test results, it is obvious that decomposed granite soils should possess high strengths. A well graded particle size distribution, low plasticity, rough particle surfaces and angular shape are all essential elements for the high strength. These might be expected to be counteracted to some extent by the weak particle strength.

Table 4.4 presents some strength parameters of the soil reported in the literature. Parameters are given as angle of shearing resistance, ϕ_p', and cohesion intercept, c_p', at the peak state. Angles of shearing resistance are quite high and vary very greatly, ranging from 32° to 51°. The cohesion intercepts are also considerable. The shearing resistance is found to depend on the particle size distribution, and especially on the fine particle fraction. Some of the data from Table 4.4 have been plotted in Figure 4.19, where the relationship between ϕ_p' and fines content is clear; ϕ_p' decreasing with an increase in fines fraction.

As discussed in the previous chapter, ϕ_p' and c_p' for peak states are not constants but depend on the current state; stress level and void ratio. The shearing resistance at the ultimate state, ϕ'_{ult} or M, is independent on the current state and could be considered as the underlying strength parameter of a soil. However data on the ultimate strength parameters of decomposed granite soils are very limited. The soil usually exists at states below the range of apparent pre-consolidation pressures and for normal engineering stress levels shows a peak with associated dilatant behaviour. Most of the tests reported in the literature were not continued to the ultimate state but were terminated just after the peak. The concept of the ultimate state has not been fully understood for these soils

or used to explain their behaviour.

Some ultimate strength parameters, which have either been reported or estimated from the data given in the literature, are shown in Table 4.5. The values of the ultimate shearing resistance, ϕ'_{ult}, are fairly uniform falling within a range of 38° - 41°. Similar values have been found from interpretation test results presented by Irfan (1985) who carried out direct shear tests on various undisturbed samples, whose void ratio, particle size distribution and mineral composition were varied. The stress-strain curves vary considerably, as expected, but, under the normal stress of 40 kPa, the ultimate strengths approach very similar stress levels, say 36 kPa, as shown in Figure 4.20, again confirming an ultimate shearing resistance, ϕ'_{ult}, of decomposed granite soil of around 42°.

In addition to current state, the shearing behaviour of the soil is affected by various other factors, such as sample disturbance (undisturbed or remoulded), sample preparation method (compaction) and water content (Onitsuka et al, 1985; Miura and O-hara, 1979; Yagi and Yatabe, 1985). The behaviour of undisturbed samples is very different from that of compacted samples as shown in Figure 4.21 (a) and (b), which show data reported by Yagi and Yatabe (1985) and Murata and Yasufuku (1987) respectively. They both carried out triaxial compression tests on disturbed and undisturbed samples with the same void ratio. Compared to the compacted samples, the undisturbed ones show similar or slightly higher peak strengths, more pronounced volumetric strains and considerably lower initial stiffness. Consequently they require larger strains to reach peak or ultimate states. However the ultimate strength is almost the same for both types of sample, as shown in Figure 4.21 (b), but at the ultimate state, the specific volume seems to be higher for the undisturbed soil.

As mentioned in the previous section, different behaviour for undisturbed (structured) and disturbed (destructured) samples is commonly observed in residual soils. The reasons for this difference are explained mainly by the bonded structure of the

undisturbed soil. In the case of the decomposed granite soil the behaviour is also affected by particle crushing during both shearing and compaction stages (Onitsuka et al, 1985; Yagi and Yatabe, 1985). Undisturbed soil is usually bonded, which might originate from the parent rock or have been developed during the latter stages of the weathering. On the other hand compacted soil loses the bonding through the sampling and compacting processes. Particles in undisturbed soil are also more randomly oriented than those in the compacted soil. Yagi and Yatabe (1985) found that individual pore spaces are much larger, although the overall total pore volume is equal, and that particle crushing is more severe for undisturbed soils. It seems that the higher peak strengths of the undisturbed soil may be attributed to the bonding and random particle arrangement and that the differences in stress-strain behaviour are caused by the larger individual pore spaces for the undisturbed soil together with the more intensive particle crushing. As a result of shearing, the undisturbed soil becomes disturbed, losing its bonding and eventually it is thought to have almost the same soil structure as the compacted soil at the ultimate state.

It has been shown by Miura and O-hara (1979) that decomposed granite soil is weakened by water. As demonstrated in Figure 4.22, which shows the results of direct shear tests carried out by Onitsuka et al (1985), soaked (saturated) samples show a significantly lower shear strength than unsaturated samples. It is clear that suctions are dissipated by complete saturation and consequently the shear strength decreases. In addition to this, increased particle crushing in the saturated samples also results in a decrease in the peak shear strength. Particle crushing results from the weak particles which constitute these soils, and Miura and O-hara (1979) have found it to be increased by the presence of water. The effects of saturation and particle crushing on the stress-strain behaviour will be discussed in detail in the later sections.

4.3.6 Effects of weathering

The weathering profile (grade) scheme, shown in Figure 2.3, may be employed to classify the state of weathering. The scheme is based on the visual evaluation of certain geological characteristics and qualitatively provides the degree of weathering of in situ materials. Many attempts have also been made to quantify the degree of weathering, of which some indices developed for the granites are shown in Table 4.6. The chemical indices, such as ignition loss (JSSMFE, 1979; Murata and Yasufuku, 1987), apparent specific gravity (JSSMFE, 1987), specific gravity of feldspar (Matsuo and Nishida, 1968) and chemical weathering index (Sueoka, 1988), are a measure of chemical alteration during the weathering process. The petrographic indices, such as degree of decomposition (Lumb, 1962), density of microcracks (Onodera et al, 1974) and micropetrographic index (Irfan and Dearman, 1978), quantify the successive mineralogical and textural changes produced by weathering.

Whatever the indices, the properties of decomposed granite soil are continuously changed as weathering progresses. Particle size distribution, void ratio and mineral composition are modified, which result in a change in engineering properties. Figure 4.23 shows the trend of changes in physical and engineering properties.

4.4 Behaviour of soils with crushable particles

4.4.1 Introduction

In the mechanics of soils, soil particles are usually assumed to be rigid and not crushable under the applied load (Rowe, 1962; Schofield and Wroth, 1968). However, microscopic examination or grading analysis before and after testing shows that there is often considerable particle crushing during the loading process. Although the crushing starts at low stress levels, it becomes more significant under high pressures. During tests on soils with microcracks or intra-particle voids, such as weathered soils or

carbonate soils, this phenomenon is frequently observed even in the engineering stress range (Miura and O-hara, 1979; Coop, 1990). Under high pressures, the gradings of rockfill materials (Marsal, 1967), granular soils (Lee and Farhoodmand, 1967) and even quartz sands (Vesic and Clough, 1968; Miura and Yamanouchi, 1975) are also changed due to particle crushing. Particle crushing changes the particle size distribution, and thus affects the stress-strain behaviour as well as the peak strength.

4.4.2 Factors influencing crushing

Though particle crushing actually begins at low stress levels in every granular soil, regardless of particle strength or the presence of fractures, the amount of particle crushing was shown by Lee and Farhoomand (1967) and Hardin (1984) to depend on the following factors: particle size distribution (size and uniformity), particle shape and strength, the confining and shear stresses, and the presence of pore fluid.

Lee and Farhoomand (1967) examined the above influences on particle crushing using crushed granite materials. Figure 4.24 shows the grading changes of materials before and after isotropic compression up to 8 MPa. The solid and dotted lines represent the gradings of the soil before and after testing respectively. The uniformity of the original materials for samples A, B, C, D and E is similar but the amount of crushing increases with the size of particle, because the normal contact forces in a soil element increase with particle size and the potential for the crushing therefore grows with its size. Initially fine soils show little crushing. Figure 4.25 (a) and (b) illustrates the effects of particle shape and confining stress. As can be seen from the figures, the amount of particle crushing increases with confining stress and is greater for angular particles. At the same confining stress, particle crushing increases with shear stress, as shown in Figure 4.25 (c) and (d), where K_c is stress ratio, σ_1'/σ_3'. Particle crushing is also increased by the presence of pore water, as shown in Figure 4.26.

4.4.3 Particle crushing measurement

The amount of particle crushing is found by grading curves measured before and after testing, however, it is convenient to define a parameter which adequately express the amount. The increase in percentage passing a specific sieve size has been often used for this purpose. Leslie (1963, 1975) used as a reference the sieve size on which the percentage of original material retained was either 100% or 90%. Miura and Yamanouchi (1975) used the 74μm and 149μm test sieves as a reference as shown in Figure 4.27 (a). The amount may be related to the particle size instead of the percentage change, as shown in Figure 4.27 (b). Lee and Farhoomand (1967) represented the amount using the change of D_{15}, the diameter at which 15% is finer, while Datta et al (1979) and Coop (1990) used D_{10} and D_{50} respectively.

The above two methods represent the amount of crushing as a single number, but they basically give information at a certain point on grading curves and may be influenced by the grading characteristics of the material. Marsal (1967) considered the overall crushing process and proposed the degree of particle breakage (crushing), B, which is the sum of the positive difference in percentage retained in each sieve size before and after testing, as shown in Figure 4.28 (a). Hardin (1985) also considered the overall crushing process and defined the parameters breakage potential, total breakage and relative breakage, as defined in Figure 4.28 (b) and (c). Breakage potential, B_p, represents the state that all the coarse particles are crushed to fine particles and is equal to the area between the original grading curve for sizes greater than 74μm sieve and the line passing through 74μm. Total breakage, B_t, is defined as the area enclosed by grading curves before and after for sizes greater than 74μm sieves. From these two parameters, relative breakage, B_r, may be defined as B_t/B_p. Relative breakage is a normalised parameter, which is independent of particle size distribution.

In addition to the above parameters, Miura and O-hara (1979)

evaluated the particle crushing as the increase in surface area of the materials and Coop (1990) investigated the changes of the relative density.

4.4.4 Effects on the soil behaviour

As mentioned in the previous sections, particle crushing during compaction causes an increase in the maximum dry density and optimum moisture content and a considerable decrease in the permeability of the soils. In addition to these, the compressibility, strength and stress-strain behaviour are also influenced by this phenomenon.

In one-dimensional or isotropic compression, particle crushing adds to the plastic volumetric strain. During shearing, particle crushing again causes additional plastic volumetric strain and consequently decreases the rate of dilation and the peak strength. Particle crushing causes a decrease in the peak strength but it appears not to influence the ultimate strength. Coop (1990) carried out triaxial tests on carbonate sands under standard and high pressures and found that the ultimate strength parameter, M, did not change with stress level, although more significant particle crushing occured under high pressures.

This crushing phenomenon is increased by the presence of pore water, because water decreases the surface energy in pre-existed or developed cracks and, in consequence, reduces the tensile strength of the particle (Lee and Seed, 1967; Miura and Yamanouchi, 1975). Lee and Seed (1967) carried out drained triaxial tests on Antioch sand, which contained weathered and cracked particles. Three sets of tests were conducted on oven dried samples, air dried samples and finally on saturated samples. The results, as shown in Figure 4.29, revealed that the peak strength in the saturated state was significantly lower than that of oven dried or air dried states. The decrease in strength is accompanied by a decrease in dilatancy rate and also by an increase in particle crushing, as shown in Figure 4.26. In the case of Toyoura sand, which has stronger

particles, Miura and Yamanouchi (1975) found the difference to be negligible even under very high pressure, as shown in Figure 4.30. From these results, it is clear that such water sensitive behaviour is due to the presence of weak particles in soils.

4.5 Partial saturation and collapse

4.5.1 Partial saturation

In situ as well as compacted residual soils are generally partially saturated. In partially saturated soils both air and water exists in the pores and the pressure of water is always less than that of the air due to the presence of capillary menisci. The pressure difference between the two pore fluids is known as soil suction.

There are two stages in partial saturation. If the degree of saturation is low, the air exists as continuous air voids and both air and water pressures influence the effective stress and the behaviour of the soil. If the degree of saturation is high, typically over 85%, the air exists as bubbles and the air pressure has little influence on the effective stress.

Soil suctions arise from the surface tension of water and are inversely proportional to the perimeter of the meniscus. In the dry season, pore water continues to evaporate and the areas occupied by menisci reduce and the soil suctions increase, giving an additional component of effective stress and increasing the stability of slopes.

4.5.2 Behaviour of partially saturated soils

As discussed in section 3.7, the behaviour of partially saturated soils is also dependent on the effective stress and the effect of the suction on the shear strength has been expressed as an apparent cohesion term, which varies linearly with the suction, $(u_a-$

$u_w)\tan\phi^b$ in equation 3.35. Typical values of ϕ^b are of the order of 20°. However, it has been found that ϕ^b is a variable which depends not only on suction but also on other parameters and ϕ^b may drop to 5° for high values of suction (Escario and Saez, 1986; Fredlund et al, 1987). This means that the increase in strength due to suction is limited.

Recently a general framework, based on critical state soil models, has been proposed to explain the behaviour of partially saturated soils. Toll (1990) carried out triaxial compression tests on compacted saturated and partially saturated Kiunyu gravel, a lateritic gravel from Kenya, with the measurement of the suction. He used the total stress q and $p-u_a$ for stress variables and specific volume v and degree of saturation S_r for volumetric variables. The critical state lines of saturated and partially saturated soils were found to be identical in q and $(p-u_w)$ space. However, no unique relationship between specific volume and mean stress was found for the critical states of partially saturated soils. This may be due to the inadequate definition of the critical state for the partially saturated soils. As the author mentioned, the end states of the tests were assumed to be critical states although the soils continued to dilate at that point.

Toll divided the stress component p' of equations of 3.8 and 3.9 into total stress $p-u_a$ and suction u_a-u_w and the critical state equations for partially saturated soils have been formulated as follows by extending equations 3.8 and 3.9.

$$q = M_a(p-u_a) + M_w(u_a-u_w) \qquad (4.1)$$

$$v = \Gamma_{aw} - \lambda_a \ln(p-u_a) - \lambda_w \ln(u_a-u_w) \qquad (4.2)$$

where subscripts a and w represent total stress and suction components respectively and Γ_{aw} describes the specific volume when $p-u_a$ and u_a-u_w equal unity.

The relationship between shear strength, total stress and suction has been found to be strongly influenced by the degree of

saturation. Figure 4.31 (a) shows that the contribution of suction to the deviator stress reduces and that of total stress increases, as the degree of saturation reduces. At high degrees of saturation, the two values towards to the saturated value, M_s, and equation 4.1 reduces to equation 3.8. Below a certain degree of saturation, 55% in this case, the suction component of the deviator stress reduces to zero. The two components M_a and M_w are equivalent to ϕ' and ϕ^b, which were assumed to be constant, but are also affected by the degree of saturation. The effects of the two stress ratio components on the volumetric behaviour are similar to those on the deviator stress, as shown in Figure 4.31 (b).

4.5.3 Collapsing and swelling

Collapse may be defined as the immediate settlement of a dry or partially saturated soil, when it is soaked under constant load (Vaughan, 1985). Dry soils with loose and bulky structure suffer most severely from collapse. Typical natural collapsing soils are wind deposited loess and some residual soils in regions with a distinct dry seasons (Mitchell and Sitar, 1982; Houston et al, 1988). This collapse may result from the following conditions,

a) a loss of the capillary menisci between particles
b) a loss of strength of the individual particles
c) a loss of strength of the bonding material

Mechanism a) is due to effective stress changes and b) is related to the fact that the strength of certain soil particles is weakened by water and so the soil shows additional deformation. It is necessary to distinguish between intrinsic collapse and increase in shear strains resulting from changes in the effective stress.

The potential magnitude of collapse may be determined by flooding a sample with water under a stress of 0.2MPa in an oedometer. The result is usually expressed in terms of the percent collapse and may be used as a guide to possible collapsing situations, as shown in

Table 4.7 (Jenning and Knight, 1975).

Soaking causes some clay soils to swell, instead of collapse, under very low effective stress. With soaking the capillary menisci are relaxed and the clay soil starts to expand. Swelling potential depends on the soil structure as well as on the type and amount of clay minerals in the soil. Soils with montmorillonite as clay minerals, vertisols, are usually highly expansive and remoulded soils swell more than undisturbed ones under the same conditions.

Chapter 5. Laboratory tests: equipment and procedures

5.1 Introduction

The mechanical behaviour of decomposed granite soil has been investigated through triaxial tests. The purpose of this chapter is to describe the triaxial apparatus used and the test procedures. The first two sections (5.2 and 5.3) have been devoted to describing the Bishop and Wesley triaxial cell and high pressure triaxial cell as used in the Geotechnical Engineering Research Centre at the City University. Some special considerations for triaxial tests on coarse grained decomposed granite soil and detailed test procedures follow in Sections 5.4 and 5.5.

The triaxial test is one of the most common tests on soils for geotechnical design or research. The principle advantages of the test are the control of drainage conditions, the measurement of volume change or pore pressure, the ability to apply principal stresses in known directions giving a versatility of stress path direction which can not be achieved with any other apparatus in common use. It also has several limitations. Its inability to examine the effects of the intermediate principal stress and the rotation of principal stress directions may cause problems. Despite these limitations, the triaxial test does combine versatility with relative simplicity in concept and performance. Other apparatus in which three unequal principal stresses can be applied, or in which the principal stresses can be rotated, do not have this versatility and are more complicated to use.

5.2. Bishop and Wesley triaxial cell

Triaxial tests at confining stresses up to 500 kPa were carried out in a standard microcomputer controlled City University stress path cell (Atkinson, 1985; Atkinson, Evans and Scott, 1985). This triaxial system consisted of Bishop and Wesley hydraulic triaxial

cell (Bishop and Wesley, 1975) with electrical instrumentation, a BBC microcomputer with peripherals and operating software. The components of the system are described in the following sections.

5.2.1 The triaxial cell

The original cell design is described in detail by Bishop and Wesley (1975). Later the drainage connections were modified and cell body was enlarged to 200 mm in diameter, the cell was originally designed for 38 mm diameter samples. To accommodate the 60 mm diameter and 120 mm high samples used in this series of tests, the top and bottom platens were enlarged and the perspex cell body was lengthened from 282 mm to 342 mm.

The pressure supplies required in this apparatus are cell pressure, pore (back) pressure and ram pressure for axial loading. The arrangement is illustrated in Figure 5.1. The air pressures to generate these pressures were provided by an air compressor at a maximum of 800 kPa. The pressures were regulated by electro-manostats under the command of a computer and transmitted to the cell through air/water interfaces. In the pore pressure supply system the Imperial College type volume gauge was used as the interface with air pressure in the lower chamber and water in the upper. The axial pressure was applied to the sample by means of a 60 mm diameter piston passing through the base of the cell. The top cap of the sample was fixed during the test and the piston moved up and down hydraulically. The piston was actuated in two different ways. With the valve, V, open, this pressure was also controlled by an air pressure regulator giving stress controlled axial loading. When the valve was closed, a fixed volume of water was contained in the loading system and the screw ram provided strain controlled axial loading.

5.2.2 Instrumentation

The instrumentation used consisted of cell and pore pressure transducers, axial load cell, volume gauge and an axial displacement

transducer as shown in Figure 5.1.

Both cell and pore pressures were measured using Druck PDCR transducers with a range of 0 - 1000 kPa. The axial load was measured using a 450 kgf Imperial College type load cell. Since all measurements were made inside the cell, errors due to the frictional losses through a piston seal were avoided.

Axial displacements were measured externally as the relative displacement of the top of the cell and the crosshead on the axial loading ram below the sample. Volume changes of a fully saturated sample were measured by observing the amount of pore water entering or leaving the sample through the drainage leads using an Imperial College 50 cc capacity volume gauge. This device consists of a piston in a chamber with bellofram seals at top and bottom. Back pressure could be applied by means of compressed air pressure in the lower bellofram. An external displacement transducer measured the movements of the piston and thereby the volume changes of the sample. In case of unsaturated samples, a specially designed inner chamber was employed for the volume change measurements. This will be described in Section 5.2.5. Radial strains were not measured directly but computed from the observed axial and volumetric strains on the assumption that the sample remained a right cylinder.

5.2.3 Calibration and accuracy

Each instrument was calibrated by applying a known load, pressure or displacement to the device as appropriate, such that a known stress and strain should be displayed on the monitor screen.

The axial load cell was calibrated by applying dead weights via a hanger. The pore pressure and cell pressure transducers were calibrated using a reference pressure meter which could apply pressures to within 0.01% of the stated values. The axial displacement transducer was calibrated using a micrometer. The volume gauge device was calibrated by displacing known quantities of

water into and out of the gauge while under pressure.

During the calibration procedure, the non linearity and hysteresis of each transducer was found to be insignificant, and the calibration constants were decided assuming that the devices were linear over their whole range.

The measured axial displacement was not only the result of displacement of the sample but also had a component arising from the flexibility of the load cell and the axial screw adjusting nut. This system compliance was calibrated by using a rigid dummy sample and varying the deviator stress. The expansion of the volume gauge bellofram under changing back pressure was also calibrated. More detailed calibration procedures are described by Atkinson, et al (1983), Clinton (1985) and Lau (1988).

The true stresses and strains on the sample are sensed by the transducers and after applying calibration factors are recorded. The errors between the true stresses and strains and the recorded ones are due to the characteristics of the measuring instruments and the electronics of the system. Experience at the City University on 38 mm samples using the conventional testing instrumentation, gives accuracy of the order of 1 to 2 kPa in pore pressure and cell pressure, of the order of 3 to 5 kPa in axial stress and of the order 0.02 to 0.03 % during the initial stages and 0.1 % at large strains in axial and volumetric strains (Coop, 1990; Lau, 1988; Richardson, 1989).

5.2.4 Data logging and control system

The stress path test control system comprises of Acorn BBC model B computer, Intercole Spectra Micro-ms interface unit. Its peripherals a printer, a disk drive and a monitor.

The arrangement is illustrated in Figure 5.2. Instruments record the axial force F_a, the pore pressure u, the radial stress σ_r, the

axial deformation ΔL and the volume change ΔV. The change of radius ΔR can be computed from the axial deformation and the volume change. The electrical transducer output is transmitted to a signal conditioning unit which selects a transducer, reads and amplifies the output and converts the signal into digital form. The basic function of the microcomputer is to receive the digital output from the interface unit, convert these to stresses and strains and command the electromanostats to supply the required pressures, by means of electrical relays, also housed in the Micro-ms interface unit.

The basic control software used was initially 'TRIAX' which was later changed to the more sophisticated program *'TRILOG3'*. Both were written in Acorn Basic Version OSI.20. Minor modifications to these programs were made, whenever it was necessary, to suit particular purposes, for instance to conduct constant p' tests or to monitor external volume change measurements. Their principal function was to record data from triaxial tests and to control the stress path followed using a feedback loop. Details of the stress path, control time interval and recording time interval are specified by the user and can be varied for each test stage. Records are stored on a sideways RAM and are printed out and dumped to disk at the end of every test stage or on request by the user. Details of these programs are given by Clinton (1986) and Pickles (1988).

5.2.5 Volume change measurements on unsaturated samples

As described in the previous section, volume changes of fully saturated samples were measured observing the amount water entering or leaving the sample during the test. This method could not be used in samples containing air due to its compressibility. In consequence some modifications were made in the volume change measurement system for the dry and partly saturated samples.

It was attempted initially to measure the volume change by observing

the quantity of water entering or leaving the triaxial cell after installing the volume gauge in the cell pressure supply system. However, considerable errors occurred resulting from the expansion of the cell, creep effects and slight leakage of the cell water under pressure. The expansion and leakage with time were observed as apparent volume changes (Figure 5.3). The volume gauge registered a change of 12.5 cc for a cell pressure increment from 30 kPa to 300 kPa and a change of 1.0 cc under constant cell pressure of 200 kPa for 30 hours.

To overcome this problem a perspex inner chamber was employed as shown in Figure 5.4. The basic principle of this inner chamber is the same that of Bishop and Donald (1961). The pressures in the inner and outer perspex chambers are always maintained equal by connecting them to the same pressure supply system. An Imperial College type 50 cc volume gauge is installed in the connection to the inner chamber to measure the volume change to and from the chamber. As can be seen in Figure 5.5, the apparent volume change decreases remarkably with this inner chamber. Compared with the system without inner chamber, the volume changes induced by the cell pressure increments reduce to one tenth and those under constant cell pressure reduce to one third.

Despite the double-walled system, some errors in volume change measurements were still evident and it was necessary to calibrate for the pressure change and the lapse of testing time. Volume changes appeared to result from air trapped in the chamber and the absorption of water into the perspex and the membrane. The errors due to the cell pressure changes were found to be repeatable and calibrated linearly in a semi-logarithmic plane (Figure 5.5 (b)). The errors under a constant cell pressure were small but also calibrated. The dotted lines in Figure 5.5 (b) and (c) represent these calibrations. The volume change resulting from the axial ram movement was calibrated and the overall performance of the inner chamber system was cross-checked using a fully saturated sample. The maximum error in volumetric strain compared to those measured with the conventional volume gauge was 0.06%.

5.3 High pressure triaxial cell

Six triaxial tests were carried out in a high pressure cell which can apply radial stresses of up to 9 MPa (Figure 5.6). The apparatus consists of a high pressure cell with electrical instrumentation, a motorised loading frame and a BBC microcomputer with peripherals and operating software. The cell body is constructed of steel in order to resist the high pressures and was large enough to accommodate the 60 mm diameter and 120 mm high samples chosen for this research.

The high cell and axial pressures were provided by pressure multipliers which could deliver hydraulic pressure at a ratio of 12:1 of the input air pressure. The output pressures were regulated by controlling the input air pressures with electromanostats. To prevent pressure fluctuations when the multipliers recharge, a damping system of fine metering valves and accumulators was used, as shown in Figure 5.6.

The main difference between Bishop and Wesley cell and the high pressure cell is the system for applying and measuring the axial stress. In the high pressure apparatus the axial load was applied by a ram passing through the top of the cell was measured with an external load cell, whereas the Bishop and Wesley cell has self-contained hydraulic axial loading through the base of the cell and internal load measurement. However in the high pressure apparatus the axial stress can be controlled by means of a hydraulic piston mounted above the axial load cell. As for the standard pressure system, constant strain rate loading was used and this was applied by the motorised 10 tonne load frame. Because the outer load cell was employed, the measured axial force included the friction between the ram and its O-ring seal at the top of the cell. To reduce the ram friction by providing lubrication, a thin layer of oil (Shell Tellus) was used on top of the cell water. The friction was assessed before and after each test and the average was taken for the correction. After accounting for this friction the axial force

was measured to an accuracy of about 3%.

Axial displacements were again measured externally and a correction was made for the expansion or contraction of the cell under changing cell pressures. An Imperial College 100 cc capacity volume gauge was used for the volume changes. The accuracy of strain measurements is similar to those from the Bishop and Wesley cell. Both cell and pore pressures were measured by Wykeham Farrance transducers with a range of 10 MPa which are of similar percentage accuracy to those for the standard pressure cell.

Data logging and control of this system was the same as that for the Bishop and Wesley cell, being performed by an Intercole Spectra which was interfaced with a BBC microcomputer.

5.4. Special considerations for the triaxial testing of decomposed granite soil

Because triaxial samples of decomposed granite soil contain quite coarse grains (up to 5 mm), some points have to be considered. These are; the choice of sample size and type of end platens, the estimation of membrane penetration, the type of drainage and the rate of loading. Details are discussed in the following sections.

5.4.1 Sample size

The test sample should be large enough to represent adequately the soil of which properties are to be determined. For fine grained soils 38 mm diameter samples are commonly used in the standard triaxial test (BS 1377:1975). If the soil contains larger particles, larger diameter samples should be used.

When coarse particles are present, smaller diameter samples give higher compressive strengths than larger samples (Holtz and Gibbs, 1956), but the larger samples require more material. In addition the capacity of the axial stress in Bishop and Wesley triaxial cell

is limited by the ratio of the sample to Bellofram cylinder areas; the larger the sample diameter, the smaller the maximum axial stress that is available with the same mains pressure supply. Thus the selection of the sample diameter is governed by the particle size and the equipment used.

Various standards have given guidelines on the ratio of triaxial sample diameter to the maximum particle size. In ASTM (1970) a sample diameter of at least 10 times the maximum particle size is recommended, or 6 times if the diameter is over 71 mm. In 'Soil Testing Procedures' by Japanese Society of Soil Mechanics and Foundation Engineering (JSSMFE, 1982) a ratio of 20 is suggested for relatively uniform river sand and 10 or 5 for a well graded soil. No recommendations were made for this ratio by British Standard until 1990. In the latest standard (BS 1377:Part 1:1990) 5 times the maximum particle size has been suggested as a minimum sample size. From these standards, greater than 10 times the maximum particle size seems to be reasonable as a sample diameter for a relatively well graded soil. In this project the material passing through a 5 mm test sieve was used for the triaxial test and 60 mm, 12 times of the maximum particle size, was chosen as the sample diameter.

5.4.2 Ends restraint

Ideally the stresses and strains in the triaxial test should be uniform throughout the test sample. It is generally considered that adequately uniform conditions will be achieved by using samples with a height greater than or equal to two diameters (Taylor, 1941). However, the non-uniform stress and strain distributions, which are produced by the frictional restraint at the sample ends, have been recognized by several researchers (Shockley and Ahlvin, 1960; Bishop and Green 1965; Kirkpatrick and Belshaw, 1968).

Various methods have been tried to reduce the effects of end restraint but only lubricated layers, which were developed by Rowe

and Barden (1964), have proved both effective and practicable. These consist of a combination of rubber membranes and silicone grease. While lubricated layers minimize the end restraint, there are associated errors in the measurement of axial and volumetric strains due to the deformation of the layers as reported by Sarsby, et al. (1980, 1982). In addition, the thickness of lubricated layers influences the strength parameters as well as the strain measurement.

Norris (1981) assessed the effect the thickness of the lubricated layers on the strength and proposed the optimum thickness of the layers to obtain consistent results. He also evaluated the differences in behaviour between the conventional triaxial test (H = 2 to 2.5 D) and the test with H equal to D with lubricated layers. Using an LVDT mounted on the sample to avoid bedding errors, he found significant variation in sand strength between tests depending on the number and thickness of end membranes employed (Figure 5.7). The sample height and confining pressure also influenced the optimum thickness, but the most significant influence was the particle size. He suggested that an initial choice of end membrane thickness should be equal to 1.5 times the average particle size. He also observed that the conventional test give a strength comparable to that of the test with frictionless end platens and an optimum end membrane thickness. Tatsuoka et al (1984) reported that the quality of the silicone grease and the composition of the layers could influence the performance of the lubricated layers.

From the available data, very thick lubricated layers of about 2.25mm at each end would be necessary to minimise the friction at the end platens for the tests on decomposed granite soil with a mean particle size of 1.5mm. This would however cause excessive uncertainty in the deformation measurements using conventional instrumentation. Internal deformation measurement devices could be used for the axial strain, but accurate measurement of volumetric strains would remain a problem. Lubricated layers were therefore not employed and samples with a length to diameter ratio of 2 were tested between the conventional platens throughout the research.

5.4.3 Membrane penetration

In the case of coarse material (i.e. mean particle size of 0.1 mm or over), membranes are deformed at the surface of the sample as the effective radial stress changes (Figure 5.8). The effect of membrane penetration is to lead to errors in the measurement of volumetric changes for drained tests or of pore pressures for undrained tests. For instance, in drained isotropic loading and unloading tests on medium dense fine sand the errors in volume change can be of the order of 20% and 40% respectively (Molenkamp and Lugar, 1981).

For drained triaxial teats, an adequate calibration between the effective radial stress and volumetric change due to membrane penetration for a given material and testing condition can be made and the measured volumetric changes are corrected by using these calibration results. Several experimental methods have been employed to measure the magnitude of membrane penetration. These are,

a) to use the isotropy of the sand samples.
(Newland and Alley, 1957; Roscoe, et al. 1963);
Volume changes due to membrane penetration can be estimated from the difference between measured volumetric strains and three times the measured axial strains.

b) to use dummy metal rods.
(Roscoe, et al. 1963b; Raju and Sadasivan, 1974);
Samples with a metal rod are used, varying the size of the rod. The soil volume within the sample and consequently the overall volume changes will differ. However, the volume changes due to membrane penetration will be the same.

c) to use hollow cylindrical samples. (Frydman, et al. 1973);
While keeping the external diameter constant, the internal diameter of a hollow cylindrical sample is varied. The

volume changes due to membrane penetration can be estimated from the relationship between the measured volume changes and the internal diameters of the sample.

The basic assumption of methods b) and c) is that the volume change of the sample is proportional to the volume of the soil.

To estimate the membrane penetration effect of decomposed granite soil, method b) was employed. As the diameter of the metal rod increases, the soil volume decreases, but the surface area remains unchanged. Therefore, with increasing core rod diameter, the volume change due to compression of the soil decreases, while the volume change due to membrane penetration remains the same.

Isotropic compression tests were carried out on 60 mm diameter cylindrical samples of soil surrounding brass core rods of 22 mm and 44 mm diameters. For each test the initial specific volume of the soil was 1.65. The penetration of a 0.6 mm thick membrane was evaluated for each value of the effective radial stress by plotting the measured volumetric changes against the brass rod diameters. The latter can be expressed as the ratio of the soil volume to the sample volume; V_s/V_o. In Figure 5.9 the two points have been connected by a straight line which has been extrapolated to give the volume changes corresponding to a brass rod of 60 mm diameter (V_s/V_o=0) for each applied effective radial stress. These volume changes represent membrane penetration. Also plotted on Figure 5.9 are points corresponding to isotropic compression tests on samples without dummy rods. These do not fall the same straight line as the other data, indicating that the stress conditions are not truly isotropic, i.e the axial stress is less than the radial stress, due to the rigid platens and stiff brass rod. This calibration may therefore lead to an overestimate of the membrane penetration.

The volumetric strain resulting from membrane penetration (ϵ_{vm}) can be used to derive the unit membrane penetration (V_m) which is the membrane penetration effect per unit membrane area. Figure 5.10 shows that the relationship between the unit membrane penetration

and the effective radial stress on a semi-log scale is close to linear. The slope of this line is related to the mean particle size and factors such as density, particle size distribution, particle shape are known to give minor effects (Frydman, et al, 1973). When the effective radial stress was changed during a test, for instance during isotropic compression or constant mean effective stress tests, the relationship shown in Figure 5.10 was used for correcting the data for the membrane penetration effect.

5.4.4 Drainage

The field drainage conditions may be approximated by unconsolidated undrained, consolidated undrained or drained triaxial tests. The type of test is selected mainly as a result of the permeability of a soil. The permeability of decomposed granite soil is the order of 10^{-3} cm/sec. In consequence excess pore pressures dissipate very rapidly, and excluding some exceptional cases the loading may be assumed to be drained. In case of undrained tests the pore pressure responses are also influenced by the membrane penetration effect. Consequently most of the triaxial tests in this research were performed in the drained condition.

5.4.5 Rate of loading

It is necessary to choose a rate of loading which allows the test to be carried out in a reasonable time without causing errors due to incomplete pore pressure dissipation. For highly permeable soils such as decomposed granite soil, permeability is not a significant factor controlling the loading rate. However, a rapid test under constant strain rate loading is not considered to be adequate to determine accurately the stress-strain behaviour of soil before failure. The rate of stress change in this loading is initially very large because the soil is stiff at small strains. On the contrary the ultimate state cannot be observed in constant stress rate loading. The tests were therefore started with constant

stress rate loading and later switched to constant strain loading (Atkinson, 1984b).

5.5 Triaxial test procedures

5.5.1 Triaxial sample preparation

Disturbed samples for the triaxial tests should be prepared in such a way that it is reproducible. The sample should have the pre-determined dry density and should be homogeneous.

Granular samples are commonly prepared by the conventional pluvial method described by Bishop and Henkel (1962). However this method is not suitable for well-graded materials because they segregate during preparation. This method also does not model the mechanical compaction to which the soil is subjected when used as a fill.

Each sample, 60 mm in diameter and 120 mm in height, was prepared in a 3-piece split mould in twelve layers by the moist tamping method (Ladd, 1978). Every effort was made to prevent material segregation. The procedures followed are detailed below.

a) After the treatment, which will be described in section 6.2.3, the material was separated and stored in seven batches according to the particle size, i.e. 5-3.35 mm, 3.35-2 mm, 2-1.18 mm, 1.18 mm-600 μm , 600-300 μm, 300-150 μm and below 150 μm. The material over 5mm was discarded, and the percentage weight of each batch to the whole was determined. The uniformity of the material, which is the ratio of D_{60} to D_{10}, in each batch was kept below 2.

b) The required dry weight of material was calculated for a sample.

c) Air-dried material was collected from the batches in the correct proportions. A slightly greater total weight was collected so as to provide a moisture content measurement from the material not

used in preparing the sample.

d) Air-dried material with a moisture content of about 0.5% was mixed with de-aired water to give about a 10% water content and then allowed to cure for about 48 hours in a vinyl bag.

e) The wet weight of material required was calculated for the whole sample and also for each of the 12 layers from the dimensions of the mould and the pre-determined dry density.

f) The required height of the sample at the top of the n-th layer was calculated. When the material was compacted in layers, the compaction of each succeeding layer could further densify the material below it. The concept of undercompaction (Ladd, 1978) was used to make a uniform sample. The optimum values of percent undercompaction were 5% for the loose samples and 0% for the dense samples.

g) The amount of material required for each layer was weighed and placed into the mould. The surface of the material was levelled using a spatula and compacted to the predetermined height. Then the compacted surface was scarified using an awl to prevent stratification..

h) Step g) was repeated until the last layer was in place. During the compaction of the last layer, the tamping rod was used until the surface of the compacted material was about 0.5mm higher than required. Then a top platen was placed into position and lightly hit with a rubber mallet until it was seated.

i) After compaction the weight of the sample was measured and a sample for a water content measurement was taken from the remaining material. Then the sample was transferred into the triaxial cell and the split mould was removed. Loose samples, above initial specific volume of 1.60, were frozen in the freezer after compaction to prevent collapse when the mould was removed. Sample dimension changes due to freezing were avoided by using

relatively dry material (water content about 10%, giving about 40% saturation) and by applying a surcharge of 15–20 kPa during freezing. The dimensions of a sample were assumed to be equal to those of the mould.

Most of samples were prepared in a wet state as described above, but some samples were prepared in a dry state. The former will be referred to as wet or wet compacted samples and the latter as dry or dry compacted samples.

Oven-dried soil, cooled in a desiccator, was used for the dry samples which were also 60 mm in diameter and 120 mm in height. The preparation procedures were quite similar to those of wet compacted samples except that the samples were prepared directly on the triaxial cell base using a sample former. The sample former, consisting of a 2-piece split mould of 61.2 mm internal diameter, was placed on the cell base with a membrane of 0.6 mm thickness and a dry porous stone (Figure 5.11). Compared to the wet compacted samples the dry ones reached the required density with less compactive effort (tamping). This was not quantified precisely but a dry sample with an initial specific volume of greater than 1.60 (dry density of about 1.60 g/cm^3) could be made without tamping, just placing the dried material into the sample former with a spoon and levelling it. After preparing the top layer, a filter disc, the porous stone, top cap and O-rings were placed and a small suction was applied to the sample. Then the sample former was removed and the exact sample dimensions were measured. The height was measured and calculated using a dial gauge and a dummy sample. Three measurements of the diameter were made using vernier callipers; one at each end and one at mid-height. The average was taken as the diameter after deducting the membrane thickness. The suction was maintained until the cell was assembled.

Some wet compacted samples were air dried in the laboratory. They dried quite quickly, and after 5 days drying, the sample weight had stabilized with a water content of 0.5% to 1%. Upon drying they became firmer and appeared to be cemented. Each sample was dried

for at least one week before testing.

5.5.2 Pre-test checks and sample setting up

Before starting a test series the measuring instruments were calibrated following the procedures given in Section 5.2.3. The calibration was then carried out regularly, at least every six months, but no significant changes in calibration factors were ever noticed. If a full calibration was not undertaken, a brief check was made as to whether all the instruments responded properly. This was done easily by applying a small pressure, load or displacement to the devices and observing the readout.

The triaxial cell was then filled with water, the surface of which was at about the middle of the sample during the test, and the zero stress readings from the load cell and the pressure transducers were recorded.

The cell was emptied and the drainage leads to the pore pressure transducer and the volume gauge were flushed with de-aired water and carbon dioxide gas respectively. Because carbon dioxide gas was going to be circulated through the connection from the volume gauge to the cell base, it was better to fill the connection lead with the gas than water at this stage. High vacuum grease was applied along the sides of the base platen and the top cap. An air dried porous stone was then placed on the platen followed by a filter paper disc, the sample, a second filter paper disc, the top porous stone and the top cap complete with rubber suction cap. Then either one thick membrane (thickness= 0.6 mm) or two thin membranes (thickness= 0.3 mm each) was put over the sample and sealed top and bottom with O-rings. Although the total thickness of membrane was same (0.6 mm), two thin membranes proved to be more effective in avoiding punctures during the tests. All tests in the Bishop and Wesley cell were carried out with a total membrane thickness of 0.6 mm, however in the high pressure cell a total membrane thickness of 1.2 mm (one thick and two thin membranes) was used. When the inner chamber was employed, it was assembled at this stage. Then the top drainage

lead was connected by simply pushing the drainage line with rubber sleeve into the hole in the top cap. This simple connection worked very well even under the highest pressure of 8 MPa. A diagrammatic view of a sample on the base platen is shown in Figure 5.12.

The cell body was placed, screwed down and filled with de-aired water. Then the cell pressure was increased to 20 kPa and the top drainage was opened to the atmosphere. The top of the sample was connected to the load cell using rubber suction cap at this stage. In the early stages of the research, the connection was made after the isotropic compression stage, and in this case it was not possible to measure the axial deformation directly during isotropic loading. Figure 5.13 shows the suction cap arrangement.

In the high pressure cell, the cell was filled with water with a layer of oil on top. The top part of the cell was assembled and the tie bars were tightened. The cell pressure was then increased to 20 kPa manually using fine metering valves and the top drainage was opened to the atmosphere. A suction cap was not used in the high pressure cell.

5.5.3 Saturation

Saturation of the sample is necessary to provide reliable measurements of the volume change in drained tests and of the pore pressure response in undrained tests. The methods which have been used for soil saturation are,

a) flushing with water (Lowe and Johnson, 1960)

b) use of back pressure (Lowe and Johnson, 1960; Black and Lee, 1973)

c) using carbon dioxide (Lade and Duncan, 1973; Been and Jefferies, 1985)

d) applying a vacuum (Rad and Clough, 1983)

Among these, the back pressure method is most frequently used to force entrapped air into solution. If this method were employed in order to saturate the compacted wet sample, which are stiff and also contains a lot of air, it would need very high pressure and extra time to ensure full saturation. To avoid the use of high back pressures while achieving rapid saturation, carbon dioxide was used.

As shown in Figure 5.14, carbon dioxide was introduced through the bottom drainage, thereby pushing the air in the sample out through the top drainage. The CO_2 was detected using calcium hydroxide from the top drainage after 5 minutes, but the supply was continued for 15 minutes. The pressure of carbon dioxide was kept within 1–2 kPa by using the regulator, R. De-aired water was then introduced through the bottom drainage and allowed to seep slowly up through the sample with very low pressure (Figure 5.14(b)), thereby pushing most of the carbon dioxide out through the top drainage and dissolving in the water. The head of de-aired water was kept below 2–3 kPa. After this water circulation the top drainage was closed and a back pressure of 100–150 kPa was applied for about 12 hours to dissolve the remaining carbon dioxide and maintained until the end of the test.

The degree of saturation was checked by measuring the pore pressure response parameter B (Skempton, 1954). The value of B was found to be 0.98–1.00, indicating that the samples were adequately saturated.

Not all samples were saturated at this stage. Some samples were kept dry or wet throughout a test and others were saturated (flooded) after isotropic compression or during the shearing stage.

5.5.4 Isotropic compression and shearing

Each test was generally conducted in the following stages.

stage 1: Isotropic compression
stage 2: Shearing 1 (stress controlled)
stage 3: Shearing 2 (strain controlled)

For the isotropic compression stage, the axial and radial stresses were increased to a pre-determined stress at the same rate. The pore pressure was kept constant for the saturated samples and the drainage valves were opened to the atmosphere for partly saturated or dry samples. Pore pressures were not measured for the partly saturated samples. The rate of the compression was in the range of 50 to 100 kPa per hour. Both axial and volumetric strains were recorded in the Bishop and Wesley cell during isotropic compression but only volumetric strains were obtained in the high pressure cell. For the over-consolidated samples, the stresses were increased to the normal compression stress range and then decreased to the certain points. The over-consolidation ratios used were 2.5 and 5.

Following isotropic compression new sample dimensions were calculated, deducting the volume change resulting from membrane penetration and assuming that the sample underwent isotropic strains if the axial strains were not measured. These new dimensions were used throughout the shearing stages unless strains were zeroed again. Three kinds of stress path were followed. In addition to the conventional drained and undrained tests, for which samples were sheared under a constant total radial stress, tests which followed a constant p' path were also carried out. For each type of test the shearing stage was initially under stress control and then switched to strain control as discussed in section 5.4.5. The rate of stress controlled shearing was 50 to 100 kPa per hour, depending on the confining stress, and 0.5 - 0.8% per hour for strain controlled.

Special procedures were taken to determine the effects of water on the behaviour of the soil. Some dry samples were flooded either after isotropic compression, at the point when the deviator stress had reached 90% of its ultimate value or at some point after the peak strength. For the first two cases the axial and radial stresses were kept constant and changes of the axial and volumetric strains were observed during flooding. But for the latter where the sample was already undergoing axial strain controlled loading, this was continued and changes of the axial stress and the volumetric strain were measured. In each case flooding was achieved using

carbon dioxide and de-aired water circulation as described in the previous section. One air-dried sample was also flooded upon reaching the 90% of the ultimate strength.

5.5.6 Post-test

After the end of the shearing stage, the sample was removed from the cell and the water content was determined by the oven drying method. The water content of the dry samples after testing was 0.35% - 0.45%. For the partly saturated samples the water contents were always within 0.1% of the original water content. A sieve analysis was carried out to observed the change of the particle size distribution during the triaxial test.

The final zero readings of the stress transducers were also checked and in all cases these were found to be within 1 kPa of the initial zero readings indicating that the drift of the instruments was negligible.

Chapter 6 Test results and discussions

6.1 Introduction

This chapter presents the results of the tests carried out at the Geotechnical Engineering Research Centre, City University. Analyses of the data and the discussion on the results are also presented. The analyses are based on the theoretical framework of critical state soil mechanics described in Chapter 3.

The Section 6.2 contains the results of the preliminary tests, such as soil description, index tests, etc. The remaining sections concentrate on the result of triaxial compression tests. Details of the triaxial testing programme and the calculation procedures are described in Section 6.3 and the results for the saturated samples follow in Sections 6.4 to 6.8. The principal points discussed are; isotropic compression and swelling, ultimate states, peak states, the state boundary surface and shear stiffness. The last section presents data for both dry and partly saturated (wet) samples. These tests were performed to investigate the possible effects of water on the behaviour of the soil and the results are compared with those from saturated samples.

In total 59 triaxial tests were carried out but the basic test data are not presented in this thesis, as they have been reported separately by the Author (1991).

6.2 Preliminary tests

6.2.1 Introduction

Decomposed granite soil samples taken from the site were transported to the laboratory. First of all, the samples were carefully examined and some simple index tests were carried out. Samples were visually examined and described according to the procedures given in

BS 5930 : 1981. The preparation of disturbed samples is then described, followed by the results of index tests, such as in-situ density and water content, specific gravity and particle size distribution. Mineralogical analyses were carried out to identify which minerals were present and compaction tests were performed to find the maximum density and optimum moisture content. For the index tests and compaction tests, the procedures described in BS 1377 : 1975 were followed.

6.2.2 Soil description

The colour of the soil is light brown in its dry state and reddish brown in a wet state, consisting principally of grey quartz, pinkish feldspar and black mica. The material is a completely weathered granite soil (grade V). The feldspars are moderately decomposed and the quartz particles are fractured. Quartz particles coated with feldspars are frequently found.

Although the soil is coarse and disturbed, the particles are not completely separated but some particles appear to be bonded and exist in the form of an aggregate. These aggregates, whose size sometimes reaches 30–40 mm in diameter, indicate the in-situ texture of the soil, which is the product of the parent rock and the weathering processes. The aggregates, which are friable and can be crumbled by hand, seem to be the result of both the pore water suction and true bonding between the particles, because some of them fall apart in water while others remain firm.

The soil particles are principally of coarse sand grain size, but gravel and silt sized particles are also found. The soil is very well graded and may be described as very gravelly sand. The particles show little or no evidence of wear and are sub-angular to angular, with a surface texture which is rough. Individual particles are frequently micro-cracked and found to be easily broken down.

6.2.3 Disturbed material preparation

The aggregations of particles should be crumbled before soil samples are prepared for classification and mechanical tests, but crushing of individual particles must be avoided for most purposes. This process may be done in a mortar with a rubber pestle (BS 1377 : 1975). However, this method would lead to the crushing of individual particles of the decomposed granite soil which has micro-cracks and is in a state of active weathering and continuous breakdown.

The free-falling method recommended by the Japanese Society of Soil Mechanics and Foundation Engineering was used as the preparation procedure (JSSMFE, 1982). Soil samples were air dried for 3-4 days on trays in the laboratory. About 500 g of the sample was put into a small vinyl bag, and the bag of soil was dropped 30 times, falling freely from the height of 1.5 m, onto a concrete floor. The amount of particle disaggregation is related to the number of drops. Figure 6.1 shows the relationship between the change of grading and the number of drops. From this diagram it can be seen that the change of grading seems to cease after 30 drops. After the treatment, however, particle aggregates were still found. Following this treatment, representative samples for various tests were obtained by riffling.

6.2.4 Index tests

In-situ water content and density were determined by the oven drying and sand replacement methods respectively. The average water content was about 7% and that of dry density was 17.13 kN/m^3. The results are shown in Table 6.1.

The specific gravity of the soil, determined by following the density bottle method specified in BS 1377 : 1975 Test 6(B), was 2.61. This value is found to be slightly lower than the usual value for decomposed granite soil, 2.65.

Wet sieve analyses, specified in BS 1377:1975 Test 7(A), were carried out both before and after the treatment described in the previous section. The results are shown in Figure 6.2, where solid and dotted lines represent the gradings before and after the treatment respectively. The grading becomes a little finer as a result of the treatment. The grading curve reveals a wide and even particle size distribution. Particles range from gravel to silt size and mean particle size of the treated material is 1.9 mm. D_{60} and D_{10}, the particle sizes for which 60% and 10% of particles are finer, are 2.5 mm and 0.185 mm respectively. The uniformity coefficient, which is the ratio of D_{60} to D_{10}, is a quite high value of 13.5. Compared with the grading curves of other decomposed granite soils in Figure 4.9, this soil is rather coarse and would be termed a 'well-graded silty sand and gravel'.

It has been observed that the grading of the soil changed with the period of time sieving. As shown in Figure 6.3, where grading changes are expressed by the changes of D_{10}, D_{30}, D_{50} and D_{60}, the grading becomes finer with the time, even after a long period of sieving. The change is more severe for coarse particles, indicating that the grading change does not result from the incomplete sieving but mainly from the particle disaggregation. It is desirable to keep the sieving time as short as possible, however, the time should be long enough to complete the sieving itself. All sieving analyses in this thesis were performed for 10 min which is recommended as the minimum period by BS 1377 using a mechanical shaker.

Because the soil is coarse and the proportion of particles finer than 425μm is below 20%, conventional Atterberg limits tests cannot be used to index the soil.

6.2.5 Mineral composition

The mineral composition of the soil was analyzed using X-ray diffraction techniques at the Geomaterials Laboratory, Queen Mary College. The X-ray diffraction analysis was carried out using a

Philips PW1050 diffractometer with a graphite monochromator. The mineralogy obtained from the analysis is given in Table 6.2.

As can be seen from the table, the soil consists mainly of quartz and feldspar with some mica and kaolinite. Comparing the mineralogy of coarse and fine particles, the fine particles consist of a lower proportion of quartz but more feldspar, mica, kaolin and smectite. The latter two clay minerals are absent in the coarse particles, indicating that feldspar and mica have broken down to fine particles and partly altered to clay minerals.

6.2.6 Compaction test

The 'Proctor' compaction test was performed to obtain a dry density-moisture content relationship. Because the soil was known to be susceptible to grading changes during compaction, materials were not reused after compaction but new materials used at each moisture content.

The compaction curve is shown in Figure 6.4, together with 0, 5 and 10% air voids lines. The maximum dry density is 1.83 Mg/m^3 (17.94 kN/m^3) and the corresponding optimum moisture content is 12%. These values are within the ranges of the soils, mentioned in section 4.3.2. Although the compaction curve shows a clear peak, dry density does not vary very much with moisture content. Thus the moisture content to achieve the 90% or 95% of the maximum dry density, which is frequently found in specifications for compaction, is not critical.

Grading changes due to compaction were observed and the changes of grading before and after the compaction tests are shown in Figure 6.5.

6.3 Triaxial tests: programme and calculation procedures

6.3.1 Test programme

In total 59 triaxial compression tests were carried out in the apparatus previously discussed. Test were performed under various moisture conditions, dry densities, radial stresses, stress paths and drainage conditions.

As discussed in Chapter 4, the behaviour of soils, especially those whose particles are breakable or contain cracks, is influenced by the presence of water. To determine the effects of water on the behaviour of decomposed granite soil, various moisture conditions of the samples were maintained throughout the tests as shown in Table 6.3.

Moisture conditions were varied from the sample preparation stage. As mentioned in section 5.5.1, soils for the sample preparation (compaction) were wet, moisture content of about 10%, or were oven dried. Samples compacted in a wet state were partly saturated. The saturation ratio depends on the water content and the density, but ranges from 40 to 60%. Most samples were saturated before or after isotropic compression and sheared in a saturated state. This type of sample or test will be described as 'saturated'. Some of the partly saturated samples were sheared without saturation. This type of sample or test will be simply referred to as 'wet'. Three of the samples were air dried and sheared, except one which was flooded during shearing. Samples compacted in a dry state were isotropically compressed in a dry state and most of them were sheared under the same condition while others were saturated or flooded either before or during shearing. This type of sample or test will be described as 'dry', irrespective of saturation or flooding in the later stage.

Both the density of samples and the confining stress were varied. The initial dry density of samples was varied from 95% to 86% of the maximum dry density determined by the compaction test at intervals

of around 3%. Samples with an initial specific volume of 1.50 are equivalent to 95% of $\gamma_{d\,max}$ and will be termed "very dense" samples, while those with an initial specific volume of 1.55, 1.60 and 1.65 will be described as "dense", "medium dense" and "loose" respectively. Effective radial stresses before shearing were applied in the range 50 to 500 kPa in the Bishop and Wesley cell and up to 8 MPa in the high pressure cell.

Two kinds of total stress path were used. One was the conventional compression test stress path in which samples were sheared under a constant radial stress after isotropic compression. Most of tests were performed under drained conditions but eight undrained tests were also carried out. The other path used was the constant p′ stress path. Because the mean effective stress p′ was kept constant, volume changes only due to dilatancy are obtained for this stress path test. Details of the triaxial test programme are shown in Tables 6.4 to 6.6.

6.3.2 Raw test data correction

Stresses and strains have been calculated from the current transducer readings by the control system. Among them the axial stress is calculated using the corrected sample area. The sample area is corrected, based on the conventional assumption that the sample deforms as a right cylinder. The current values of stresses and strains are stored at regular intervals and usually stored on a floppy disk at the end of each test stage.

In addition to the sample area correction, several other corrections were also made either as the tests were running or during later analyses of the test data. These corrections are for the compressibility of the load cell and the cell body, the expansion of the volume gauge, the membrane penetration, the ram friction in the high pressure cell and the membrane stiffness. All the corrections, except that for the membrane stiffness, were estimated using the procedures described in chapter 5 and are mostly allowed for in the

control programs 'TRIAX' or 'TRILOG3'.

The use of membranes may have an effect on the deviator stress measurement due to its stiffness. The amount of contribution by the membrane depends on the properties of the membrane, sample failure modes, stress paths and strains. The corrections for the membrane stiffness in a bulging failure were derived analytically by Duncan and Seed (1967) and later amended by Richardson (1986). They took into account both axial and volumetric strains and corrected both axial and radial stresses, applying elastic shell theory. Accumulated axial and volumetric strains throughout a test were used for the correction.

Based on their work, the results of test 50, in which the radial stress was only 50 kPa, have been corrected and the effect of the correction is shown in Figure 6.6 (a) and (b), where the plots of q' against ϵ_s and q'/p' against ϵ_s are presented. As can be seen from the figures, the stress-strain curves are only slightly affected by these corrections. The corrections made to q' are 1.5 kPa at the peak and 5.5 kPa at the end of the test respectively and that to q'/p' is 0.03 at the end of the test. The corrections may be overestimated at large strains due to possible relative movement between the two materials as well as buckling of the membrane, indicating that the corrections may not be necessary. In addition, at larger radial stresses, the relative importance of the membrane correction becomes smaller, because the membrane correction is almost independent of the radial stress. The correction for the membrane stiffness has therefore been applied only to tests in which radial stress at the ultimate state was 50 kPa or less.

6.3.3 Analysis

The raw test data, which was generated by a BBC microcomputer, was transferred to the IBM compatible PC and analyzed to produce further parameters, such as q', p', v, ϵ_s, etc, using the VP planner spreadsheet software.

The recorded strains in the raw data are ordinary or linear ones, defined as the change in a dimension divided by the initial reference dimension. Since the strains in the tests are relatively large, however, accurate and consistence results are to be obtained only when natural strains are used. The importance of the use of natural strain in the analysis of soil tests has been demonstrated by Richardson (1984), and only natural strains are used for data analyses in this thesis. The conversion between ordinary strains (ϵ_{ord}) and natural strains (ϵ_{nat}) is given by

$$\epsilon_{nat} = - \ln (1 - \epsilon_{ord}) \qquad (6.1)$$

The specific volumes of the sample are usually back calculated from the final water content and the volumetric strains. In this research, however, the initial density of the sample was used instead of the final water content. For the fully saturated samples, the final water contents may be used but corrections have to be made for the volume changes due to membrane penetration. On the other hand, the initial density can be controlled and is always available at the sample preparation stage, regardless of the sample moisture state. This method seems to provide more consistent results for both fully saturated and unsaturated samples.

The potential errors are larger in the measurement of the initial density of the sample. Compared with the determination of the final water content, larger errors occur as a result of inaccuracies in the measurement of the sample dimensions. The specific volume calculated from the initial density is compared with that from the final water content in the Table 6.7. As can be seen from the table, the differences between the two values are mostly within the range of ±0.007, which is equivalent to ±0.27% in terms of water content. For the dry samples, this comparison cannot be made. However, from the results of tests 19 and 22, which were prepared in dry state but saturated after isotropic compression, the specific volume determination based on the initial density of the sample is quite convincing for dry samples as well.

6.4 Isotropic compression and swelling

As mentioned in Chapter 2, the parameters for the normal compression line are the basis of critical state soil models. The isotropic compression and swelling tests were initially carried out in a Bishop and Wesley cell with quite loose samples, for which the initial specific volumes were around 1.67. The results showed that the deformations remained quite small so that normal compression line as well as yielding point could not be determined, indicating that isotropic compression tests on this material should be performed using higher pressures.

Several isotropic compression and swelling tests were performed in the high pressure cell described previously. One sample, HP1, was exclusively performed to find the isotropic compression and swelling properties of the soil and others, HP2 to HP6, were compressed (or later swelled) isotropically before shearing. Details of the results are shown in Table 6.8, together with those of the tests in Bishop and Wesley cell and they are plotted in v:lnp' space in Figure 6.7.

It can be seen in Figure 6.7 that loose samples are more compressible than dense ones in the initial stage, however, they eventually constitute a single, straight normal compression line in v:lnp' space. The unload-reload curves produce swelling lines, of which the gradient appears to be constant. The parameters for the isotropic normal compression line and swelling lines are given in Table 6.9, together with those of other soils. The value of λ of 0.09 is within the range for decomposed granite soils as mentioned in Section 4.3.4, while that of κ is much lower than usual values. Compared with river sands, the values of N and λ are very small, presumably due to the grading, as well graded soils might be expected to show higher density than uniform soils under the same confining stresses. Uniformly graded soils are also known to be more compressible than well graded (Lee and Farhoomand, 1967). The values of N and λ of the decomposed granite soil are comparable with those of a well graded soil, such as a till.

The slope of swelling lines, κ, is very small and the ratio to the slope of normal compression line, λ/κ, is quite large, indicating that most of the volumetric strains during the compression are irrecoverable. This may be due to the particle crushing which has been identified by the sieve analysis before and after the isotropic compression and swelling. Figure 6.8 shows the sieve analyses of test HP1. The fact that particles are crushed during compression means that the volumetric strains during isotropic compression are the results of particle crushing as well as particle movement. The volumetric strains which result from the crushing are totally plastic, therefore, the ratio of λ/κ is higher than other fine grained soils, where particles are not crushed. A high value of λ/κ has been also reported by Coop (1990) for tests on Carbonate sands, where a considerable amount of particle crushing was observed. It is clear that a higher value of λ/κ is a characteristic of crushable soils.

As can be seen in Figure 6.7, the compacted soils exist on the left side of the normal compression line, i.e over-consolidated states. However, their behaviour seems to be different from that of the truly over-consolidated soils, which reach the current states by unloading. Near point x in Figure 6.7, the current states of HP1, HP2 and HP3 are very similar, however, the shape of compression curves are rather different. The compression line of HP2, which is for first loading, is curved and does not show a distinct yield point. In contrast, the compression curves of HP1 and HP3, which are for reloading, are almost straight up to their pre-compression pressures at which the yield stress is very distinct.

The traces of normal compression of the soil, where volume changes resulted from particle crushing as well as particle movement, have been found to give a straight line in v:lnp' space. This means that the particle crushing effects on the volume changes during isotropic compression changes with the logarithm of the pressure applied.

Because of its coarse grading, any excess pore pressures dissipate very rapidly. However, the soil shows time dependent deformation

during isotropic compression under a high pressure. The additional volume changes, which take place after reaching the required pressure, are plotted against the square root of time in Figure 6.9. From the figure, the time dependent volume changes can be seen to continue for many hours and are independent of the rate of compression, indicating the feature does not result from incomplete primary compression. Similar phenomena have been observed in silica sand or coarse granite materials at very high pressures (Miura and Yamanouchi, 1975; Lee and Farhoomand, 1967) and in carbonate sands at usual laboratory pressures (Coop, 1990), but in both cases the pressures were large enough to cause particle crushing. Miura and Yamanouchi reported that it took about 350 and 570 hours to complete the isotropic compression of silica sand samples under the pressure of 30 and 50 MPa respectively. From these observations the time dependent deformation under high pressures seems to be due to progressive particle crushing.

The relationship between the axial strain (ϵ_a) and the volumetric strain (ϵ_v) during isotropic compression in the Bishop and Wesley cell is shown in Figure 6.10. If the soil behaves isotropically, the slope of ϵ_v:ϵ_a should be 3:1. Axial strain measurements were not available in the high pressure cell during isotropic compression and so the ratio of ϵ_v:ϵ_a for the soil on the normal compression line is unknown. However the degree of anisotropy decreases with the compression of the soil, tending towards 3:1 at higher stresses.

6.5 Shearing and ultimate states

This section is devoted to the behaviour of saturated samples. The behaviour of wet or dry samples will be considered later. The samples were prepared by compaction in a wet state and saturated either before or after the isotropic compression stage. In total 33 tests were conducted in this test series and details of each test have been summarized in Table 6.4. Typical test results from the Bishop and Wesley cell and in the high pressure cell are shown in Figures 6.11 and 6.12 respectively.

6.5.1 General trends of shearing data

The stress-strain curves of compacted decomposed granite soil are quite similar to those of other soils. The behaviour is very much influenced by the confining stress as well as the initial density. Figure 6.13 shows the results of the tests with various initial densities under the same confining stress of 100 kPa. As can be seen in the figure, the initial density dominates the patterns of the behaviour. Dense samples, 61 and 81, show peaks and dilative volume changes and are approaching an ultimate state at the end of the test. The loose samples, 51 and 70, show no peaks but reach the ultimate state with compressive volume changes. The initial part of the stress-strain curves becomes stiffer and the peak strength increases with the increase of the density. However, it is clear that each test approaches the same deviator stress level and specific volume at the ultimate state (point C), regardless of the initial density. This ultimate state is the critical state.

Figure 6.14 shows the results of tests with the similar initial specific volume of 1.60, showing that the behaviour of the soil is affected by the confining stress. At the low confining stress (test 50) the sample shows a peak and dilative volume changes but it behaves like looser soils under the higher confining stress (test 51). This feature is emphasized in high pressure tests. Although sample HP5 is quite dense (specific volume of 1.481 before shearing), the data shown in Figure 6.12 are similar to those for loose samples.

Seven undrained tests were also carried out and some of the results are shown in Figure 6.15. As can be seen in the figure, the strength depends on the initial density of a sample, however, the stress ratio at the ultimate state is almost the same, regardless of the density or the confining stress. All samples show slight peaks, and there is only a small post peak reduction in stress ratio. The shape of the $\Delta u:\epsilon_s$ curves are very similar to those of $\epsilon_v:\epsilon_s$ for the drained tests. While positive pore pressures are generated for loose samples (test 26 and 45) negative pore pressures are generated

for the dense sample (test 24). These are equivalent to compressive and dilative volume changes respectively for drained tests.

As mentioned in Section 5.4, the pore pressure response in undrained tests is affected by membrane penetration. In consequence, the effective stress path and the strength are also influenced. In the case of a loose sample, the pore pressure increases and the effective confining stress decreases during shearing. This causes a membrane to be deformed outward, resulting in sample volume increase. This contradicts the basic assumption of the undrained test of constant volume during loading. The undrained tests are therefore actually partially drained tests. The pore pressure responses are decreased under a partially drained condition, which results in higher effective confining stresses and shear stresses. In a dense sample, the opposite might be observed. However, the effective strength envelope seems not to be influenced by this effect (Lade and Hernandez, 1977). The volume changes arising from the pore pressure changes might be estimated from the relationship between the volume changes which result from the membrane penetration and the changes of effective radial stress which were shown in Figure 5.10.

Although the current states were similar, the behaviour of compacted samples was found to be different from that of truly over-consolidated samples during isotropic compression. This feature is also observed in shearing stage. As can be seen in Figure 6.16, the current states of test 41 and 51 are very similar, however, the stress-strain responses are quite different. While the sample of test 41 was isotropically compressed to 500 kPa and swelled to 100 kPa, that of test 51 was only isotropically compressed to 100 kPa. Compared with compacted soil, the truly over-consolidated soil (test 41) is initially stiffer and later in the test progressive compressive volume changes continue under an almost constant shear stress. However, the ultimate strengths of the two samples seem to be the same and the difference in the final volumes is small.

6.5.2 Particle crushing

Particle crushing, which takes place during sample preparation, compaction and isotropic compression is also observed during shearing. Particle crushing has been again identified by the grading changes before and after loading. Figure 6.17 shows the grading changes during triaxial tests. The figure represents the grading changes which result from shearing as well as isotropic compression. However, if the results of HP4 and HP6 were compared with that of HP1, which is shown in Figure 6.8, it is clear that shearing also causes grading changes. The two sheared samples, whose isotropic compression pressures were lower than that of HP1, show a greater grading change.

As observed in Antiochi sand (Lee and Seed, 1967) and carbonate sands (Coop, 1990), particle crushing is usually caused by the breakage of individual particles, however, in decomposed granite soils it seems to result from the separation of the aggregation of particles as well as the breakage of individual particles. It is very difficult to quantify these two effects. Thus the term 'particle degradation' is more appropriate in this case. However, it will be shown that the effects of particle grading changes on the soil behaviour seem not to be influenced by the causes of the changes. In addition, the term 'particle crushing' is more widely used, and has been used to described the grading changes throughout this thesis.

The amount of particle crushing during the triaxial test has been measured using the parameters of breakage potential, total breakage and relative breakage, which were proposed by Hardin (1985) and described in Section 4.4.3. He defined these parameters for the particle sizes greater than 74 μm sieve, however, 63 μm sieve has been used here for convenience. The breakage potential, B_p, of the triaxial sample before test was found to be 1.23. Total breakage, B_t, was calculated from the area enclosed by grading curves before and after the test for sizes greater than 63 μm sieve and was scaled down using B_p, yielding a normalised parameter, relative breakage,

B_r. The amount of particle crushing during the tests has been summarized in Table 6.10.

As can be seen in Figure 6.17, the grading changes are negligible under low pressures but noticeable under high pressures. It is logical to assume that the amount of particle crushing is proportional to the pressures applied to the sample throughout a test. The relationship between the two has been shown in Figure 6.18, where the amount of particle crushing, expressed in relative breakage, is plotted against the maximum pressure of p' and q' of a test. Although the data are scattered in low stress range, the trend is clear. The amount of particle crushing increases with the pressures, as expected. The trend is more distinct in B_r–q' space than B_r–p' space, indicating that particle crushing mainly depends on the shear stress, q', and as previously discussed the crushing which occurred for HP4 and HP6 far exceeded that of HP1, which was isotropically compressed up to 8 MPa but was not sheared. The amount of particle crushing is shown in Figure 6.18 (b) to be proportional to the square root of the maximum shear stress, indicating that the crushing is independent of the stress path but only depends on the shear stress suffered.

The shearing behaviour of this soil is very much affected by this particle crushing and this effect will be discussed where appropriate.

6.5.3 Identification of the ultimate state

The concept of critical state has been defined in Section 3.4.2 as a state where deformations occur without further changes of stresses or of volume. However, in practice, slight changes may take place in the critical state due to the limitations associated with the measurement system or sample boundary conditions. Some practical criteria have been made to identify the state. For this work a sample has been assumed to have reached critical state when the changes of the stress ratio (q'/p') and the volumetric strain are

below 0.03 and 0.1% respectively during the last 3% of axial strain before the end of a test. In undrained tests, a pore pressure change of 5 kPa is used instead of the volumetric strain criterion.

Loose samples usually reached critical states between 15 to 20% of axial strain. Dense samples, which reached the states with strain softening, needed greater axial strain unless confining stresses were reasonably high. As can be seen for Test 81 or 61 of Figure 6.13, the dense samples were obviously approaching a critical states but the tests sometimes had to be terminated prematurely because of the limit of the axial strain which was only about 20% in the Bishop and Wesley cell. Thus some of the critical states of dense samples could not be properly determined. Under high pressures, all samples were normally compressed and show very soft behaviour. More than 25% axial strain and 10% volumetric strain were required to arrive at critical states for drained conditions.

6.5.4 The ultimate strength and the critical state line

The critical states, determined according to the above criteria, are summarized in Table 6.11, together with the peak states. In Figure 6.19, where the critical states are plotted in q':p' space, the critical states appear to lie on a straight line, which is defined as the critical state line by the Equation 3.8. The gradient of the line gives a critical state friction parameter, M, of 1.59, which is equivalent to friction angle of 39°. Although a considerable amount of particle crushing has occurred at high pressures, there is no sign of curvature in the critical state line, indicating that the critical state friction parameter, M, is independent of the stress level. The independence of the value of M from particle crushing was also observed for carbonate sands by Coop (1990). The M value of 1.59 seems to be rather high, but is comparable with the value of 1.60 for other decomposed granite soils reported in the literature.

As mentioned in Section 4.3.5, the M value of many decomposed granite soils seems to be almost constant at 1.60, although their

origins, particle size distributions and mineralogies are different. This may be due to the following reasons. Decomposed granite soils always contain considerable amount of feldspars. Because they are initially weathered, feldspar particles are usually finer than the other components, and the voids between the larger particles are filled with feldspar particles. The frictional properties of the soils may therefore be determined by the friction between the feldspar particles. This may explain why the frictional parameters of the soils hardly vary and are similar to those of feldspars, whose friction angle of 42° at constant volume has been reported by Lee, I.K. (1966).

Figure 6.20 shows the critical states in v:lnp' space. The best fit critical state line has also been drawn in the figure. The critical specific volumes of undrained tests, which are denoted with □ in the figure, have been corrected for the volume changes due to the membrane penetration effect. The critical state parameters λ and Γ are 0.087 and 2.04 respectively. The critical state line is found to be almost parallel with the normal compression line, indicating that the soil conforms to the basic assumption of the critical state soil models.

As mentioned before, the grading of the soil changes during shearing. It is obvious that the grading changes depend on stress path and on stress level. However, the location of the critical state line seems not to be influenced by the stress path to reach the critical state or by the stress level. If this were not true, there would not exist a unique critical state line in v:lnp' space. This also suggests that the effects of the grading changes on the specific volume at the critical state also depend on the logarithm of the applied stresses.

From the critical state lines of several clayey soils, Schofield and Wroth (1968) proposed the existence of the Ω point, through which all critical state lines pass. The coordinates of this point are 1.25 and 10.3 MPa for v and p' respectively. The critical state parameters determined in Figure 6.20 give the specific volume of

1.24 for p' of 10.3 MPa. The mechanism to arrive the critical state is very different in the decomposed granite soil, where grading changes occur, but the critical state line of this soil shows the same feature as those of other soils, where particle crushing is not normally observed. This agreement is another example of the uniqueness of the critical state line of soils.

6.6 Dilation and peak states

6.6.1 Dilation

Figure 6.21 shows the mobilised stress ratio (q'/p') against the shear strain (ϵ_s) and the corresponding volumetric strain (ϵ_v). Two of the tests, 81 and 83, show distinct peaks, which are accompanied by dilative volume changes, and others reach the ultimate states without peaks. However, as expected, the ultimate stress ratio seems to be unique. As discussed in Chapter 3, the mobilised stress ratio depends on the friction parameter, M, and the rate of volume change during shearing, i.e dilation. Any stress ratio greater than the ultimate is solely due to a certain rate of dilation.

The relationships between the mobilised stress ratio and the rate of dilation ($d\epsilon_v/d\epsilon_s$) of the tests in Figure 6.21 are shown in Figure 6.22. Elastic strain components are excluded from the measured total strains. In each figure, the horizontal axis indicates the rate of dilation and following the usual practice a negative sign is used for volume expansion. The results for normally compressed samples, HP5 and HP6, show that they are initially highly compressive but the rate of volume change decreases to zero at the ultimate state. The data are rather scattered in the low stress range, which may be due to the effects of creep after normal compression. However, the relationship can be approximated by a straight line passing through critical state stress ratio, M, at $d\epsilon_v/d\epsilon_s = 0$. The gradients of the lines are found to be 0.76 and 0.97 for HP5 and HP6 respectively. The slope of constant p' test (HP6) is steeper than that of constant σ'_r test (HP5), because the volume

changes due to the change of p' were avoided in the constant p' test. The stress-dilatancy relationship which is exclusively due to shearing is therefore given by equation 6.2, which is very similar to the Cam-clay plastic work equation given in Equation 3.14.

$$(q'/p') = M - 0.97 \times (d\epsilon_v/d\epsilon_s) \qquad (6.2)$$

The above equation reveals that the mobilised stress ratio depends on the volumetric behaviour of a soil. As can be seen in the results of test 81, the sample initially contracts and starts to dilate near the stress ratio of 1.6, which was identified as the M value of the soil. The maximum stress ratio also appears to coincide with the maximum rate of dilation and the ultimate stress ratio is approached again towards the end of the test. The stress ratio is less than M during volume contraction and is greater than M during volume expansion. These observations are quite consistent with the concept of the above equation.

The relation between the stress ratio and the rate of dilation was approximated to be linear. However, the slope becomes less steep beyond the ultimate stress ratio. The data of test 84, which was also sheared under a constant p' condition, show that the relationship beyond the ultimate stress ratio still seems to be linear but the slope of 0.74 is less than that of 0.97 for the lower stress ratio range. This trend is clearer in Figure 6.23, where the relationship for peak states is presented. The relationship is found to be linear and passes through the critical stress ratio again with a gradient of 0.74, which is independent of the stress path.

Some unusual relationships are found for constant p' tests on soils with initial states on the dry side of critical. As can be seen from the data of test 83, the sample shows an almost constant volume up to a stress ratio of 1.0 and then starts to dilate. The maximum stress ratio is associated with the maximum rate of dilation and the rate of dilation tends to zero at the end of the test, where the stress ratio approaches M. However, the relationship described in

equation 6.2 is not valid for this test from the beginning of dilation to the peak state. Similar patterns are found in tests of 62 and 52. This deviation may be explained by possible errors in strain measurements, particularly by the membrane penetration correction, or by severe non-uniformity in the stress and strain distribution. At A in the figure, where the sample starts to dilate, the axial and volumetric strains read by the transducers were 0.15% and -0.06% respectively. However, most of the volume change was due to membrane penetration. The effective radial stress had decreased from 100 to 67 kPa, which caused 0.11% of apparent volumetric strain, and the corrected volumetric strain was 0.05%. For constant p' tests of this type, where the sample is very stiff but the radial stress is changing, the measured volumetric strains are influenced strongly by the membrane penetration correction, and the accuracy is not comparable with those of the strain measurements for other tests with constant σ'_r.

As mentioned in the previous section, the behaviour of compacted samples is different from that of the truly over-consolidated samples. The difference has been illustrated in Figure 6.16, but is more apparent in the stress-dilatancy plots, presented in Figure 6.24. The compacted sample, 51, shows plastic volumetric strains from the beginning, although it exists on the dry side of critical. In contrast, the truly over-consolidated sample, 41, shows almost no volume changes up to the stress ratio of 1.3, where the sample yields. The behaviour of the latter complies with the critical state theoretical framework, as samples on the dry side of critical should remain on an elastic wall until yield.

6.6.2 Peak states

Peak states are generally associated with dense soils, as for loose soils the states are not determined separately but coincide with the ultimate states. The maximum stress ratio (q'/p') has been used for the selection of the peak states instead of the maximum deviatoric stress, as this is more suitable if the data from different types of

test are to be correlated or compared. The maximum stress ratio occurs at the same state as the maximum deviatoric stress for a drained test, but it may be different in the case of an undrained test. The peak states of the series of the tests have been summarised in Table 6.11.

Figure 6.25 shows the peak states plotted in q':p' space. The stress ratio at peak is found to be high and ranges from 1.60 to 2.10, which is equivalent to a friction angle of 39° to 51°. All the peak states, as expected, lie above the critical state line, but no clear relationships, such as peak state line, are not found, as the samples had different initial states. Unlike the critical stress ratio, which is a property of a soil, the peak stress ratio of a soil depends on initial density as well as effective stress.

The peak states plotted in v:lnp' are shown in Figure 6.26. The states lie to the left of the critical state line. The numbers in the figure represent the stress ratio at the peaks. The ratio appears to increase as the distance between the state and the critical state line increases, and constant peak stress ratio contours may be drawn, which lie parallel to the critical state line. Because the stress ratio is linearly related to the rate of dilation, each contour line should be associated with the same rate of dilation. These observations are consistent with the stress-dilatancy model described in Section 3.4.

The farther to the left side of the critical state line is the initial state of a soil, the higher is the rate of dilation during shearing. The stress ratio at a peak, which is related to the maximum rate of dilation, therefore depends on the initial state of a soil. As mentioned in Section 3.5.4, the initial state of a soil may be represented by the state parameter (ψ). The relationship between the maximum stress ratio of the soil and the parameter is shown in Figure 6.27 (a) and (b). A negative sign for the parameter represents the dry side of critical. As expected, a soil with a higher negative state parameter shows a higher peak stress ratio. Figure 6.27 (a) also indicates that the peak stress ratio is

affected by the stress path followed. For the same initial state, Tests 52 and 51 shows that a constant p' path gives a higher peak stress ratio than constant σ'_r path. As shown in Figure 6.27 (b), however, a unique relationship has been found between the peak stress ratio and the state parameter at the peak, which coincides with the observations made in Figure 6.26. The state parameter is an alternative to the over-consolidation ratio (OCR) and influences the peak stress ratio. However, the peak stress ratio cannot be estimated from the parameter alone, as shown in Figure 3.13 (Been and Jefferies, 1986), as it is also dependent on the stress path.

Figure 6.28 shows normalised peak and ultimate states. The normalising parameters of p'_p and v_λ have been described in Section 3.5. As can be seen in the figure, more consistent results are found after normalisation. While the ultimate states fall close to a unique critical state point, the peak state points form a straight line which represents a Hvorslev surface. The critical state point is defined by the soil parameters M and Γ and the Hvorslev surface, as given in Equation 3.20, may be defined using the slope H and the intercept J in q'/p'_p:p'/p'_p space. The values for H and J are 1.48 and 0.045 respectively. As shown in Equations 3.20 and 3.21, if the Hvorslev surface is assumed to be a straight line for elastic wall sections (p'_p), the surface will be curved in constant p' sections (v_λ), and vice versa. However, in this case the data are too scattered to show which normalisation gives the better straight line.

6.7 The state boundary surface

6.7.1 State paths

Effective stress paths for drained and undrained tests at standard pressures are presented in Figure 6.29 and 6.30 respectively. The stress paths for drained tests are straightforward. While the paths are inclined at a slope of 3:1 for constant σ'_r tests, the paths are vertical for constant p' tests. As expected, loose samples reach

the ultimate state directly and dense samples reach peaks first and retrace the path to arrive the ultimate state.

The stress paths for undrained tests show some unusual features as well as features commonly found in other soils. Like other soils, the excess pore pressure increases for a loose sample, such as 26, as the shear stress is increased. For dense samples, such as 24 and 25, the excess pore pressures increase initially but decrease later due to the effect of dilatancy, which causes the path to move to the right. As mentioned in Section 6.5.1, the pore pressure responses are affected by membrane penetration. If this effect were not present, the stress paths would lie to the left of their current locations, because the pore pressure responses are positive. Unlike other soils, all undrained tests show peaks, after which the deviator stresses decrease at a stress ratio close to that at the critical state, indicating that positive pore pressures are being generating. These continued decreases could be due to the effects of continued particle crushing. When the soil reaches a critical stress ratio, the soil particles are still in turbulent motion which may cause continued particle crushing, resulting in additional volume changes for drained tests and positive pore pressures for undrained tests. This has been demonstrated for drained tests in Test 51 of Figure 6.11 and HP5 of Figure 6.12, where samples show continued small volume changes after a constant deviator stress is reached. This means that a constant stress ratio state precedes a constant volume state. However, all samples appears to reach ultimate states eventually.

Stress paths for high pressure tests are shown in Figure 6.31. As all of these samples were normally consolidated, they show typical loose soil behaviour and the end of test points all fall close to a critical state line regardless of the stress level.

Figure 6.32 shows state paths during shearing in v:lnp' space. Only results for the tests shown in Figures 6.29 to 6.31 are presented. As expected, the path depends on the initial state and the stress path followed. The end of test points lie close to a critical state

line regardless of the initial state or the stress path.

6.7.2 The state boundary surface

The normalised state paths for all drained tests are shown in Figure 6.33. The normalising parameters p'_p and v_λ have again been used. The figure clearly reveals the existence of a state boundary surface. The traces of two tests on normally consolidated samples, HP5 and HP6, form the same Roscoe surface and the Hvorslev surface is defined by the envelope of the peak states. As described in Section 3.5.3, all the critical states reduce to a single point in the normalised sections. While the paths of normally consolidated or lightly over-consolidated samples terminate at this point, those of heavily over-consolidated samples generally do not reach the critical state point probably due to the localised strain and stress distribution after the peak. In the constant p' section, the value of v_λ at the critical state is slightly greater than the Γ value. This is because the slope of the normal compression line, which was used for the calculation of v_λ values, is slightly larger than the slope of the critical state line.

In Figure 6.34, the state boundary surface is compared with those of the Cam-clay and modified Cam-clay models, which have been drawn using the critical state parameters determined previously. It can be seen in the figure that the state boundary surface of the soil lies between the two Cam-clay surfaces up to the stress ratio of 1.0. Beyond this stress ratio, however, the path crosses the Roscoe surface of the Cam-clay model and reaches the critical state, which is to the left of the critical states of the Cam-clay or modified Cam-clay models. This is probably the result of volume changes due to particle crushing during shearing. Unusually, the state boundary surface in elastic wall sections shows a peak. This feature has been theoretically predicted by Chandler (1985), who applied plasticity to granular materials, assuming that volume changes resulted from particle crushing as well as particle movement.

Particle crushing, which causes additional volume changes in drained tests, affects the plastic strain increments. The plastic strain increment vectors from a high pressure constant p' test, HP6, are plotted in Figure 6.35, together with the state boundary surface. For many other soils, where the normality condition applies, these vectors are orthogonal to the state boundary surface. For the decomposed granite soil, the vectors seem to be normal to the state boundary surface up to the stress ratio of 1.0. However, the normality condition seems not to be valid in the later stages.

If the state boundary surface is assumed to be a yield surface, as described in Section 3.6, soils suffer only elastic strains below the surface. Below the surface, therefore, the normalised stress paths of constant p' tests should be vertical and those of constant σ'_r tests should be a straight line at a slope of 3:1. Figure 6.33 shows that heavily over-consolidated samples seem to follow these paths but for lightly over-consolidated samples this is not the case. For example, constant p' test paths, 73 and 75, and constant σ'_r test path, 71, deviate very much from the theoretical stress paths. This means that compacted soils, when on the wet side of critical, start to yield below the state boundary surface. On the other hand, truly over-consolidated samples, such as 41 and 42, follow the elastic paths and yield only when the state boundary surface is reached, as shown in Figure 6.36. While the states of the compacted and the truly over-consolidated samples are limited by the same Roscoe surface on the wet side of the critical, it is a yield surface only for the truly over-consolidated soils. This difference seems to result from the different particle crushing mechanisms of the two types of sample during shearing, which will be discussed in more detail later.

In Figure 6.37, the normalised state paths for undrained tests are shown, together with the state boundary surface obtained from the drained tests. The paths are believed to be shifted slightly due to membrane penetration as explained earlier. All the paths reach the critical state point and form a state boundary for undrained tests.

The undrained stress paths for normally consolidated samples are generally assumed to define the state boundary surface for a soil. However, for the decomposed granite soil, they appear to lie inside the state boundary surface for drained tests, indicating that undrained tests are not suitable to determine the boundary surface. The difference between the two types of stress paths, drained and undrained, may be due to particle crushing. As mentioned in Section 6.5.2, considerable particle crushing occurs during shearing under high pressures. In undrained tests, positive pore pressures have to be generated to compensate the volume changes due to particle crushing and the pore pressure increases are large because of the low κ value of this soil. This large positive pore pressure seem to locate the undrained paths below the drained paths. However, the location of the critical state point is not changed by the type of test. This type of behaviour has also been observed during triaxial tests on a crushable carbonate sands by Coop (1990).

It has been demonstrated for drained tests that the behaviour of compacted samples differs from that of truly over-consolidated samples. This is also the case for undrained tests. As can be seen in Figure 6.37, the initial normalised states of 25 and 45 are almost the same, but the behaviour of the two is quite different. The current state of 25 was achieved by compaction, followed by isotropic compression, while 45 was normally compressed and then swelled back to a similar state. As discussed in Section 3.5.3, the undrained stress path below the state boundary surface should be vertical if the soil is isotropic. From the results of drained tests, the truly over-consolidated sample, 45, might be expected to show a vertical stress path, however, the path is slightly curved, which may be due to membrane penetration, reducing the pore pressure response. Considering the membrane penetration effect, the path of 25 is very far from the elastic one, indicating that the compacted soil again begins to yield below the state boundary surface. As mentioned before, this difference may result partly from particle crushing. The truly over-consolidated samples had experienced higher stresses than the compacted samples, and the former would therefore suffer less particle crushing during shearing, especially

below the state boundary surface. In contrast, compacted samples would undergo severe particle crushing even below the surface and this would be shown as yielding in the stress-strain relationship.

6.8 Shear stiffness

Throughout the previous sections, it has been demonstrated that the stress-strain relationships of the soil depend on various factors. The basic characteristics of the stress-strain behaviour are revealed qualitatively in Figure 6.38, where the normalised stress paths for four constant σ'_r tests and four constant p' tests are shown, together with contours of shear strain. Solid lines are used for the constant σ'_r tests and dotted lines for the constant p' tests. From the figure, three points can be made. Firstly, the strain contours seem to be almost parallel to the horizontal axis, indicating that the behaviour is affected by the current state, as described by over-consolidation ratio or a state parameter. The further to the left of the figure the state of the soil, the higher stress ratio is at the same level of strain. Secondly, the strain contours of the constant p' tests lie rather higher than those of the constant σ'_r tests. This demonstrates the effect of the stress path on the behaviour. If the behaviour of the soil were elastic and isotropic, the strain contours would not depend on the stress path. Finally, the strain contours increase approximately logarithmically, indicating that the behaviour of the soil is not linear even below the state boundary surface.

The stress-strain behaviour may be described quantitatively by the shear stiffness

$$3G' = dq'/d\epsilon_s \qquad (6.3)$$

which is the gradient of the stress-strain curve. The shear stiffness has been defined in terms of small increments of stress and strain and, therefore, is a tangent stiffness. Figure 6.39 shows the variation of the shear stiffness for the constant p' tests

which have been presented in Figure 6.38, against the shear strain on a logarithmic scale. The stiffnesses have been normalised with respect to the current stress and specific volume. This figure, first of all, demonstrates the non-linear stress-strain behaviour as the stiffness decreases continuously with strain. This feature has been also observed in other soils by Jardine et al (1984), Richardson (1984) and others. For test 84, the normalised stiffness drops from about 400 at a strain of 0.05% to about 100 at a strain of 0.3%. The figure also illustrates the effect of the current state of the soil on the normalised stiffness. Well compacted samples, which are apparently heavily over-consolidated and have therefore higher negative values of a state parameter, show higher initial stiffness. However, the stiffness tends to be independent of the current state after a certain strain.

Figure 6.40 shows the normalised stiffness of constant σ_r' tests at strains of 0.1, 0.25 and 0.5% plotted against the state parameter ψ. The data are scattered but the trend is clear, showing that the normalised stiffness varies approximately linearly with the value of the state parameter. This feature agrees with the fact that the stiffness of a soil increases with the logarithm of over-consolidation ratio, which is commonly found for other soils (Little and Atkinson, 1988).

Although the current state is similar, the stress-strain behaviour for compacted soils has been found to be different from that of the truly over-consolidated soils. Figure 6.41 shows the difference in stiffness for the two soils. As expected, the stiffness of the truly over-consolidated sample is very much higher than that of the compacted sample, indicating that the stiffness is affected by the way the current state has been achieved as well as the values of the current state parameter.

Figure 6.42 shows stiffness data for various stress path tests on normally consolidated samples. The data again reveal that the stiffness also depends on the stress path followed. The constant p' test and the undrained test show higher stiffnesses than the

constant σ'_r test. The dependence of the stiffness on the stress path may be expected from the definition of the stiffness as given in Equation 6.3. For elastic and isotropic soils, shear strains are exclusively due to shear stress and the stiffness is independent of the stress path. For other soils, shear strains may result from changes in the mean effective stress and the stiffness may therefore depend on the stress path.

6.9 Effects of the presence of water

6.9.1 Introduction

So far, test results only for saturated samples have been discussed. However, as mentioned in Chapter 4, the behaviour of soils with weak particles may be influenced by the presence of water. To determine the effects of water on the behaviour of decomposed granite soil a series of drained triaxial compression tests on both dry and wet (partly saturated) samples have been performed and the results are compared with those of saturated samples.

Sixteen tests were carried out on dry samples and nine on wet samples. The sample preparation methods of dry and wet samples have been described in Sections 5.5.1 and 6.3.1. The details of each test have been summarized in Tables 6.5 and 6.6 and typical test results are shown in Figure 6.43.

All tests were conducted in a drained condition. Top and bottom drainage tubes were open to the atmosphere for the free drainage (Figure 5.4), and the pore air pressures are assumed to be constant and zero throughout a test. In a wet sample, pore water suction will be generated, but as no attempt has been made to measure this, in the following discussion the effective stresses of the dry and wet samples are assumed equal to the total stresses, and the implications for the possible magnitudes of the pore suction will be discussed.

6.9.2 Shearing behaviour of dry and wet samples

The stress-strain curves for dry and wet samples are compared in Figure 6.44 with those of saturated samples. The initial specific volumes of the samples are very similar and the confining stresses are the same. From the figure, some differences as well as similarities in their behaviour can be seen. The dry sample shows a much greater peak strength than the others. Associated with this higher peak strength, the dry sample is a greater tendency to dilate. The initial stiffness of the dry sample is lower than that of the others, which may result from the difference in sample preparation. As mentioned before, dry samples needed less tamping and therefore energy to reach a certain density than wet samples. Wet and saturated samples show similar behaviour, indicating that pore water suctions are very small relative to the total stresses for these tests. If this were not the case, the wet sample would show higher strength than the saturated sample. It appears that at 40 to 60% saturation, which is generally achieved by compaction near optimum moisture content, wet samples exhibit similar behaviour to saturated ones. The ultimate state of the wet sample is very well defined. At the ultimate state, the saturation ratios of wet samples were around 50% and in view of Toll's work (Figure 4.31) this may result in higher ultimate stress ratio. However, the ultimate state is found to be the same as that of the saturated sample. In contrast, the dry sample does not reach an ultimate state even after modest strains (ϵ_s= 20%). However, it is clear that the dry sample is approaching an ultimate state when the test was ended. The ultimate strength of the dry sample seems to be comparable with that of saturated sample, but the ultimate specific volume is significantly higher.

The ultimate states of dry and wet samples are summarized in Tables of 6.12 and 6.13, together with the peak states. Although dry samples do not reach the ultimate strengths, they have been estimated from the stress ratio at the minimum sample volume states. Figure 6.45 shows the ultimate states in q'-p' space, which appear to lie on the critical state line defined from saturated samples,

indicating that the critical state friction parameter, M, does not depend on the sample moisture conditions. This emphasises the importance of the ultimate strength as a unique material property, the importance of which was also highlighted by the fact that the ultimate strength of undisturbed soil is almost equal to that of disturbed sample, as discussed in Section 4.3.5 and demonstrated in Figure 4.21.

The specific volume at the ultimate state appears, however to depend on the sample moisture condition. As can be seen in Figure 6.46, where the ultimate (or end) states are presented in v–lnp' space, the dry samples show higher specific volumes than saturated or wet samples, even though the tests on dry samples were still dilating. The data for wet samples lie on the same unique critical state line as the saturated samples. In contrast, the specific volumes of the dry samples are quite scattered, presumably due to different dilation rates at the end states. It is not clear from the present data whether the ultimate states of the dry samples lie parallel to the critical state line of the saturated samples or not.

The higher ultimate specific volumes of the dry samples may be the result of a differing degree of particle crushing. The amount of particle crushing during triaxial tests has been summarized in Table 6.14 and also shown in Figure 6.47, where the relative particle crushing (B_r) and the maximum shear stress (q') are again chosen as the parameters which should be correlated. As can be seen in this figure, the amount of particle crushing varies with the sample moisture condition, indicating that the grading of samples at the ultimate state depends on the sample moisture condition as well as the stresses suffered. The increase of particle crushing with the presence of water was also observed by Miura and O–hara (1979) for decomposed granite soils. The particle crushing in wet samples is comparable with that of saturated samples, which supports the hypothesis that there is a unique critical state line for these two types of samples. The particle crushing which occurred for the dry samples was much smaller than that for the other samples, and this seems to result in the higher specific volume at the ultimate state,

as particle crushing causes compressive volumetric strain.

This water sensitive behaviour accords very well with the results reported by Onitsuka et al (1985) for direct shear tests on decomposed granite soils and by Lee and Seed (1967) for triaxial tests on Antiochi sand, of which some particles were weathered and cracked. As mentioned in Section 4.4.4, Antiochi sand showed lower peak strength and an increase in particle crushing in a saturated state than a dry state. These results were shown in Figures 4.26 and 4.29. From these observations it seems that the water sensitive behaviour of a soil is linked with the presence of particles with cracks.

From Figure 6.47, it is clear that particle crushing is promoted by the presence of pore water. This may be prompted by the loss of suction or bonding in the micro-cracks of the individual particles, i.e intra-particle suction or bonding. For dry samples, soil particles were oven dried before sample preparation and consequently the suctions between the particles were expected not to exist in this case. (This was confirmed from the fact that soil particles flowed freely when dry.) However, intra-particle suctions or bonding may exist or be even increased by oven drying. These suctions or bonding may disappear or be weakened by moistening. Therefore particles seem to be weaker and accordingly more particle crushing is observed in a wet state than a dry state.

Figure 6.48 shows the mobilised stress ratio (q'/p') against the shear strain (ϵ_s) and the corresponding volumetric strain (ϵ_v) for two dry samples, 8 and 35, and one wet sample, 14. As shown in Figure 6.44, the dry sample, 8, exhibits a higher peak stress ratio than the wet sample, 14, although their initial states are similar. All samples shows peaks and dilative volumetric strains, but after around 20% strain only the wet sample has reach an ultimate stress ratio which is equal to that of saturated samples. As mentioned before, the ultimate stress ratio of dry samples has been estimated from the values at the minimum sample volume, and these are too found to be comparable to the value for the saturated samples. This

indicates that the difference in the strength of dry and wet or saturated samples is not due to the change of friction parameter, M, but solely due to the difference in volume change characteristics.

Figure 6.49 shows the relationship between the mobilised stress ratio and the rate of dilation of two dry samples. They are initially very compressive and start to dilate near the stress ratio of 1.6, which was identified as the ultimate value of M of the soil. The maximum stress ratio is associated with the maximum rate of dilation. The relationship appears to be linear but the gradient of the contraction range is different from that of the dilation range, which is also observed for saturated samples. The peak stress ratios and the dilation rates at those points are presented in Figure 6.50. The relationship can be approximated as a single line for both dry and wet samples and the location of the line is found to be very similar to that of saturated samples, indicating that the relationship at peaks is not influenced by the sample moisture conditions. This also suggests that the higher strengths of dry samples are due solely to the different volume change characteristics.

It has been observed that dry samples show higher peak strengths and higher ultimate specific volumes than saturated or wet samples but that the ultimate strengths and the stress-dilatancy relationships seem to be similar. From these facts a possible model can be postulated that the state boundary surface of the dry soil is expanded in the direction of specific volume, compared with that of the saturated soil. However, the projection of the critical state line in the q'-p' space is identical. This model would explain the different peak strength and volumetric strain behaviour for the dry and saturated samples. Although the initial states of samples are the same, if the moisture conditions are different, their behaviour could be different as a result of their relative distances from their respective critical state lines as shown in Figure 6.51. The further to the dry side of the critical state line, the higher the peak strength and dilatancy rate they exhibit will be. If the critical state line of dry sample is outside that of the saturated

samples, dry samples will show behaviour indicative of a greater density, i.e higher peak strength and greater dilatancy even though the initial specific volume is equal to that of the saturated sample under a particular mean effective stress.

6.9.3 Flooding tests

The effects of moisture condition on the behaviour of the soil were examined more closely by flooding samples during triaxial tests. Firstly both dry and wet samples were flooded after the isotropic compression. The results have been tabulated in Table 6.15 and some data are shown in Figure 6.52. As can be seen from the table and the figure, wet samples are hardly affected by flooding, which again confirms that the pore water suctions in the samples are not significant. In contrast, dry samples are prone to collapse on flooding. The magnitude of collapse varies with the specific volume and the confining stress; the looser the sample and the higher the confining stress, the greater the amount of collapse.

Because the soil particles were dried before sample preparation, the collapse seems not to result from a loss of the suction or bonding between the particles but seems to result from the weakening of the individual particles. As mentioned in the previous section. dry soil particles are strong due to the possible intra-particle suctions or bonding, however, the suctions or bonding may disappear or be weakened upon flooding and soil particles become weaker and consequently are crushed. This seems to be seen as collapsing. This mechanism is quite different from that of other collapsible soils, where collapsing is triggered by weakening of bonding materials (Houston et al, 1988).

The collapse results in the densification of soils and this feature has been often utilized as a compaction method on site, especially where mechanical compaction is difficult to achieve, such as for the backfill behind a retaining wall. This method has been locally known as 'water compaction' and seems to be very effective to

prevent further settlements due to saturation.

The behaviour of the soils formed by the collapse is found to be different from that of the mechanically compacted soils. Figure 6.53 presents a comparison of the two soils. While sample 61 was compacted in wet state, saturated and isotropically compressed to 100 kPa, sample 20 was compacted in dry state, isotropically compressed to 100 kPa and then flooded. The resulting specific volumes were 1.540 and 1.538 respectively. As mentioned before, the compaction energy was greater for the wet sample, although the current state is very similar. As shown in the figure, the peak and ultimate strengths are comparable to each other, however, the stiffness is much lower in the flooded sample, indicating that the behaviour of the soil is also influenced by the sample moisture condition when the soil is compacted.

Figure 6.54 shows the effects of flooding on the stiffness of the soil. Both samples were initially prepared at a specific volume of 1.60 in a dry state and sample 19 was flooded under the confining stress of 100 kPa, while sample 4 was kept dry. Flooding caused sample 19 to be denser. As expected, the strength of the flooded sample is lower than that of the dry sample, however, the initial stiffnesses are almost equal. Figures 6.53 and 6.54 suggest that whereas the stiffness of the soil is not increased by the collapse and densification induced by flooding, it is increased by mechanical compaction.

In the previous section, dry samples were found to show higher peak strengths and higher ultimate specific volumes than wet and saturated samples. This feature is dramatically demonstrated by flooding dry samples during shearing, data for which have been presented in Figure 6.55. While sample 4 was kept dry throughout the test, sample 31 was flooded when 90% of the ultimate strength had been reached and sample 30 was flooded after the peak state. The ultimate strength was estimated from the results of the saturated soils. The value of 90% of this strength was chosen because the effects of flooding were assumed to be greater for a

higher stress level and catastrophic failure may occur above the ultimate strength.

Up to the flooding points, the three samples show very similar behaviour. Upon flooding, however, the samples show abrupt changes in the volumetric strain and either the shear stress or the shear strain, sample 31 being flooded whilst maintaining constant total stresses and sample 30 whilst maintaining control of the axial strain. When 90% of the ultimate strength had been reached, sample 31 was allowed to rest overnight to avoid creep effects and was then flooded. Although the axial stress was maintained constant, the sample suffered axial and volumetric strains of 2.97 and 1.19% respectively due to flooding alone. After the peak sample 30 was flooded, while the test was under constant strain rate loading. This caused a decrease of the shear stress from 484 to 171 kPa and a volumetric strain of 1.81%, again clearly demonstrating the effect of water on the soil behaviour. After further straining, both samples recovered their strengths, but the peak for test 31 is far lower than that of the dry sample, 4. Once flooded, the behaviour which follows is very similar to that of other flooded samples, as shown in Figure 6.56, where sample 22 was flooded immediately after the isotropic compression.

The same test results are presented in v:lnp' space on the right side of Figure 6.55. As expected, the dry sample, 4, approaches a much higher specific volume than the critical state of a similar saturated sample. In contrast, samples of 30 and 31 deviate from this upon flooding and eventually reach the same critical state as the saturated samples. This difference can be attributed to the greater amount of particle crushing which occurs in wet or saturated samples which was again confirmed in this series of tests. As shown in Figure 6.47, the flooded sample, 31, shows a greater amount of particle crushing than the dry sample, 4, although the former suffered lower stresses than the latter.

Figure 6.57 shows the results for samples 46 and 48, which were compacted in a wet state and then air-dried. They show the brittle

failure of bonded soils and their strengths and stiffnesses are very high. Even an unconfined test gives a peak strength of 220 kPa. These demonstrate that these soils may be exceptionally strong and very stable in the dry season.

The source of the high strengths and stiffnesses seems to be mainly the suctions or bonding developed between the particles. As mentioned before, pore water suctions were very small when samples were compacted at their optimum moisture content, but the suctions seem to be increased by desiccation. This has been confirmed by flooding the sample during shearing. The test results are shown in Figure 6.58, which shows that sample 47 was flooded when 90% of the ultimate strength had been reached. Once flooded, the sample suffered axial and volumetric strains of 2.84 and 1.17% respectively and subsequently followed almost the same path as that of a fully saturated sample with a similar density (sample 51). In v:lnp' space, the sample deviates from the path upon flooding and approaches the critical state of the saturated sample. This suggests that the high strengths and stiffnesses in compacted and later desiccated soils result from suction between the soil particles.

Chapter 7 Conclusions

Laboratory tests were carried out on a completely weathered granite soil (grade V) taken from Seoul, Korea. The soil is rather coarse and can be described as a well-graded silty sand and gravel. Quartz, feldspar and mica provide the main mineral constituents of the soil. The soil particles are frequently aggregated and contain micro-cracks.

7.1 General behaviour of saturated soil

The results of triaxial compression tests on saturated compacted samples show that the soil conforms the basic features of critical state soil models. A unique isotropic normal compression line has been identified and although a considerable amount of particle crushing takes place during shearing, the soil eventually reaches an ultimate state, or critical state, where deformations occur without further change of stresses or volume. The critical states form unique straight lines in the $q':p'$ and $v:\ln p'$ planes and the critical state line is found to be almost parallel to the normal compression line. A state boundary surface, which limits all possible states of the soil, has also been identified. The surface includes the isotropic normal compression states, critical states and peak states.

It is rather curious that the behaviour of decomposed granite soil conforms to critical state soil models, where soil particles are generally assumed to be rigid. Particle crushing seems to cause the soil behaviour to deviate from the current soil models. However, the research on carbonate sands, where particle crushing also occurred during loading, revealed that the behaviour of carbonate sands was consistent with the principal features of critical state soil models (Coop, 1990). These indicate that the framework of critical state soil mechanics may be more widely applicable to other granular soils in range of stresses where particles crush.

The relationship between the mobilised stress ratio and the rate of dilation has been found to be linear in both side of critical. However, the slope becomes less steep beyond the ultimate stress ratio. Any stress ratio greater than the ultimate is solely due to dilation and peak states are associated with the maximum rate of dilation. Normalised peak states define the Hvorslev surface. Like other soils, the stress-strain behaviour is non-linear even below the state boundary surface and depends on the stress path.

In general, the behaviour of decomposed granite soil is similar to that of clayey soils. In detail, however, the soil shows a number of unusual features such as high peak and ultimate strengths, particle crushing and changes in the behaviour with moisture condition.

The friction angle at peak states ranges from 39° to 51°. The value depends on the initial state (density and effective stress) and the sample moisture condition. The ultimate states give a friction angle of 39°, which is independent of the initial state or sample moisture condition. Both peak and ultimate friction angles are unusually high but are typical of decomposed granite soils. They probably result from the soil's well graded particle size distribution, rough particle surface, angular particle shape and mineral composition. Decomposed granite soils contain a large quantity of feldspars (around 50%), whose friction angle reaches 42° at a constant volume state, and the frictional properties of the soil therefore seems to be governed by the friction between the feldspar particles.

An ultimate friction angle of 40° was observed in carbonate sands (Coop, 1990). It is somewhat premature to relate particle crushing to a high friction angle, however, it is interesting that two completely different crushable soils give significantly higher ultimate friction angle than other soils.

7.2 Effects of particle crushing

Particle crushing has been observed during the isotropic and shearing stages, and has been identified from the grading changes before and after the test and quantified using relative breakage (B_r) proposed by Hardin (1985). Unlike other soils, particle crushing of the soil seems to result from the breakage of individual particles and also from the separation of aggregations of particles. However, the type of crushing is not important as far as engineering behaviour is concerned. The amount of particle crushing has been found to be proportional to the square root of the maximum shear stress applied but independent of the stress path.

Particle crushing results in plastic volumetric strains during both isotropic compression and shearing. In spite of the plastic volumetric strains due to particle crushing, the traces of both normal compression and ultimate states of the soil have been found to be straight lines in v:lnp' plane, indicating that the soil may still be described within the framework of critical state soil mechanics. The effect of particle crushing also appears in an unusually high value of λ/κ (=18), indicating that most of the volumetric strains during compression are irrecoverable. Particle crushing has also been shown to influence the location and shape of the state boundary surface and to give different normalised state paths under drained and undrained loading. The critical state point of the state boundary surface is located further to the left than those of either Cam-clay model and in an elastic wall section the Roscoe surface unusually shows a peak, as predicted by Chandler (1985). Due to the peak the normality condition cannot hold. The undrained state paths for normally consolidated samples appear not to traverse the state boundary surface found for drained tests but to lie inside it. This seems to result from large positive pore pressures which are generated to compensate the volume changes caused by particle crushing. This also suggests that the state boundary surface of the soil should be determined from drained tests.

7.3 Effects of the presence of water

The amount of particle crushing has been found to increase with the presence of water. The increase of particle crushing seems to be due to the loss of intra-particle suction or bonding by wetting and to be the source of the water sensitive behaviour, for which the presence of micro-cracks on the particles may be a necessary condition. Dry soils show much greater peak strengths and higher ultimate specific volumes than wet or saturated soils, but the ultimate strength of the soil is not affected by its soil moisture condition. As particle crushing produces compressive volumetric strains, the smaller amount of particle crushing in dry soils seems to result in a higher specific volume at the ultimate state and consequently the critical state line of dry soil is outside that of saturated soil in the v:lnp' plane. For the same initial state dry samples are therefore further away than saturated samples from their respective critical state lines, and dry samples exhibit behaviour indicative of a greater density. The peak stress states are related to the rate of dilation and the relationship has been found to be a single straight line regardless of the sample moisture condition, indicating that the difference in the strength of dry and wet or saturated samples is not due to the change of friction properties but solely due to the difference in volume change characteristics, i.e particle crushing. This water sensitive behaviour has been clearly demonstrated by flooding tests. Once flooded, initially dry samples also show similar peak strengths to and approach the same critical state as saturated samples.

7.4 Effects of compaction and collapsing

The strength and stiffness of the soil are improved by compaction. Well compacted samples show higher strength and stiffness than less compacted ones. Compacted samples usually exist on the dry side of critical, however, their behaviour has been found to be different from that of truly over-consolidated samples. Compared with the latter, the former are initially less stiff and do not produce

distinct yield points. Although the states of both samples are limited by the same state boundary surface, compacted samples seem to yield below the surface, while truly over-consolidated samples yield only when they traverse it.

Dry samples can be densified by flooding and this feature has been frequently used as a compaction method on site. However, the behaviour of the collapsed soil has been found to be different from that of the mechanically compacted soil, although the initial density is same. The peak and ultimate strengths are comparable to each other but the initial stiffness is much lower in the collapsed soil, indicating that large strains are required to develop the strength in the soil. This also suggests that the behaviour depends on the water content during compaction.

Samples which were compacted in a wet state and later air-dried show extremely high strengths and stiffnesses. This partly explains the good stability of the soil in the dry season. Once flooded, however, this soil exhibits similar behaviour of the saturated sample with the same density. This indicates that the high strength and stiffness are mainly due to the suction developed between the soil particles.

7.5 Practical implications

The mechanical behaviour of compacted decomposed granite soil has been investigated using a completely weathered soil. The values for the basic soil parameters may depend on the particular soil, however, the principal features of the soil behaviour seem to be applicable to other decomposed granite soils, except perhaps for clayey ones.

Laboratory tests reveal that decomposed granite soil is a very good earthwork fill material. The soil is well graded and easy to compact. Well compacted soil shows low compressibility and high strength and stiffness. For the compacted soil, the range of water

contents of the soil is not usually designated but only the required density is specified as a percentage of the maximum dry density obtained in a compaction test. In the case of decomposed granite soil, however, soils should be compacted near the OMC and it may be better to specify the range of water content of the soil as well. The reason is that while the soil is easily compacted in a dry state, it may later collapse and show additional strains upon flooding.

Due to particle crushing, the distance between the normal compression line and critical state lines is wider than for other soils, where the particles are not crushed. This means that the range where the behaviour of loose soil is expected is wide. Properly compacted samples, of which the apparent over-consolidation ratio is high, do not therefore always show peaks but may show the behaviour of loose soil, and the high strength of the soil is only mobilised with large strains.

Compacted soils are very stable in the dry season, when they show significantly high strengths and stiffnesses. However, these strengths and the stiffnesses are not their genuine properties but result from the suction or bonding developed between the soil particles and will disappear upon wetting. Therefore, these strengths and stiffnesses should not be used for design purposes.

7.6 Recommendations for further work

Together with the work on carbonate sands (Coop, 1990), the research on decomposed granite soil provides the basis for the behaviour of crushable soils. For the further understanding of the behaviour of the material, however, more research on other crushable soils or granular soils in higher stress ranges is needed.

The behaviour of compacted decomposed granite soil has been described in this thesis. For the better understanding of the behaviour of the soil, the following recommendations are made for

further work.

a) Tests on undisturbed soils.
   Although it is difficult to obtain undisturbed samples and the results probably will not form a compatible set of data because of the sample variability, tests on undisturbed samples would provide insight into the behaviour of undisturbed soils.

b) Tests at low confining stresses.
   For the analysis of shallow slope failures, tests at low confining stresses are necessary.

c) Tests under repeated loading.
   These soils are frequently used as a road base material, which will be placed under repeated loading. Repeated loading might cause continuous particle crushing and consequently a decrease of strength parameters.

References

The following abbreviations have been used in this section.

ASCE: American Society of Civil Engineers

ASTM: American Society for Testing and Materials

BS: British Standard

GERC: Geotechnical Engineering Research Centre

JSSMFE: Japan Society of Soil Mechanics and Foundation Engineering

ASTM (1970) Standard test method for unconsolidated undrained strength of cohesive soils in triaxial compression. ASTM D 2850-70.

Atkinson, J.H. (1984a). Some procedures for normalising soil test results, The City University, GERC research report GE/84/3.

Atkinson, J.H. (1984b). Rates of loading in drained and undrained stress path and triaxial tests, The City University, GERC research report GE/84/1.

Atkinson, J.H. (1985). Simple and inexpensive pressure control equipment for conventional and stress path triaxial testing of soils, Geotechnique 35, No.1, 61-63.

Atkinson, J.H. and Bransby, P.L. (1978). The mechanics of soils: An introduction to critical state soil mechanics, McGraw-Hill.

Atkinson, J.H., Evans, J.S. and Scott, C.R. (1983). Stress path testing equipment, Spectra system – operating manual, The City University, GERC research report GE/83/1.

Atkinson, J.H., Evans, J.S. and Scott, C.R. (1985). Developments in microcomputer controlled stress path testing equipment for measurement of soil parameters, Ground Engineering 18, No.1, 15-22.

Baynes, F.J. and Dearman, W.R. (1978). The microfabric of a chemically weathered granite, Bulletin of Int'l Association of Engineering Geology 18, 91–100.

Been, K. and Jefferies, M.G. (1985). A state parameter for sands, Geotechnique 35, No.2, 99–112.

Been, K. and Jefferies, M.G. (1986). Reply to discussion on 'A state parameter for sands', Geotechnique 36, No.1, 123–132.

Bishop, A.W., Alpan, I., Blight, G.E. and Donald, I.B. (1960). Factors controlling the strength of partially saturated cohesive soils, Proc. ASCE Research Conference on Shear Strength of Soils, Boulder, 503–532.

Bishop, A.W. and Henkel, D.J. (1962). The measurement of soil properties in the triaxial test (2nd edition), Edward Arnold.

Bishop, A.W. and Donald, I.B. (1961). The experimental study of partly saturated soil in the triaxial apparatus, Proc. 5th Int'l Conference on Soil Mechanics and Foundation Engineering, Paris, Vol.1, 13–21.

Bishop, A.W. and Green, G.E. (1965). The influence of end restraint on the compression strength of a cohesionless soil, Geotechnique 15, No.3, 243–266.

Bishop, A.W. and Wesley, L.D. (1975). A hydraulic triaxial apparatus for controlled stress path testing, Geotechnique 25, No.4, 657–670.

Black, D.K. and Lee, K.L. (1973). Saturating laboratory samples by back pressure, Journal of the Soil Mechanics and Foundations Division, ASCE, Vol.99, SM1, 75–93.

Brand, E.W. (1985). Predicting the performance of residual soil slopes, Proc. of the 11th Int'l Conference on Soil Mechanics

and Foundation Engineering, San Francisco, Vol.5, 2541-2578.

Brand, E.W. and Phillipson, H.B. (1985). Review of international practice for the sampling and testing of residual soils, Sampling and testing of residual soils (ed. E W Brand and H B Phillipson), Scorpion Press, Hong Kong, 7-21.

BS 1377:1975. Methods of test for soils for civil engineering purposes, British Standards Institution.

BS 1377:Part1:1990. Methods of test for soils for civil engineering purposes, Part 1, General requirements and sample preparation, British Standards Institution.

de Carvalho, J.B.Q. (1985). Topic 1.3 Geotechnical classifications, Progress report (1982-1985) 'Peculiarities of geotechnical behaviour of tropical lateritic and saprolitic soils', Committee on tropical soils of the ISSMFE, Brazilian Society for Soil Mechanics, 21-39.

Chandler, H.W. (1985). A plasticity theory without Drucker's postulate, suitable for granular materials. Journal of Mechanics and Physics of Solids 33, 215-226.

Cheung, C.K. and Greenway, D.R. (1987). Direct shear testing of a granitic soil, Special project report SPR 5/87, Geotechnical Control Office, Hong Kong.

Clinton, D.B. (1985). User manual for 'TRIAX': A programme for computer control of triaxial stress path tests, The City University, GERC research report GE/85/5.

Coop, M.R. (1990). The mechanics of uncemented carbonate sands, Geotechnique 40, No.4, 607-626.

Datta, M., Gulhati, S.K. and Rao, G.V. (1979). Crushing of calcareous sands during shear, Proc. of the 11th Offshore

Technology Conference, 1459–1467.

Dearman, W.R., Baynes, F.J. and Irfan, T.Y. (1978). Engineering grading of weathered granite, Engineering Geology 12, 345–374.

Dearman, W.R. and Turk, N. (1985). Sampling and testing of residual soils in the United Kingdom, Sampling and testing of residual soils (ed. E W Brand and H B Phillipson), Scorpion Press, Hong Kong, 175–181.

Do, D.H. (1979). CBR characteristics of weathered granite soils, Proc. of Korean Society of Civil Engineers, Vol.27, No.2, 67–78, (in Korean).

Duncan, J.M. and Seed, H.B. (1967). Corrections for strength test data. Journal of the Soil Mechanics and Foundations Division, ASCE, Vol.94, SM5, 121–137.

Escario, V. and Saez, J. (1986). The shear strength of partly saturated soils, Geotechnique 16, No.3, 453–456.

Fredlund, D.G. and Morgenstern, N.R. (1978). The shear strength of unsaturated soils, Canadian Geotechnical Journal 15, No.3, 313–321.

Fredlund, D.G., Rahardjo, H. and Gan, J.K.M. (1987). Non-linearity of strength envelope for unsaturated soils, Proc. of the 6th Int'l Conference on Expansive Soils, New Delhi, 49–54.

Frydman, S., Zeitlen, J.G. and Alpan, I. (1973). The membrane effect in triaxial testing of granular soils, Journal of Testing and Evaluation 1, No.1, 37–41.

Geological Society (1990). Tropical residual soils, Engineering Group Working Party Report, Quarterly Journal of Engineering Geology 23, No.1, 1–101.

Hardin, B.O. (1985). Crushing of soil particles, Journal of Geotechnical Engineering, ASCE, Vol.111, No.10, 1177–1192.

Holtz, W.G. and Gibbs, H.J. (1956). Triaxial shear tests on pervious gravelly soils, Journal of the Soil Mechanics and Foundations Division, ASCE, Vol.82, SM1, 1–22.

Hovrslev, M.J. (1937). Uber die Festigkeiseigenschaften Gestorter Bindiger Boden, Copenhagen.

Houston, S.L., Houston, W.N. and Spadola, D.J. (1988). Prediction of field collapse of soils due to wetting, Journal of Geotechnical Engineering, ASCE, Vol.114, No.1, 40–58.

Irfan, T.Y. (1988). Fabric variability and index testing of a granitic saprolite, Proc. of 2nd Int'l Conference on Geomechanics in Tropical Soils, Singapore, Vol.1, 25–35.

Irfan, T.Y. and Dearman, W.R. (1978). The Engineering petrography of a weathered granite in Cornwall, England, Quarterly Journal of Engineering Geology 11, 233–244.

JSSMFE (1974). Special soils in Japan, Library of Soil and Foundation Engineering, Series 10, (in Japanese).

JSSMFE (1979). Engineering properties of decomposed granite rock and soil and their application, Library of Soil and Foundation Engineering, Series 16, (in Japanese).

JSSMFE (1982). Soil testing methods (2nd revised edition), Japan Society of Soil Mechanics and Foundation Engineering, (in Japanese).

Jardine, R.J., Symes, N.J. and Burland, J.B. (1984). The measurement of soil stiffness in the triaxial apparatus, Geotechnique 34, No.3, 445–483.

Jennings, J.E. and Knight, K. (1975). A guide to construction on or with materials exhibiting additional settlement due to 'collapse' of grain structure, Proc. of the 6th African conference of SMFE, Durban, 99-105.

Kirkpatrick, W.M. and Belshaw, D.J. (1968). On the interpretation of the triaxial test, Geotechnique 18, 336-350.

Koirala, N.P. (1982). Direct shear tests on decomposed granite, Materials Division Report No.29, Geotechnical Control Office, Hong Kong.

Komoo, I. (1985). Engineering properties of weathered rock profiles in peninsular Malaysia, Proc. of the 8th Southeast Asian Geotechnical Conference, Vol.1, (3)81-86.

Korean Institute of Energy and Resources (1981). Geological Map of Korea, 1:50,000, Ddug Seom Sheet, KIER, Seoul, Korea.

Korean Institute of Energy and Resources (1982). Geological Map of Korea, 1:50,000, Seoul Sheet, KIER, Seoul, Korea.

Ladd, R.S. (1978). Preparing test specimens using undercompaction, Geotechnical Testing Journal 1, No.1, 16-23.

Lade, P.V. and Duncan, J.M. (1973). Cubical triaxial tests on cohesionless soil, Journal of the Soil Mechanics and Foundations Division, ASCE, Vol.99, SM10, 793-812.

Lade, P.V. and Hernandez, S.B. (1977). Membrane penetration effects in undrained tests, Journal of Geotechnical Engineering Division, ASCE, Vol.103, GT2.

Lambe, T.W. and Whitman, R.V. (1979). Soil mechanics, SI version, John Wiley and Sons.

Lau, W.H.W. (1988). The behaviour of clay in simple shear and

triaxial tests, PhD Thesis, The City University.

Lee, I.K. (1966). Stress-dilatancy performance of feldspar, Journal of the Soil Mechanics and Foundations Division, ASCE, Vol.92, SM2, 79-103.

Lee, In-Keun (1991). Triaxial tests on compacted decomposed granite soil, The City University, GERC research report GE/91/06.

Lee, K.L. and Farhoomand, I. (1967). Compressibility and crushing of granular soil in anisotropic triaxial compression, Canadian Geotechnical Journal 4, No.1, 68-86.

Lee, K.L., Seed, H.B. and Dunlop, P. (1967). Effect of moisture on the strength of a clean sand, Journal of the Soil Mechanics and Foundations Division, ASCE, Vol.93, SM6, 17-40.

Lee, S.G. (1987). Weathering and geotechnical characterization of Korean granites, PhD Thesis, University of London.

Leroueil, S. and Vaughan, P.R. (1990). The general congruent effects of structure in natural soils and weak rocks, Geotechnique 40, No.3, 467-488.

Leslie, D.D. (1963). Large scale triaxial tests on gravelly soils, Proc. of the 2nd Panamerican Conference on Soil Mechanics and Foundation Engineering, Brazil, Vol.1, 181-202.

Leslie, D.D. (1975). Shear strength of rockfill, Physical Properties Engineering Study No.526, South Pacific Division, Corps of Engineers Laboratory, 124.

Little, J.A. and Atkinson, J.H. (1988). One dimensional consolidation characteristics of a glacial till, Quarterly Journal of Engineering Geology 21, No.2, 183-199.

Lowe, J. and Johnson, T.C. (1960). Use of back pressure to increase

degree of saturation of triaxial test specimen, Proc. of the ASCE Conference on Shear Strength of Cohesive Soils, Boulder, 819-836.

Lumb, P. (1962). The properties of decomposed granite, Geotechnique 12, No.3, 226-243.

Lumb, P. (1965). The residual soils of Hong Kong, Geotechnique 15, No.2, 180-194.

Lumb, P. (1975). Slope failure in Hong Kong, Quarterly Journal of Engineering Geology 8, 31-65.

Marsal, R.J. (1967). Large scale testing of rockfill materials, Journal of the Soil Mechanics and Foundations Division, ASCE, Vol.93, SM2, 27-43.

Massey, J.B. (1983). Shear strength of Hong Kong residual soils, A review of work carried out by the Geotechnical Control Office, Transcript of a lecture to the HK Institution of Engineers Geotechnical Group.

Matsuo, S. and Fukumoto, T. (1976). Influence of particle breakage on the compaction characteristics of decomposed granite soil, Proc. of JSSMFE, Vol.16, No.4, 93-102, (in Japanese).

Matsuo, S. and Fukumoto, T. (1977). Significant drop of permeability due to particle breakage of decomposed granite soils, Proc. of JSSMFE, Vol.17, No.4, 87-97, (in Japanese).

Matsuo, S. and Nishida, K. (1968). Physical and chemical properties of decomposed granite soil grains, Soils and Foundations 8, No.4, 10-20.

Mitchell, J.K. (1976). Fundamentals of soil behaviour, John Wiley & Sons.

Mitchell, J.K. and Sutar, N. (1982). Engineering properties of tropical residual soils, Proc of the ASCE Conference Engineering and Construction in Tropical and Residual Soils, Honolulu, 30-37.

Miura, N. and O-hara, S. (1979). Particle-crushing of a decomposed granite soil under shear stresses, Soils and Foundations 19, No.3, 1-14.

Miura, N. and Yamanouchi, T. (1975). Effect of water on the behaviour of a quartz-rich sand under high stresses, Soils and Foundations 15, No.4, 23-34.

Molenkamp, F. and Luger, H.J. (1981). Modelling and minimization of membrane penetration effects in tests on granular soils, Geotechnique 31, No.4, 471-486.

Moye, D.G. (1955). Engineering geology for the Snowy Mountains Scheme, Journal of Institution of Engineers, Australia, Vol.27, 281-299.

Murata, H. and Yasufuku, N. (1987). Mechanical properties of undisturbed decomposed granite soils, Proc. of the 8th Asian Regional Conference on SMFE, Vol.1, 193-196.

Murata, H., Yasufuku, N., Kondoh, Y. and Okamura, M. (1985). Factors affecting the mechanical and compressive properties of decomposed granite soils, Proc. of the 20th Annual Meeting of JSSMFE, 233-234, (in Japanese).

Newland, P.L. and Alley, B.H. (1957). Volume changes in drained triaxial tests on granular materials, Geotechnique 7, No.1, 17-34.

Norris, G.M. (1981). Effect of end membrane thickness on the strength of frictionless cap and base tests, Laboratory shear strength of soil, Edited by R N Young and F C Townsend, ASTM

STP 740, 303-314.

Ollier, C. (1984). Weathering (2nd Edition), Longman.

Onitsuka, K., Yoshitake, S. and Nanri, M. (1985). Mechanical properties and strength anisotropy of decomposed granite soil, Soils and Foundations 25, No.2, 14-30.

Onodera, T., Oda, M. and Minami, K. (1976). Shear strength of undisturbed sample of decomposed granite soil, Soils and Foundations 16, No.1, 17-26.

Peltier, L. (1950). The geographic cycle in periglacial regions as it is related to climatic geomorphology,

Pickles, A.R. (1988). 'TRILOG3' Triaxial data logging and control programme, The City University, GERC research report GE/88/12.

Rad, N.S. and Clough, G.W. (1984). New procedure for saturating sand specimens, Journal of Geotechincal Engineering, ASCE, Vol.110, No.9, 1205-1218.

Raju, V.S. and Sadasivan, S.K. (1974). Membrane penetration in triaxial tests on sands, Journal of Geotechnical Engineering Division, ASCE, Vol.100, GT4, 482-489.

Richardson, D. (1984). The importance of natural strains in soil mechanics, The City University, GERC research report GE/84/23.

Richardson, D. (1986). Effect of membrane and filter paper stiffness on the stress-strain behaviour of triaxial samples, The City University, GERC research report GE/86/4.

Richardson, D. (1989). Investigations of threshold effects in soil deformation, PhD Thesis, The City University.

Roscoe, K.H., Schofield, A.N. and Thurairajah, A.L. (1963a).

Yielding of clays in states wetter than critical, Geotechnique 13, No.3, 211-240.

Roscoe, K.H., Schofield, A.N. and Thurairajah, A.L. (1963b). An evaluation of test data for selecting a yield criterion for soils, Symposium on Laboratory shear testing of soils, ASTM STP 361, 111-128.

Rowe, P.W. (1962). The stress-dilatancy relation for static equilibrium of an assembly of particles in contact, Proc. of Royal Society, London, A269, 500-527.

Rowe, P.W. and Barden, L. (1964). Importance of free ends in triaxial testing, Journal of the Soil Mechanics and Foundations Division, ASCE, Vol.90, SM1, 1-27.

Ruenkrairergsa, T. and Petchgate, K. (1985). Stress-strain and strength characteristics of compacted granite soil, Proc. of the 8th South Asian Geotechnical Conference, Vol.1, (3)10-17.

Sarsby, R.W., Kalteziotis, N. and Haddad, E.H. (1980). Bedding errors in triaxial tests on granular media, Geotechnique 30, No.3, 302-309.

Sarsby, R.W., Kalteziotis, N. and Haddad, E.H. (1982). Compression of 'Free-ends' during triaxial testing, Journal of Geotechnical Engineering, ASCE, Vol.108, No.1, 83-107.

Shelton, J.C. and Cooper, A.J. (1984). The shear strength of decomposed granite from Glenealy Area, Geotechnical Control Office Technical Note No.1/84, GCO, Hong Kong.

Shockley, W.G. and Ahlvin, R.G. (1960). Non uniformity in triaxial test specimens, Proc. of the ASCE Research Conference on Shear Strength of Cohesive Soils, Boulder.

Schofield, A.N. and Wroth, C.P. (1968). Critical state soil

mechanics. McGraw-Hill.

Seoul Metropolitan Government (1989). Seoul: Metropolitan Administration.

Skempton, A.W. (1954). The pore pressure coefficients A and B, Geotechnique 4, 143-147.

Sueoka, T. (1988). Identification and classification of granitic residual soils using chemical weathering index, Proc. of 2nd Int'l Conference on Geomechanics in Tropical Soils, Singapore, Vol.1, 55-61.

Tatsuoka, F., Molenkamp, F., Torii, T. and Hino, T. (1984). Behaviour of lubrication layers of platens in element tests, Soils and Foundations 24, No.1, 113-128.

Taylor, D.W. (1941). Seventh progress report on shear research to US Engineers, MIT.

Taylor, D.W. (1948). Fundamentals of soil mechanics, Wiley.

Toll, D.G. (1990). A framework for unsaturated soil behaviour, Geotechnique 40, No.1, 31-44.

Townsend, F.C. (1985). Geotechnical characteristics of residual soils, Journal of Geotechnical Engineering, ASCE, Vol.111, No.1, 77-94.

Vaughan, P.R. (1985). Mechanical and hydraulic properties of in situ residual soils, Proc. of the 1st Int'l Conference on Geomechanics in Tropical Lateritic and Saprolitic Soils, Brasilia, Vol.3, 231-263.

Vaughan, P.R. (1988). Characterizing the mechanical properties of in situ residual soil, Proc. of the 2nd Int'l Conference on Geomechanics Tropical Soils, Singapore, Vol.2.

Vaughan, P.R., Maccarini, M. and Mokhtar, S.M. (1988). Indexing the engineering properties of residual soil, Quarterly Journal of Engineering Geology 21, 69-84.

Vesic, A.S. and Clough, G.W. (1968). Behaviour of granular materials under high stress, Journal of the Soil Mechanics and Foundations Division, ASCE, Vol.94, SM3, 661-688.

Wallace, K.B. (1973). Structural behaviour of residual soils of the continually wet Highlands of Papua New Guinea, Geotechnique 23, No.2, 203-218.

Wesley, L.D. (1988). Engineering classification of residual soils, Proc. of 2nd Int'l Conference on Geomechanics in Tropical Soils, Singapore, Vol.1, 77-84.

Wesley, L.D. (1990). Influence of structure and composition on residual soils, Journal of Geotechnical Engineering, ASCE, Vol.116, No.4, 589-603.

Yagi, N. and Yatabe, R. (1985). A microscopic consideration on shearing characteristic of decomposed granite soil (in Japanese), Proc. of Japanese Society of Civil Engineers, No.364, 133-141.

Soil location and type	Atterberg limits natural $W_L : W_P$	air dried $W_L : W_P$	oven dried $W_L : W_P$	% finer than 2 μm natural	air dry	oven dry
Costa Rica:						
Laterite	81:29		56:19			
Andosol	92:67		66:47			
Dominica:						
Allophane	101:69	56:43				
Latosolic	93:56	71:43				
Smectoid	68:25	47:21				
Hawaii:						
Humic latosol	164:162	93:89		9	0.6	
Hydrol latosol	206:192	61:NP		30	5	
Java:						
Andosol	184:146		80:74			
Kenya:						
Red clay, Sasumua	101:70	77:61	65:47	79		47
Malaysia:						
Weathered shale	56:24	48:24	47:23	25	36	34
Weathered granite	77:42	71:42	68:37	20	17	18
Weathered basalt	115:50	91:49	69:49	80	82	63
New Guinea:						
Andosol	145:75		NP			
Vanuatu:						
Volcanic ash, Pentecost	261:184	192:121	NP	92	57	6

NP indicates non-plastic.

Table 4.1 Drying effects on classification test results (after Geological Society,1990)

Soil type and location (1)	Liquid Limit		Plasticity Index		Source (6)
	Natural (2)	Remolded (3)	Natural (4)	Remolded (5)	
Red clay, Kenya	74	84	36	45	Newill, 1961
Red clay, Kenya	77	91	16	32	Newill, 1961
Lateritic Cuba	46	53	15	22	Winterkorn and Chandrasekharan, 1951
Lateritic, Panama	60	70	21	30	Townsend, 1969

Table 4.2 Remoulding effects on Atterburg limits (after Townsend, 1985)

Location	Grading				LL	PL	PI	Reference
	G	S	Si	C				
Korea	46	47	7	–	NP	NP	NP	Do (1979)
	40	51	9	–	NP	NP	NP	
	31	48	17	4	44	34	10	
	5	82	13	–	NP	NP	NP	
Japan	37	45	12	6	49	29	20	Onitsuka et al (1985)
	40	56	2	2	45	24	21	
	36	51	7	6	48	31	17	
	24	63	9	4	NP	NP	NP	
	–	–	–	–	NP	NP	NP	Matsuo and Fukumoto (1976)
Thailand	16	62	8	14	27	20	7	Ruenkrairergsa and Petchgate (1985)
	4	52	24	20	56	28	28	
	6	64	23	7	NP	NP	NP	
Malaysia					59	36	23	Komoo (1985)
					50	37	13	
					46	30	16	
					41	31	10	

Table 4.3 Consistency of decomposed granite soils

Location	ϕ' (°)	c' (kPa)	Test[1)]	e_o	Sample[2)]	Fines (%)	Reference
Japan	33-38 40 45-51	10-40 0 0	SB	0.95-1.35 0.69-1.07 0.39-0.58	U U U	30-40 15 3-12	Onodera et al (1976)
"	33.4 33 37-42	58 16 14-41	"	0.89 0.89 0.53-0.59	U C C	18 18 13	Onitsuka et al (1985)
"	36 38 42 45	15 12 15 22	T (CD)	0.98 0.78 0.78 0.47	U U U U	26 - 15 12	Murata and Yasufuku (1987)
Hong Kong	35.6 ±0.3	0-90	"	-	U & C	-	Lumb (1962)
"	38-42	9	SB	1.05-1.26	U	18-30	Cheung and Greenway (1987)
"	43	13	T (CU)	14.3 kN/m^3	U	12	Shelton and Cooper (1984)
"	45 32	32 62	SB	-	U	11	Koirala (1982)
"	35 38 40 36	0 14 17 0	" " " T(CU)	$0.85\gamma_{dmax}$ $0.98\gamma_{dmax}$ $1.02\gamma_{dmax}$ $0.85\gamma_{dmax}$	C C C C	- - - -	Massey (1983)
Thailand	36-40 32-37	20-70 0-80	 T(CU)	$0.85\gamma_{dmax}$ "	C C	22 44	Ruenkrairergsa and Petchgate (1985)

1) SB: Shear box test
T: Triaxial test (CU: Consolidated undrained test, CD: Consolidated drained test)
2) U: Undisturbed sample, C: Compacted sample

Table 4.4 Strength parameters for decomposed granite soils

Location	ϕ' (°)	M	Test[1)]	Remarks	Reference
Japan	39	1.59	T (CD)	Compacted sample	Miura and O-hara (1979)
"	39	1.59	"	Compacted, sandy sample	Yagi and Yatabe (1985)
"	39 38 41	1.58 1.56 1.70	" " "	Undisturbed, 26% fines[2)] " 20% " " 12% "	Murata and Yasufuku (1987)
Hong Kong	39	1.59	SB	Undisturbed sample Grade V	Cheung and Greenway (1987)

[1)] T: Triaxial test (CD: Consolidated drained test), SB: Shear box test

[2)] silt + clay fraction

Table 4.5 Ultimate strength parameters for decomposed granite soils

Index & Definition	Comments	References
Ignition loss <L_i> L_i = Loss by ignition/Mass x 100 (%)	– Clay minerals increase with weathering – Quantify the crystalized water in clay minerals – Higher values indicate more advanced weathering	– JSSMFE (1979) – Murata and Yasufuku (1987)
Apparant specific gravity <G_a> Specific gravity of a soil, assuming the intra-particle voids to be part of the soil particles	– Intra-voids are developing with weathering – Reduces with weathering	– JSSMFE (1979)
Specific gravity of feldspar <G_{sf}> Specific gravity of feldspar grains	– Feldspar grains are altered by weathering – Change of G_{sf} is related to the compressive strength of the grains – Reduces with weathering	– Matsuo and Nishida (1968)
Degree of decomposition <X_d> $X_d = (N_q - N_{qo})/(1 - N_{qo})$ N_q: Weight ratio of quartz and feldspar in the soil N_{qo}: Weight ratio of quartz and feldspar in the original rock	– Weight percentages of quartz and feldspars in both the weathered and parent rock – Fresh rock: $X_d = 0$ Completely decomposed rock: $X_d = 1$	– Lumb (1962)
Density of microcracks <ρ_{cr}> ρ_{cr}: Percentage of total width of cracks to length of measuring line	– Represents the physical weathering of a granite – Microcrack determination for undisturbed soil – Increases with weathering	– Onodera et al (1974)
Micropetrographic Index <I_p> $I_p = \frac{\%\ \text{Sound constituents}}{\%\ \text{Unsound constituents}}$	– Includes the structural fabric elements, microcracks and voids, together with changes of mineral constituents – Quantifies the fabric elements of undisturbed soil – Reduces with weathering	– Irfan and Dearman (1978)
Chemical weathering index <CWI> Percentage of sesquioxide and loss on ignition in soils	– Identifies and classifies the granitic residual soils both for geological and engineering purposes	– Sueoka (1988)

Table 4.6 Weathering indices

Collapse (%)	Severity of the problem
0–1	no problem
1–5	moderate trouble
5–10	trouble
10–20	severe trouble
>20	very severe trouble

Table 4.7 Collapse percentage and the potential severity (after Jennings and Knight, 1975)

	Bulk density (kN/m^3)	W/C (%)	Dry density (kN/m^3)
	19.28 17.69 18.05	7.45 6.53 7.27	17.94 16.61 17.13
Average	18.34	7.08	17.13

Table 6.1 In-situ water content and density

Mineral	Whole sample	Coarse particles (over 2 mm)	Fine particles (below 300μm)
Quartz	33 %	45 %	17 %
Feldspar	50	51	56
Mica	9	4	10
Kaolinite	6	n.d	16
Smectite	2	n.d	1

Table 6.2 Mineral composition

Stages				Remarks
Sample preparation	Before isotropic compression	Before shearing	During shearing	
Wet compaction (43)	Saturated (30)	Saturated (29)	Saturated (29)	'Saturated'
	Wet (4)	Saturated[1] (4)	Saturated (4)	
	Wet (6)	Wet (6)	Wet (6)	'Wet'
	Air dried (3)	Air dried (3)	Air dried (2) Flooded (1)	
Dry compaction (16)	Dry (16)	Dry (12)	Dry (10) Flooded (2)	'Dry'
		Saturated[1] (4)	Saturated (4)	

[1] Flooding was followed by saturation.
* Number of samples tested is in brackets.

Table 6.3 Moisture conditions during the triaxial tests

Group	Test No.	v_o	Isotropic compression	$v^{1)}$	Test[2)] type	Remarks
1	70	1.649	100 kPa	1.623	D	Loose samples
	71	1.643	150	1.611	D	
	72	1.654	50	1.647	D	
	73	1.646	300	1.594	P	
	74	1.649	100	1.630	P	
	75	1.647	400	1.581	P	
	76	1.646	50	1.640	D	
2	50	1.600	50	1.596	D	Medium dense samples
	51	1.606	100	1.593	D	
	52	1.600	100	1.591	P	
	53	1.600	300	1.568	P	
3	60	1.556	50	1.552	D	Dense samples
	61	1.548	100	1.540	D	
	62	1.549	100	1.540	P	
	63	1.557	300	1.531	P	
4	80	1.496	50	1.496	D	Very dense samples
	81	1.500	100	1.496	D	
	83	1.500	100	1.496	P	
	84	1.498	300	1.483	P	
	99	1.465	100	1.461	D	
5	24	1.578	100	1.570	U	
	25	1.601	300	1.564	U	
	26	1.648	300	1.591	U	
6	40*	1.642	500 → 100	1.580	D	Over-consolidated samples
	41*	1.670	500 → 100	1.598	D	
	42*	1.667	500 → 200	1.600	D	
	44*	1.672	500 → 100	1.599	U	
	45	1.674	500 → 250	1.580	U	
7	HP1	1.652	8000 → 50	1.395	–[3)]	High pressure tests
	HP2	1.577	5100	1.396	U	
	HP3	1.579	3100	1.440	U	
	HP4	1.651	4000	1.430	U	
	HP5	1.650	1800	1.495	D	
	HP6	1.649	2500	1.458	P	

All samples were saturated before isotropic compression except those with asterisk, which were saturated after isotropic compression.

1) Specific volume after isotropic compression
2) D: Drained test, U: Undrained test, P: Constant p' test
3) Isotropic compression and swelling only.

Table 6.4 Test programme for wet compacted and saturated samples

Group	Test No.	v_o	Isotropic compression	$v^{1)}$	Test[2)] type	Remarks
1	11	1.622	100 kPa	1.606	D	
	12	1.567	100	1.555	D	
	14	1.556	100	1.544	D	
	15	1.609	100	1.590	D	
	16	1.541	50	1.537	D	
	17	1.597	50	1.592	D	
2	46	1.607	100	1.599	D	Wet compacted, then air-dried samples
	47[3)]	1.610	100	1.598	D	
	48[4)]	1.606	-	1.606	D	

1) Specific volume after isotropic compression
2) D: Drained test
3) Flooded when 90% of the ultimated strength had been reached.
4) Unconfined test

Table 6.5 Test programme for wet compacted samples

Group	Test No.	v_o	Isotropic compression	$v^{1)}$	Test[2)] type	Remarks
1	3	1.626	50 kPa	1.621	D	
	4	1.600	100	1.592	D	
	5	1.626	100	1.611	D	
	8	1.556	100	1.543	D	
	9	1.691	100	1.671	D	
	10	1.673	150	1.641	D	
	13	1.690	200	1.651	D	
2	19[3)]	1.603	100	1.565	D	Saturated samples
	20[3)]	1.564	100	1.538	D	
	22[3)]	1.637	100	1.574	D	
3	30[4)]	1.590	100	1.571	D	Flooded or saturated samples
	31[5)]	1.596	100	1.567	D	
	33[3)]	1.625	500	1.526	P	
4	34	1.650	500	1.583	P	
	35	1.658	300	1.596	P	
	36	1.647	200	1.611	P	

1) Specific volume after isotropic compression
2) D: Drained test, P: Constant p' test
3) Flooded, then saturated after isotropic compression
4) Flooded after the peak state
5) Flooded when 90% of the ultimate strength had been reached.

Table 6.6 Test programme for dry compacted samples

Test No.	From the initial density		From the final water content			Δ (2)−(5)
	v_o (1)	v_f (2)	w/c (3)	v (4)	v_f*) (5)	
70	1.649	1.585	22.16 %	1.578	1.583	0.002
73	1.646	1.546	21.20	1.553	1.560	−0.014
75	1.649	1.616	23.40	1.611	1.614	0.002
51	1.606	1.561	21.54	1.562	1.567	−0.006
52	1.602	1.612	23.56	1.615	1.618	−0.006
61	1.548	1.572	21.87	1.573	1.578	−0.006
62	1.549	1.603	23.09	1.603	1.606	−0.003
63	1.557	1.549	20.87	1.545	1.552	−0.003
81	1.500	1.551	21.09	1.550	1.555	−0.004
84	1.500	1.525	20.25	1.529	1.536	−0.011
41	1.670	1.581	22.31	1.582	1.587	−0.006
42	1.671	1.546	20.62	1.538	1.546	0.000
19	1.603	1.578	22.09	1.577	1.582	−0.004
22	1.637	1.572	21.97	1.573	1.573	−0.006
HP2	1.577	1.386	14.41	1.376	1.383	0.003
HP5	1.650	1.336	12.41	1.324	1.340	−0.004
HP6	1.649	1.366	13.49	1.352	1.365	0.001

*) Specific volume corrected for the volume change by membrane penetration.

Remarks: (2) = (1) x (1 − ϵ_v/100)
(4) = G_s x (3)/100 + 1

Table 6.7 Specific volumes calculated from the initial density and from the final water content

Test No.	Stage[1)]	v_i	Pressure (kPa)	v_f	Remarks
40	C	1.642	500	1.572	Bishop and
	S	1.572	100	1.580	Wesley cell
41	C	1.670	500	1.586	
	S	1.586	100	1.598	
42	C	1.671	500	1.591	
	S	1.591	200	1.600	
45	C	1.662	500	1.588	
	S	1.588	250	1.591	
HP1	C	1.652	500	1.585	High pressure
	S	1.585	50	1.594	cell
	C	1.594	8000	1.376	
	S	1.376	50	1.395	
HP2	C	1.577	3100	1.435	
	S	1.435	100	1.447	
	C	1.447	5100	1.393	
HP3[2)]	C	1.579	3100	1.440	
HP4	C	1.651	4000	1.430	
HP5	C	1.650	1800	1.495	
HP6	C	1.649	2500	1.458	

[1)] C: Compression, S: Swelling
[2)] During the sample saturation stage, the sample of HP3 was accidentally compressed with a pressure of about 500 kPa and unloaded.

Table 6.8 Summary of isotropic compression and swelling tests

Soils	λ	κ	N	λ/κ	Reference
Decomposed granite soil	0.09	0.005	2.17	18	
River sands					
-Chattahoochee	0.175	-	3.28	-	Vesic and Clough(1968)
-Toyoura	0.198	-	3.57	-	Miura and Yamanouchi (1975)
Carbonate sands					
-Dogs bay sand	0.335	0.0075	4.80	44.7	Coop (1990)
Tills					
-Cowden till	0.077	0.015	1.915	5.1	Lau (1988)
-St.Albans	0.065	0.030	1.863	2.2	Little (1984)
London clay	0.161	0.062	2.759	2.6	Atkinson and Bransby (1978)

Table 6.9 Isotropic normal compression parameters

Test No.	Maximum pressures (kPa)		B_r
	q'	p'	
70	335	212	0.048
71	495	315	0.043
72	164	104	0.021
73	476	300	0.045
74	155	100	0.018
75	607	402	0.046
50	217	123	0.019
51	342	214	0.033
52	179	100	0.010
53	476	300	0.039
60	247	133	0.056
62	196	100	0.035
63	525	300	0.040
81	502	267	0.062
83	210	100	0.045
26	306	300	0.030
40	350	500	0.042
41	330	500	0.033
42	627	500	0.046
44	275	500	0.032
45	328	500	0.035
HP1	–	8000	0.065
HP2	2695	5100	0.135
HP3	1771	3100	0.092
HP4	2158	4000	0.110
HP5	5650	3676	0.183
HP6	3896	2500	0.157

Table 6.10 Particle crushing during the triaxial tests

Test	Peak state				Critical (or end*) state			
No.	q'[1)]	p'[1)]	q'/p'	v	q'[1)]	p'[1)]	q'/p'	v
70	–	–	–	–	335	212	1.58	1.585
71	–	–	–	–	495	315	1.57	1.554
72	–	–	–	–	164	104	1.57	1.613
73	–	–	–	–	476	300	1.59	1.546
74	–	–	–	–	155	98	1.58	1.616
75	–	–	–	–	627*	402*	1.56*	1.522*
76	83	50	1.67	1.643	78*	48*	1.60*	1.643*
50	217	123	1.77	1.596	167	107	1.57	1.616
51	–	–	–	–	342	214	1.60	1.561
52	179	100	1.79	1.596	158	98	1.61	1.612
53	491	300	1.63	1.549	476	300	1.59	1.549
60	247	133	1.87	1.560	178*	110*	1.62*	1.604*
61	457	252	1.81	1.542	357*	219*	1.63*	1.572*
62	196	100	1.96	1.556	161	99	1.63	1.603
63	525	300	1.75	1.530	477	300	1.59	1.549
80	306	153	2.01	1.513	186*	113*	1.65*	1.573*
81	502	267	1.88	1.506	375*	225*	1.67*	1.551*
83	210	100	2.10	1.519	166*	100*	1.66*	1.580*
84	555	301	1.85	1.493	478	299	1.60	1.525
99	537	279	1.92	1.477	375*	225*	1.67*	1.526*
24	271[2)]	158	1.71	1.568	331	204	1.62	1.570
	347	210	1.65	1.570				
25	402	244	1.65	1.560	376	234	1.61	1.559
26	306	190	1.61	1.585	271	171	1.59	1.585
40	–	–	–	–	350	217	1.61	1.567
41	–	–	–	–	330	210	1.57	1.581
42	–	–	–	–	627*	409*	1.53*	1.546*
44	275	170	1.62	1.598	244	151	1.61	1.597
45	328	205	1.60	1.576	295	183	1.61	1.575
HP2	–	–	–	–	2699	1683	1.60	1.386
HP3	–	–	–	–	1771	1073	1.65	1.429
HP4	–	–	–	–	2158	1290	1.67	1.422
HP5	–	–	–	–	5650	3676	1.54	1.336
HP6	–	–	–	–	3896	2509	1.55	1.366

*) End state

1) Unit: kPa

2) Peak state defined at the maximum stress ratio

Table 6.11 Peak and critical (or end) states of saturated samples

Test No.	At the minimum volume state			Peak state				End state			
	q'	p'	q'/p'	q'	p'	q'/p'	v	q'	p'	q'/p'	v
3[1)]	155	102	1.52	311	154	2.02	1.648	270	140	1.93	1.674
4	371	224	1.66	514	271	1.89	1.596	383	228	1.68	1.650
5	353	218	1.62	480	260	1.85	1.611	391	230	1.70	1.655
8	359	220	1.63	575	292	1.97	1.556	415	238	1.74	1.612
9	329	210	1.57	433	245	1.77	1.670	373	224	1.66	1.701
10	525	325	1.61	620	357	1.74	1.620	547	332	1.65	1.641
13	689	430	1.60	800	467	1.71	1.609	717	439	1.63	1.629
19	337	212	1.59	420	240	1.75	1.553	368	223	1.65	1.578
20	339	213	1.59	453	252	1.80	1.534	381	227	1.68	1.568
22	364	222	1.64	414	238	1.74	1.551	371	223	1.66	1.572
30	324	208	1.56	515	272	1.89	1.581	385	229	1.68	1.572
31	344	214	1.60	419	239	1.75	1.549	396	232	1.71	1.568
33	786	500	1.57	838	500	1.67	1.505	825	503	1.64	1.512
34	797	500	1.60	870	500	1.74	1.567	850	501	1.70	1.580
35	464	300	1.55	532	301	1.77	1.591	506	300	1.69	1.617
36	296	200	1.48	364	200	1.82	1.627	339	200	1.70	1.661

* Unit - q': kPa, p': kPa
[1)] Test was terminated at the axial strain of 11%.

Table 6.12 Peak and end states of dry samples

Test No.	Peak state				Critical (or end*) state			
	q'	p'	q'/p'	v	q'	p'	q'/p'	v
11	348	216	1.61	1.583	334	211	1.58	1.588
12	416	239	1.74	1.550	358	219	1.63	1.579
14	436	246	1.77	1.554	362	221	1.64	1.580
15	376	225	1.67	1.576	342	214	1.60	1.587
16	259	136	1.90	1.553	208*	120*	1.73*	1.601*
17	223	124	1.79	1.597	189*	114*	1.67*	1.631*
46	695	331	2.10	1.601	434*	244*	1.78*	1.657*
47	347	216	1.61	1.571	339	213	1.59	1.566
48	220	73	3.0	-	-	-	-	-

Unit - q': kPa, p': kPa

*) End state

Table 6.13 Peak and critical (or end) states of wet samples

Test No.	q'_{max} (kPa)	B_r	Moisture condition
3	311	0.021	Dry
4	514	0.016	"
5	480	0.025	"
8	575	0.012	"
9	433	0.023	"
10	620	0.018	"
34	870	0.044	"
35	532	0.039	"
36	364	0.024	"
11	348	0.024	Wet
12	416	0.022	"
14	436	0.057	"
15	376	0.036	"
16	259	0.008	"
17	223	0.02	"
31	419	0.038	Flooded
33	838	0.06	Flooded

Table 6.14 Particle crushing during the triaxial tests (dry and wet samples)

Test No.	Moisture condition	v[1)]	σ_r (kPa)	Strains due to flooding	
				ϵ_a (%)	ϵ_v (%)
40	Wet	1.642	500	0.07	0.1
41	"	1.670	"	0.05	0.1
42	"	1.671	"	0.05	0.14
19	Dry	1.603	100	0.46	1.08
20	"	1.564	"	0.35	0.34
22	"	1.637	"	–	–
33	"	1.625	500	1.03	2.20

[1)] specific volume before isotropic compression

Table 6.15 Axial and volumetric strains due to flooding

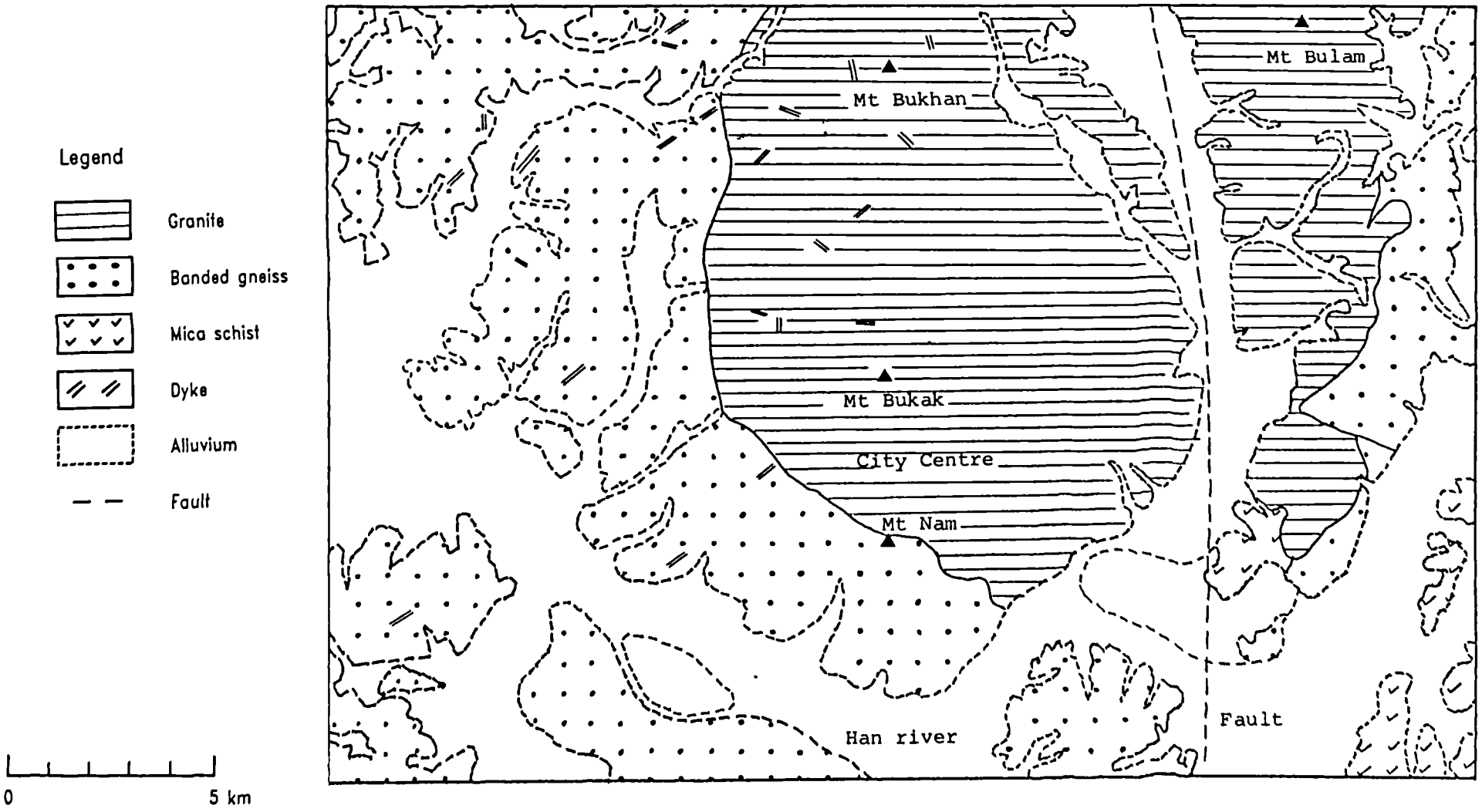

Figure 2.1 Geological map of Seoul

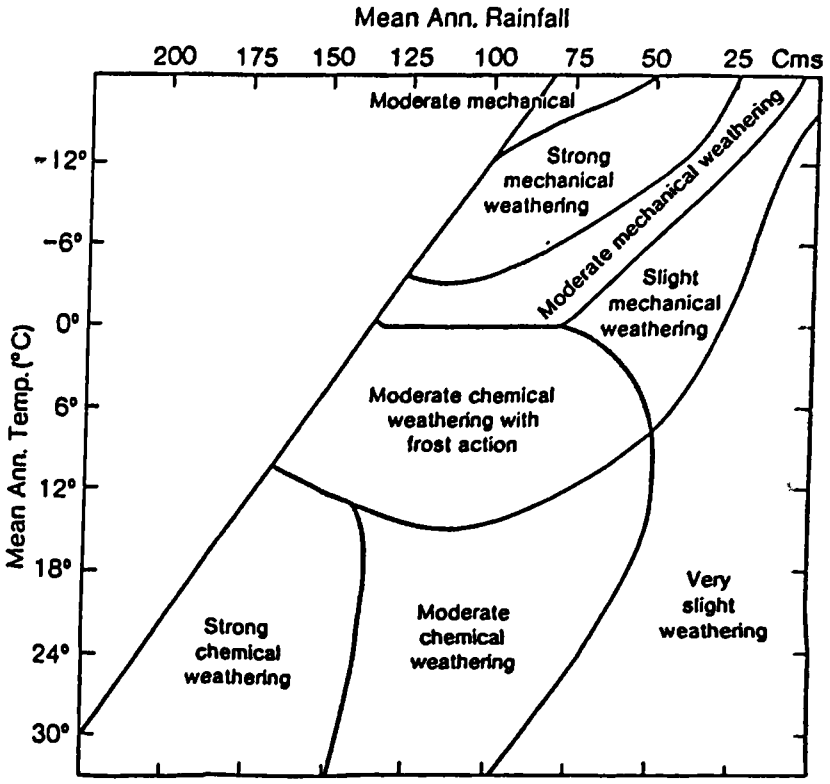

Figure 2.2 The relationship between climate and the type of weathering (after Peltier, 1950)

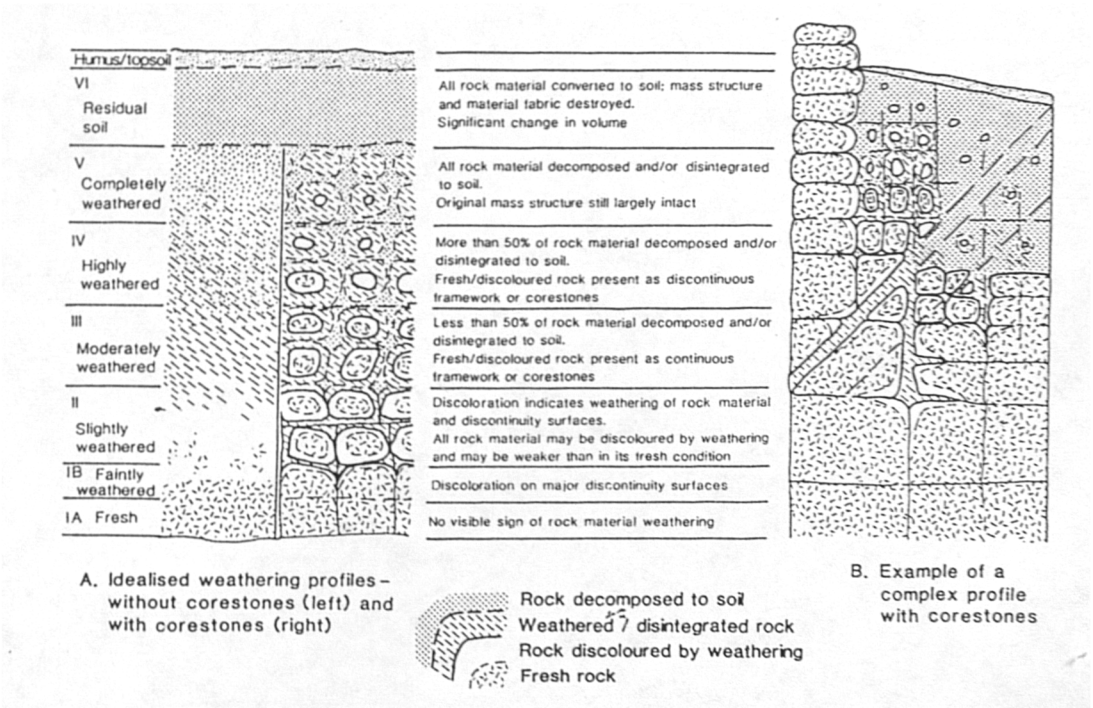

Figure 2.3 Typical weathering profile (after Geological Society, 1990)

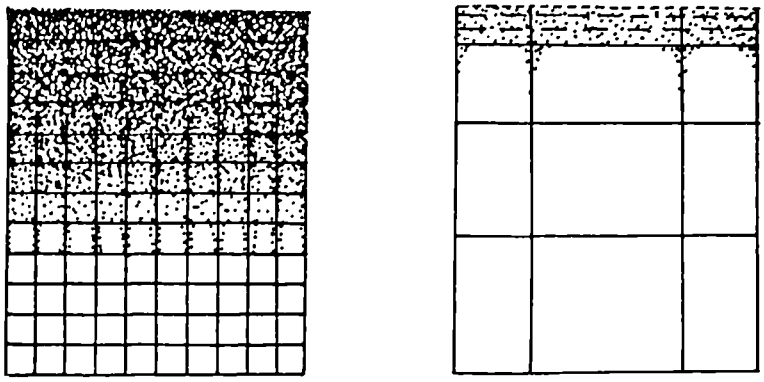

Figure 2.4 Typical weathering profiles in Korean granites (after Lee, S.G., 1987)

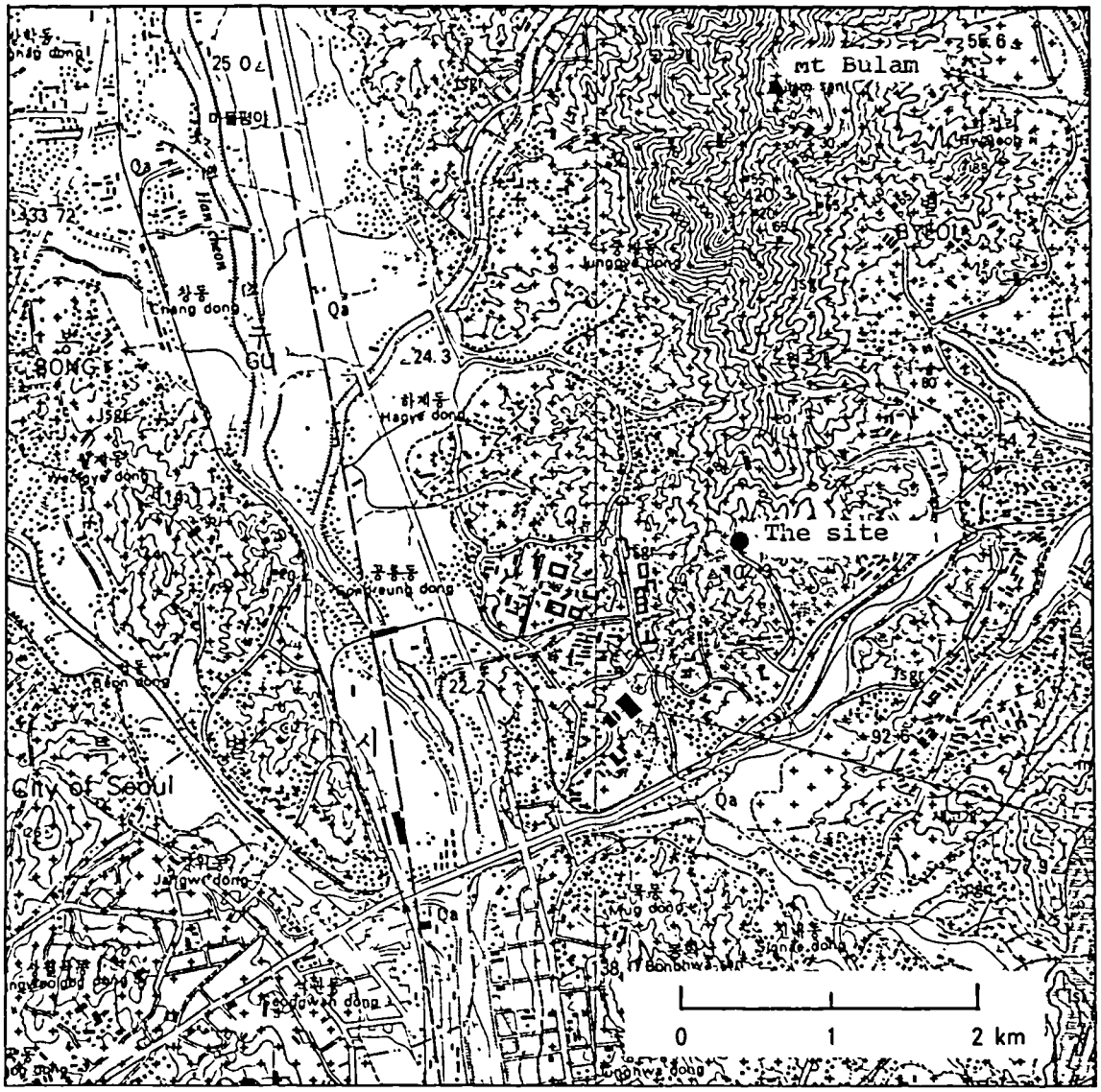

Figure 2.5 Sampling area

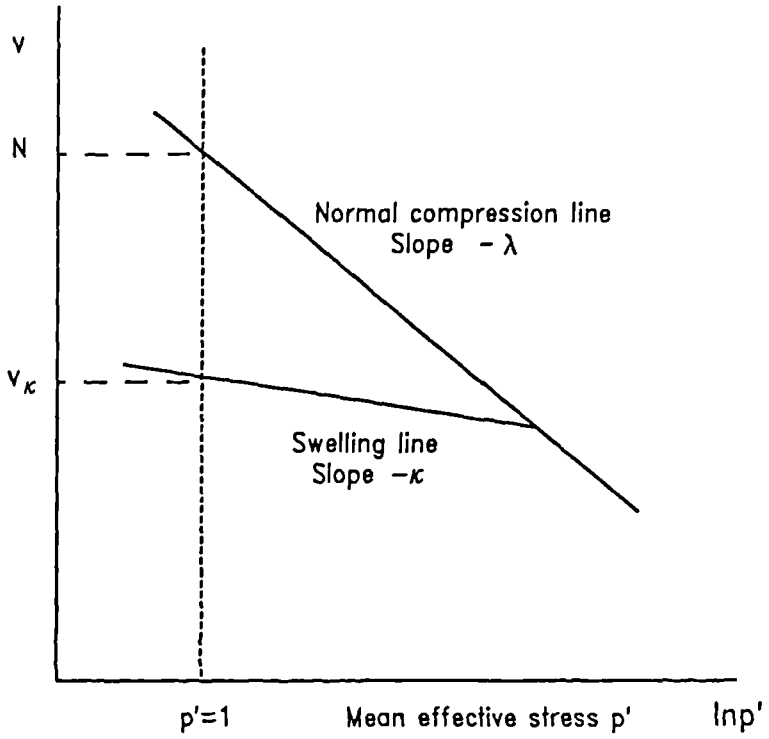

Figure 3.1 Isotropic compression and swelling in v–lnp' plane

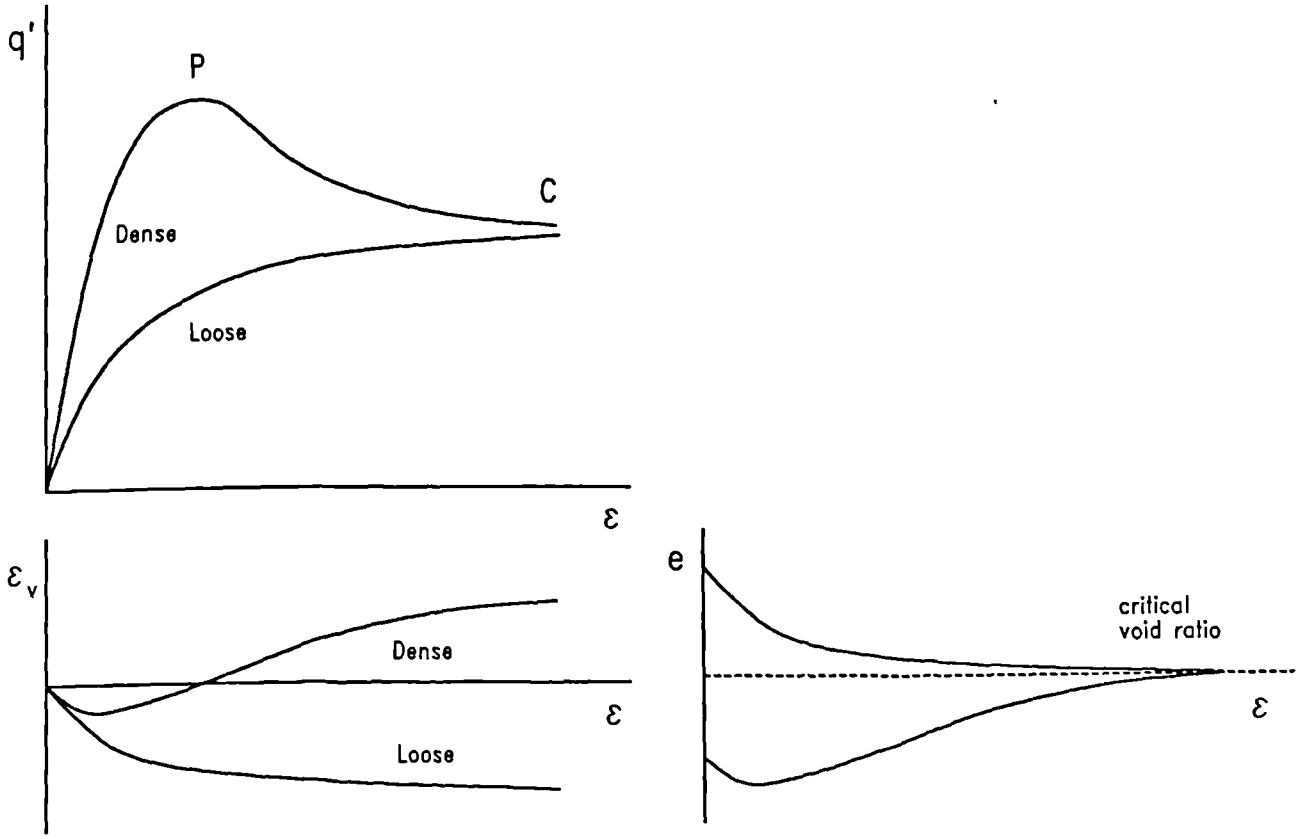

Figure 3.2 Typical stress–strain behaviour of soils

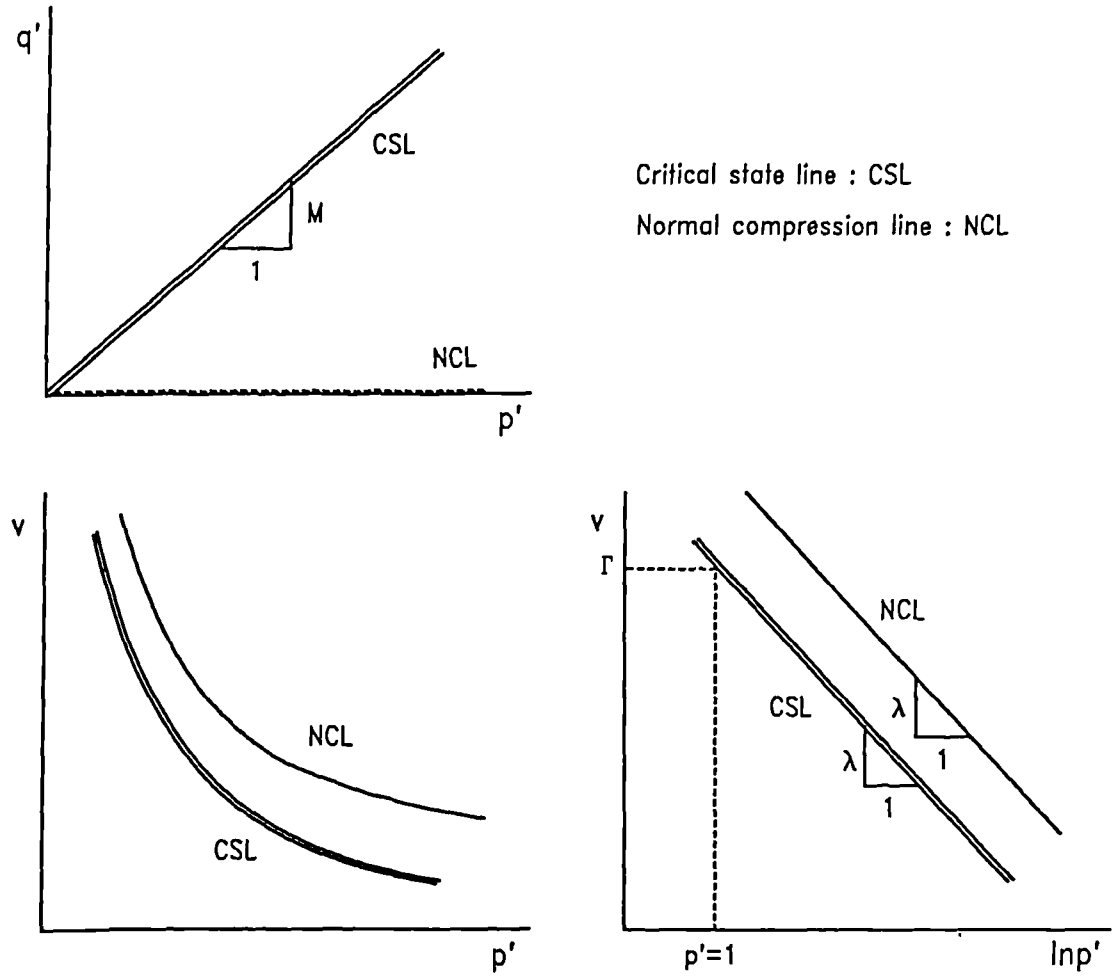

Figure 3.3 The critical state line

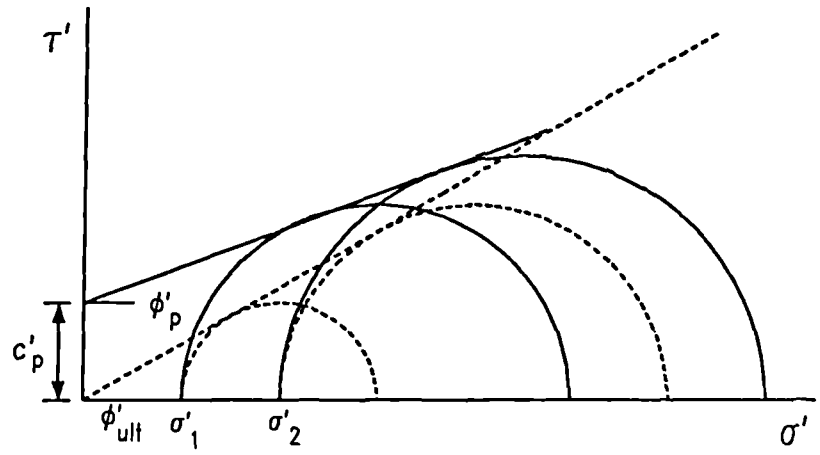

Figure 3.4 Mohr–Coulomb failure criteria

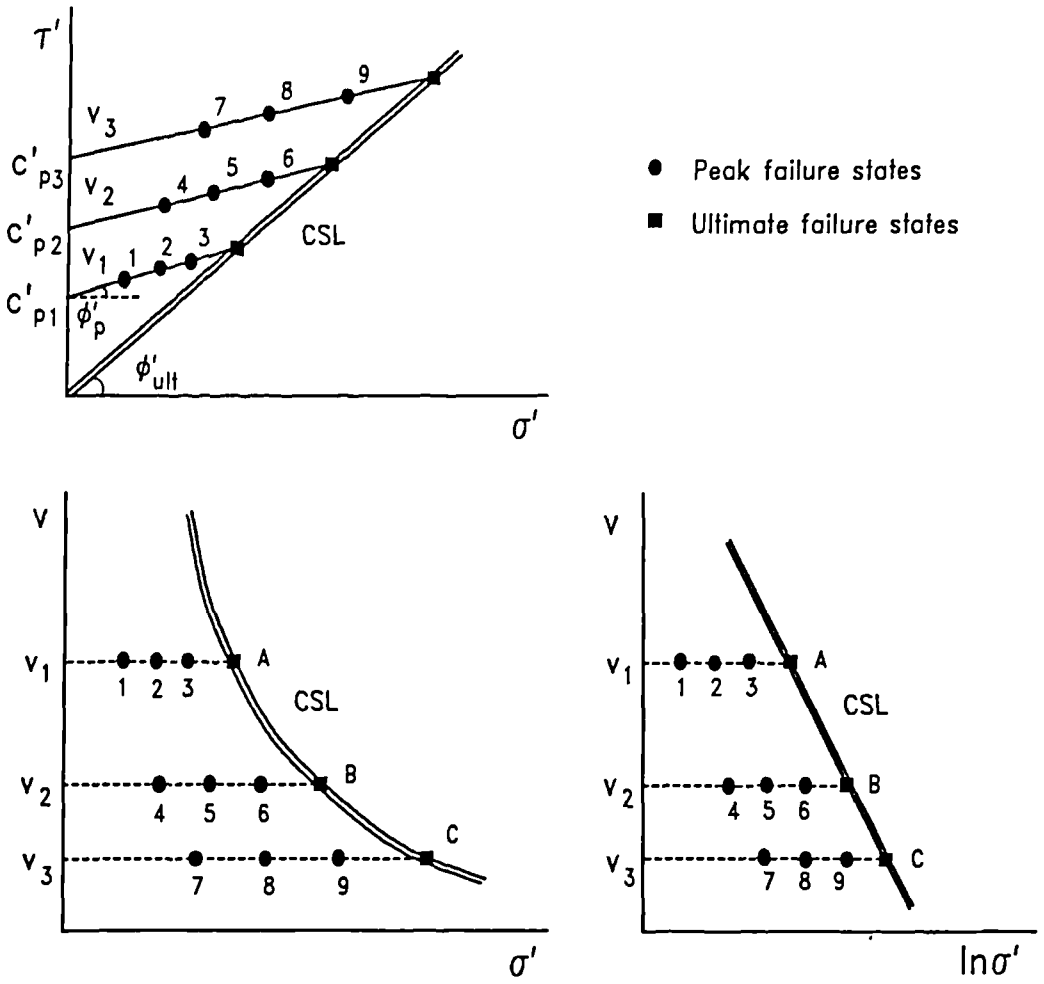

Figure 3.5 Failure states (Coulomb–Hvorslev model)

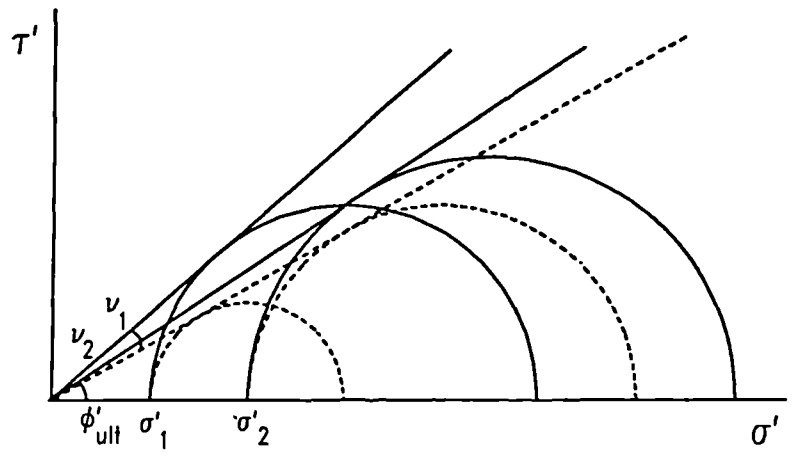

Figure 3.6 Peak states and angle of dilation

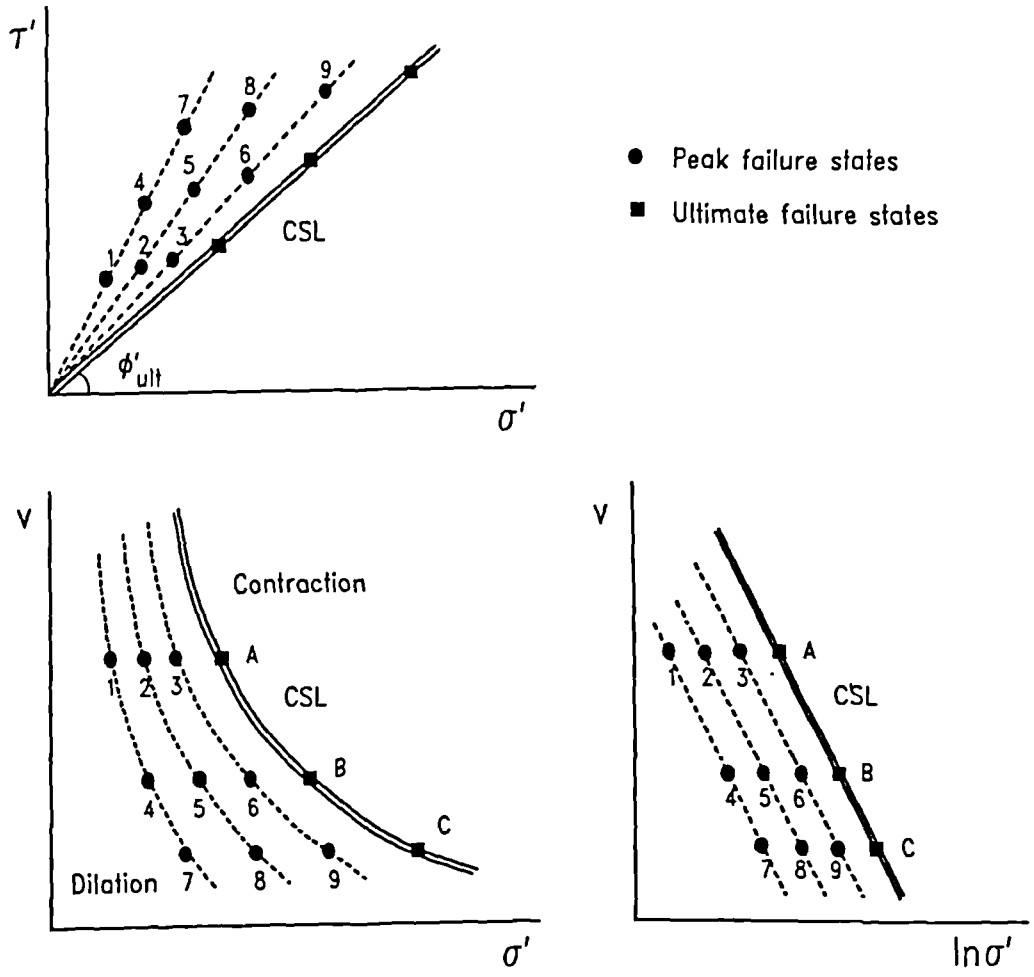

Figure 3.7 Peak states (stress–dilatancy model)

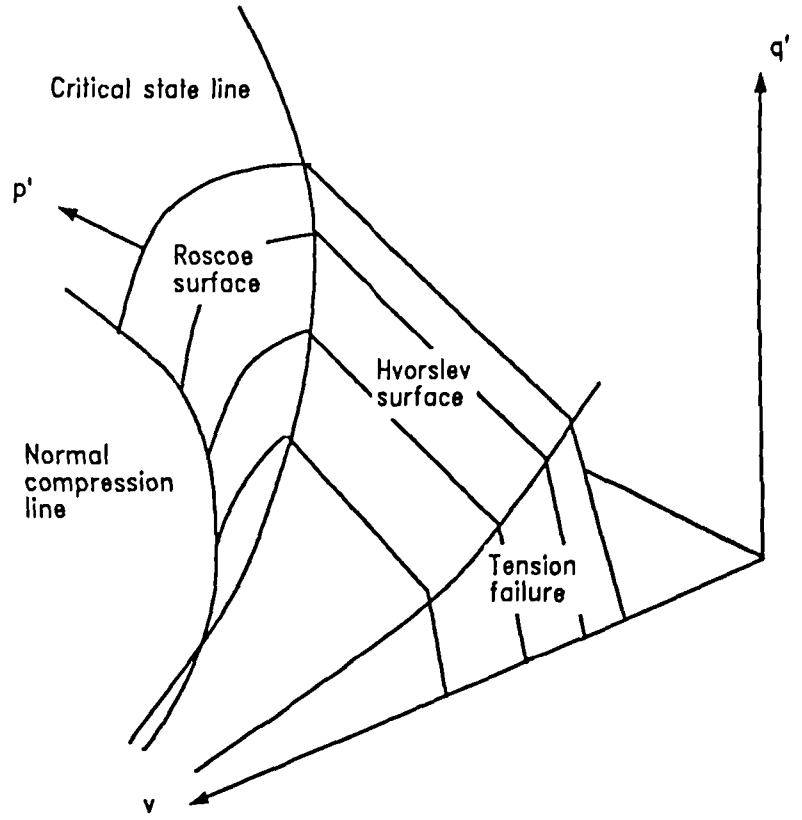

Figure 3.8 The state boundary surface in q':p':v space (after Atkinson and Bransby, 1978)

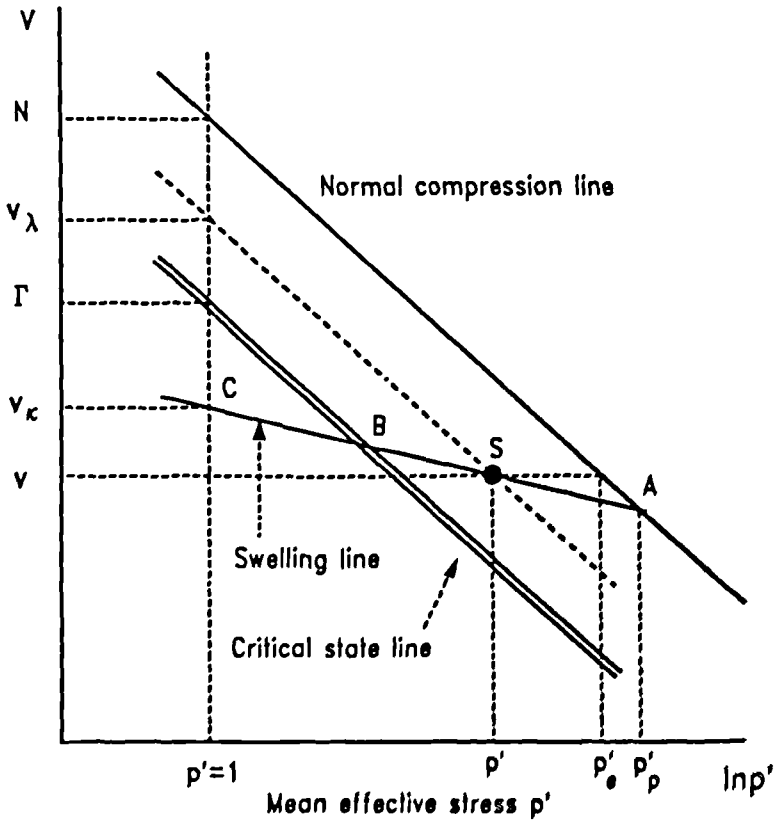

Figure 3.9 Normalising parameters

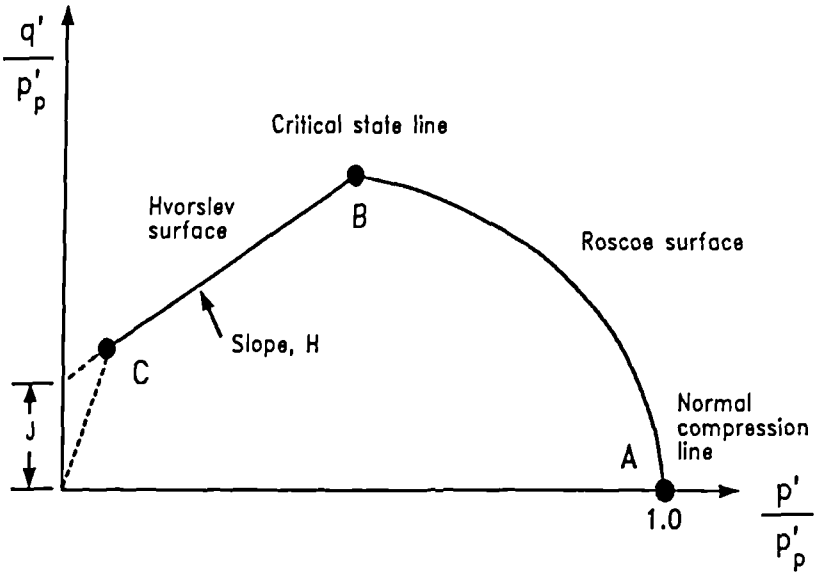

(a) Elastic wall section

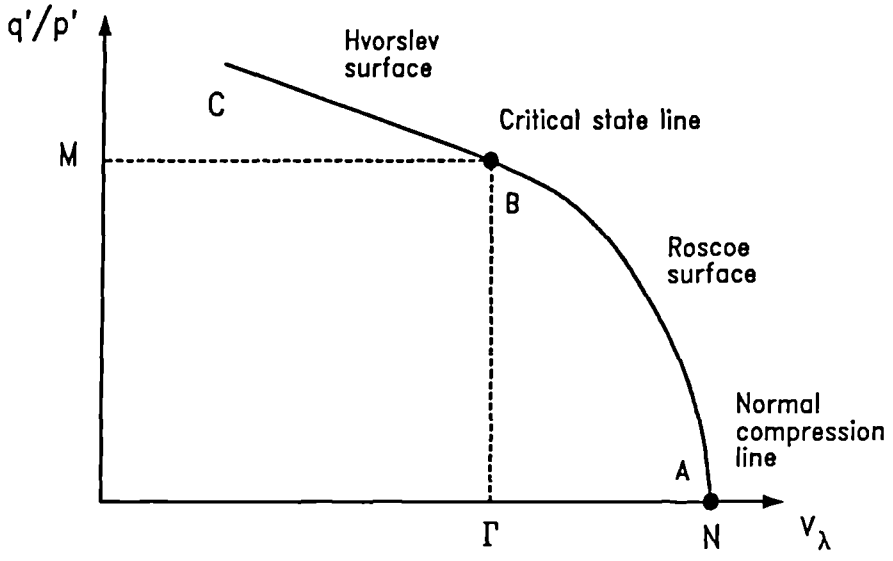

(b) Constant p' section

Figure 3.10 Normalised sections of a state boundary surface

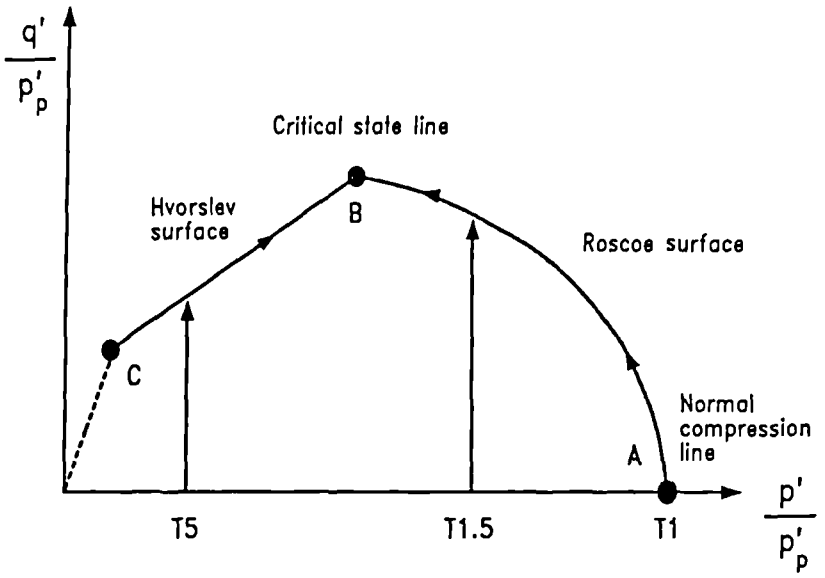

(a) Elastic wall section

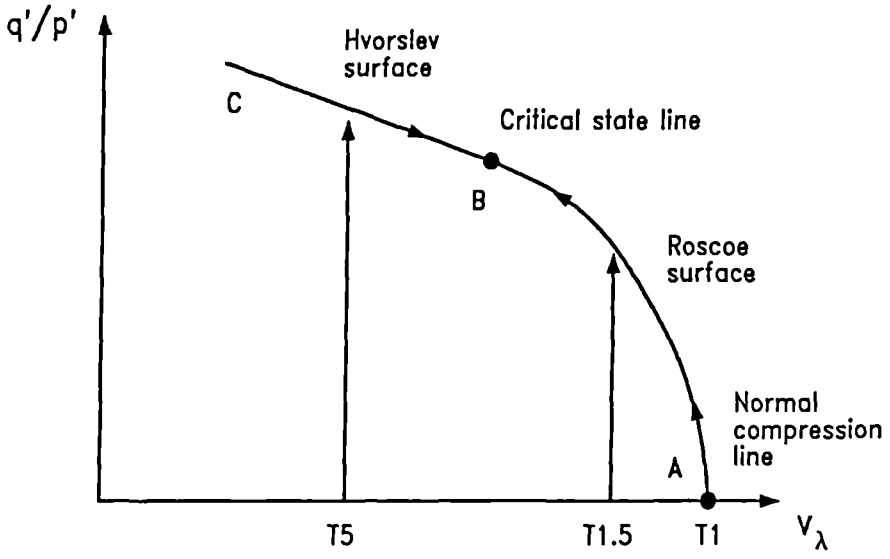

(b) Constant p' section

Figure 3.11 Normalised behaviour of soil in triaxial compression tests

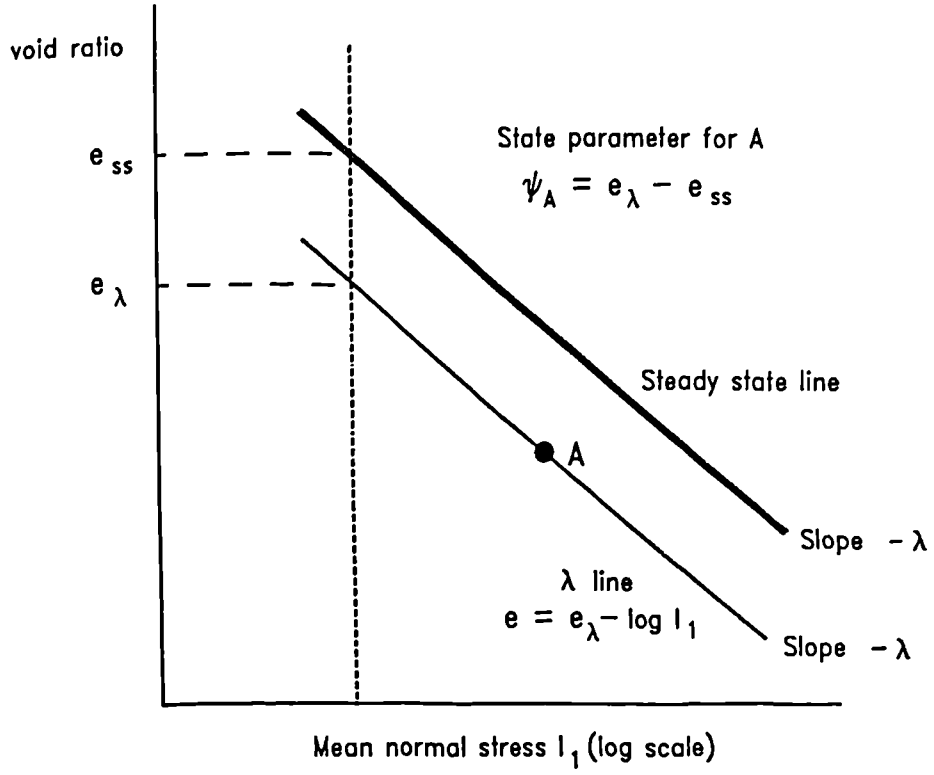

Figure 3.12 Definition of state parameter (after Been and Jefferies, 1985)

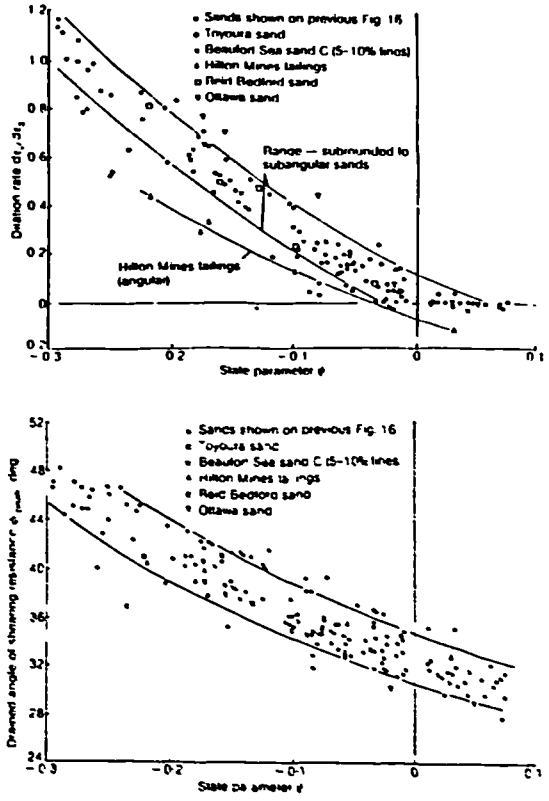

Figure 3.13 Angle of shearing resistance and peak dilation rate as a function of state parameter (after Been and Jefferies, 1986)

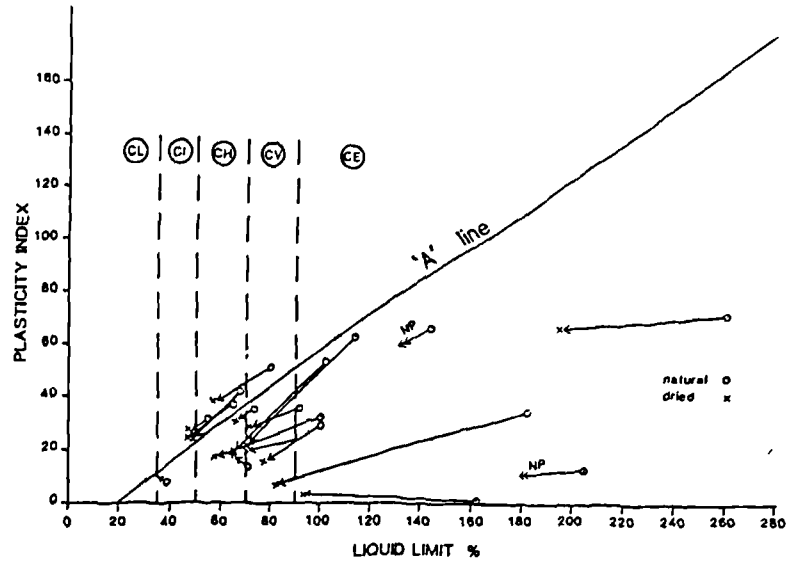

Figure 4.1 Drying effects on plasticity (after Geological Society, 1990)

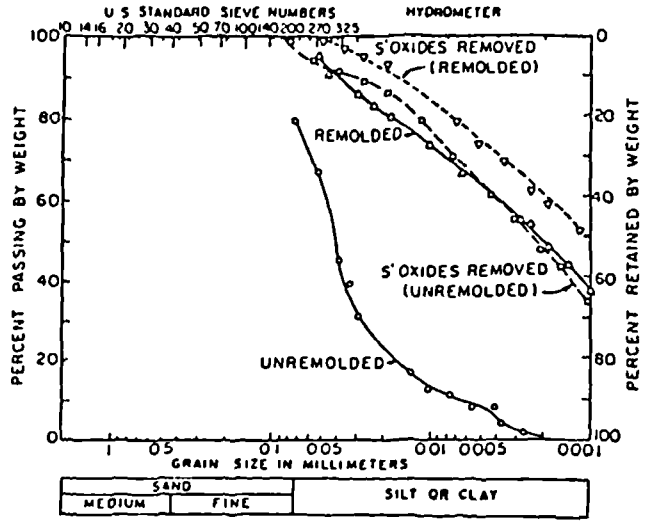

Figure 4.2 Remoulding effects on grading (after Townsend, 1985)

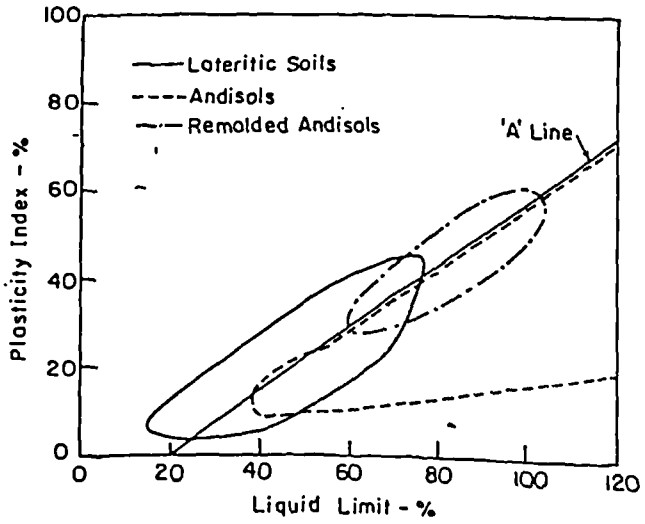

Figure 4.3 Ranges of Atterburg limits for residual soils (after Mitchell and Sitar, 1982)

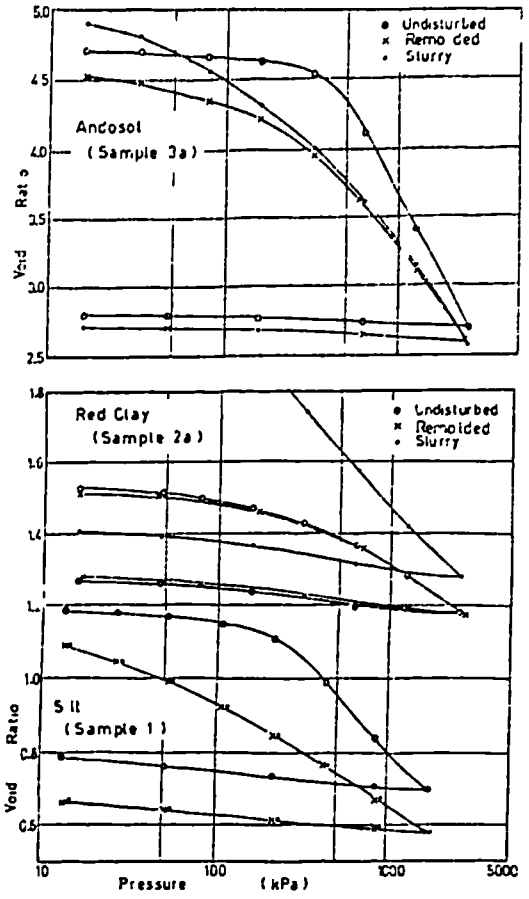

Figure 4.4 Oedometer test results on residual soils (after Wesley, 1990)

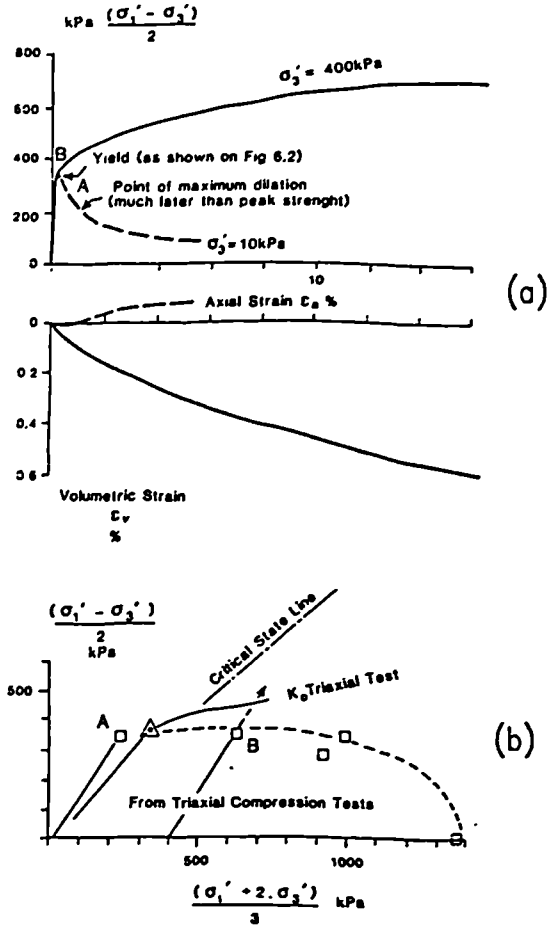

Figure 4.5 (a) Drained triaxial test
(b) Yield curve
(After Geological Society, 1990)

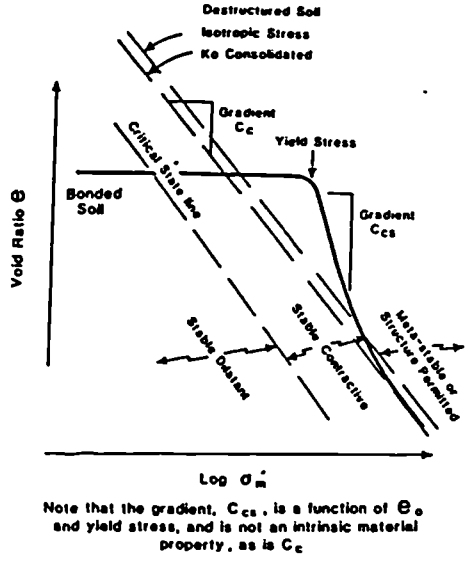

Figure 4.6 Possible states for structured and destructured soils (after Vaughan, 1988)

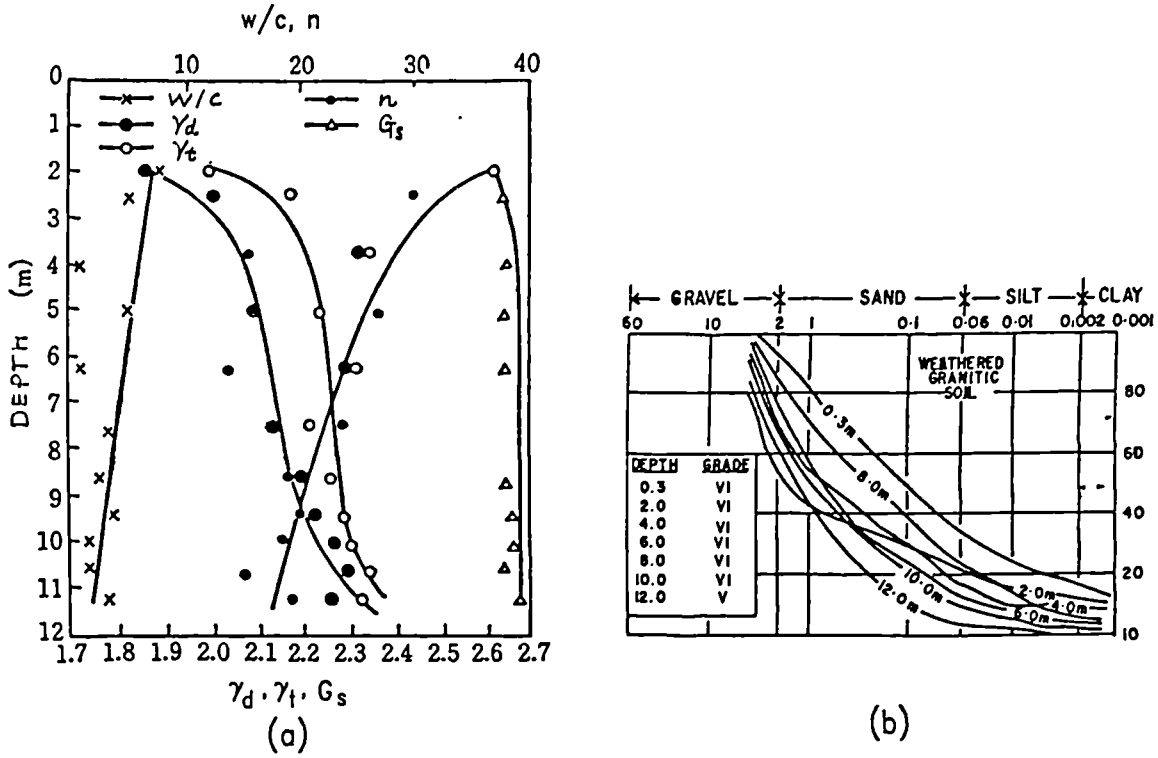

Figure 4.7 Vertical variations of properties of weathered granites
(a) Japan (after JSSMFE, 1974)
(b) Malaysia (after Komoo, 1985)

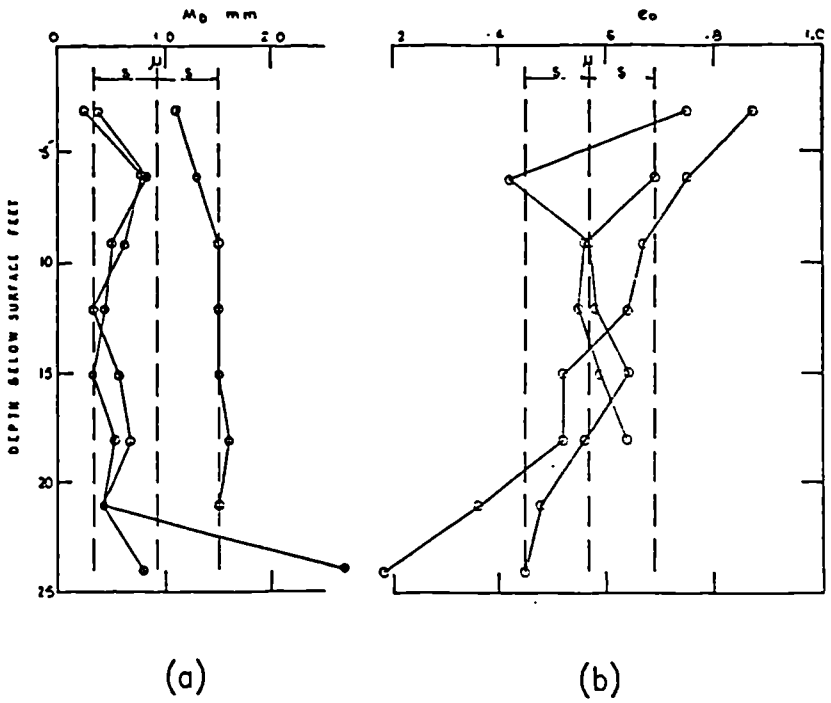

Figure 4.8 Horizontal and vertical variations of
(a) Mean particle size
(b) Void ratio
(after Lumb, 1962)

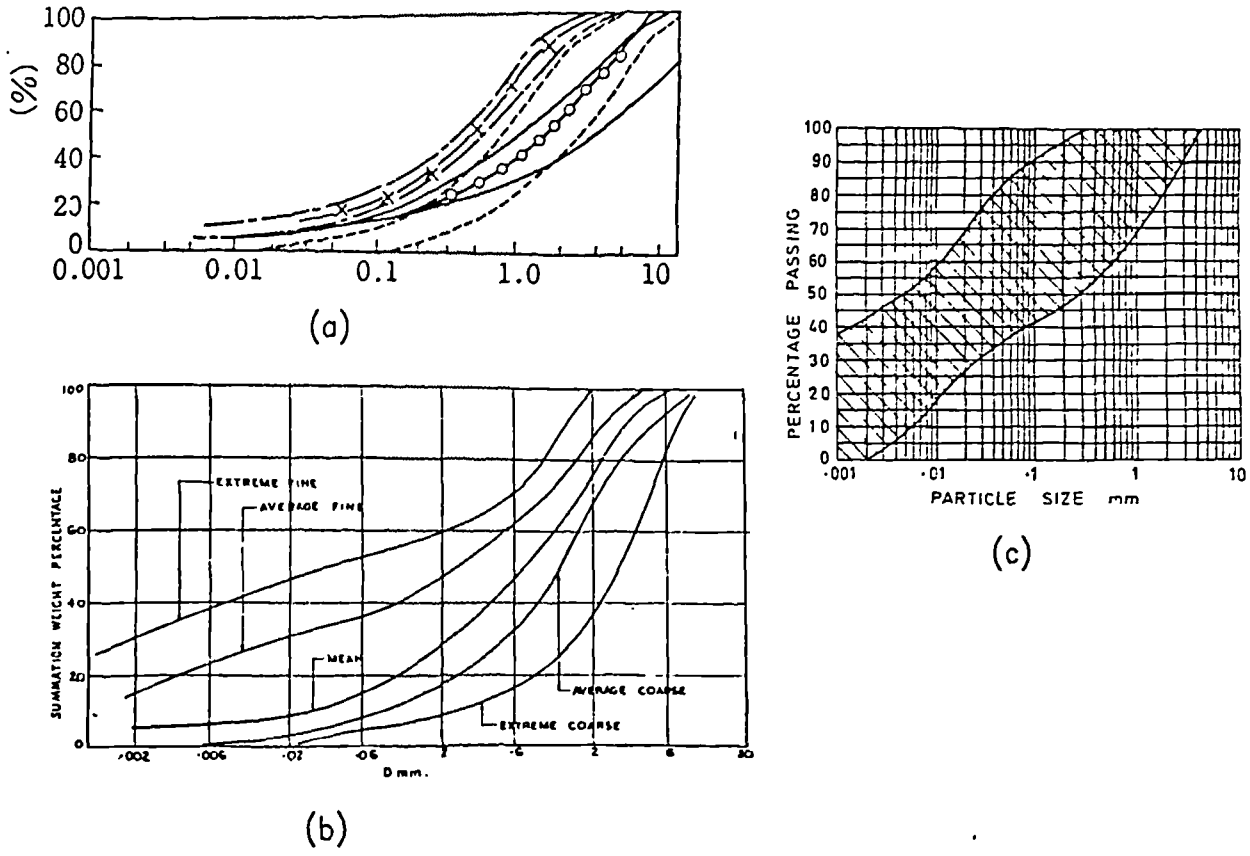

Figure 4.9 Typical grading curves of decomposed granite soils
(a) Japan (after JSSMFE, 1979)
(b) Hong Kong (after Lumb, 1962)
(c) Singapore (after Poh et al., 1985)

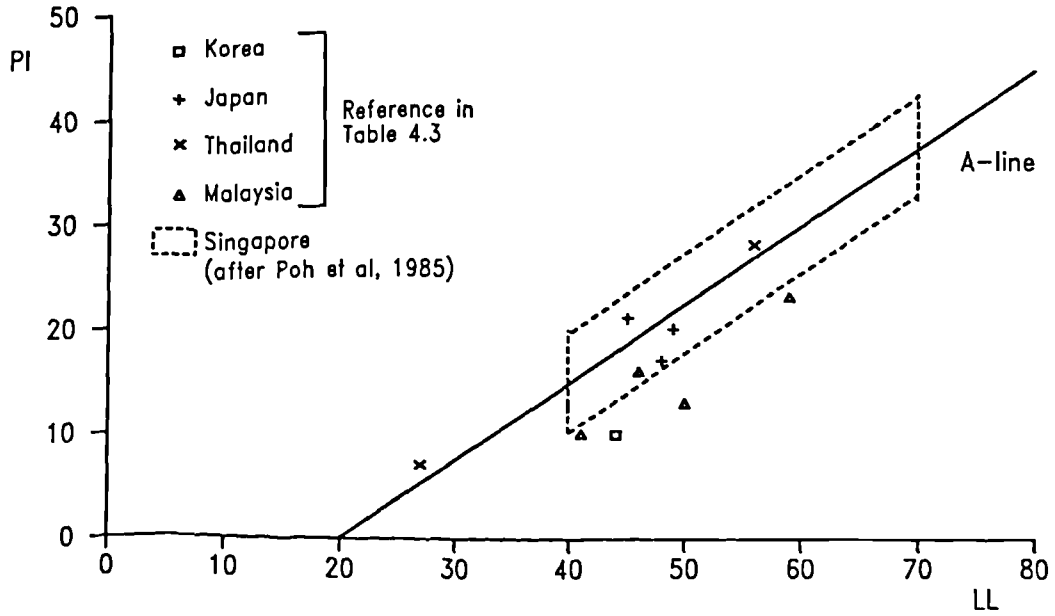

Figure 4.10 Plasticity of decomposed granite soils

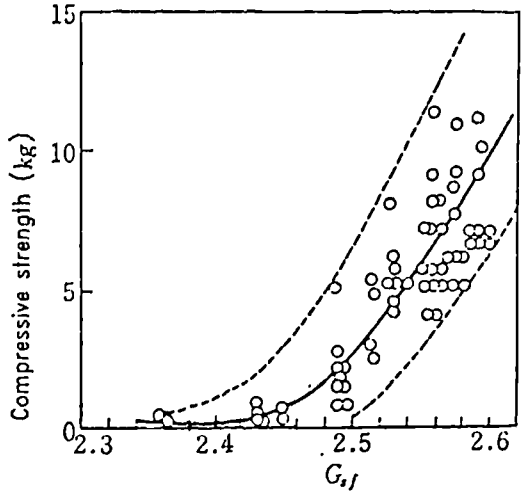

G_{sf}: Specific gravity of feldspar used for weathering index

Figure 4.11

Grain strength and weathering (after Matsuo and Nishida, 1968)

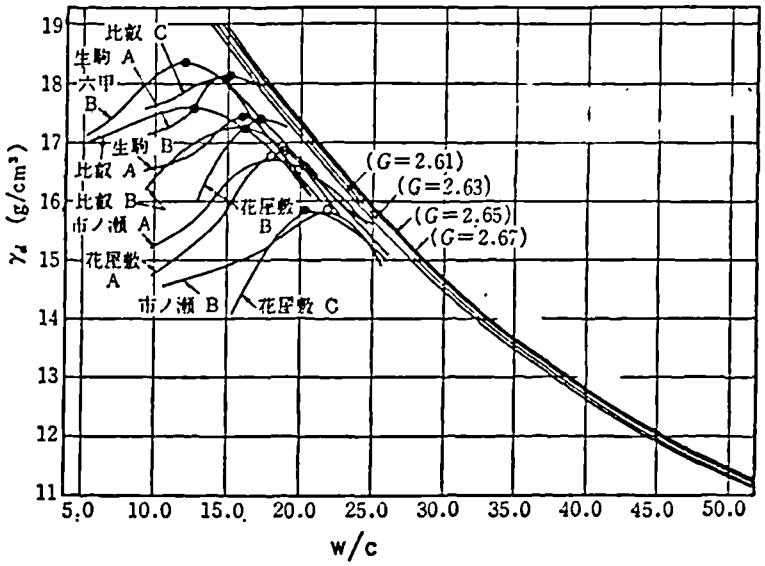

Figure 4.12 Typical compaction curves of decomposed granite soils (after JSSMFE, 1974)

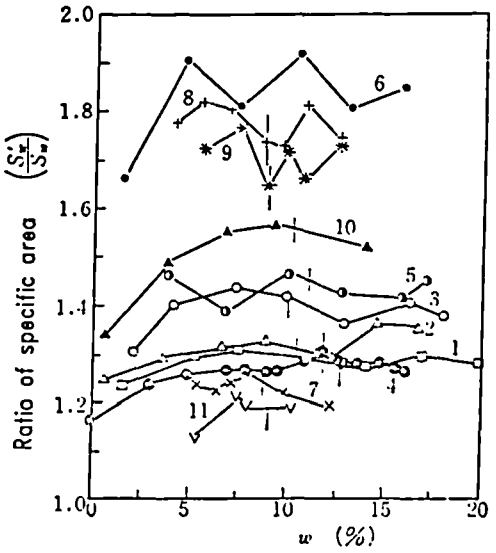

Figure 4.13
Crushing as a result of compaction (after Matsuo and Fukumoto, 1976)

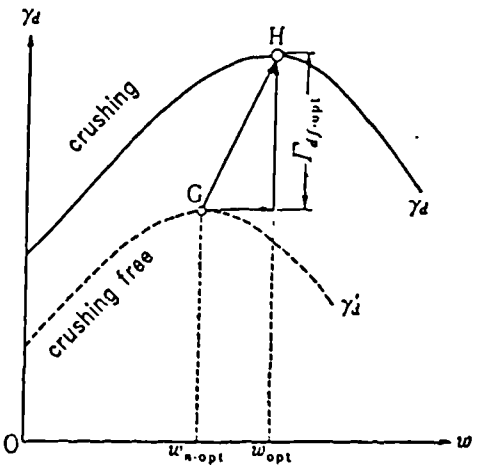

Figure 4.14
Changes of dry density and OMC as a result of crushing (after Matsuo and Fukumoto, 1977)

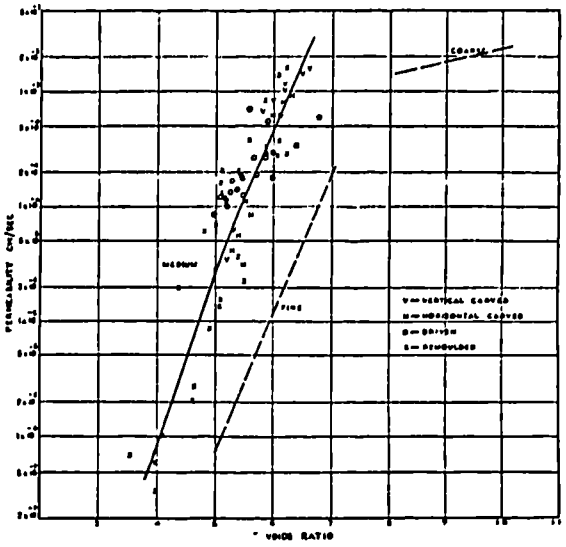

(a)

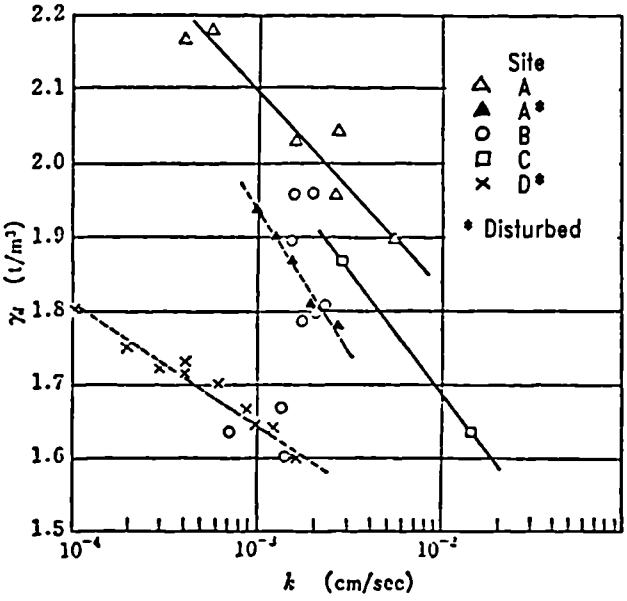

(b)

Figure 4.15 Permeability of decomposed granite soils
(a) Hong Kong (after Lumb, 1962)
(b) Japan (after JSSMFE, 1979)

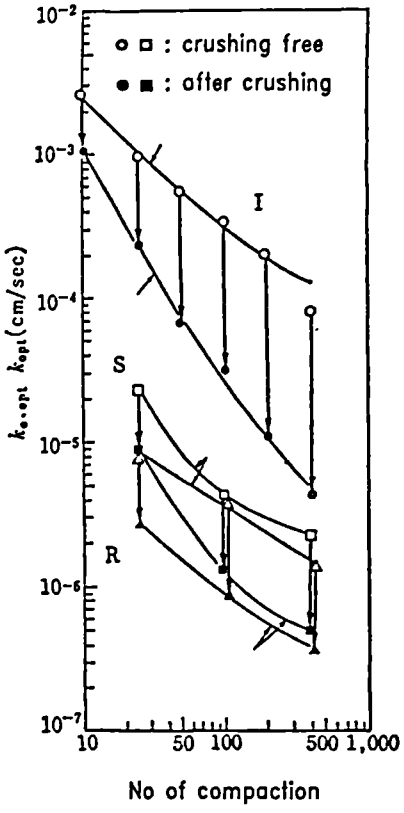

Figure 4.16 Effect of particle crushing on permeability
(after Matsuo and Fukumoto, 1977)

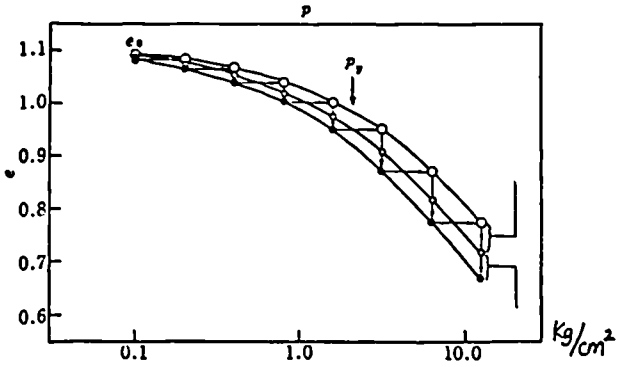

Figure 4.17 Oedometer test on undisturbed decomposed granite soil (after JSSMFE, 1979)

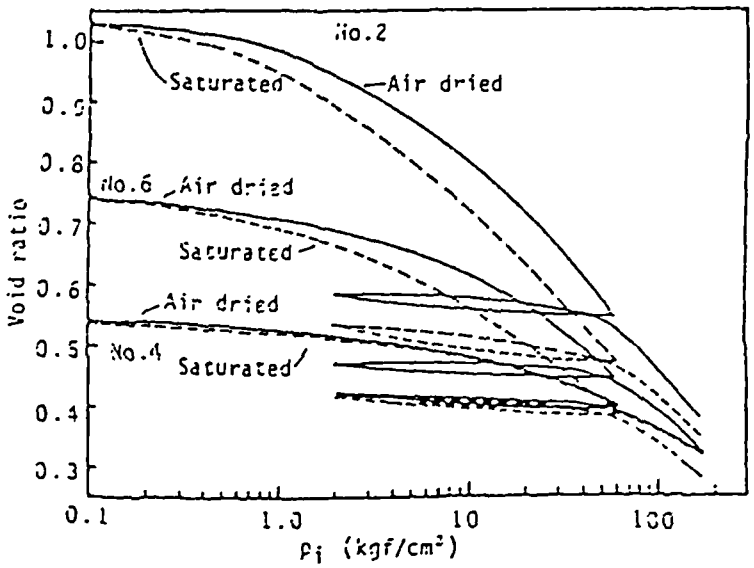

Figure 4.18 Isotropic compression of compacted samples (after Murata et al, 1985)

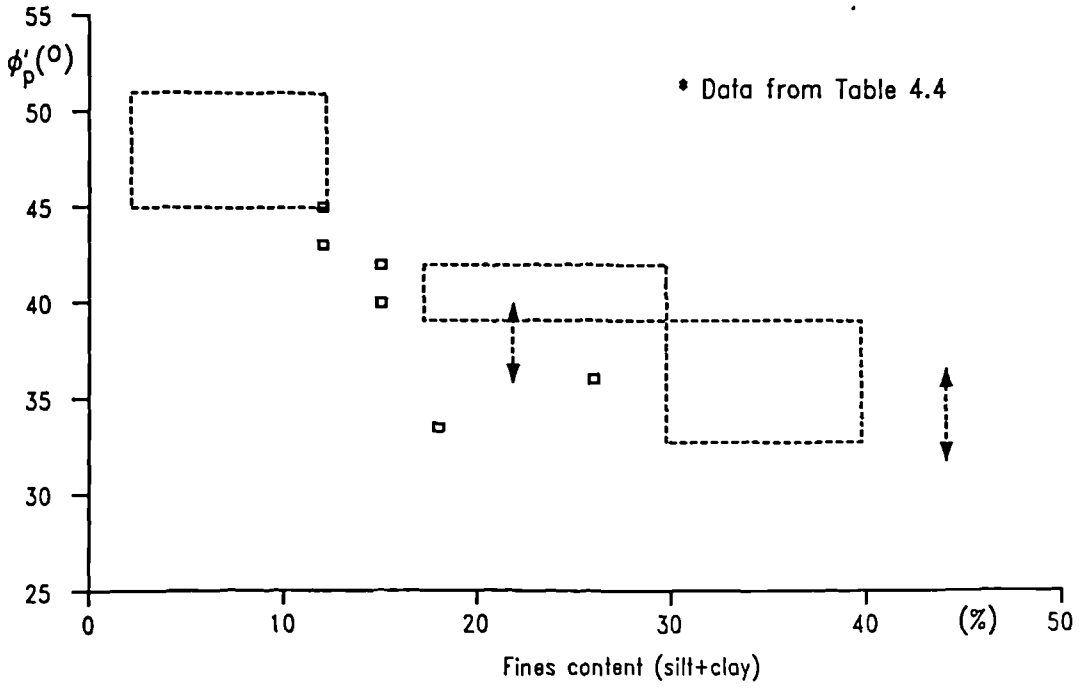

Figure 4.19 Shearing resistance and fine content

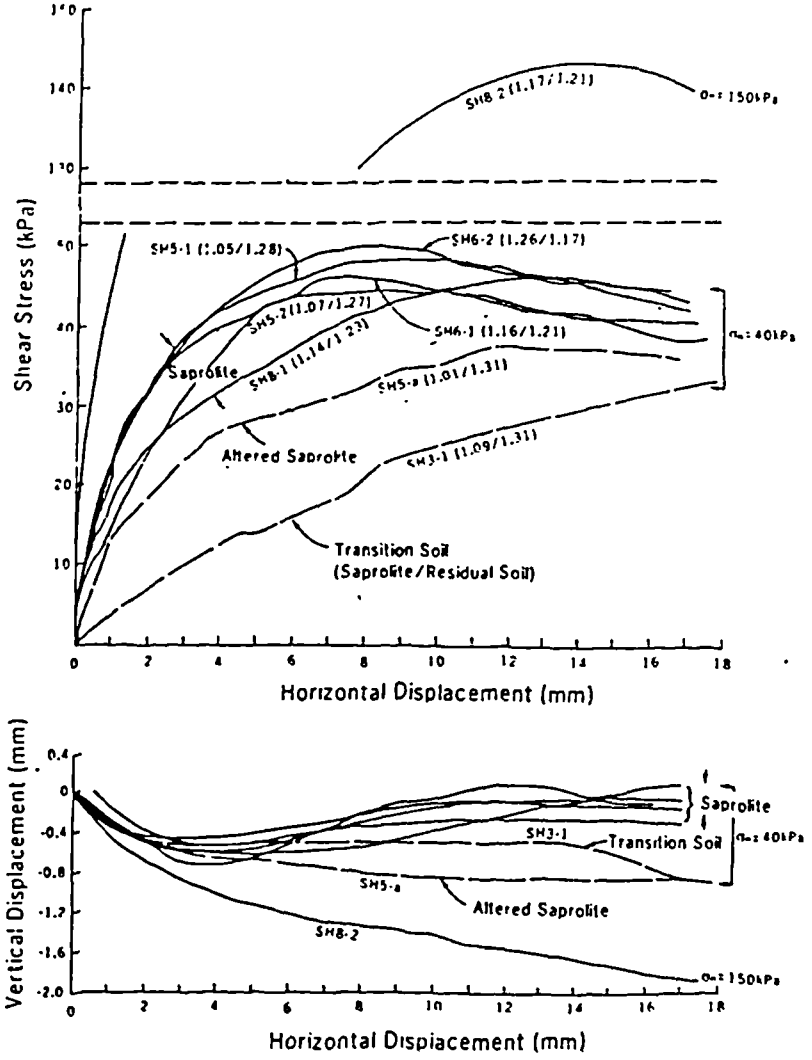

Figure 4.20 Stress–deformation curves for various decomposed granite soils (after Irfan, 1985)

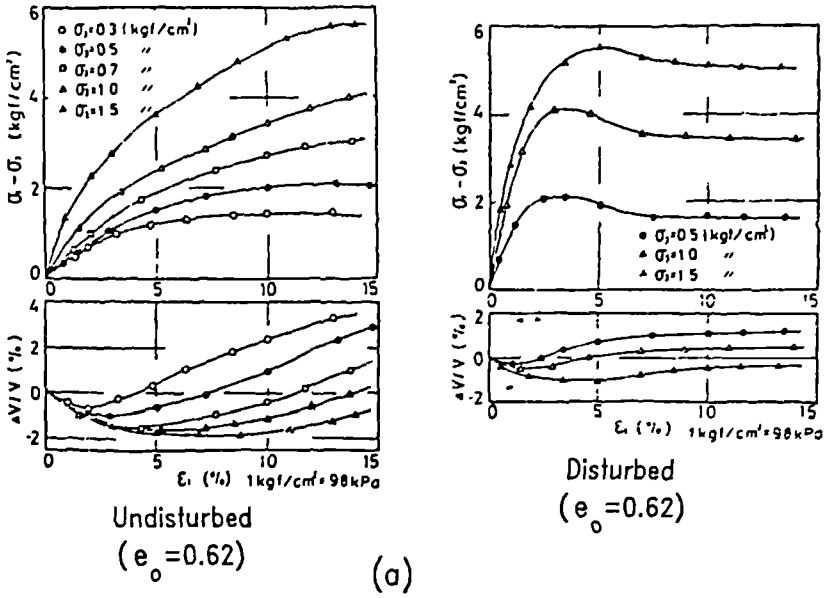

(a)

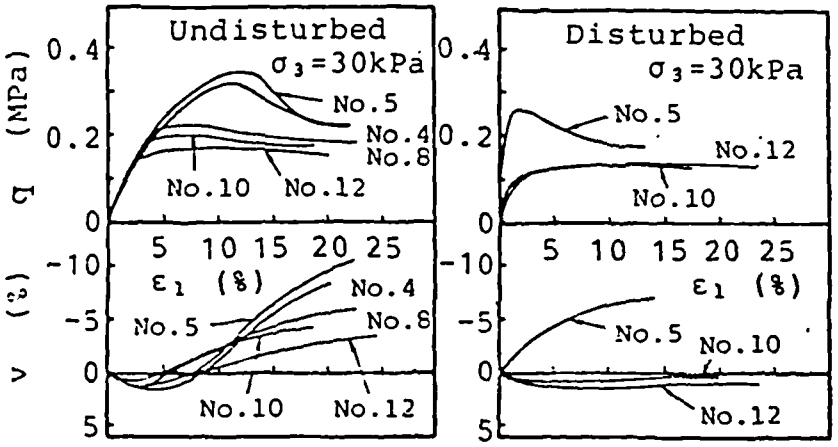

(b)

Figure 4.21 Comparision of stress–strain curves for undisturbed and disturbed samples
(a) (after Yagi and Yatabe, 1985)
(b) (after Murata and Yasufuku, 1987)

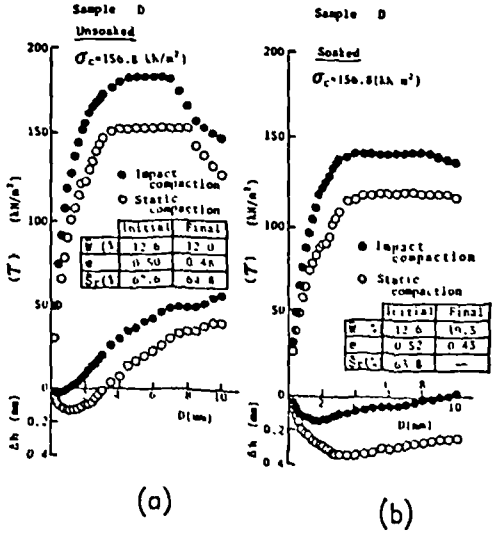

(a) (b)

Figure 4.22

Effects of soaking on stress-deformation curves
(a) unsoaked
(b) soaked
(after Onitsuka et al, 1985)

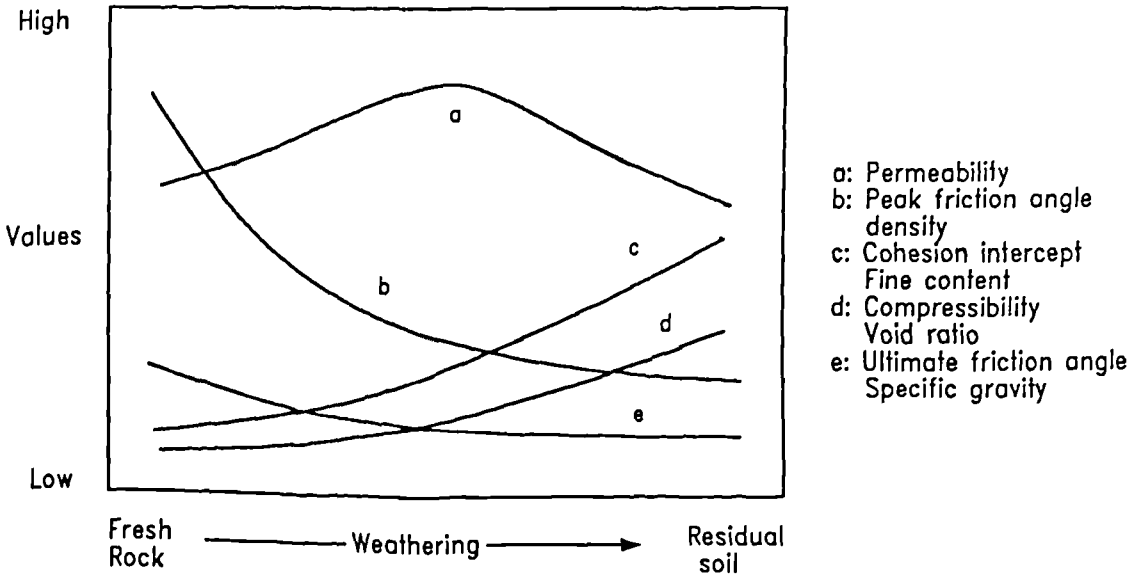

Figure 4.23 Trend of property changes caused by weathering

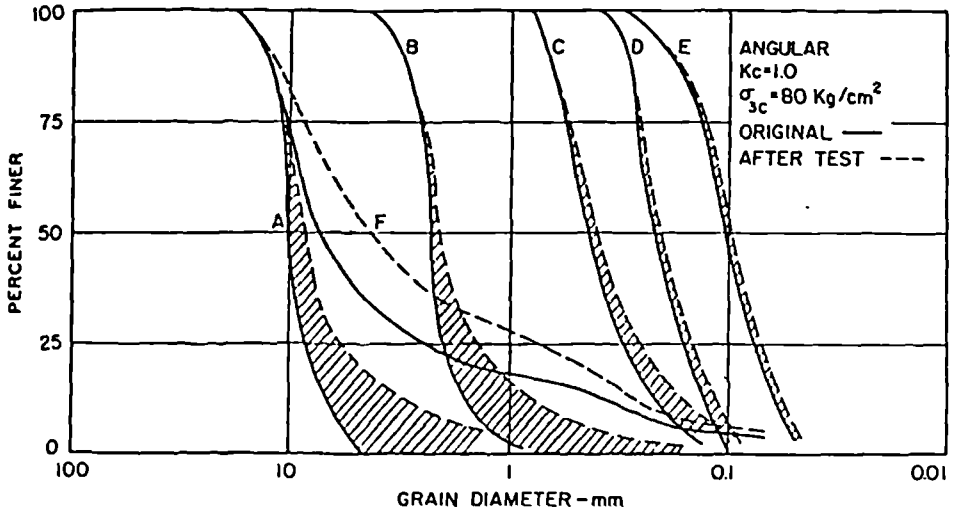

Figure 4.24 Effects of particle size on crushing (after Lee and Farhoomand, 1967)

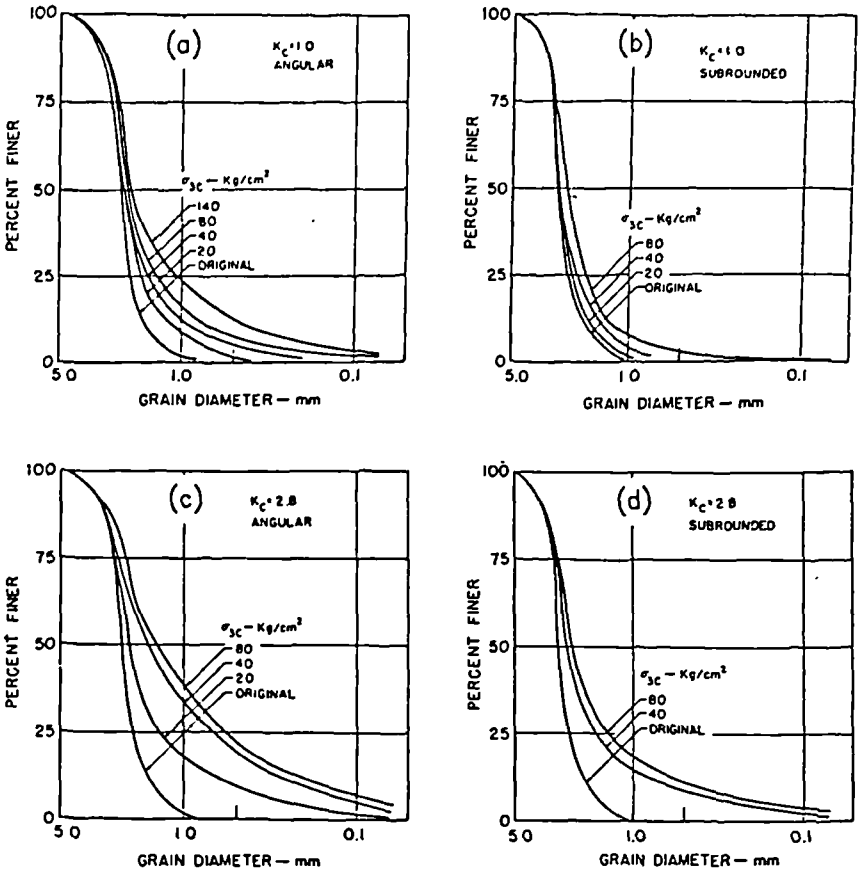

Figure 4.25 Effects of particle shape, confining stress and shear stress on crushing (after Lee and Farhoomand, 1967)

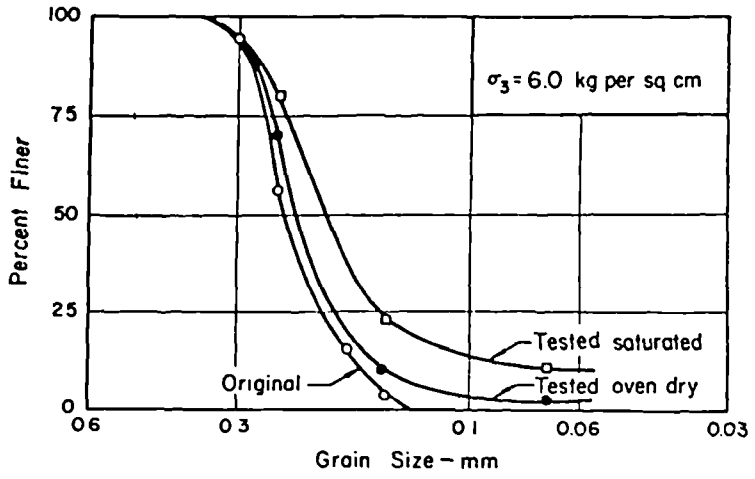

Figure 4.26 Effects of saturation on particle crushing (after Lee and Seed, 1967)

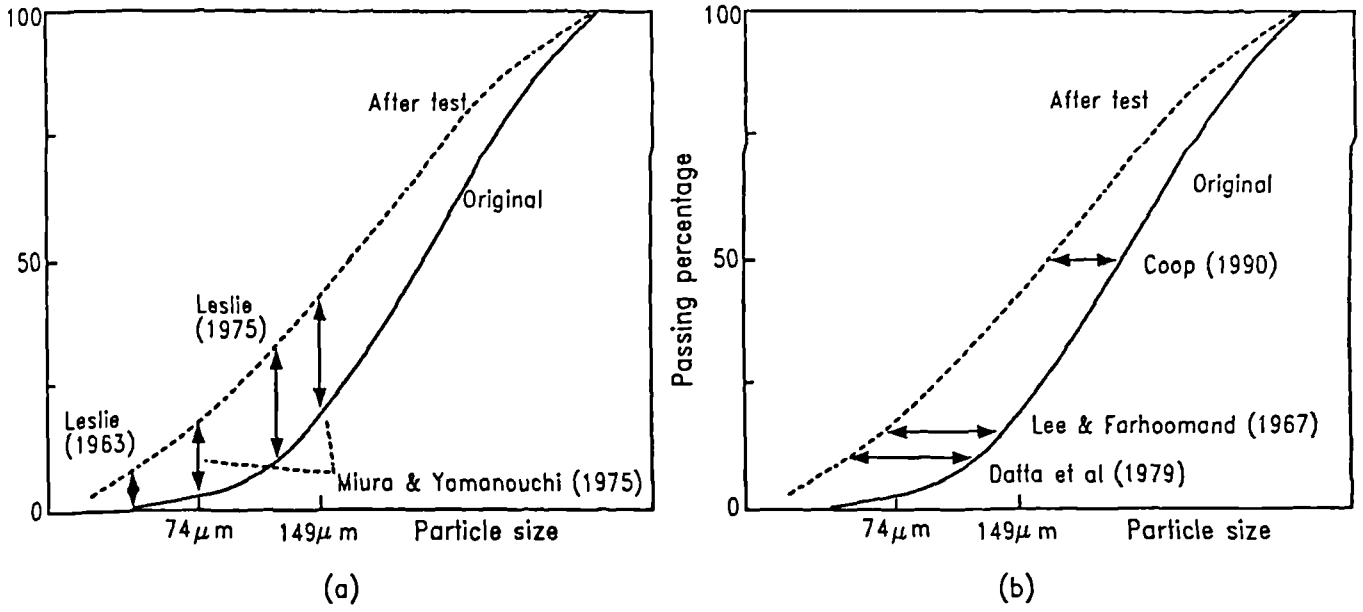

Figure 4.27 Particle crushing measurement

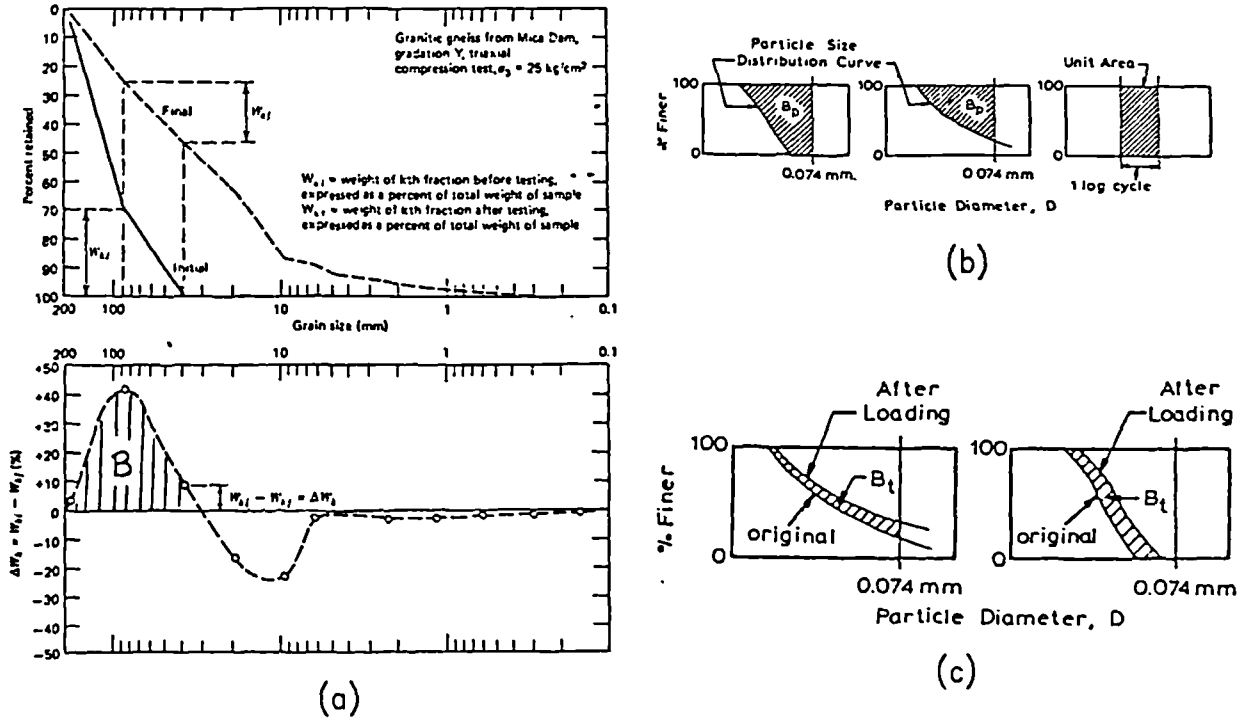

Figure 4.28 Particle crushing measurement
(a) Particle breakage B (shaded area) (after Marsal, 1975)
(b) Breakage potential B_p (after Hardin, 1985)
(c) Total breakage B_t (after Hardin, 1985)

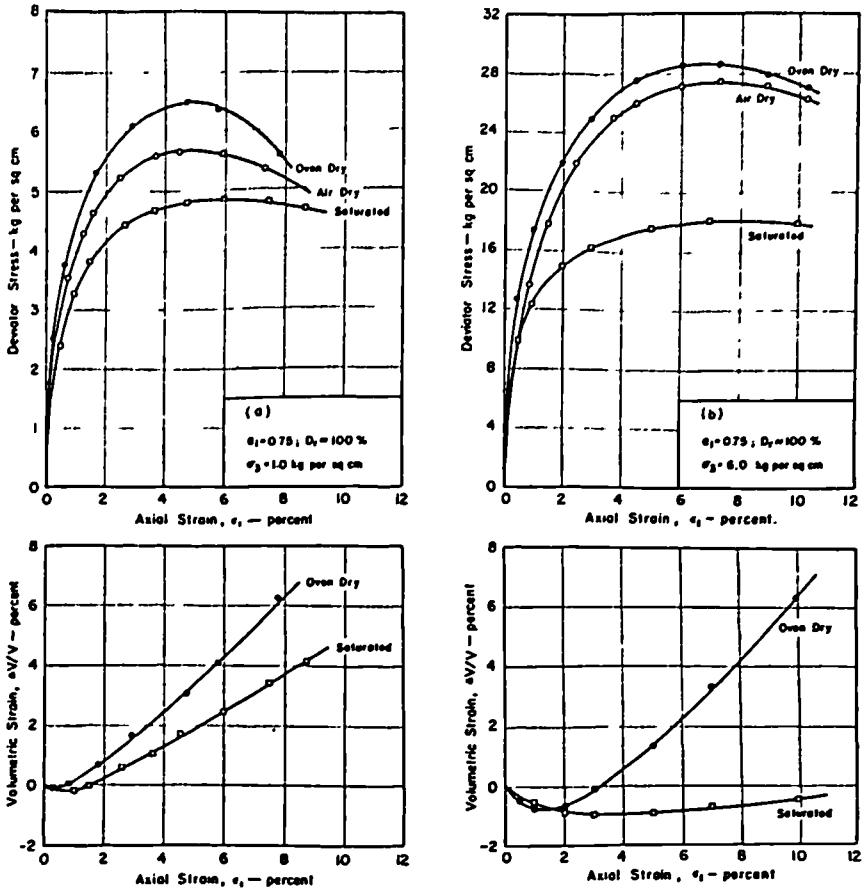

Figure 4.29 Effect of water on the stress–strain behaviour of Antioch sand (after Lee and Seed, 1967)

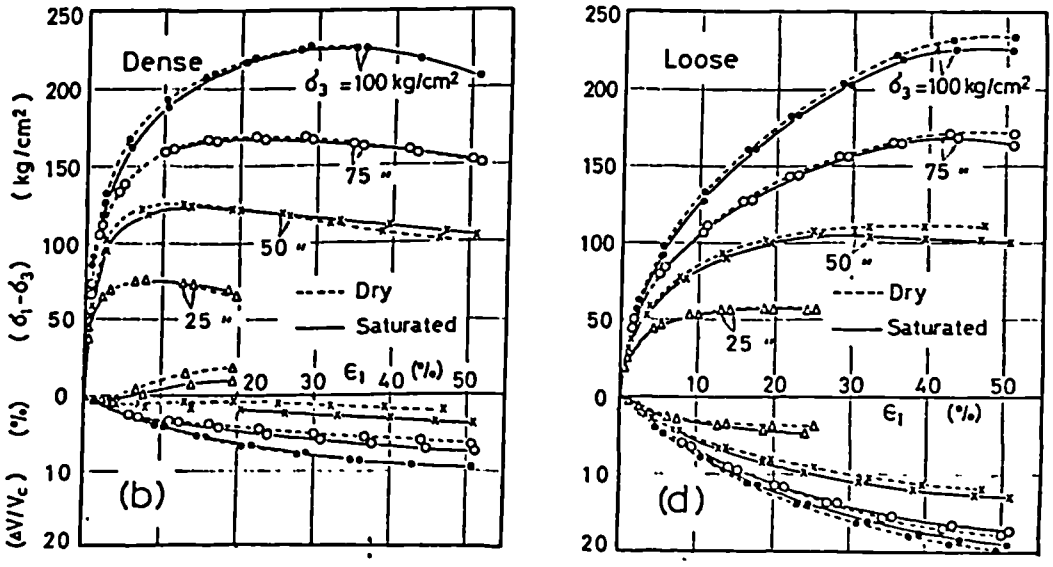

Figure 4.30 Effect of water on the stress–strain behaviour of Toyoura sand (after Miura and Yamanouchi, 1975)

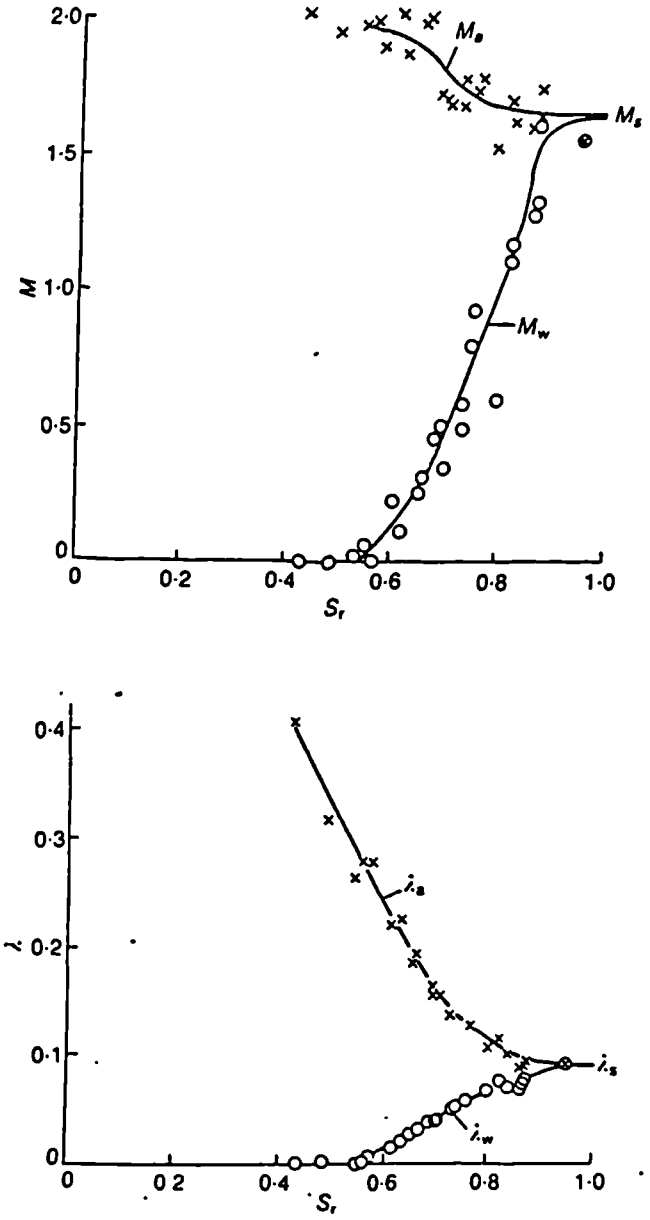

Figure 4.31 Variation of M and λ parameters at critical state with degree of saturation (after Toll, 1990)

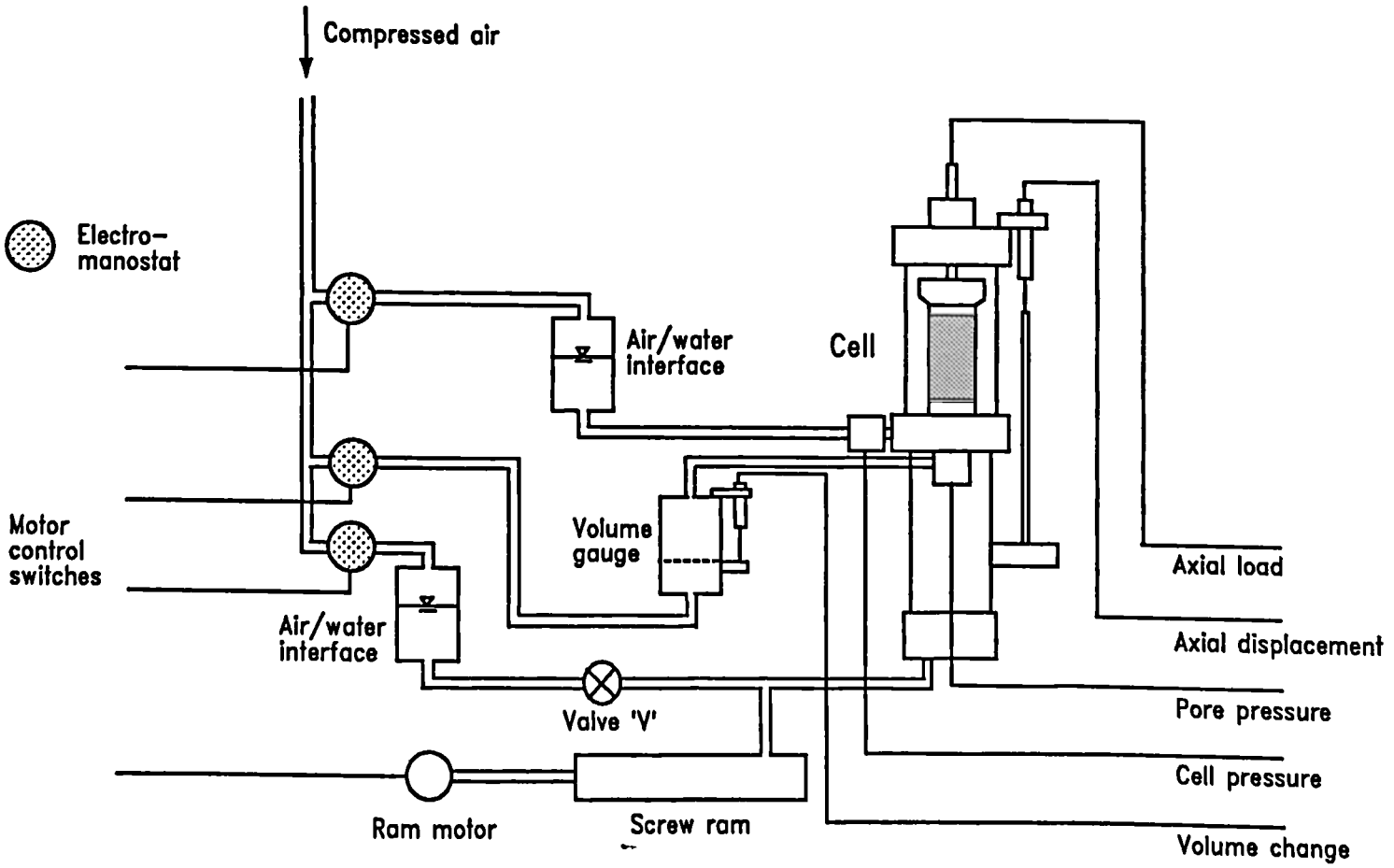

Figure 5.1 Hydraulic triaxial cell for stress path tests

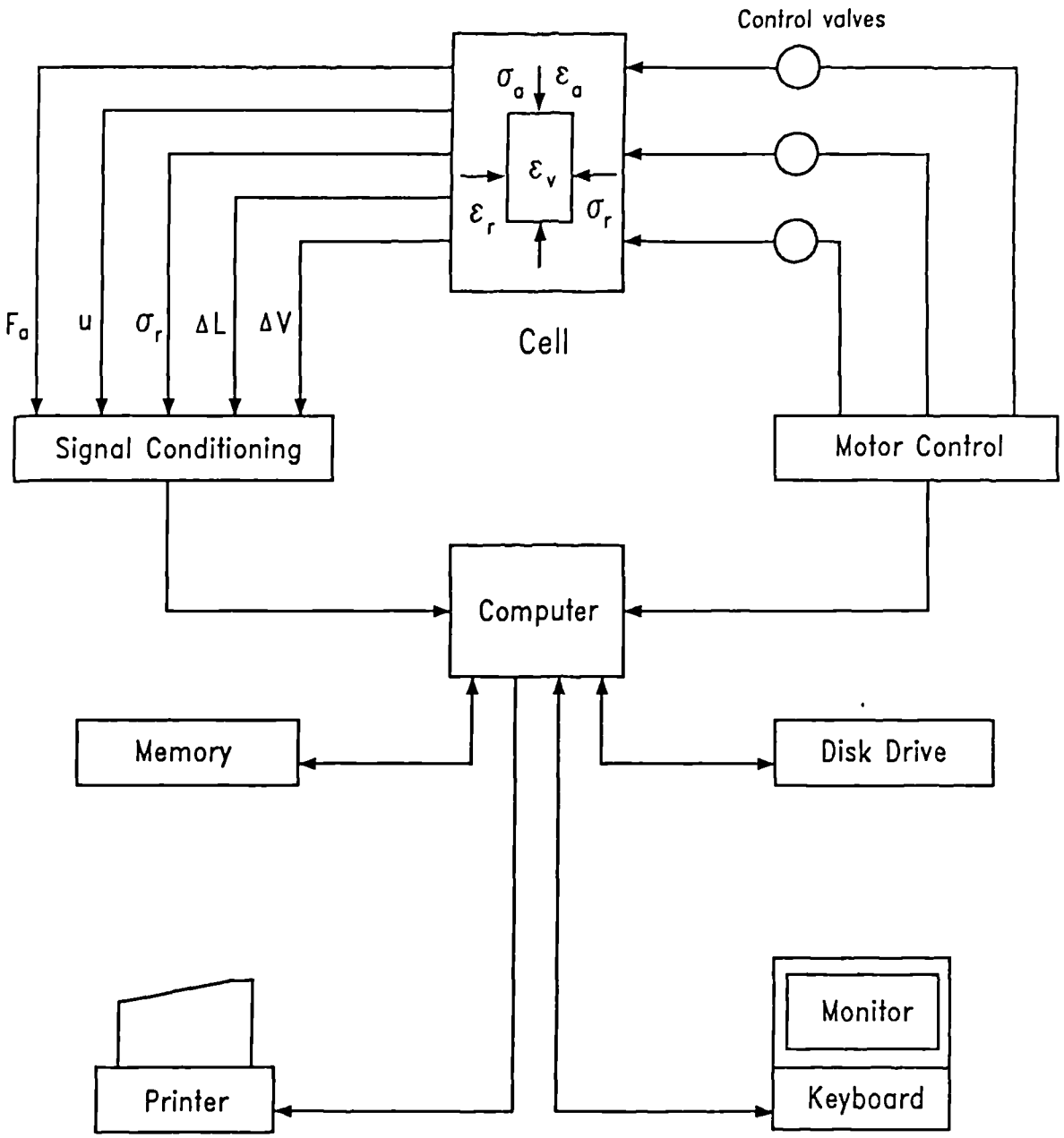

Figure 5.2 Stress path test control system

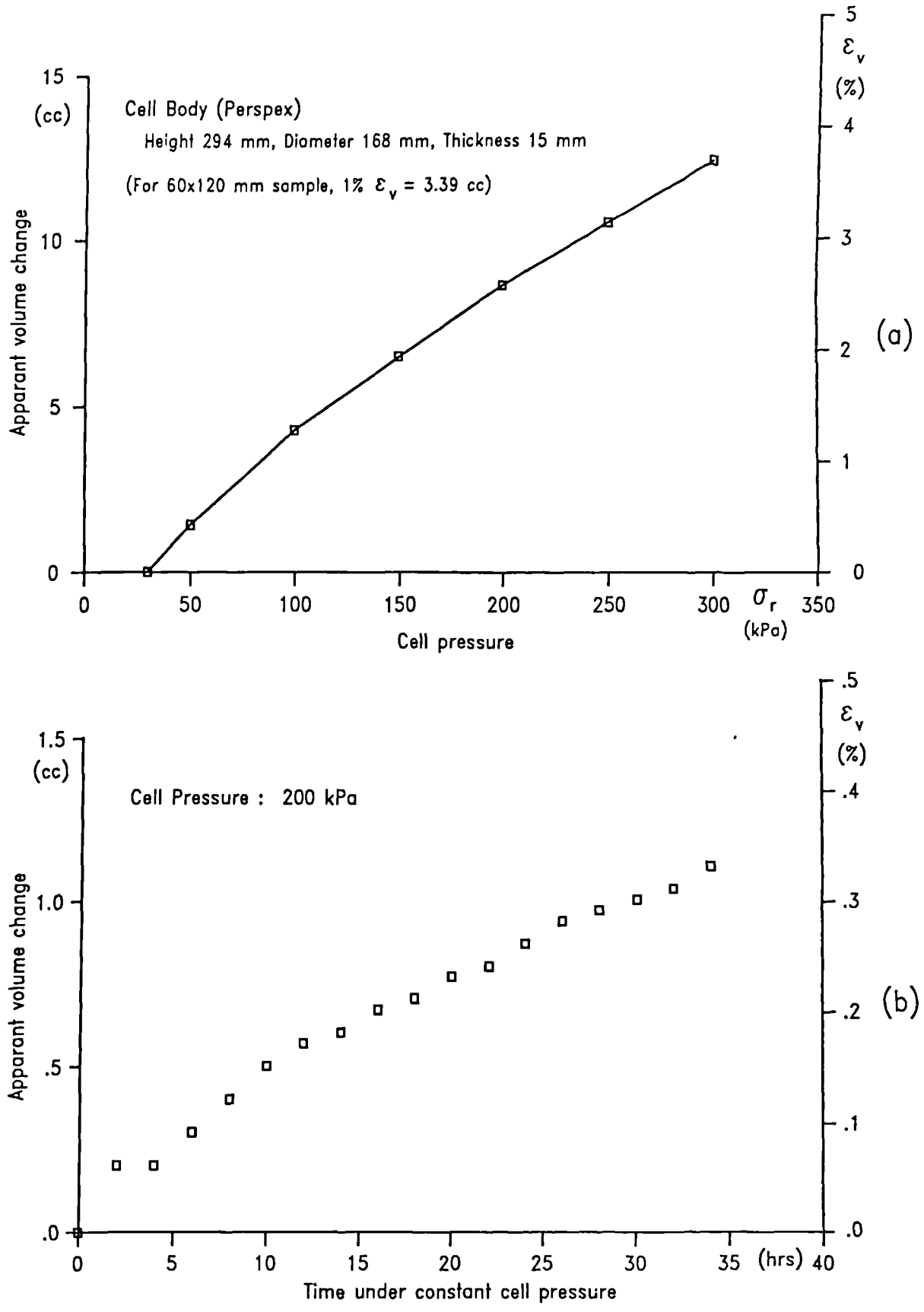

Figure 5.3 Triaxial cell volume changes with (a) pressure changes, (b) time

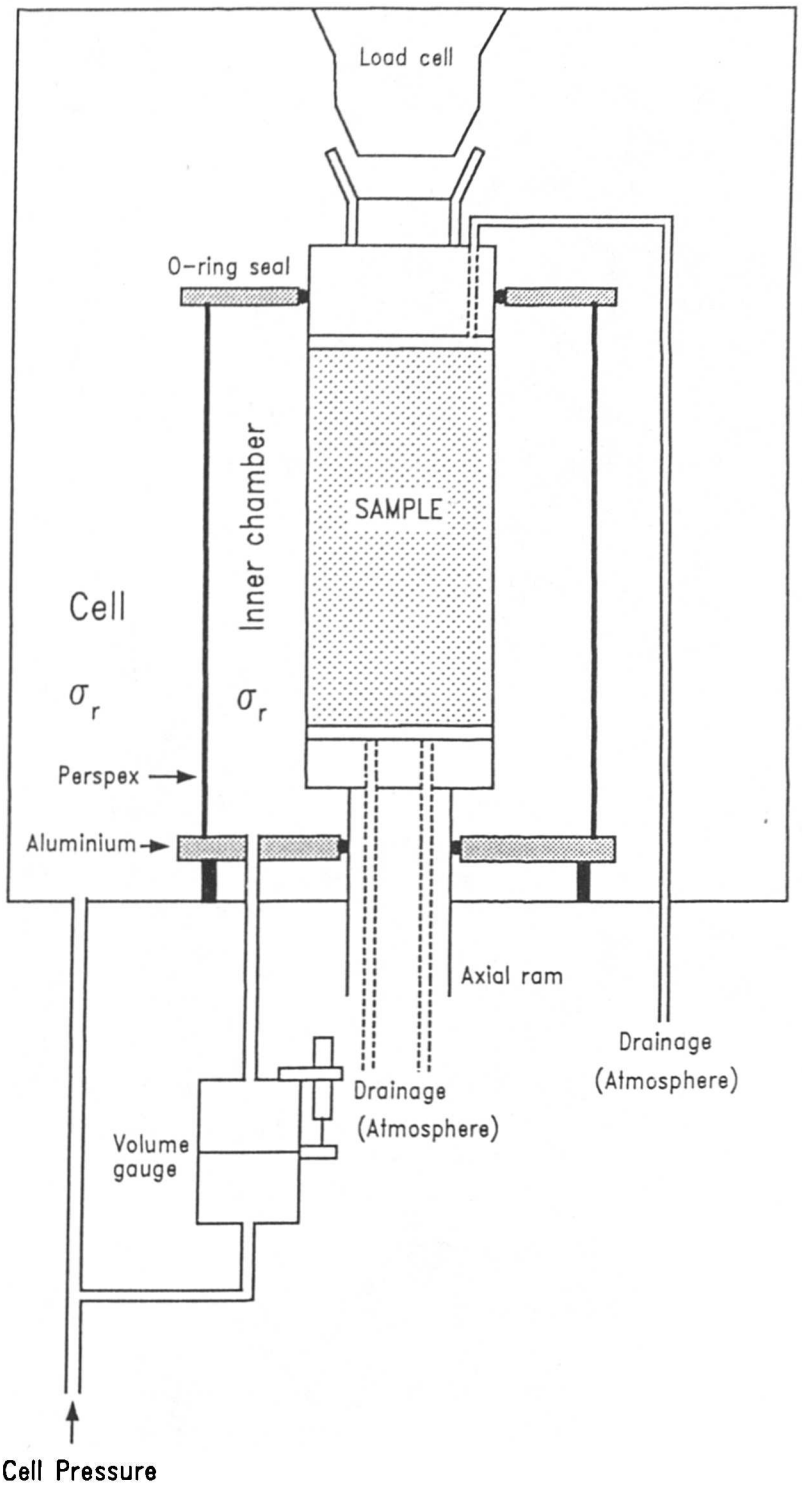

Figure 5.4 Diagrammatic plan of the inner chamber system

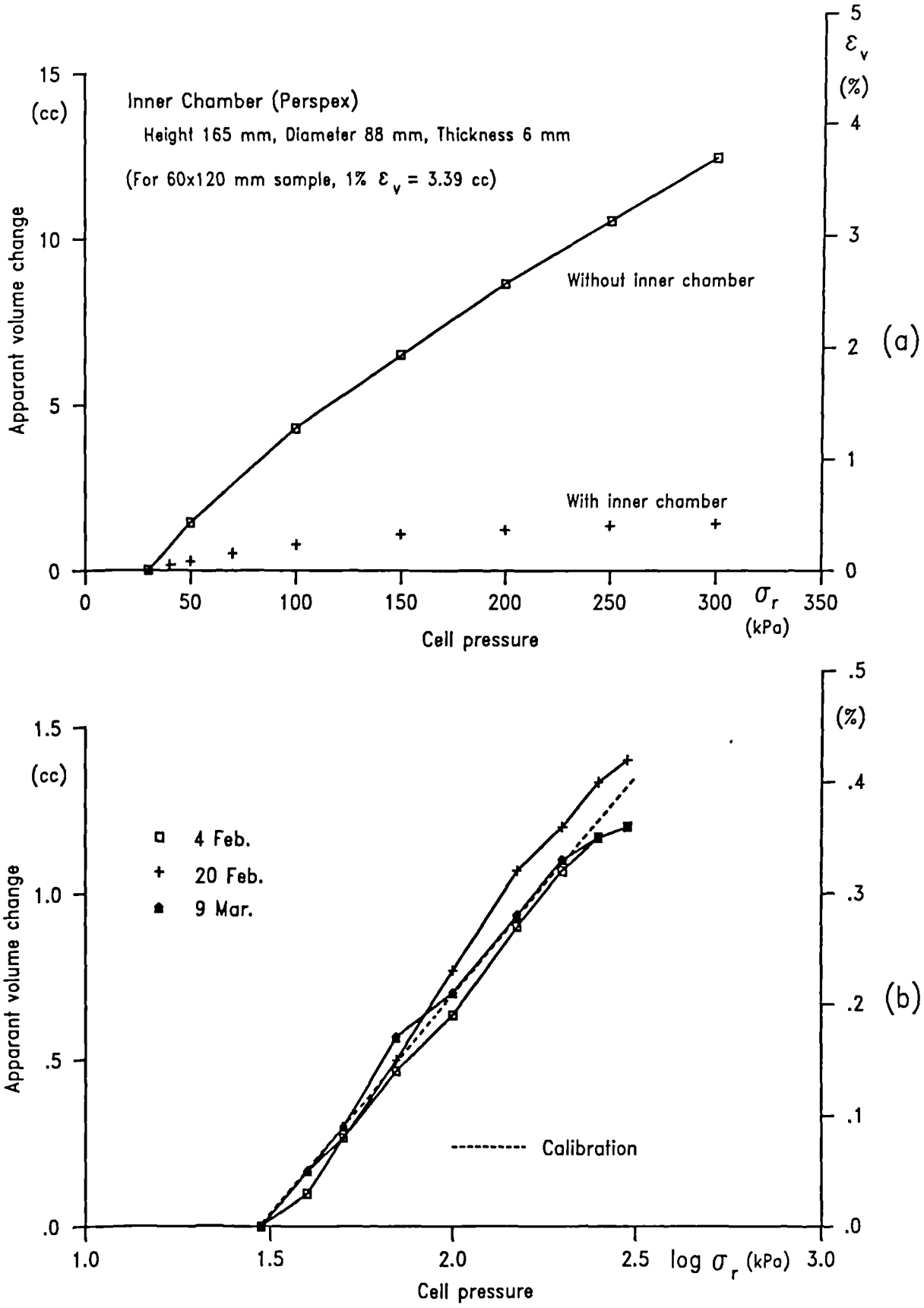

Figure 5.5 Triaxial cell volume changes with inner chamber (continued)

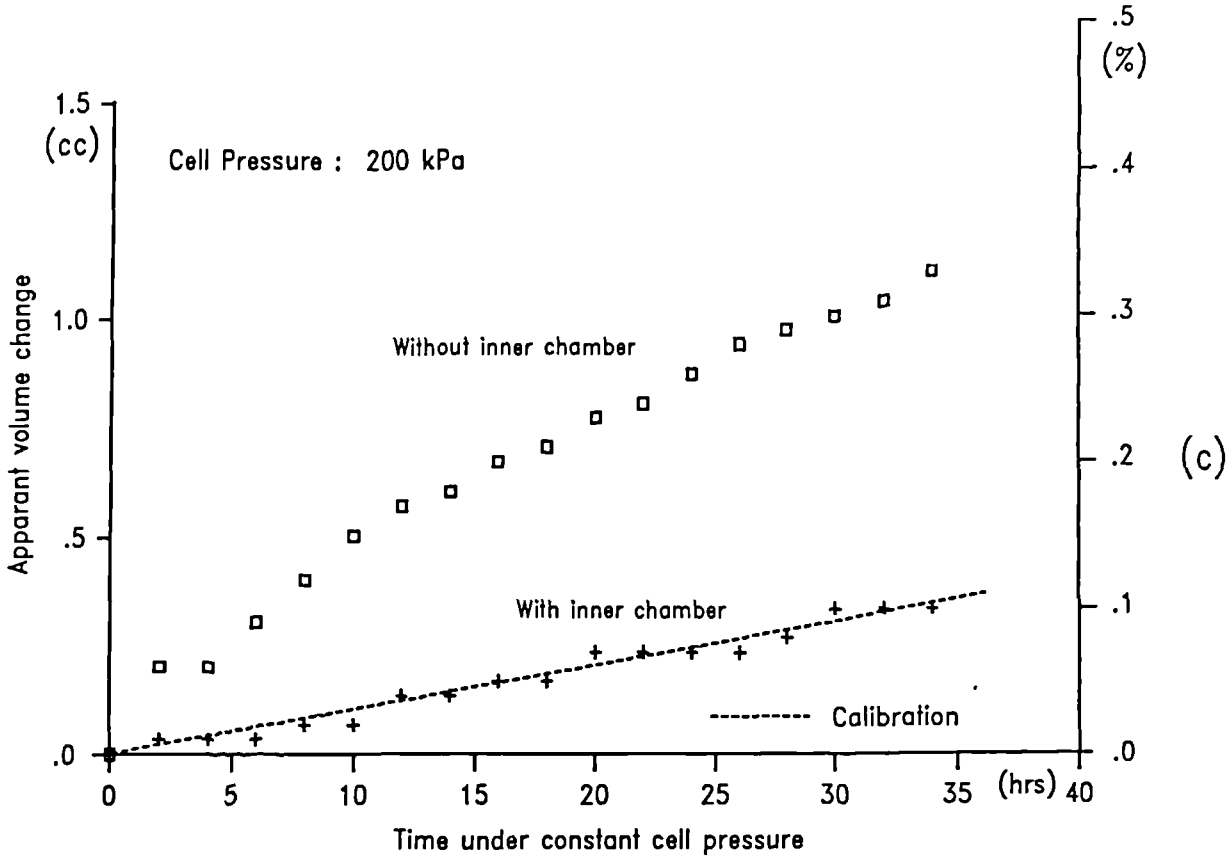

Figure 5.5 Triaxial cell volume changes with inner chamber with (a) and (b) pressures changes, (c) time

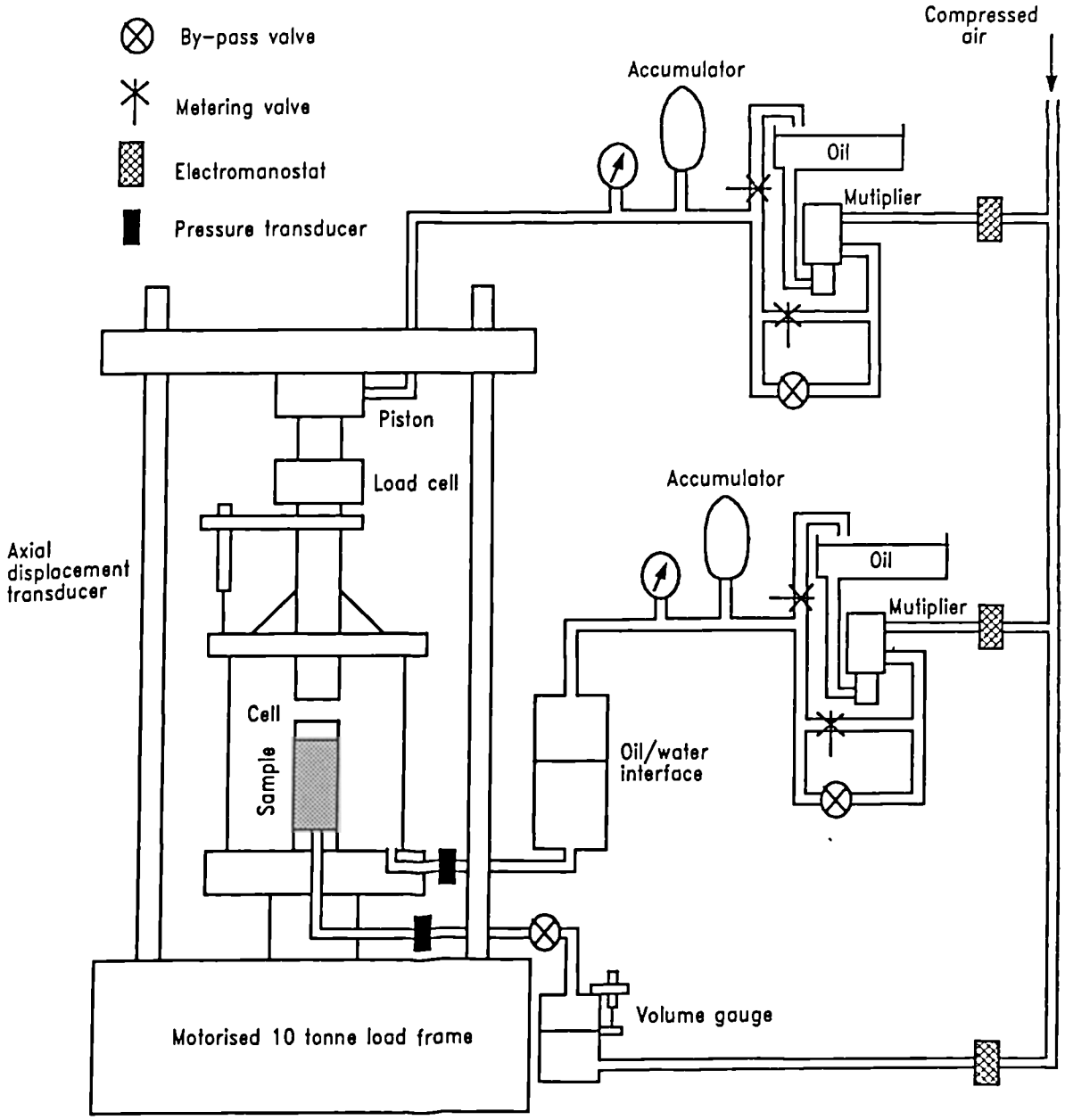

Figure 5.6 High pressure triaxial apparatus

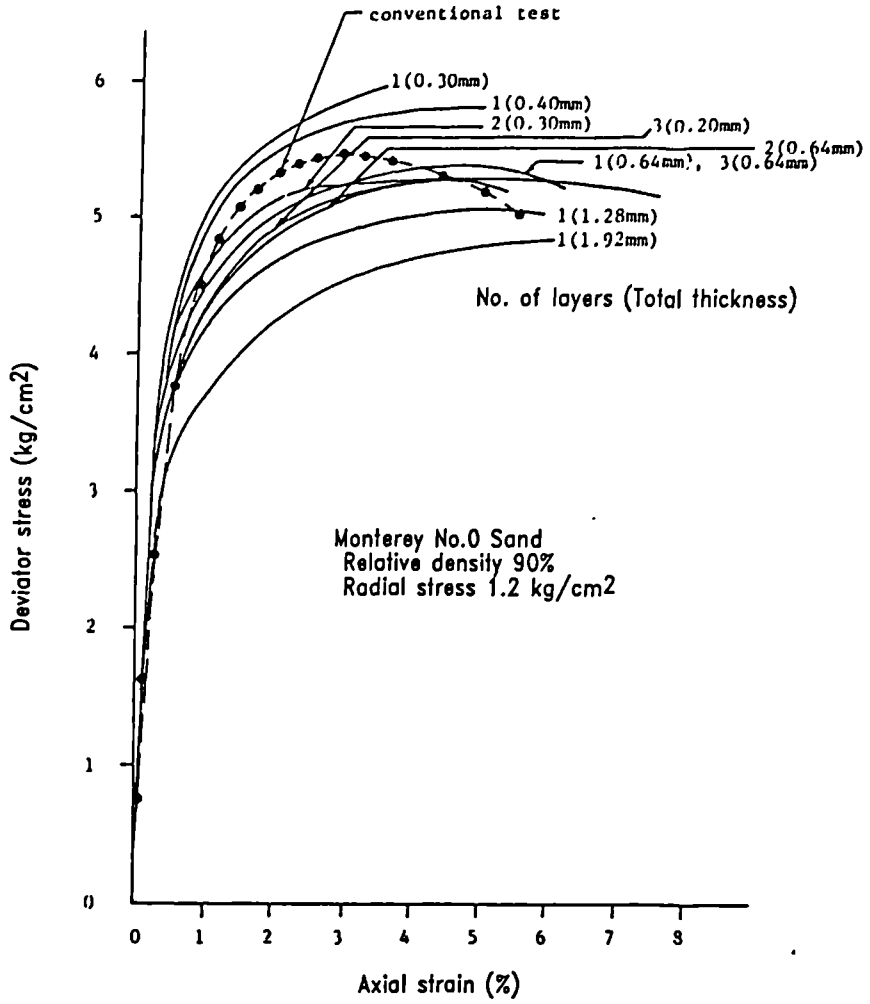

Figure 5.7 Influence of number and thickness of lubricated layers on the results of drained triaxial tests (after Norris, 1981)

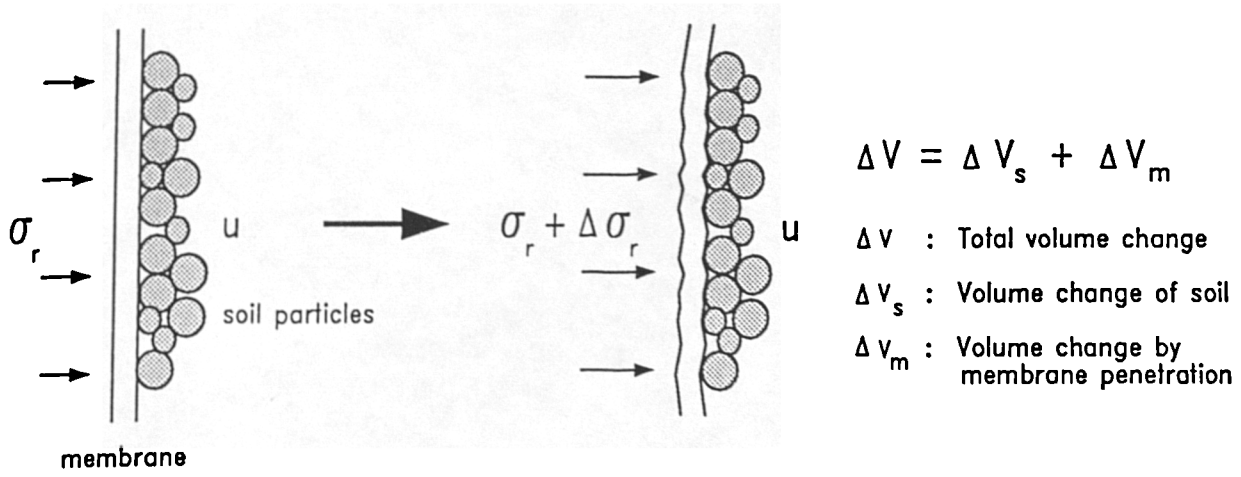

Figure 5.8 Membrane penetration due to the change of effective radial stress

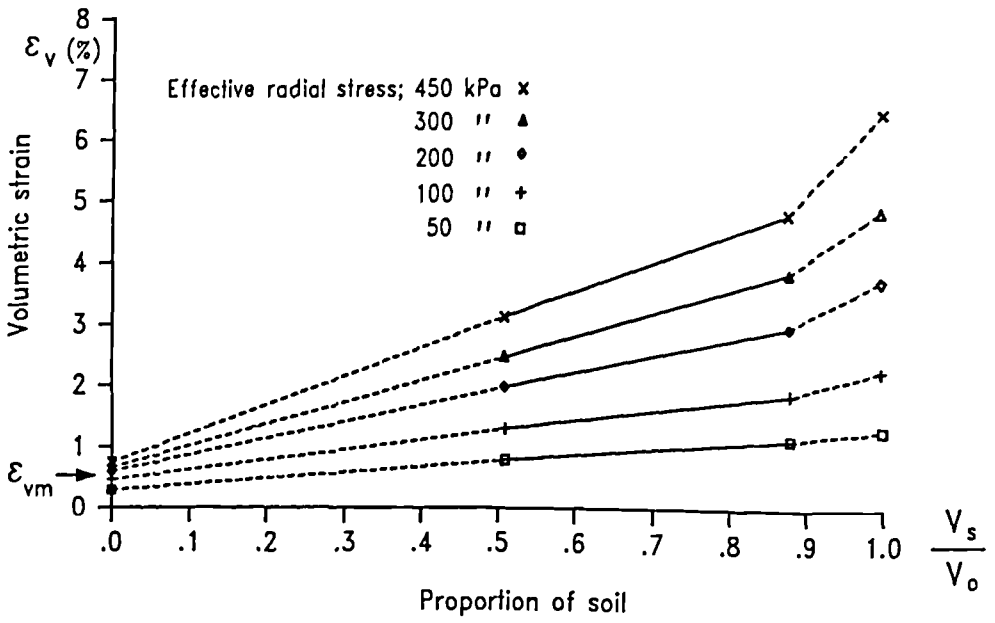

Figure 5.9 Volumetric strain resulting from membrane penetration

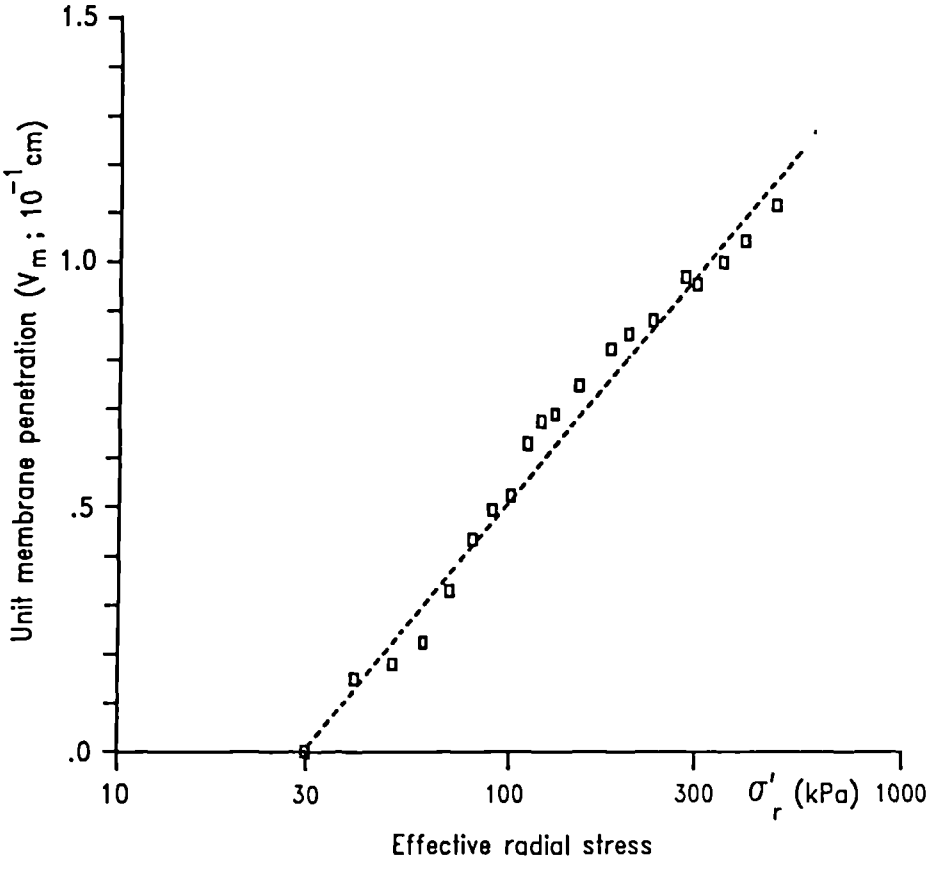

Figure 5.10 Unit membrane penetration and effective radial stress

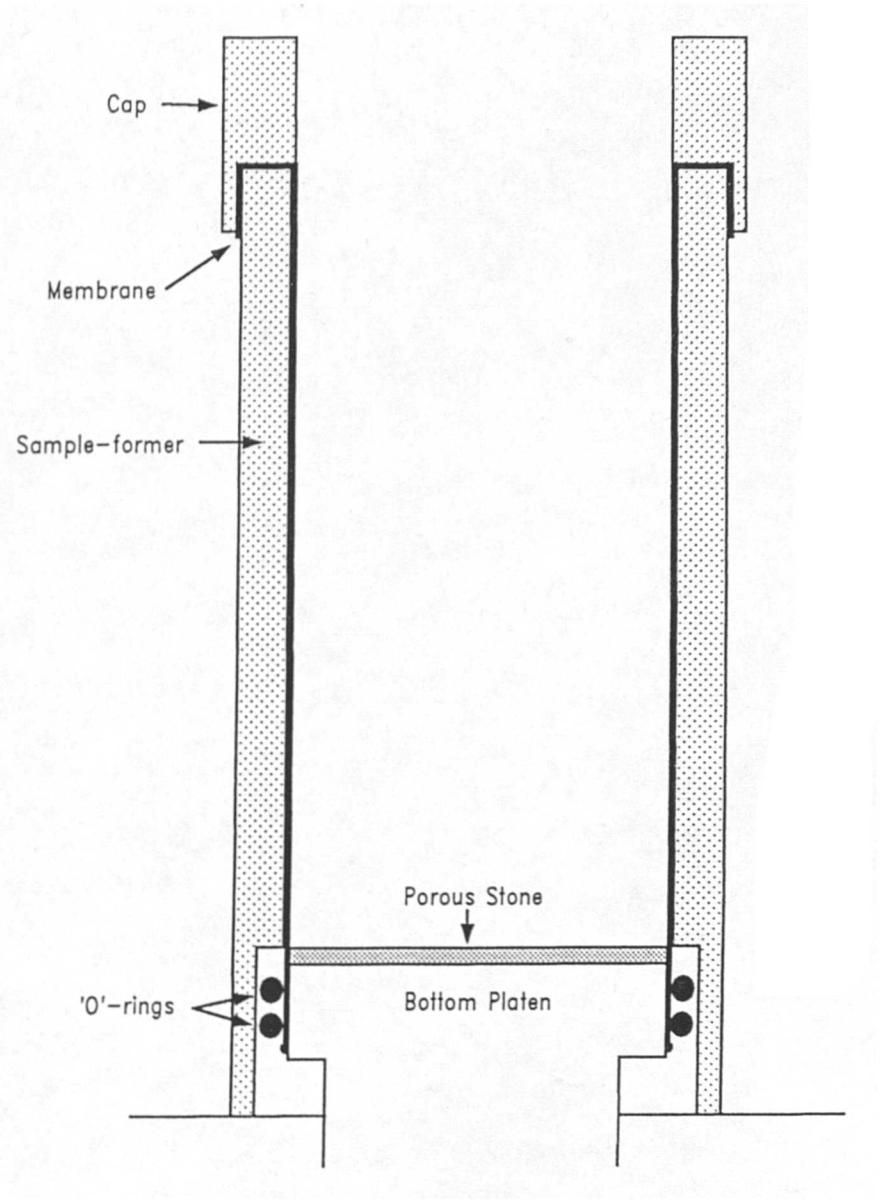

Figure 5.11 Sample former on the bottom platen

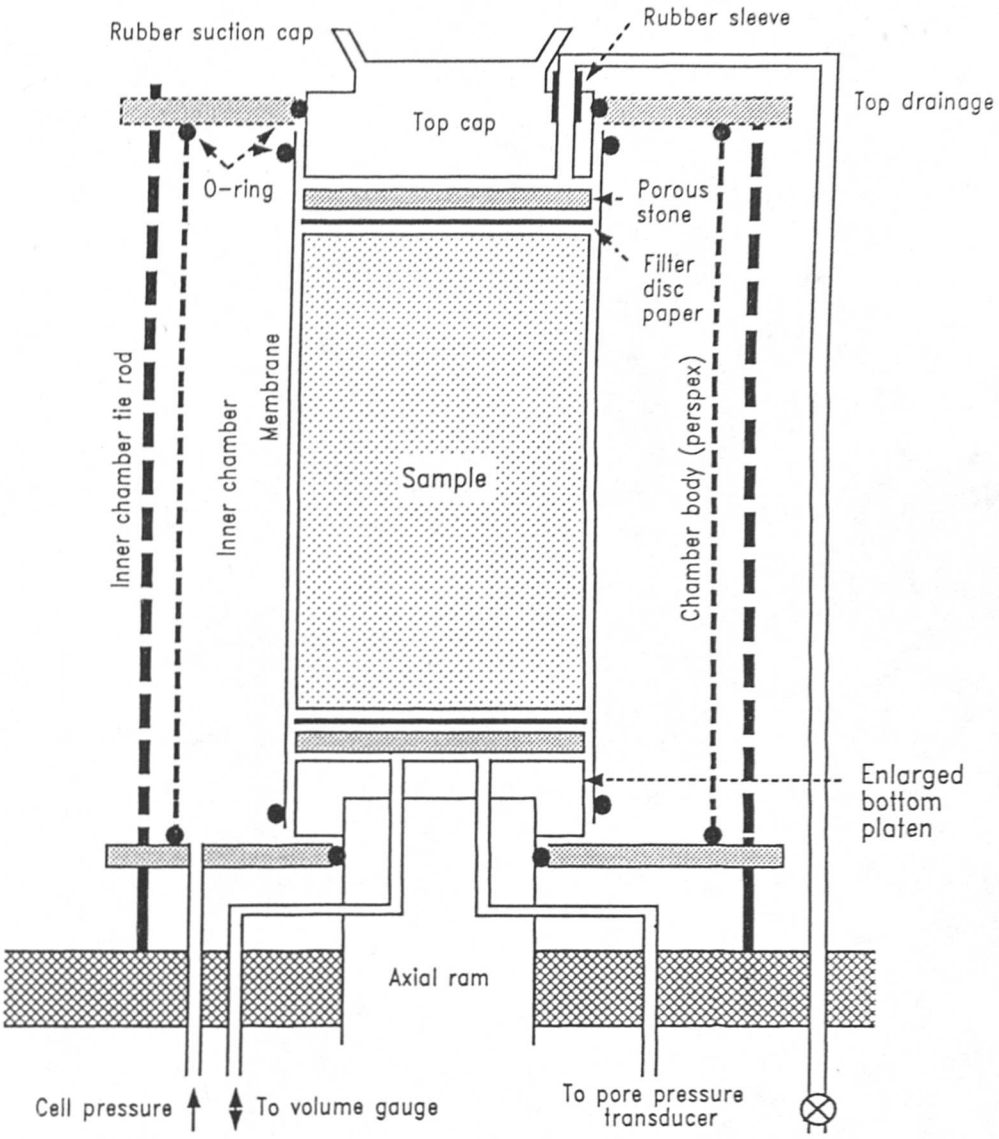

Figure 5.12 Diagrammatic view of sample set-up on the cell base

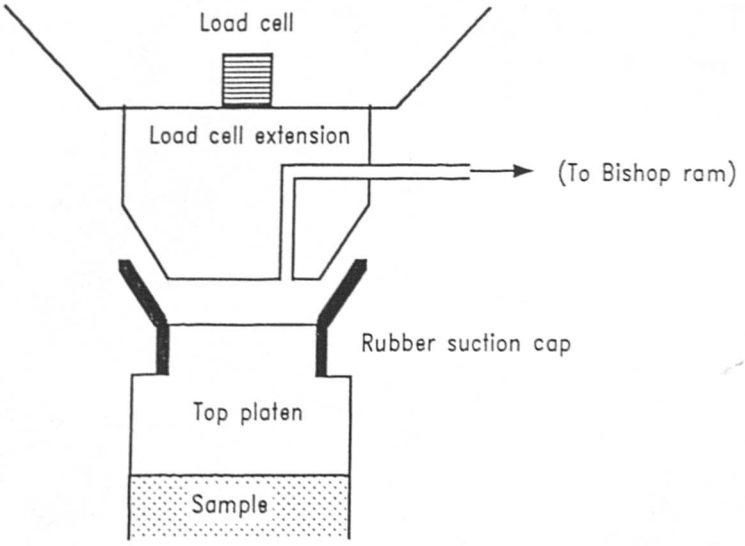

Figure 5.13 Suction cap arrangement

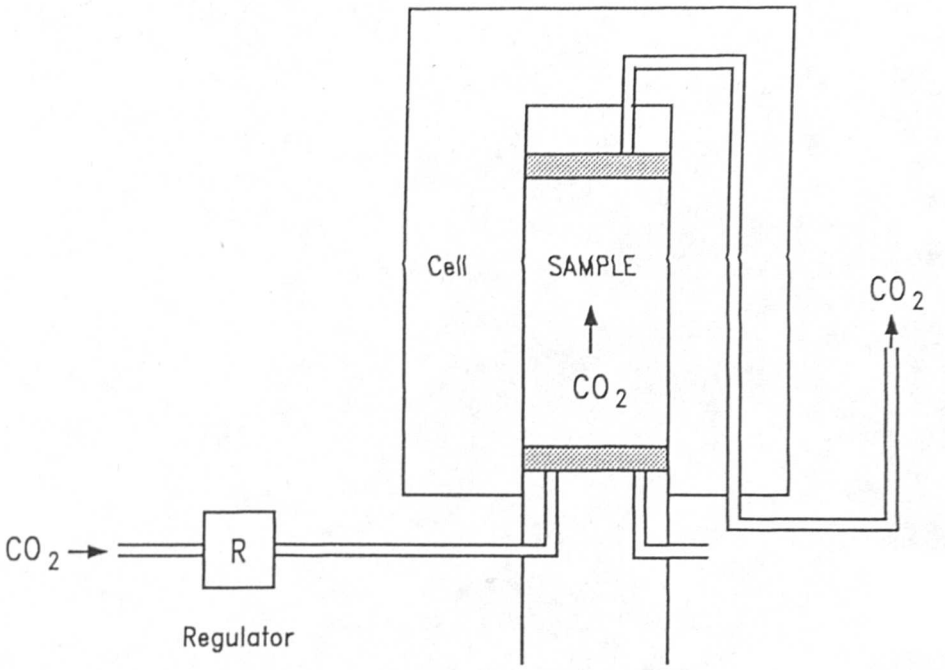

(a)

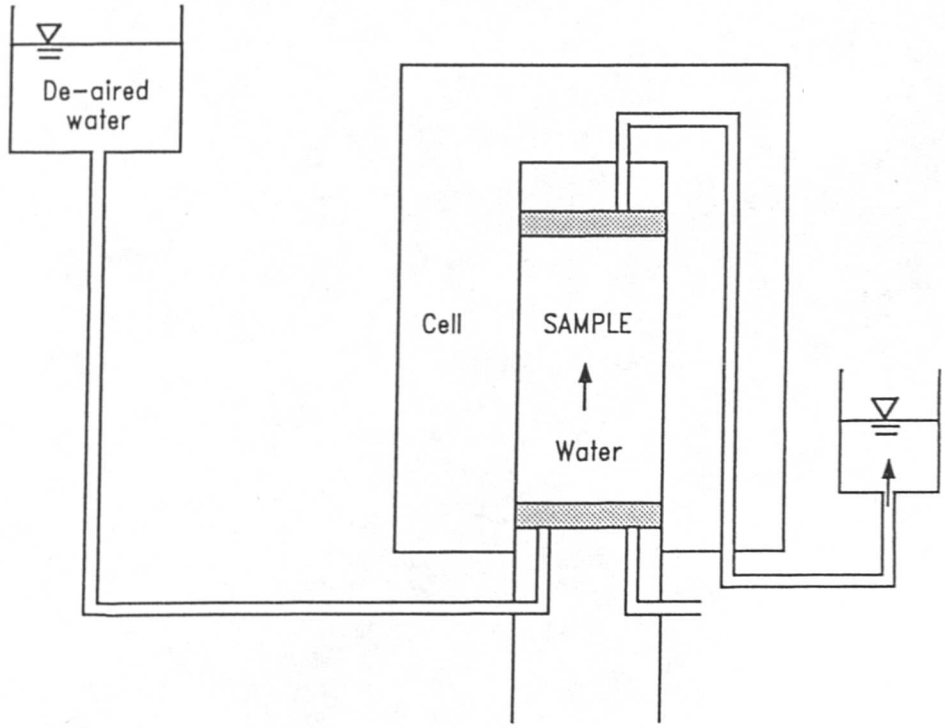

(b)

Figure 5.14 Sample saturation arrangement
(a) CO_2 circulation
(b) De-aired water circulation

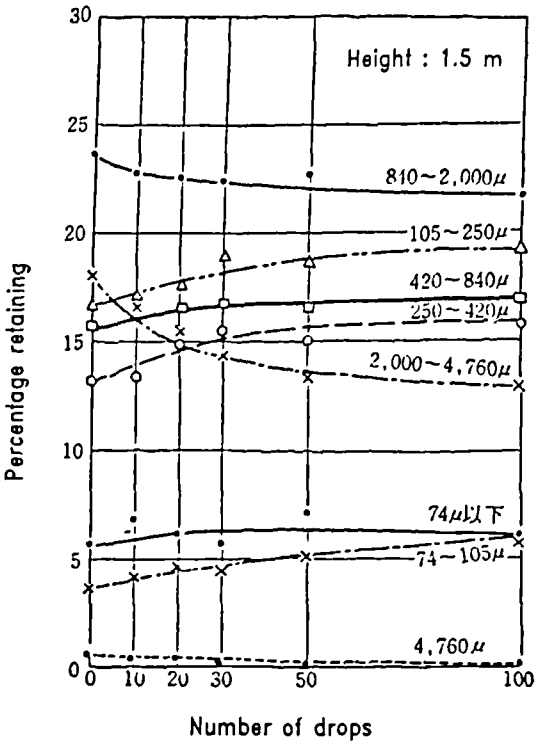

Figure 6.1 Relationship between the grading changes and the number of drops (after JSSMFE, 1982)

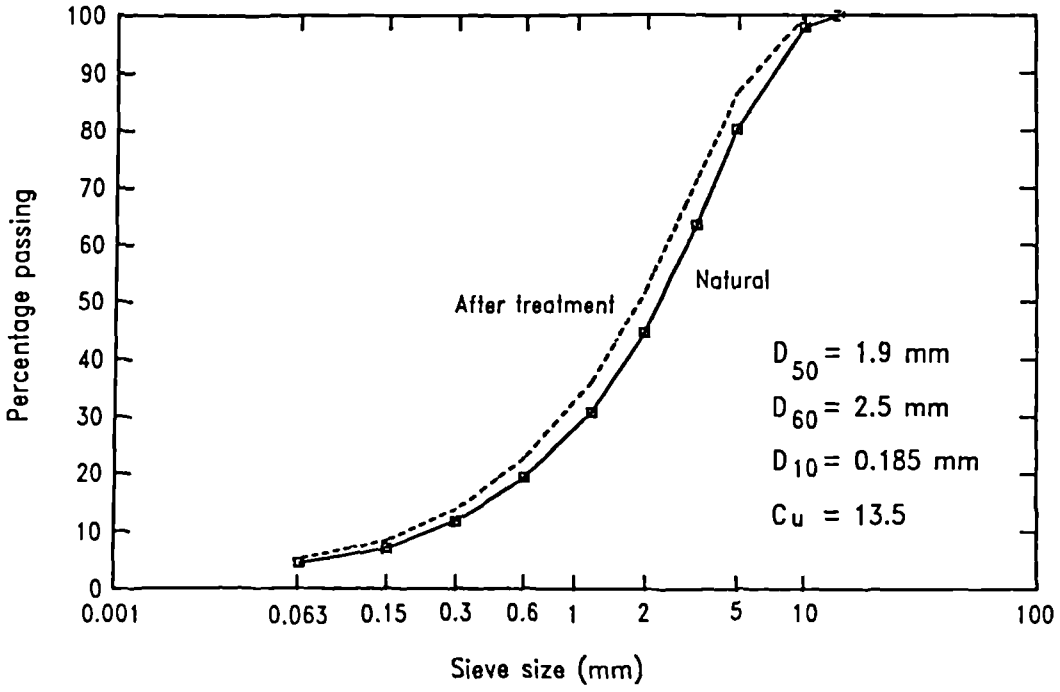

Figure 6.2 Particle size distribution

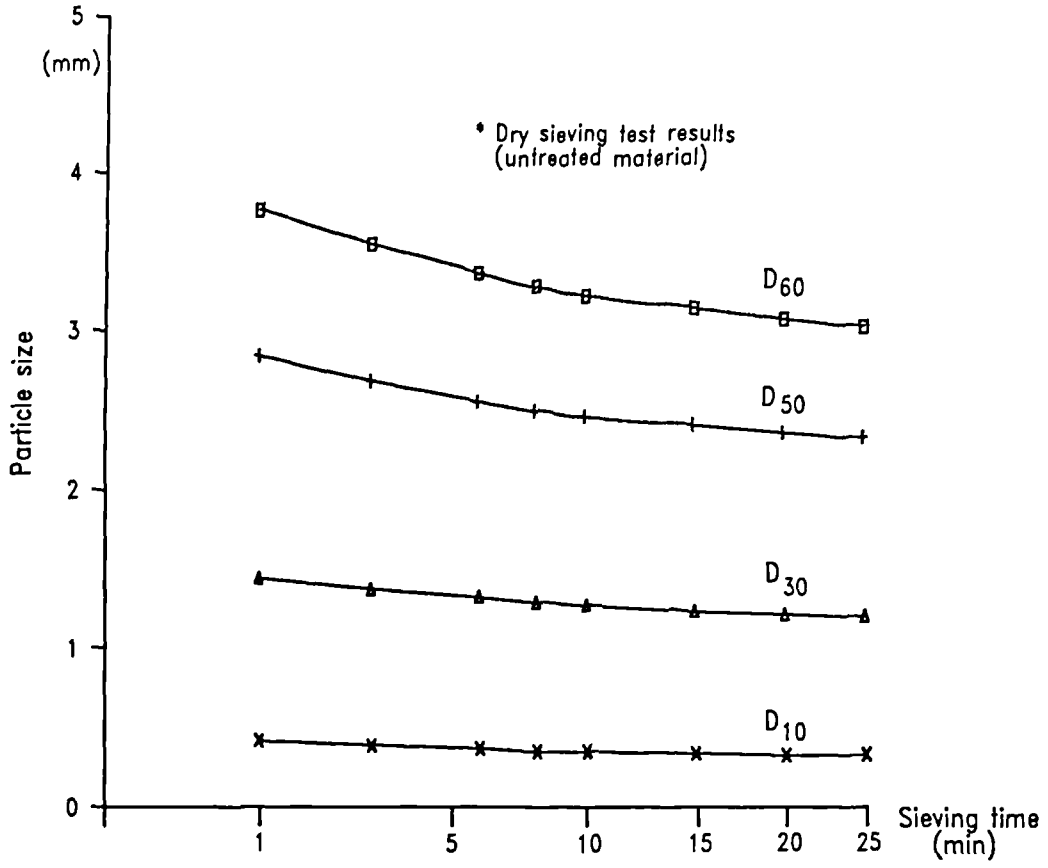

Figure 6.3 Grading changes resulting from sieving time

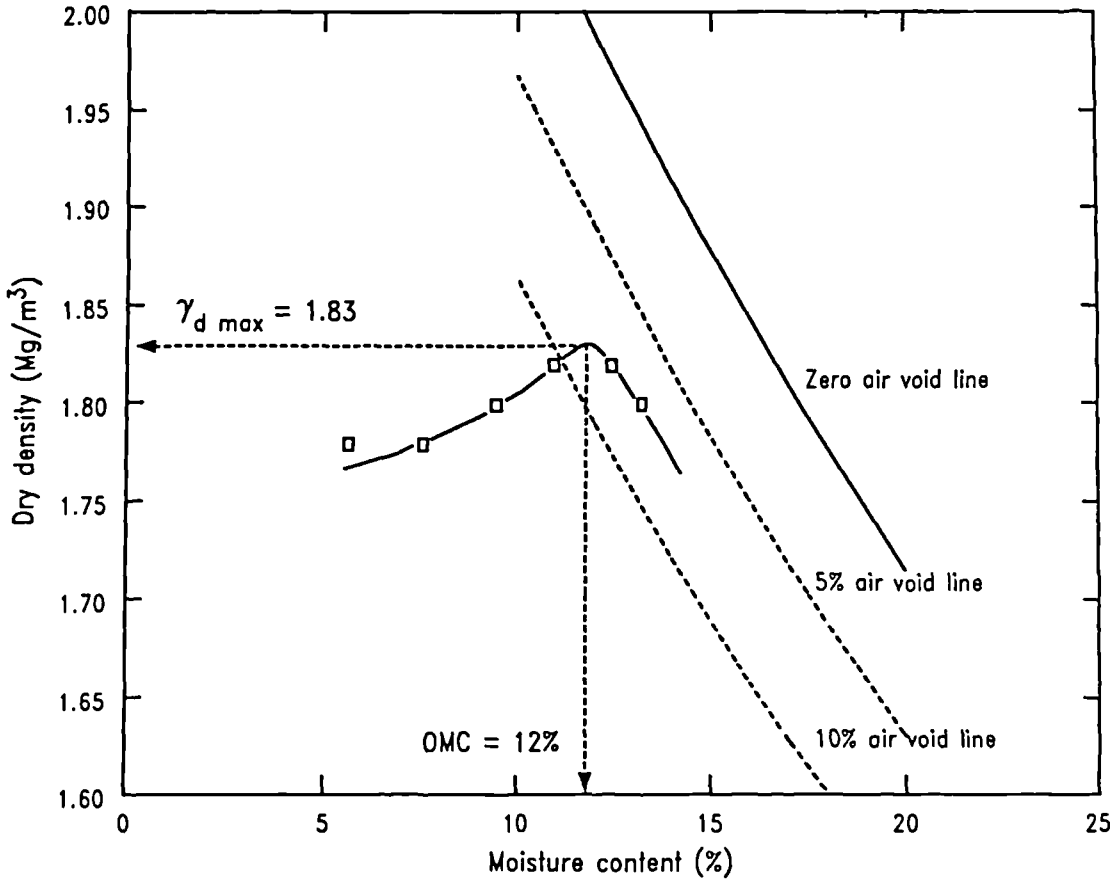

Figure 6.4 Relationship between dry density and moisture content

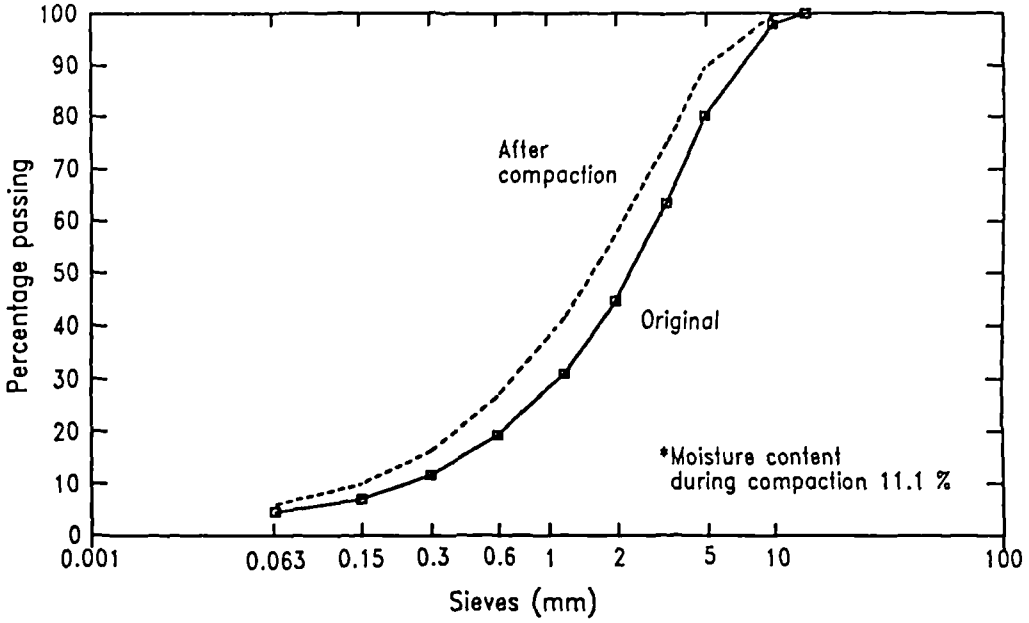

Figure 6.5 Grading changes resulting from compaction

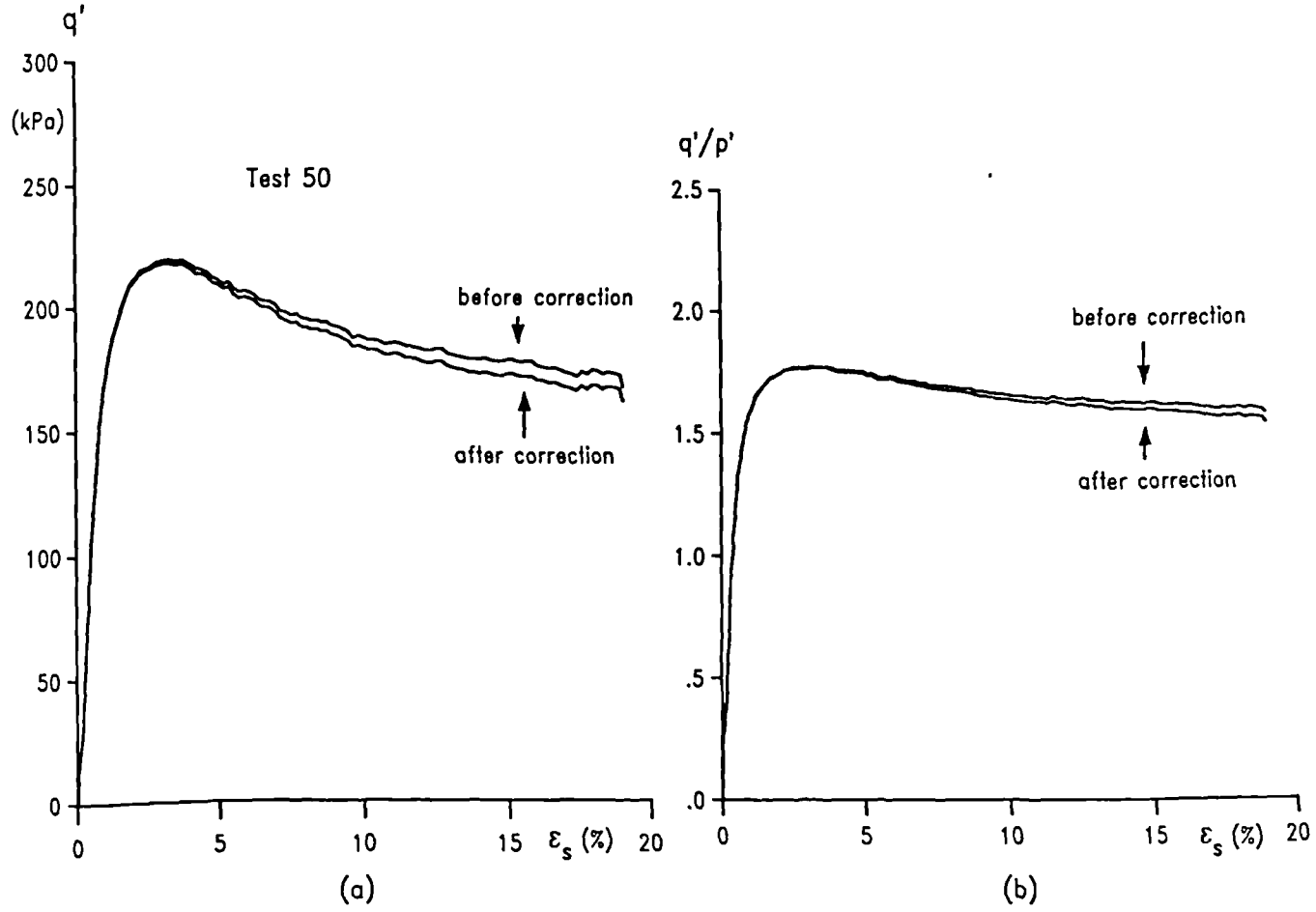

Figure 6.6 The effect of membrane stiffness correction
(a) on the deviator stress
(b) on the stress ratio

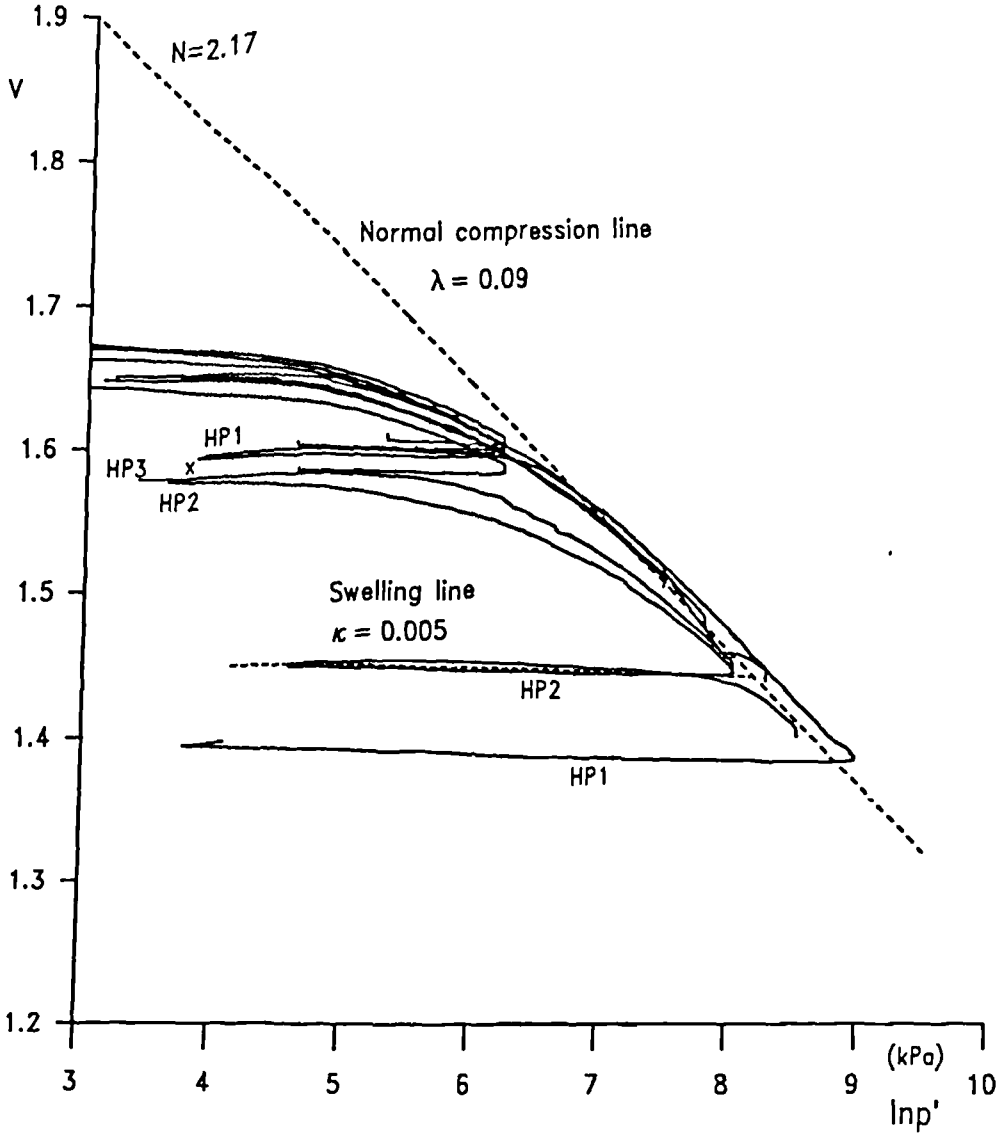

Figure 6.7 Isotropic compression and swelling

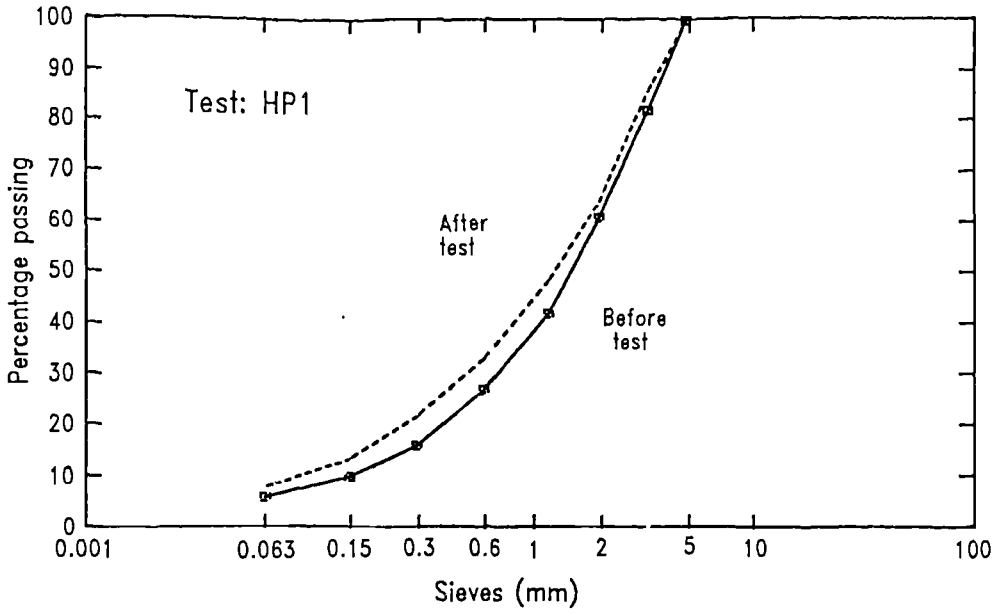

Figure 6.8 Grading changes due to isotropic compression and swelling

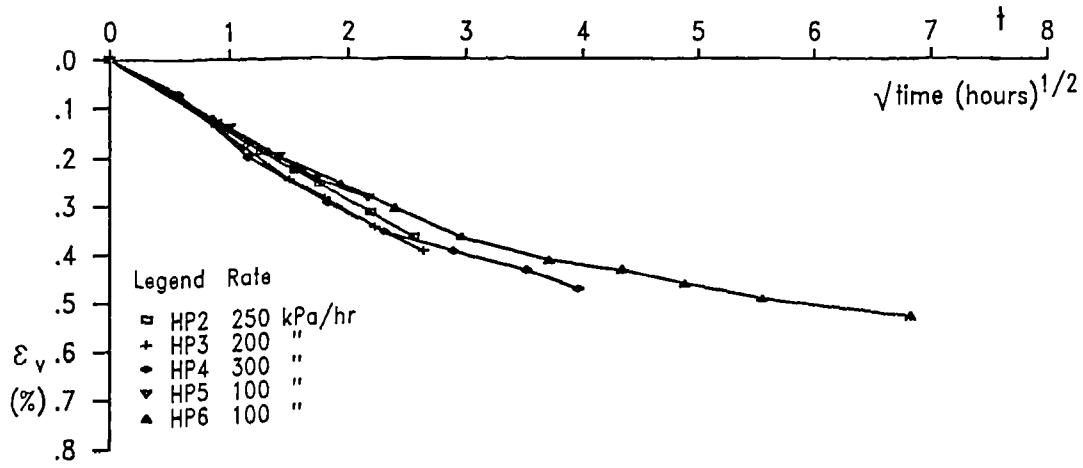

Figure 6.9 Creep effects during isotropic compression

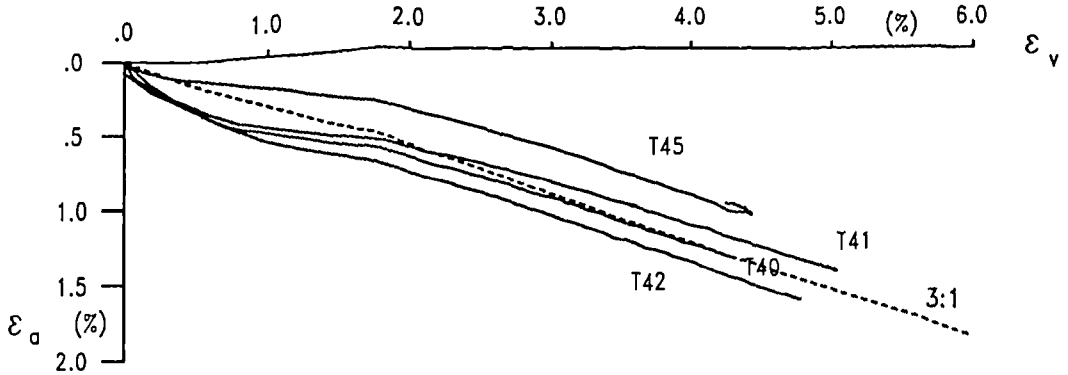

Figure 6.10 $\varepsilon_v - \varepsilon_a$ during isotropic compression

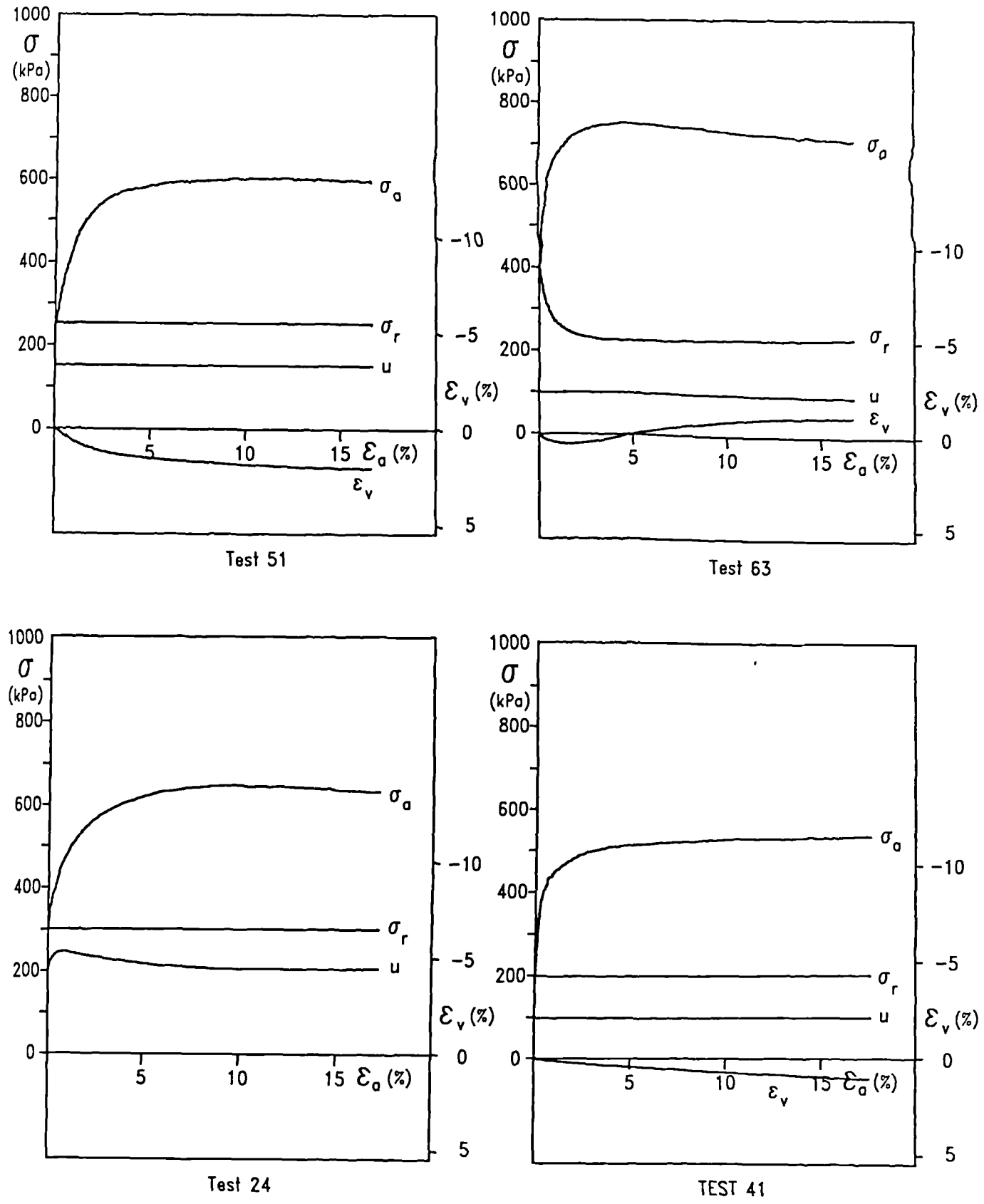

Figure 6.11 Typical test results (Standard pressure test)

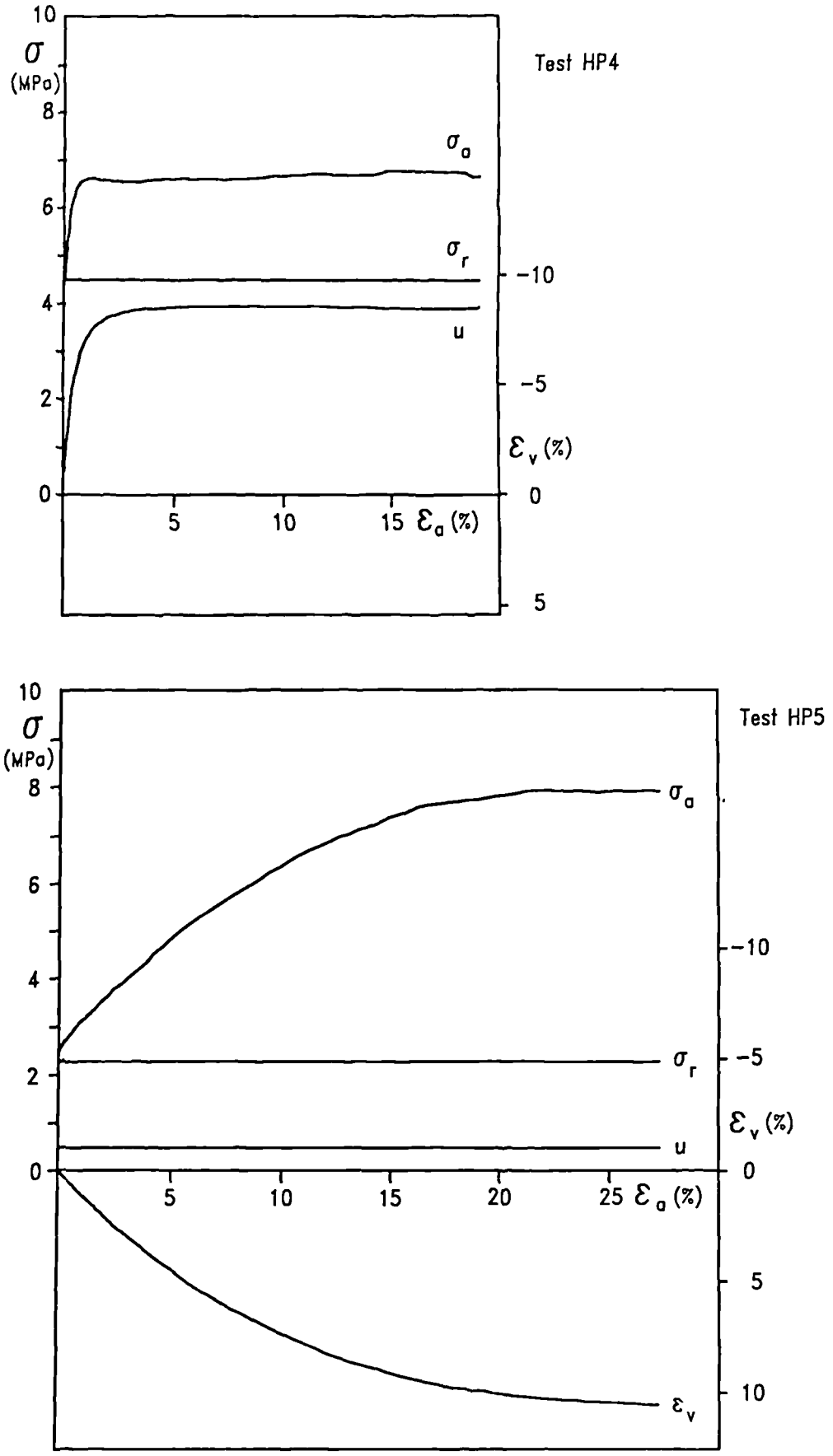

Figure 6.12 Typical test results (High pressure test)

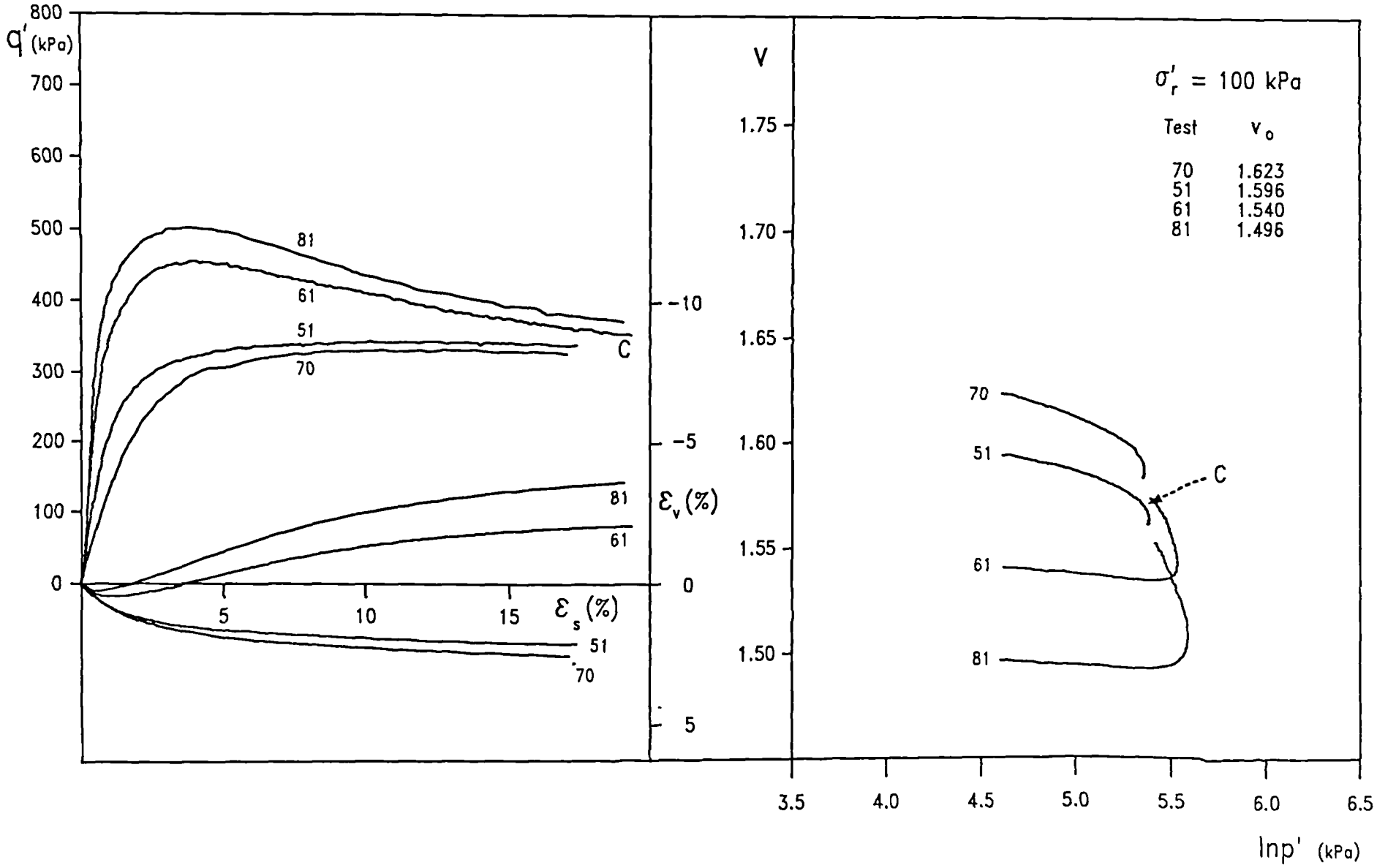

Figure 6.13 Behaviour of the soil under the same confining stress

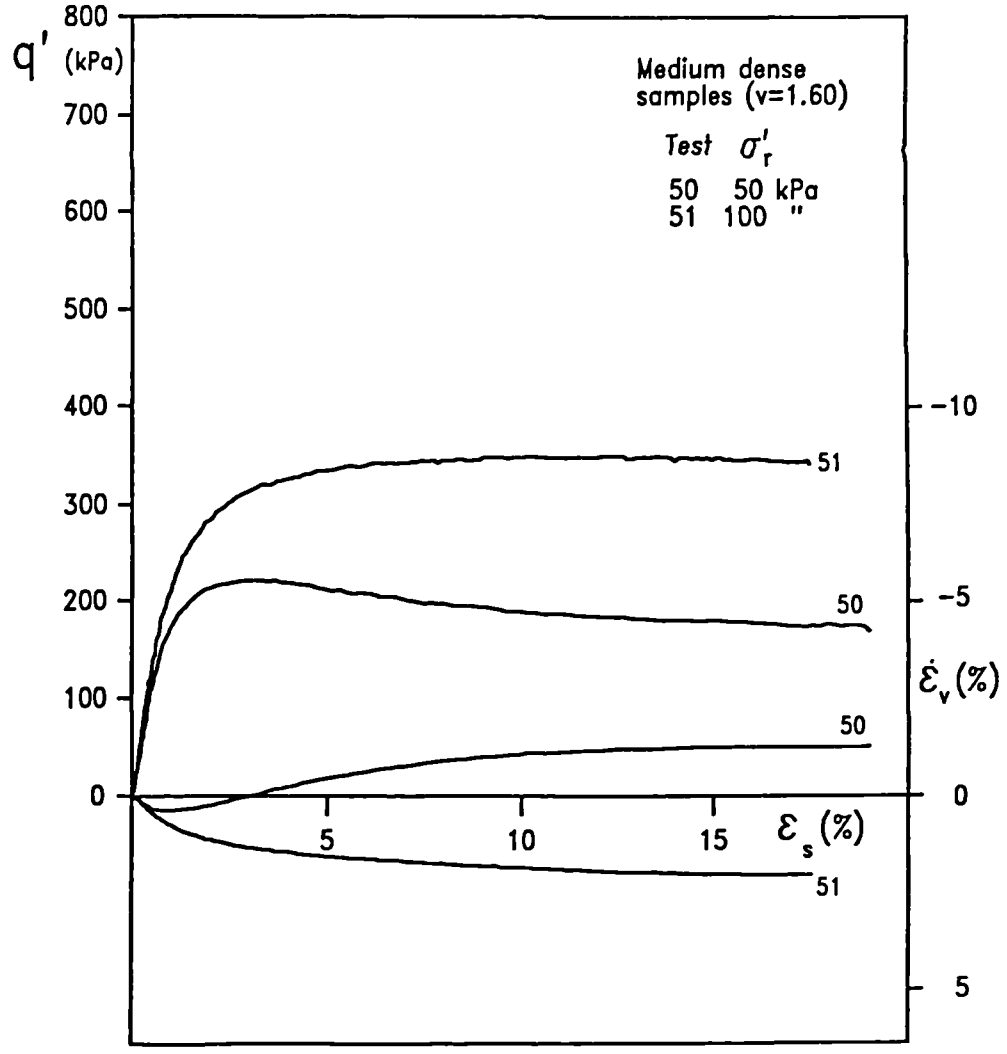

Figure 6.14 Behaviour of soils with same density under different confining stresses

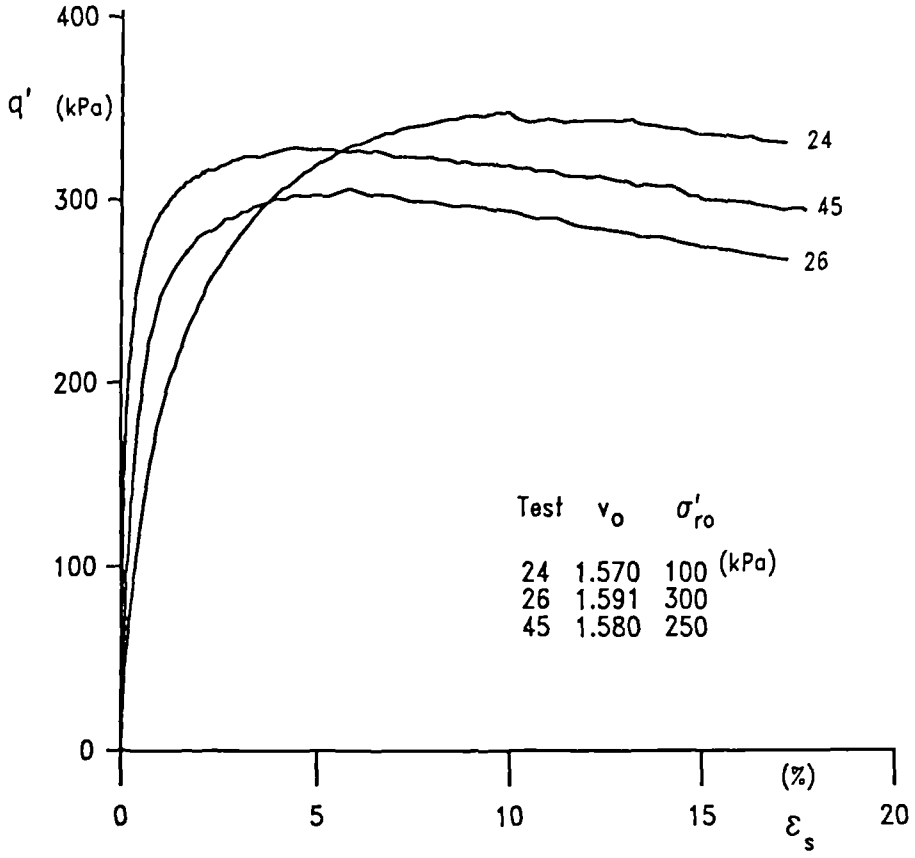

(a)

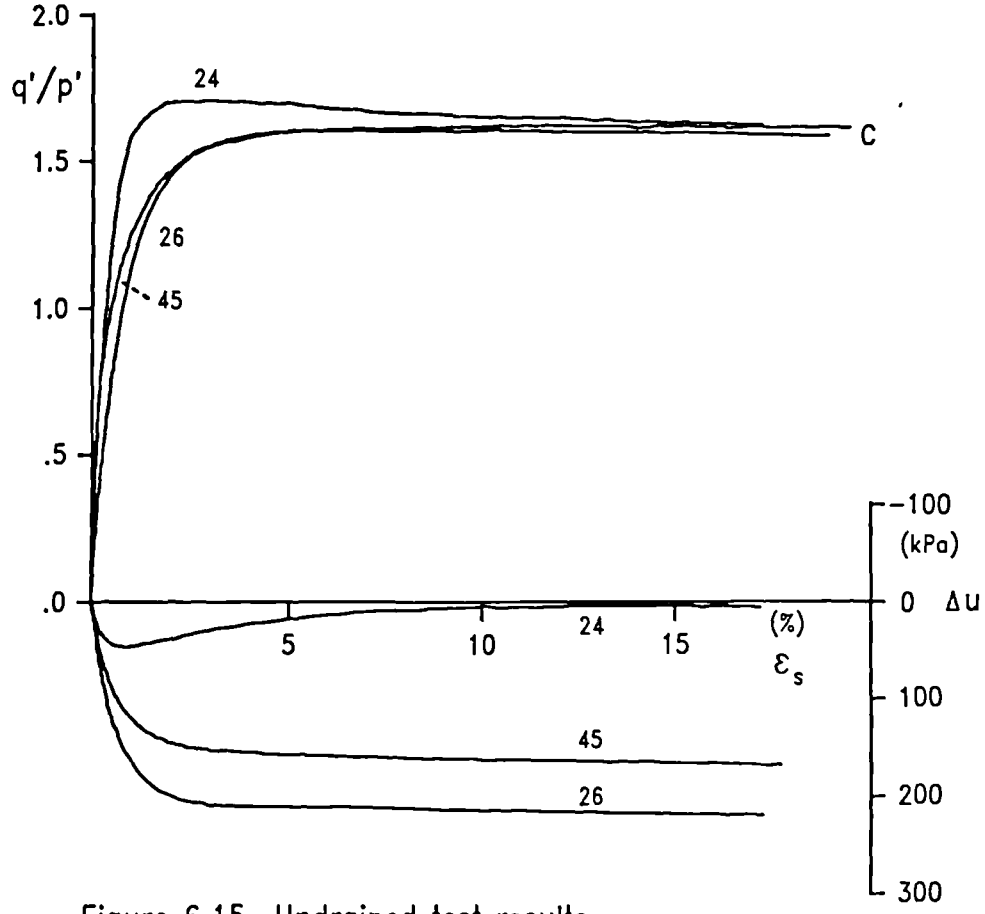

(b)

Figure 6.15 Undrained test results
(a) $q' - \varepsilon_s$
(b) stress ratio and pore pressure response

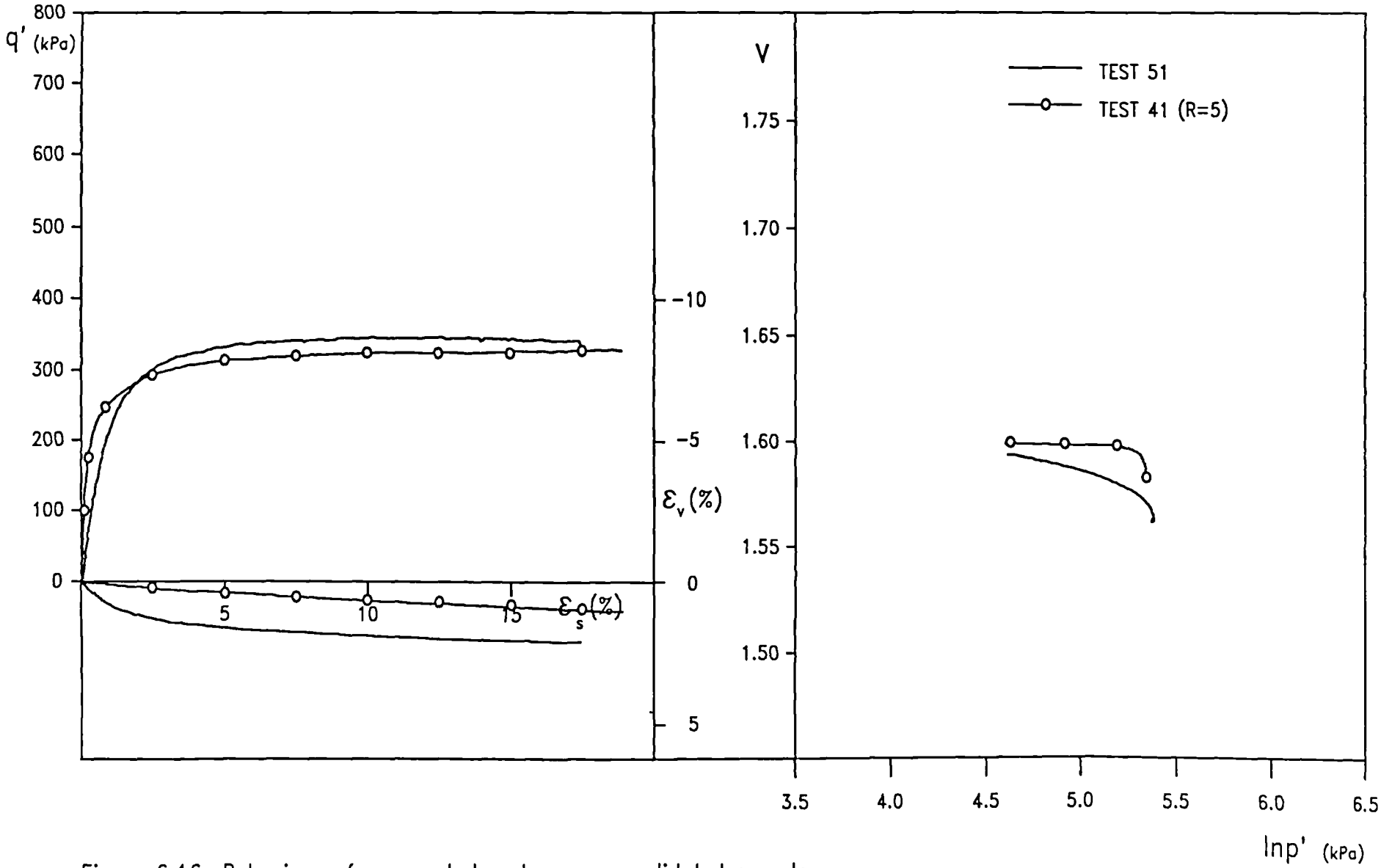

Figure 6.16 Behaviour of compacted and over-consolidated samples

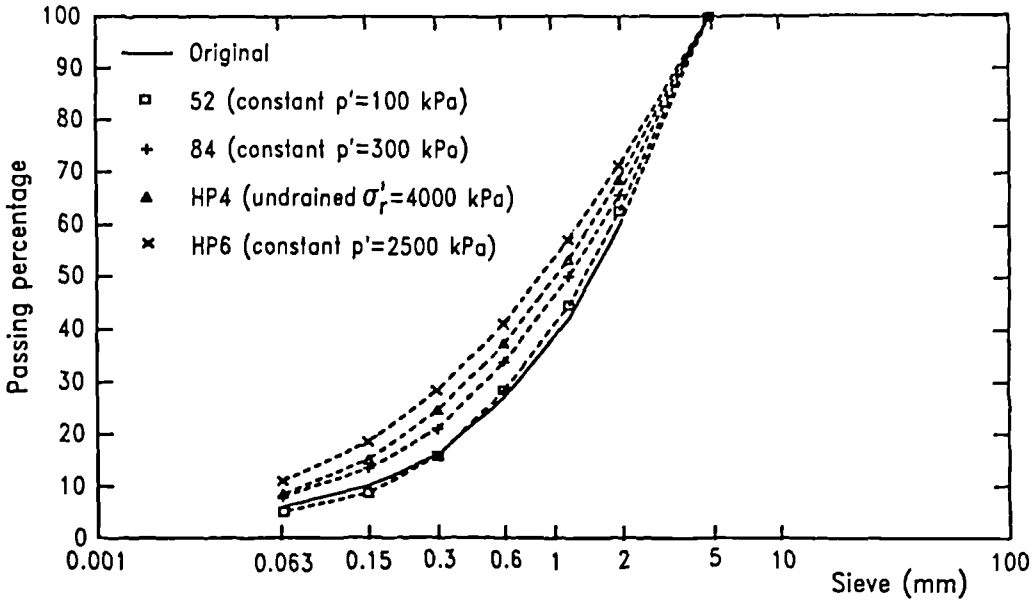

Figure 6.17 Grading changes during triaxial tests

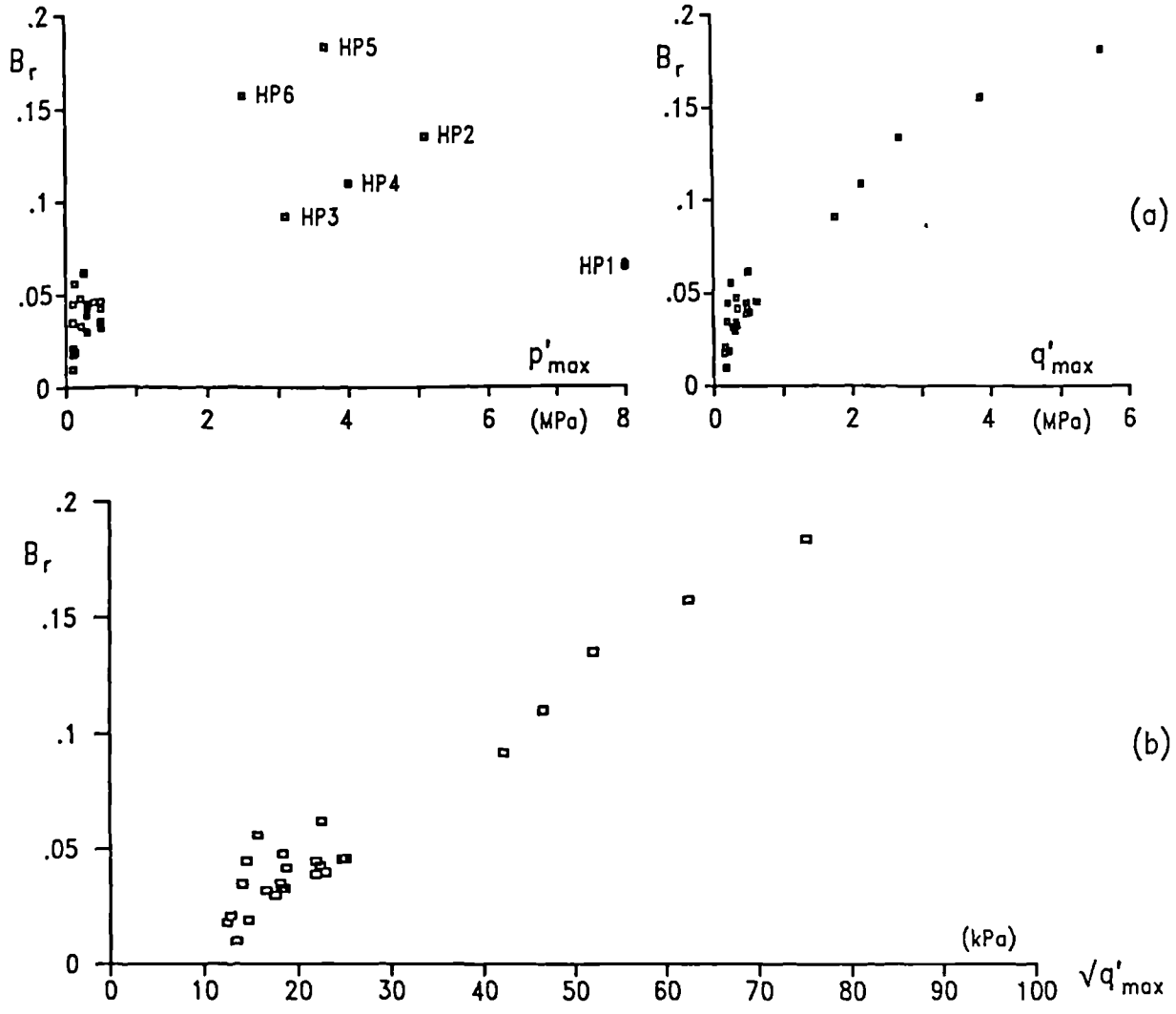

Figure 6.18 Relationship between particle crushing and pressures

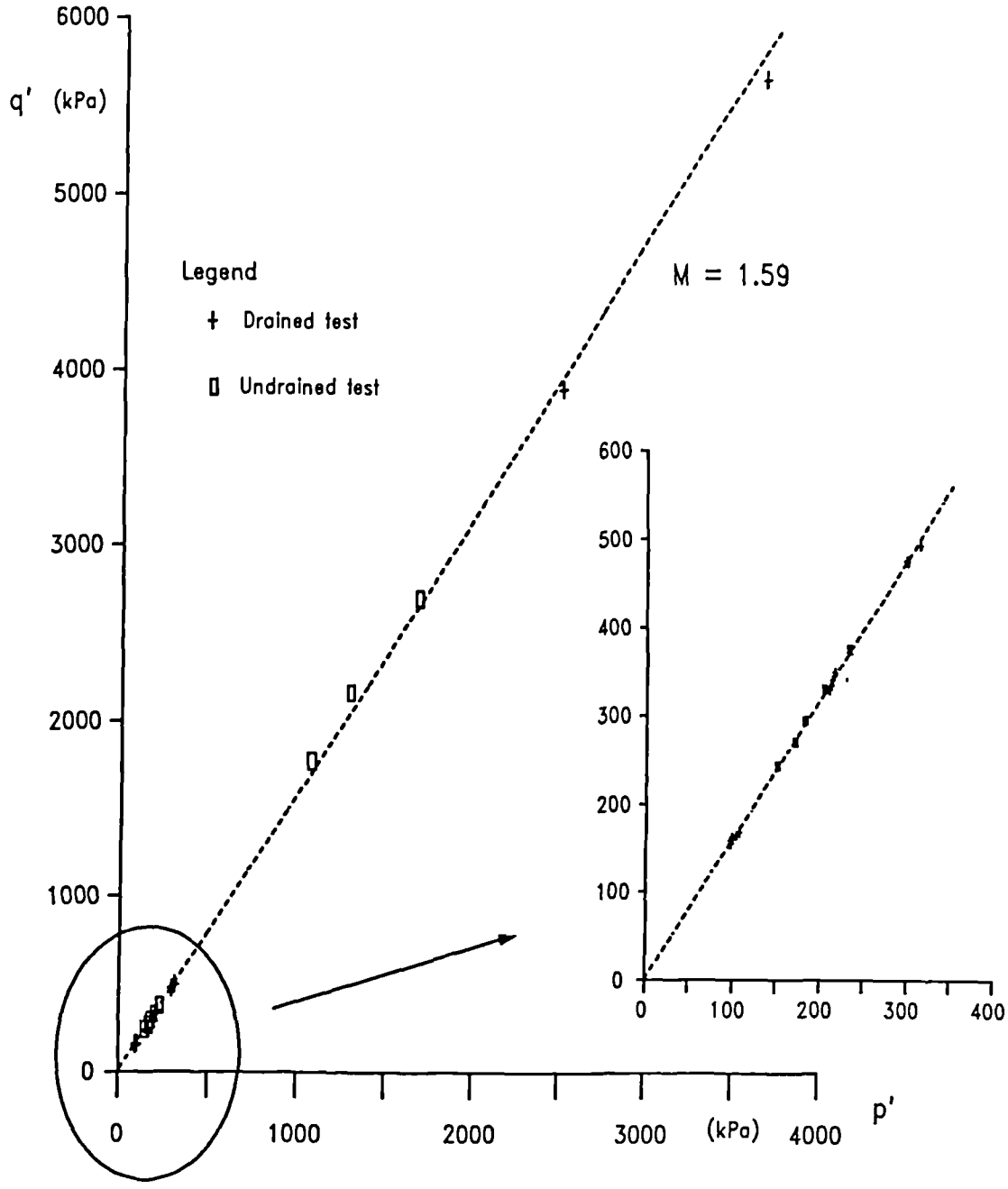

Figure 6.19 The critical states in q':p' space

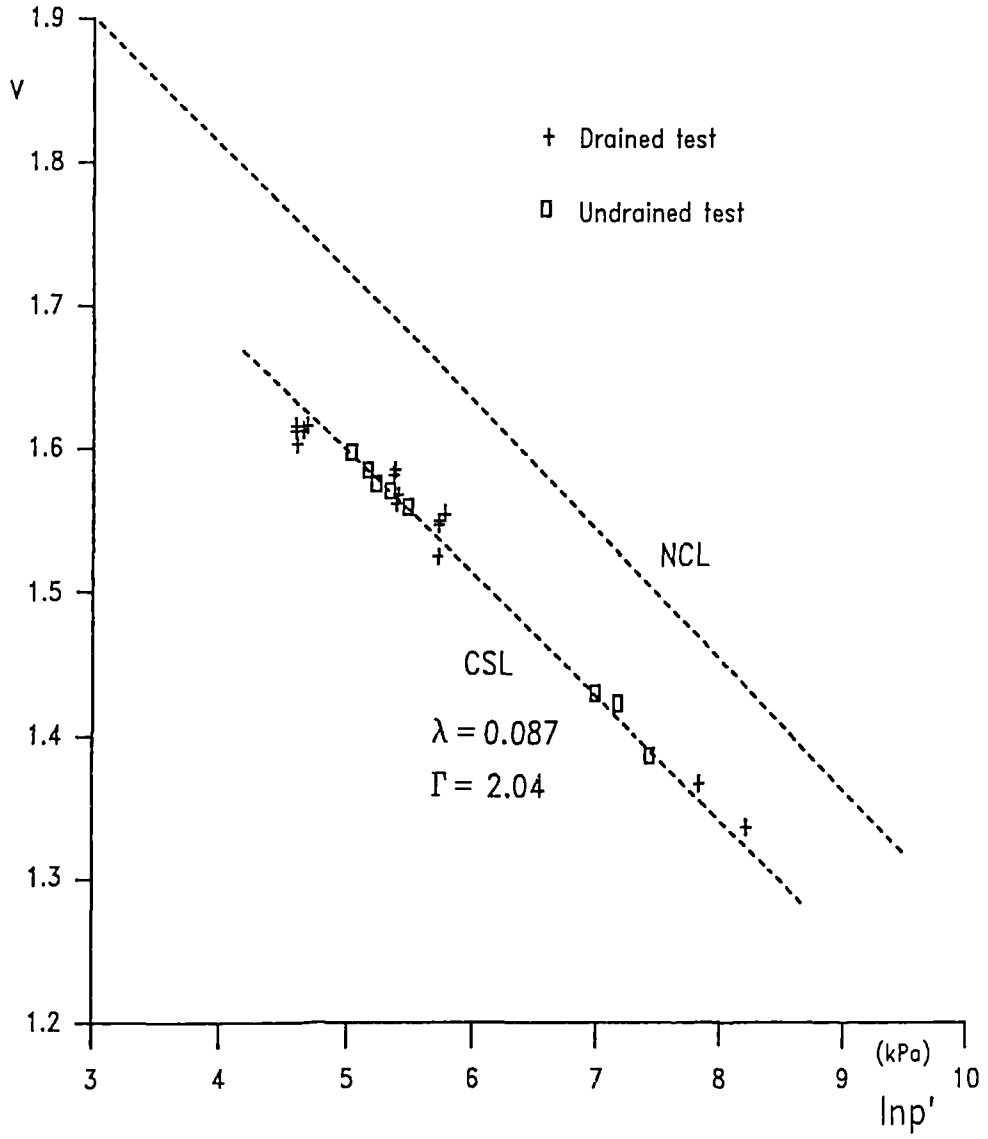

Figure 6.20 The critical states in v:lnp' space

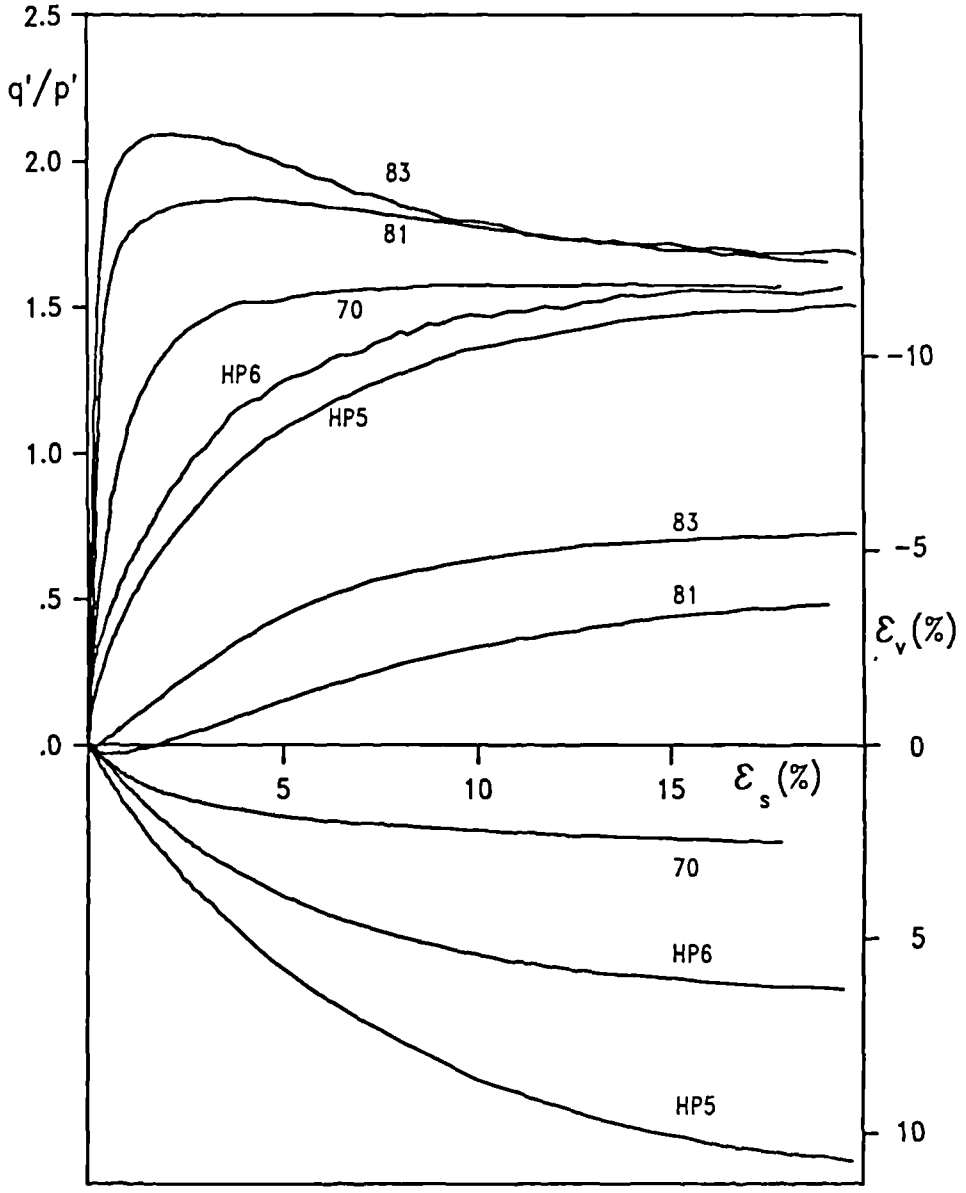

Figure 6.21 Stress ratio – shear and volumetric strains

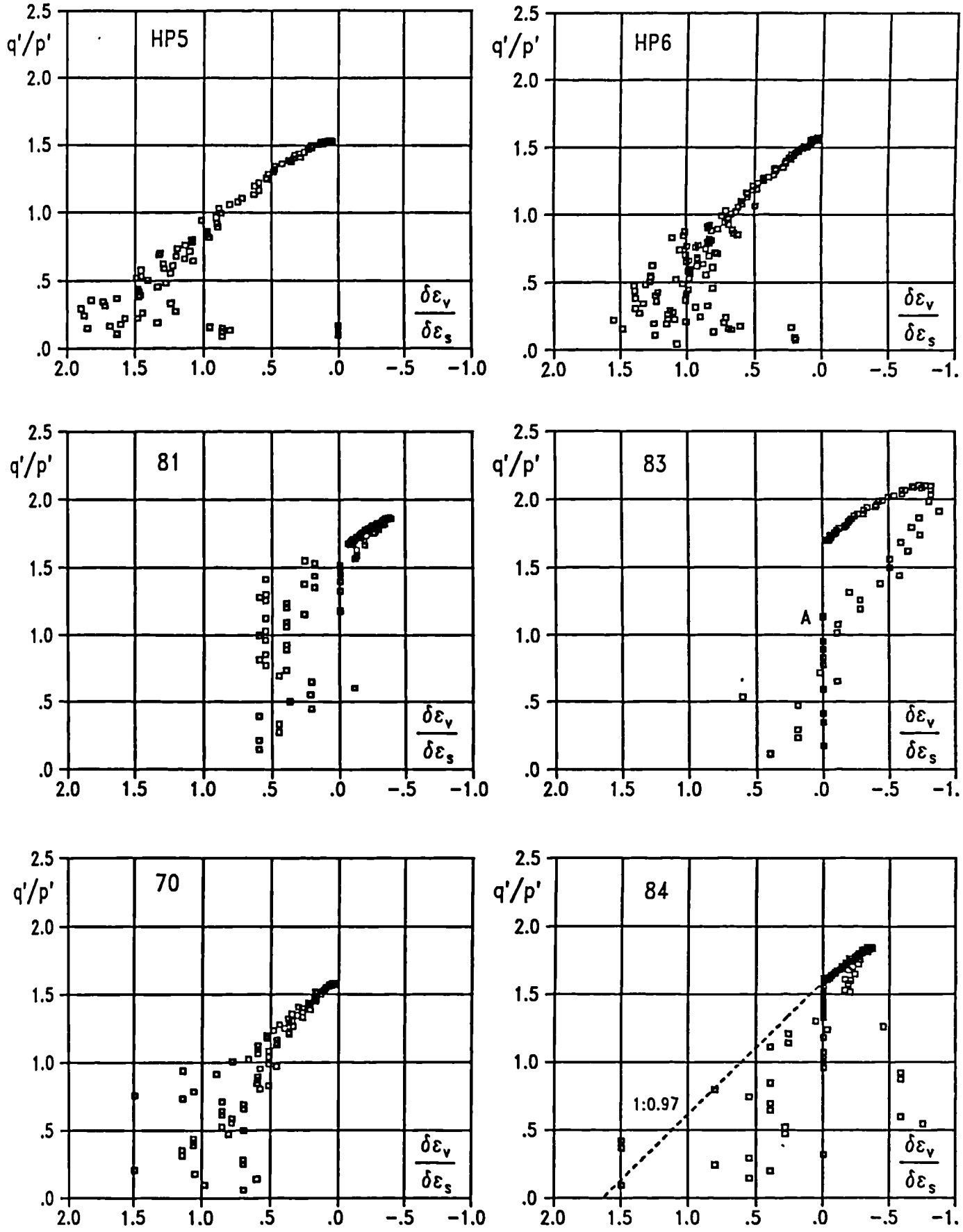

Figure 6.22 Stress–dilatancy relationships

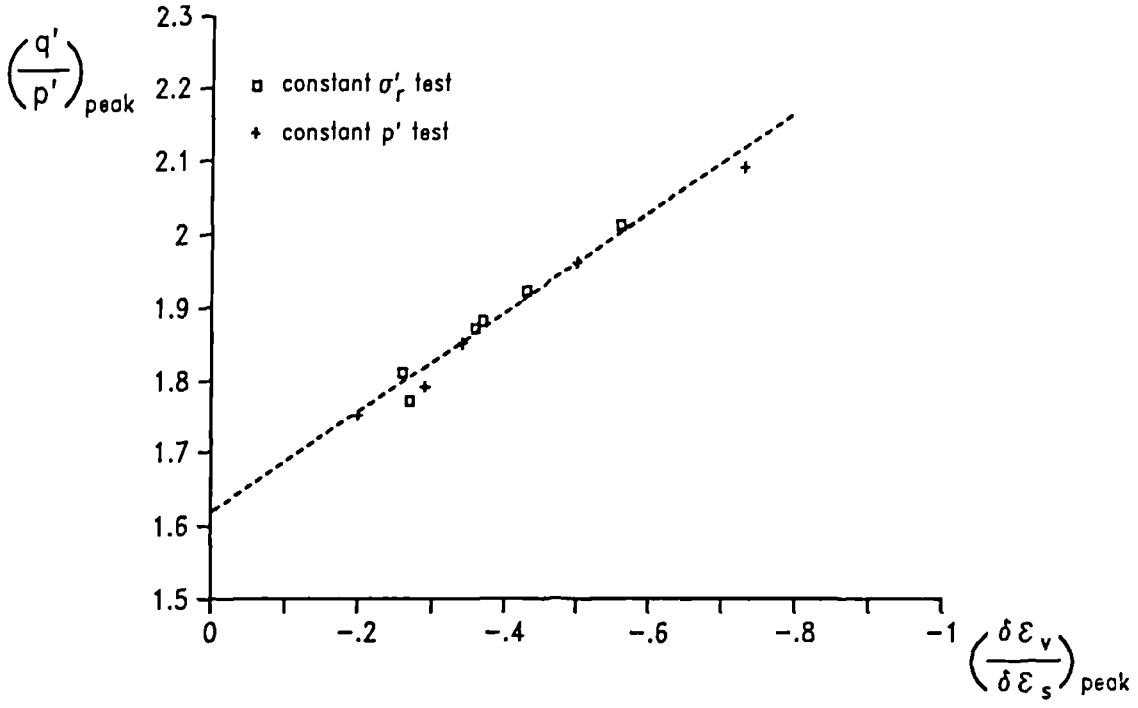

Figure 6.23 Stress–dilatancy relationship for peak states

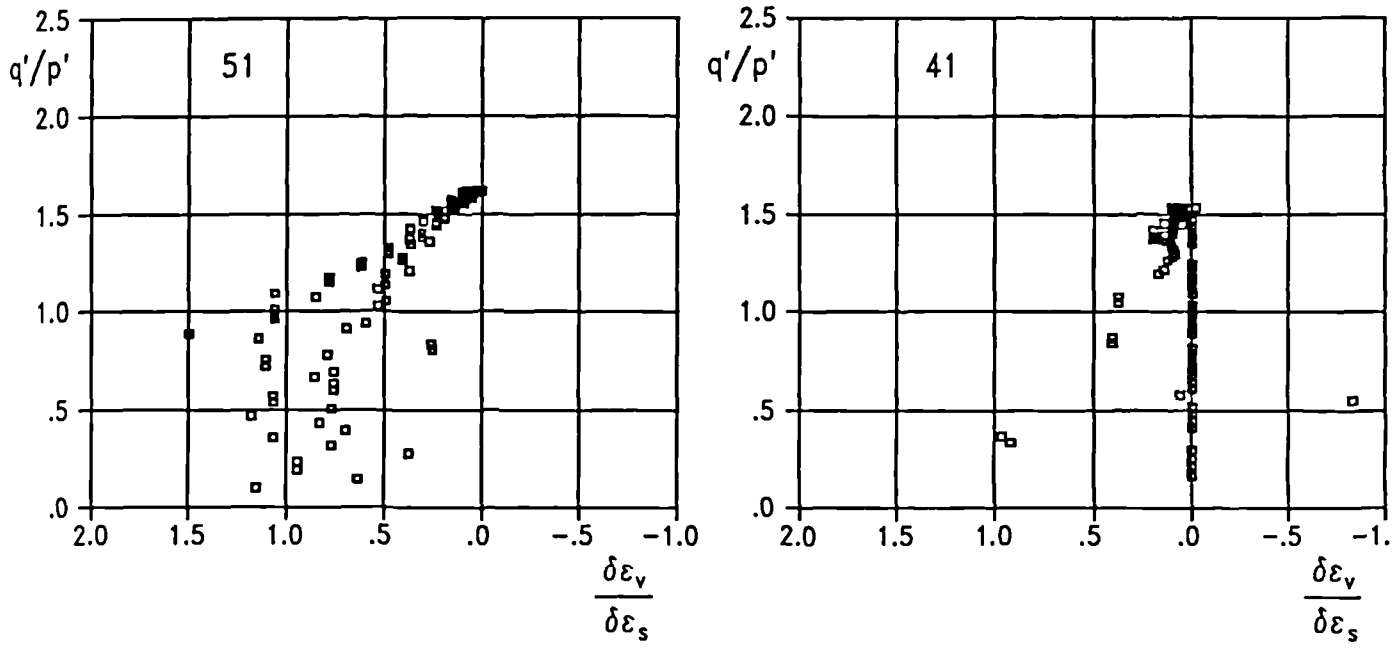

Figure 6.24 Stress–dilatancy of compacted and over–consolidated samples

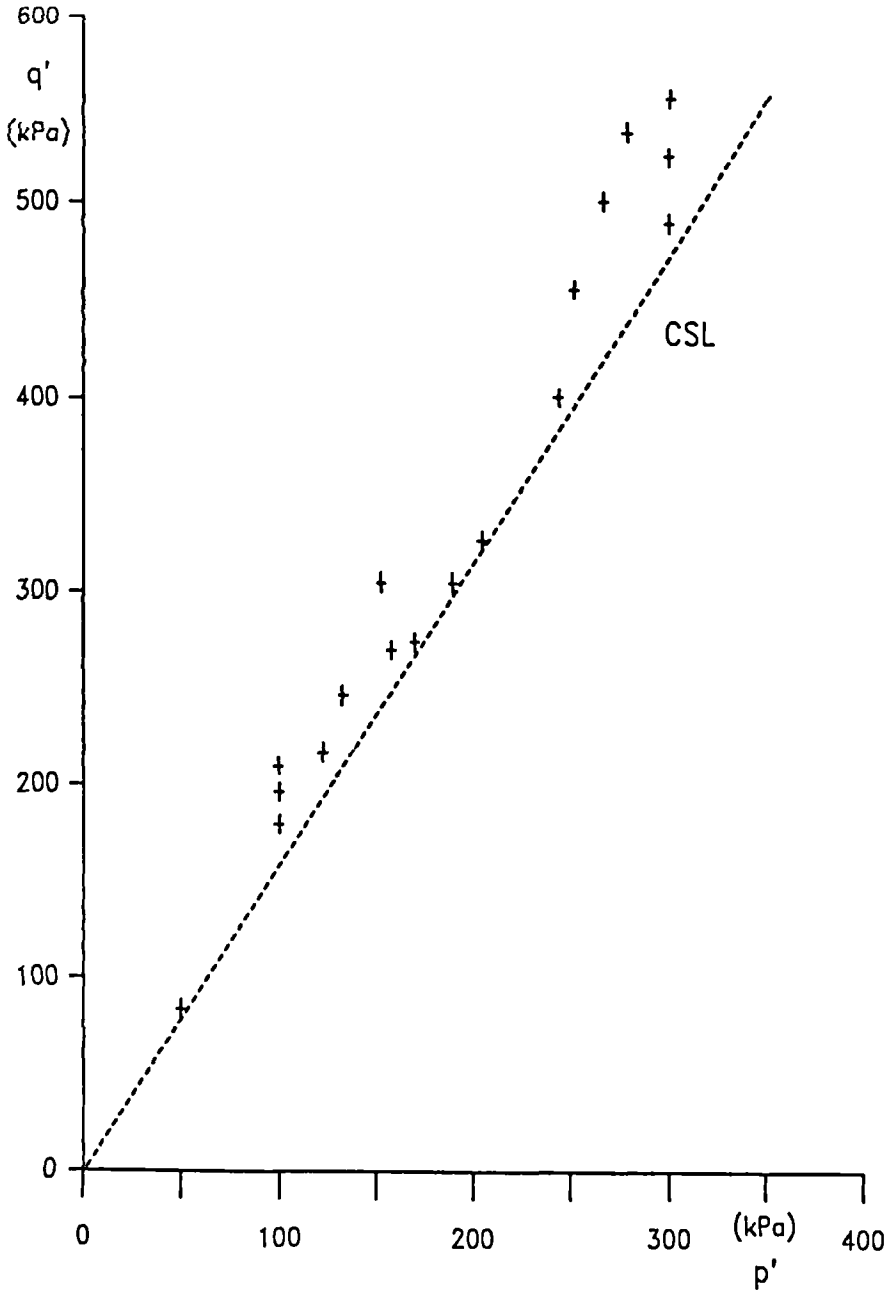

Figure 6.25 Peak states in q':p' space

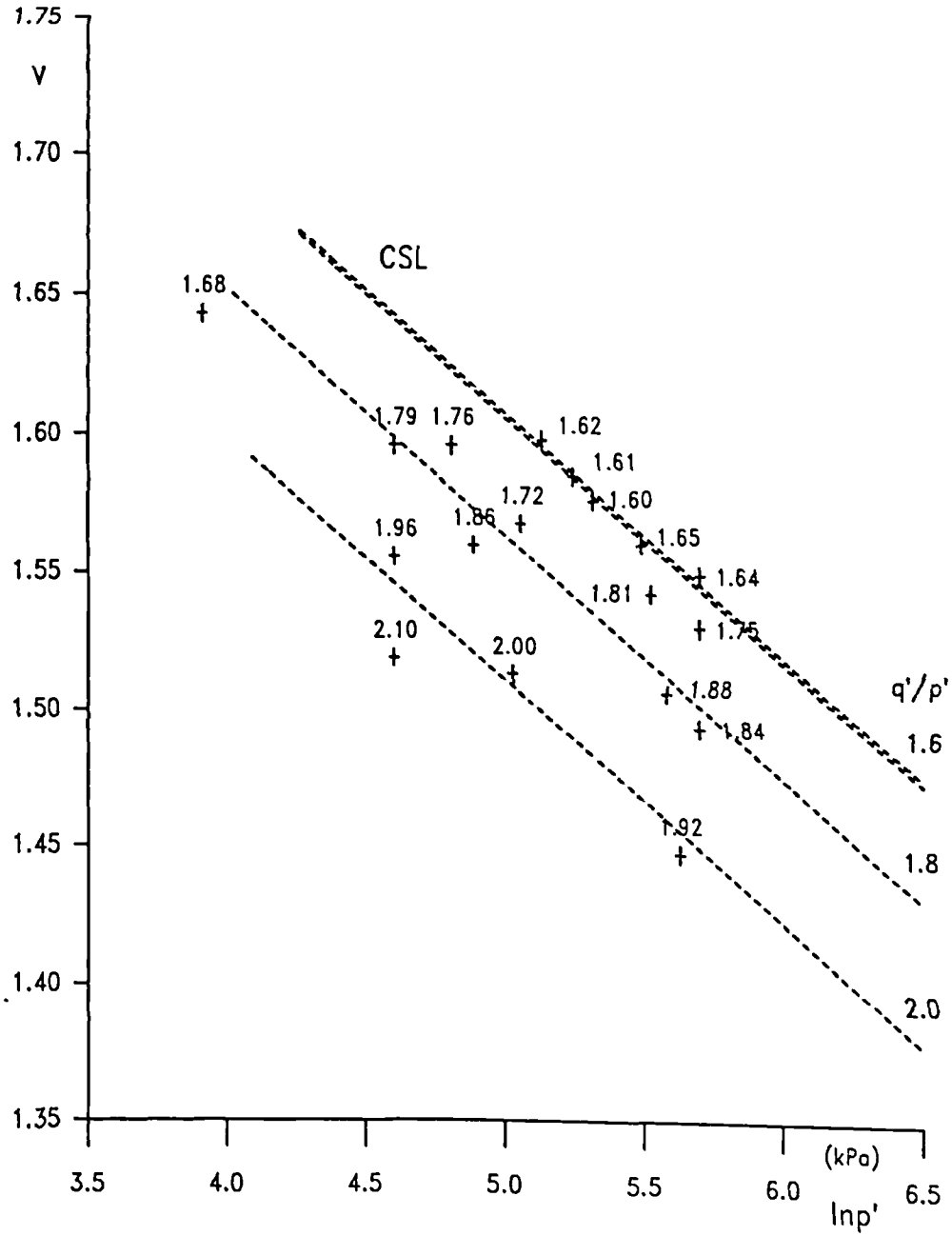

Figure 6.26 Peak states in v:lnp' space

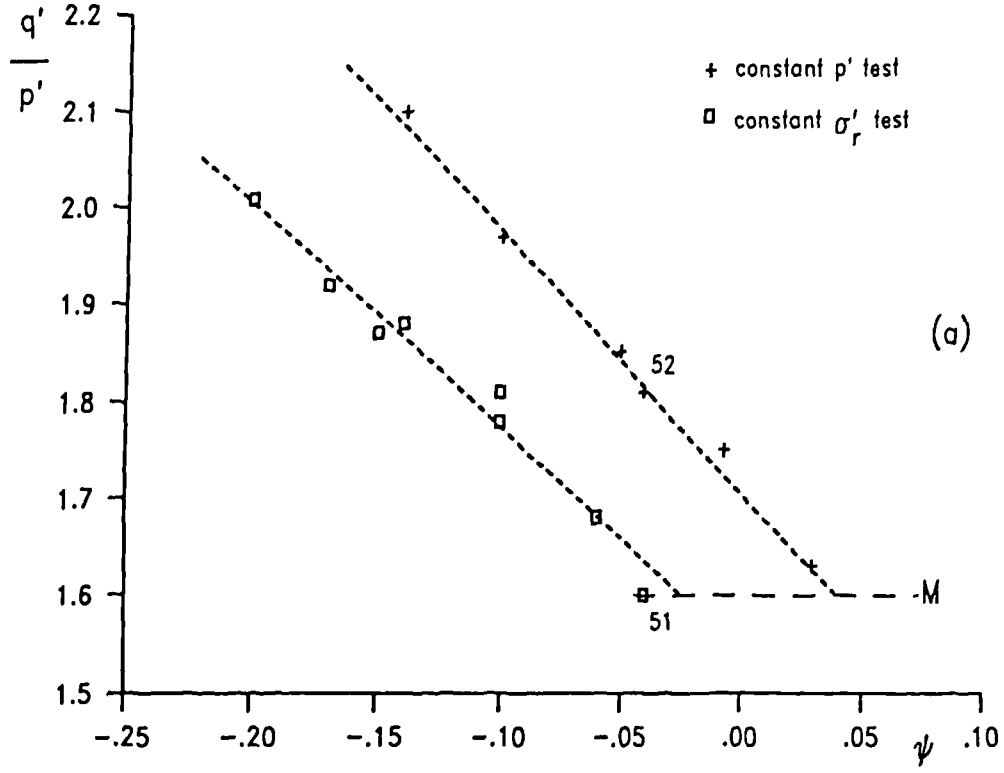

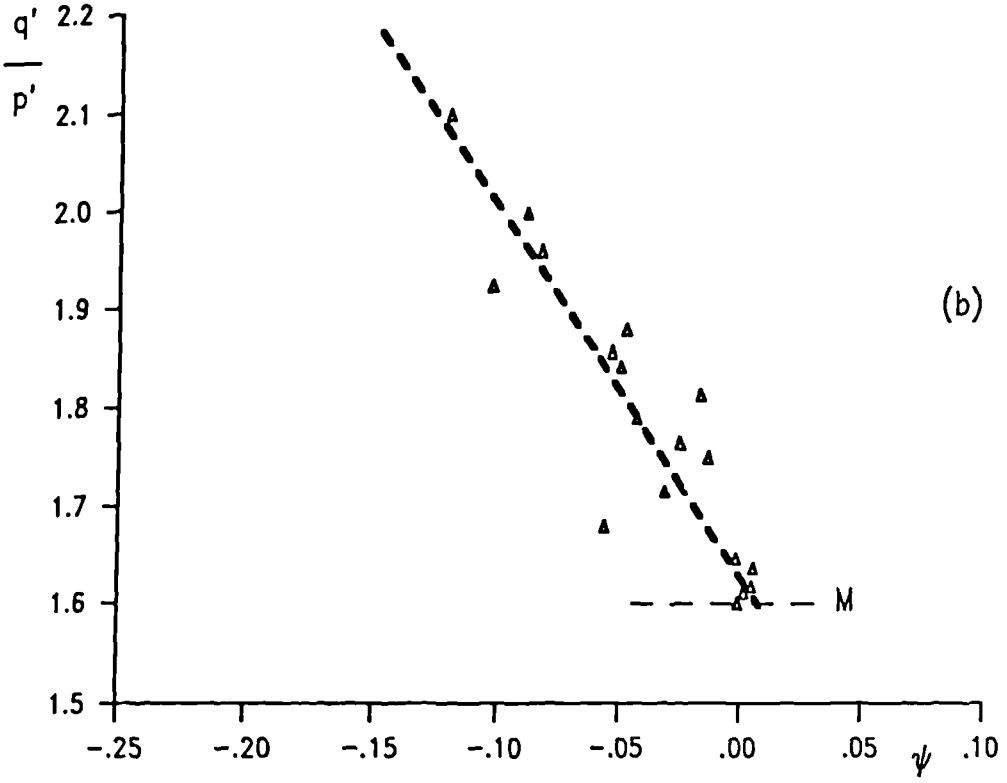

Figure 6.27 The state parameter and the peak stress ratio
(a) the initial state parameter
(b) the state parameter at peaks

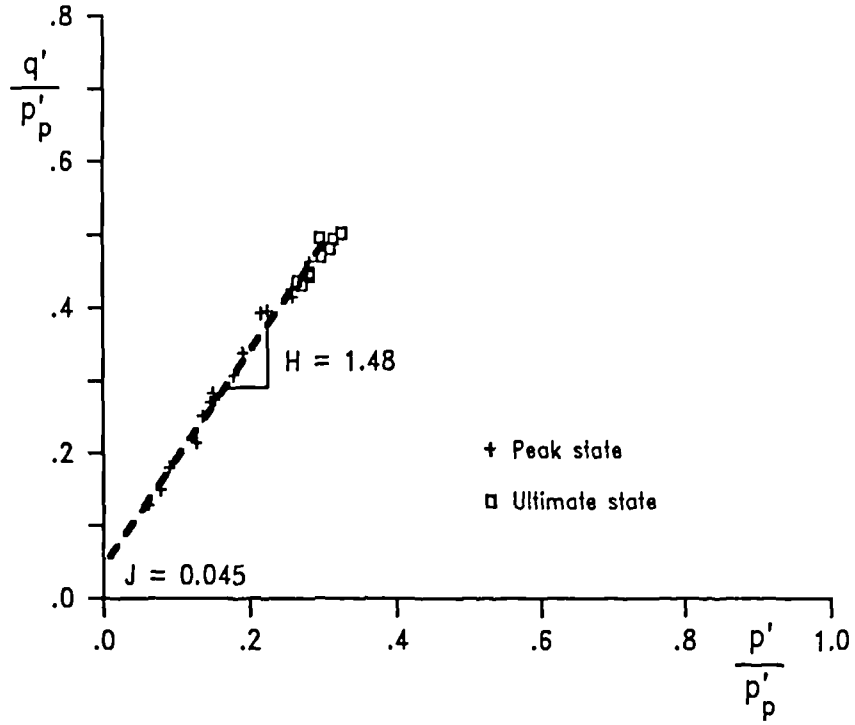

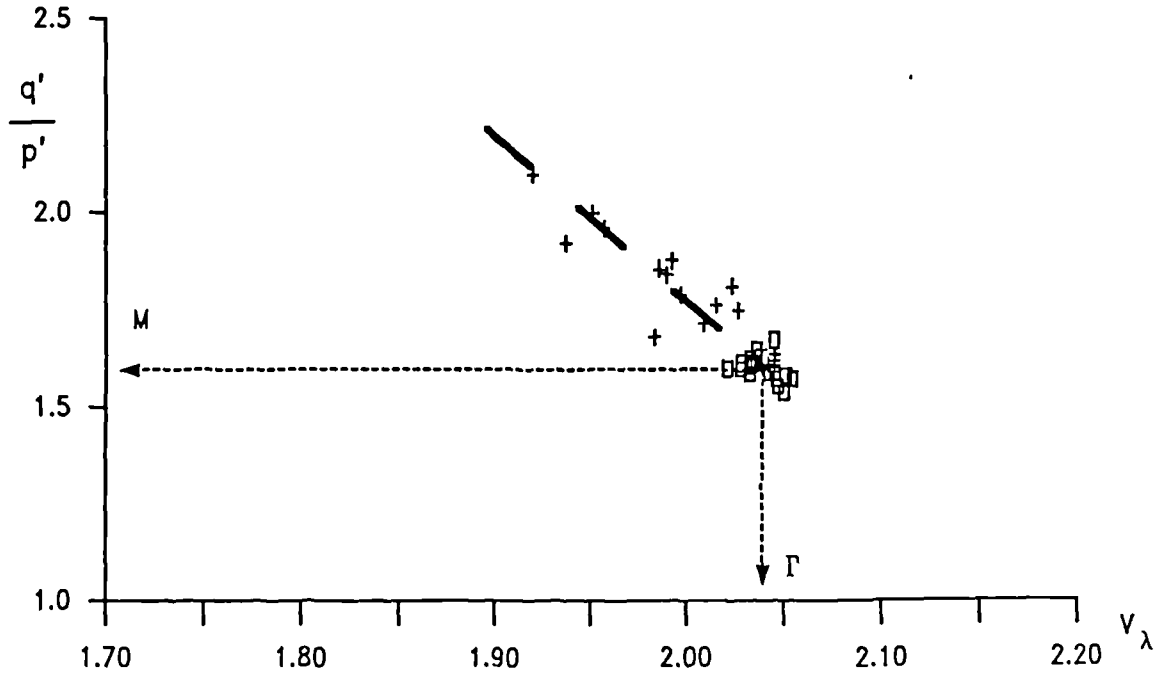

Figure 6.28 Normalised peak and ultimate states

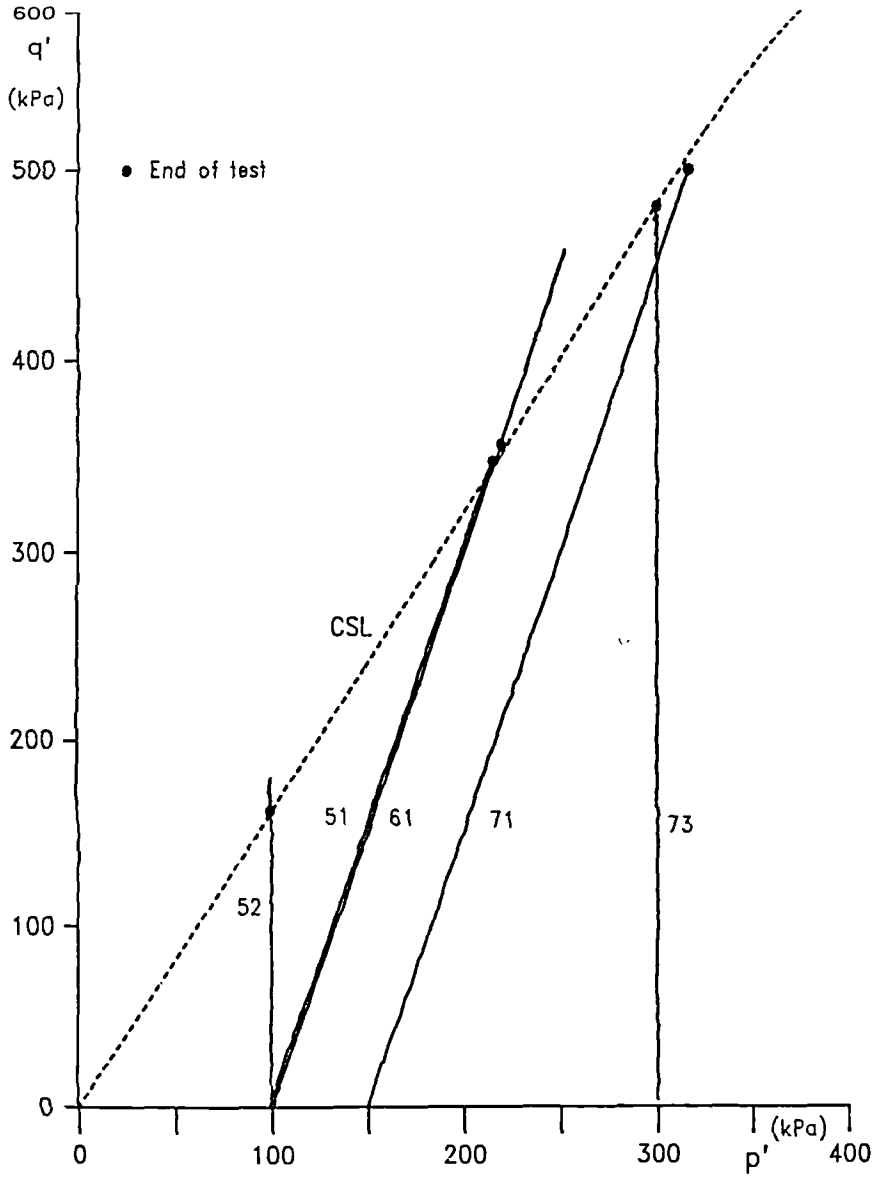

Figure 6.29 Stress paths for drained tests (standard pressures)

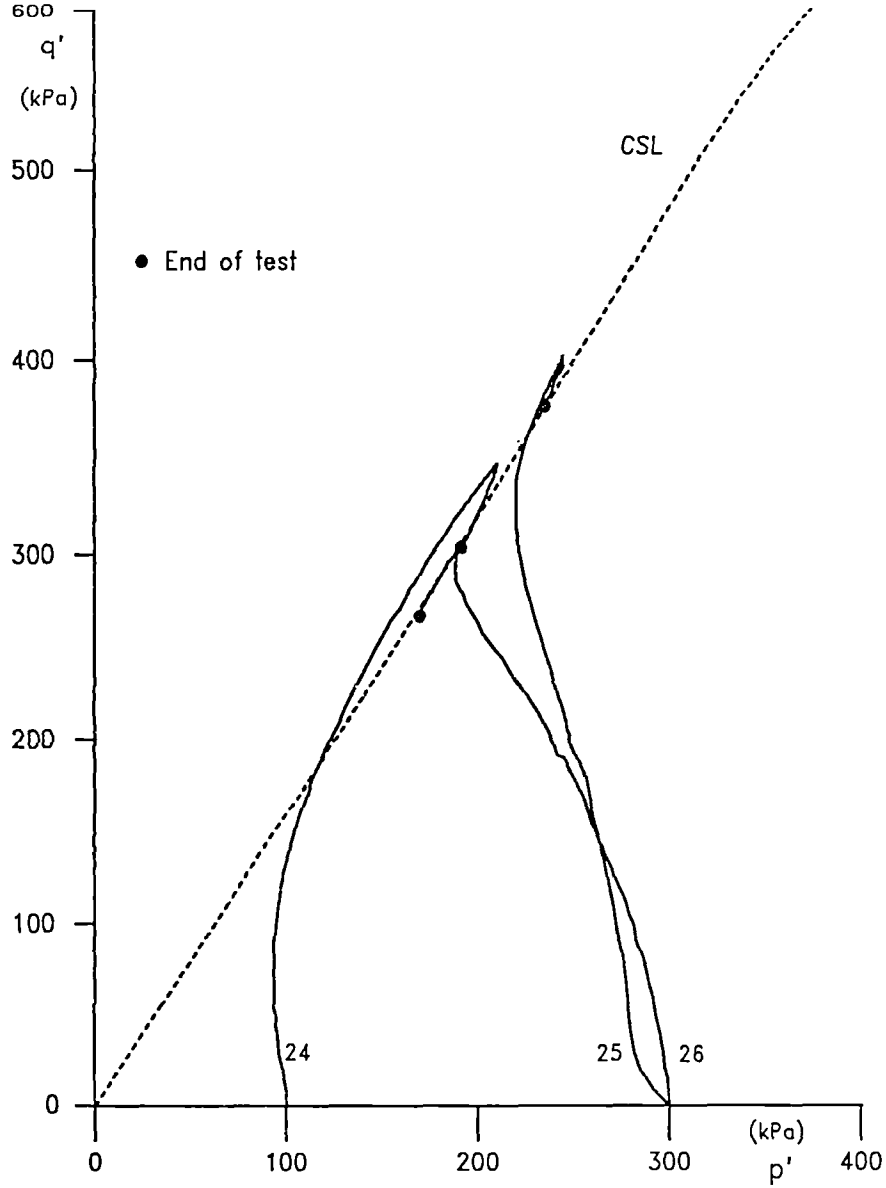

Figure 6.30 Stress paths for undrained tests (standard pressures)

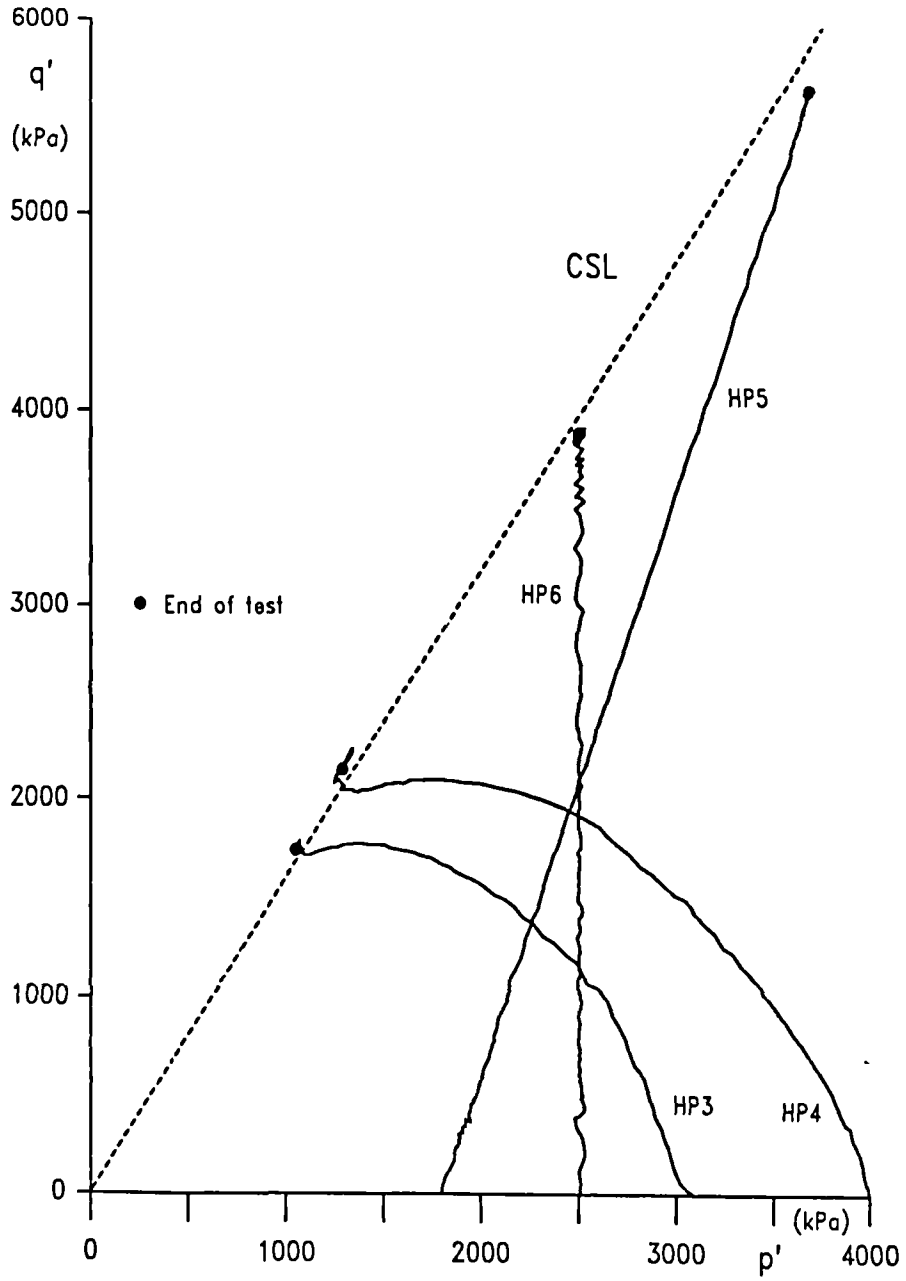

Figure 6.31 Stress paths for high pressure tests

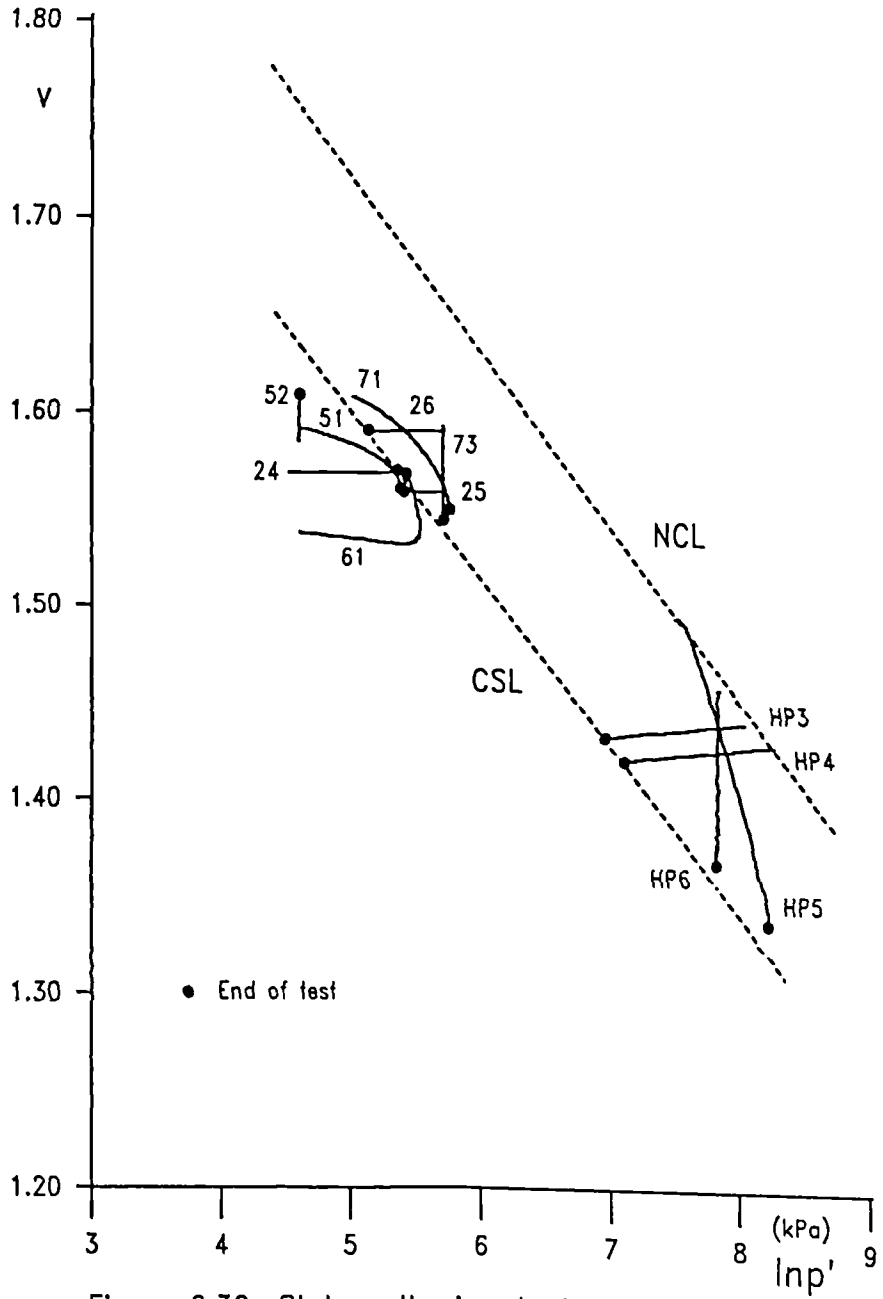

Figure 6.32 State paths in v:lnp' space

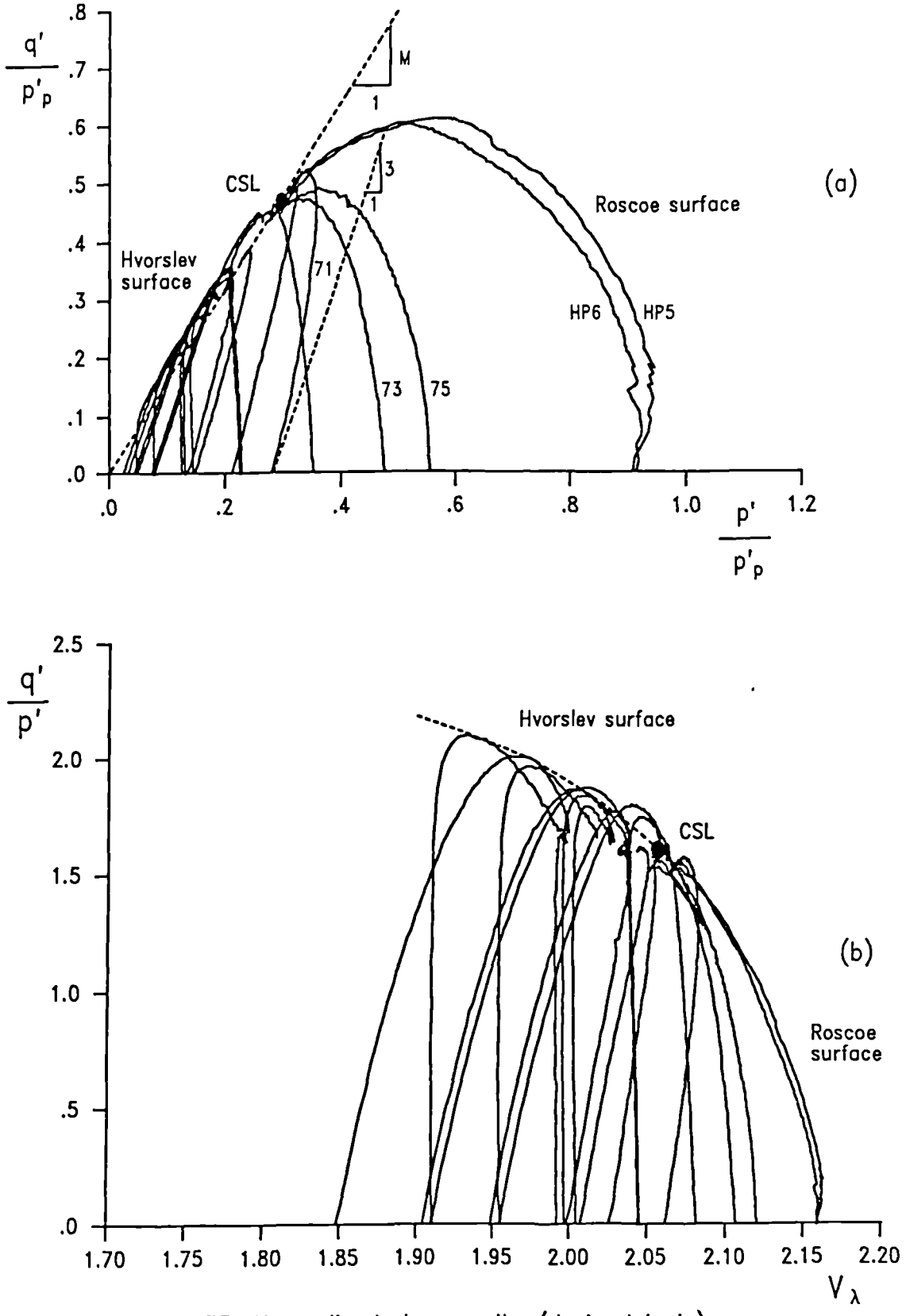

Figure 6.33 Normalised stress paths (drained tests)
(a) Elastic wall section
(b) Constant p' section

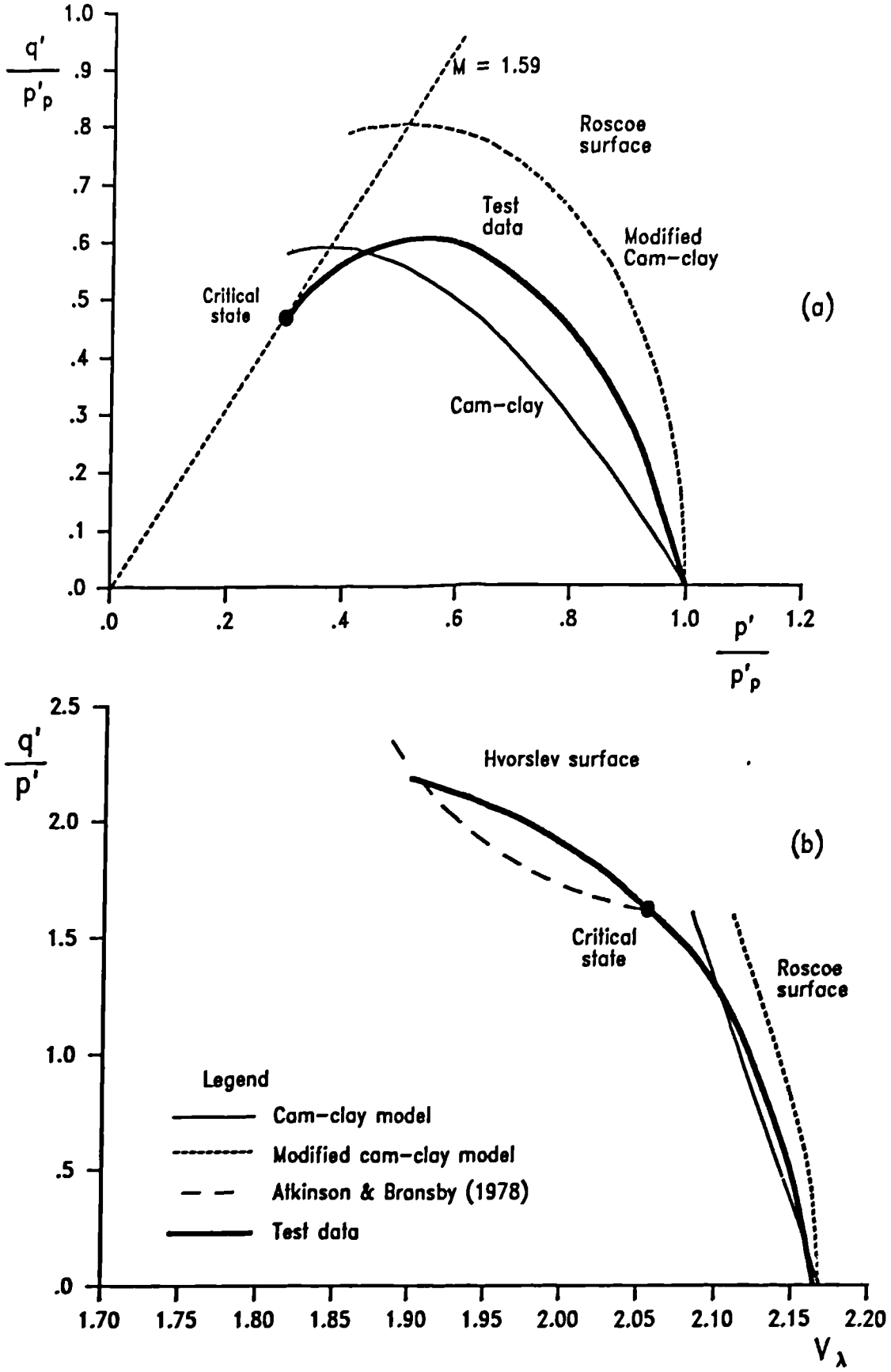

Figure 6.34 Comparision with Cam-clay soil models
(a) Elastic wall section
(b) Constant p' section

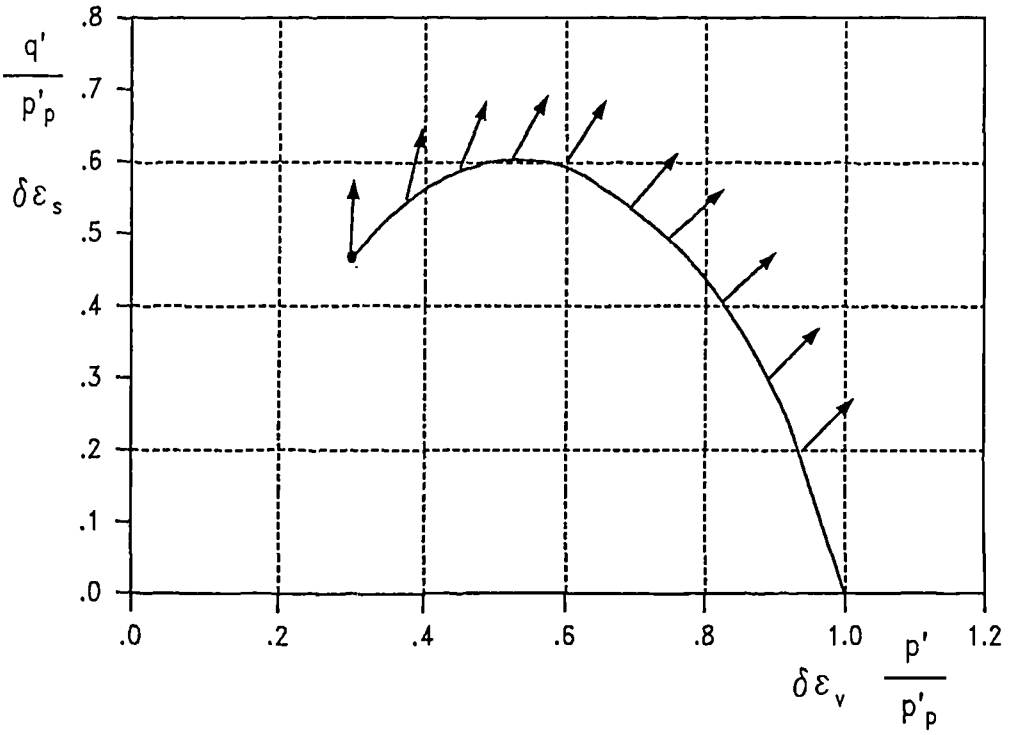

Figure 6.35 Strain increment vectors for test HP6

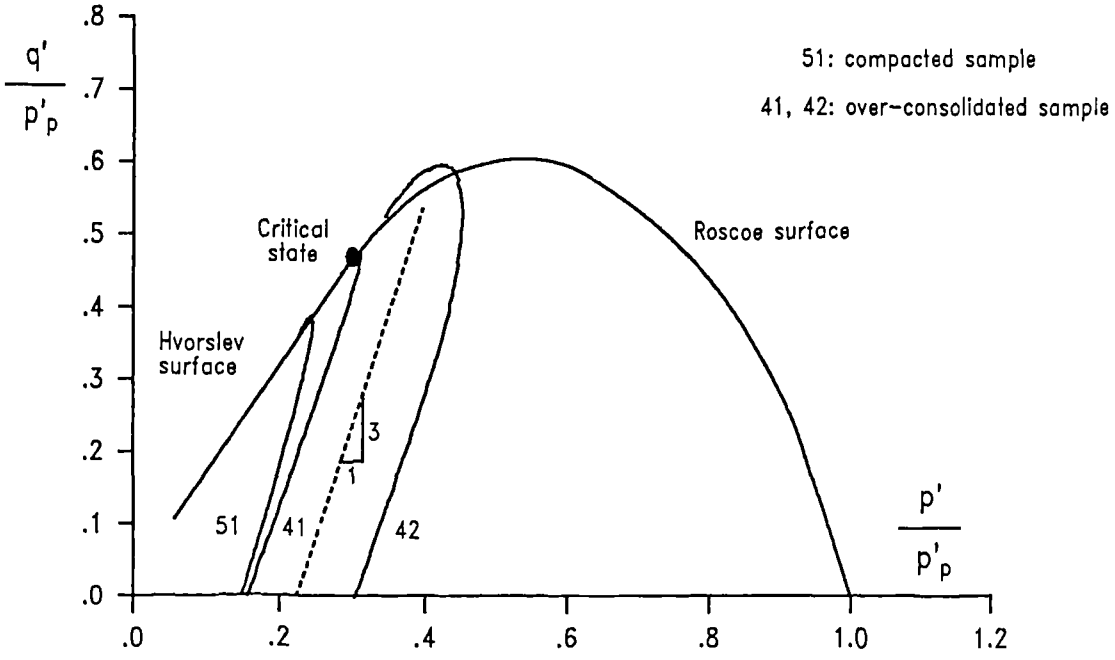

Figure 6.36 Normalised behaviour of compacted and truly over-consolidated samples

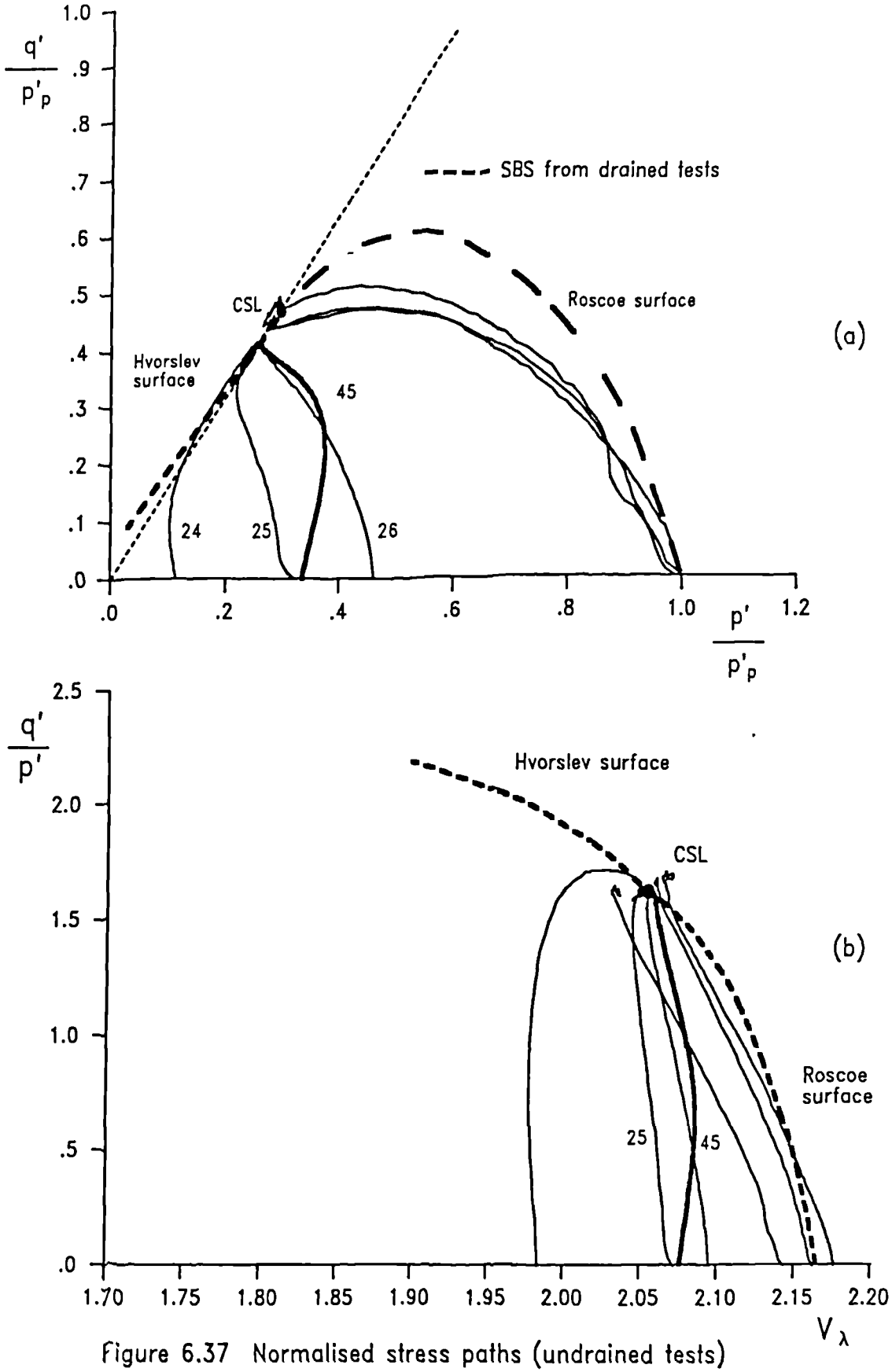

Figure 6.37 Normalised stress paths (undrained tests)

(a) Elastic wall section
(b) Constant p' section

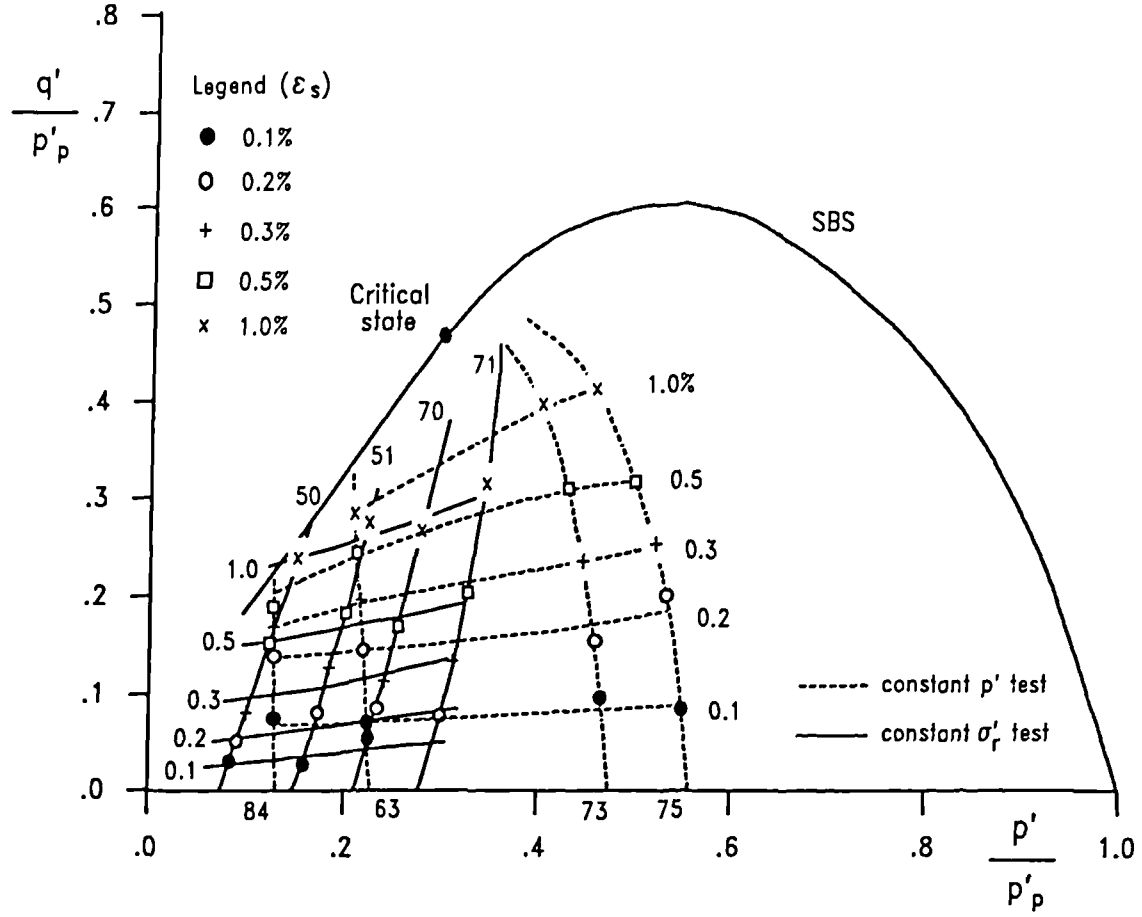

Figure 6.38 Shear strain contours below the state boundary surface

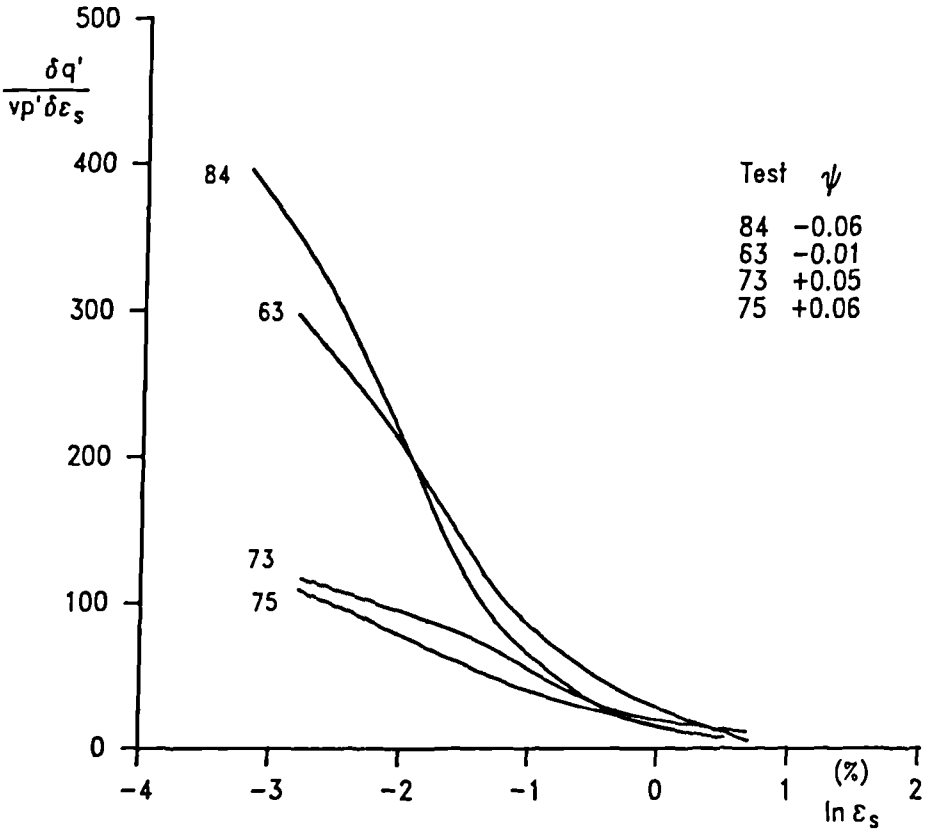

Figure 6.39 Normalised shear stiffnesses for constant p' tests

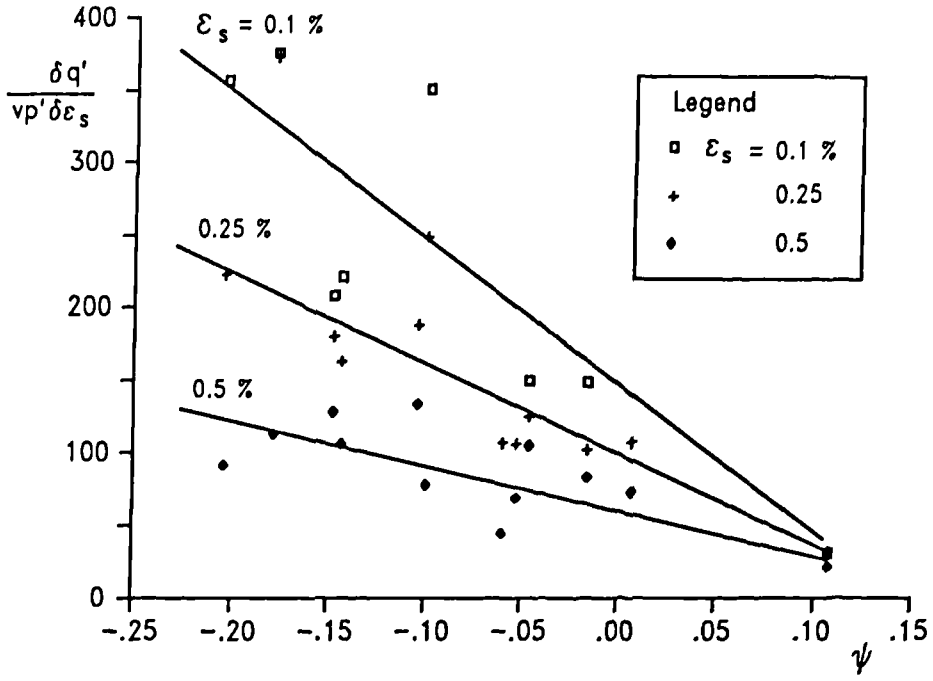

Figure 6.40 Normalised shear stiffness and the state parameter

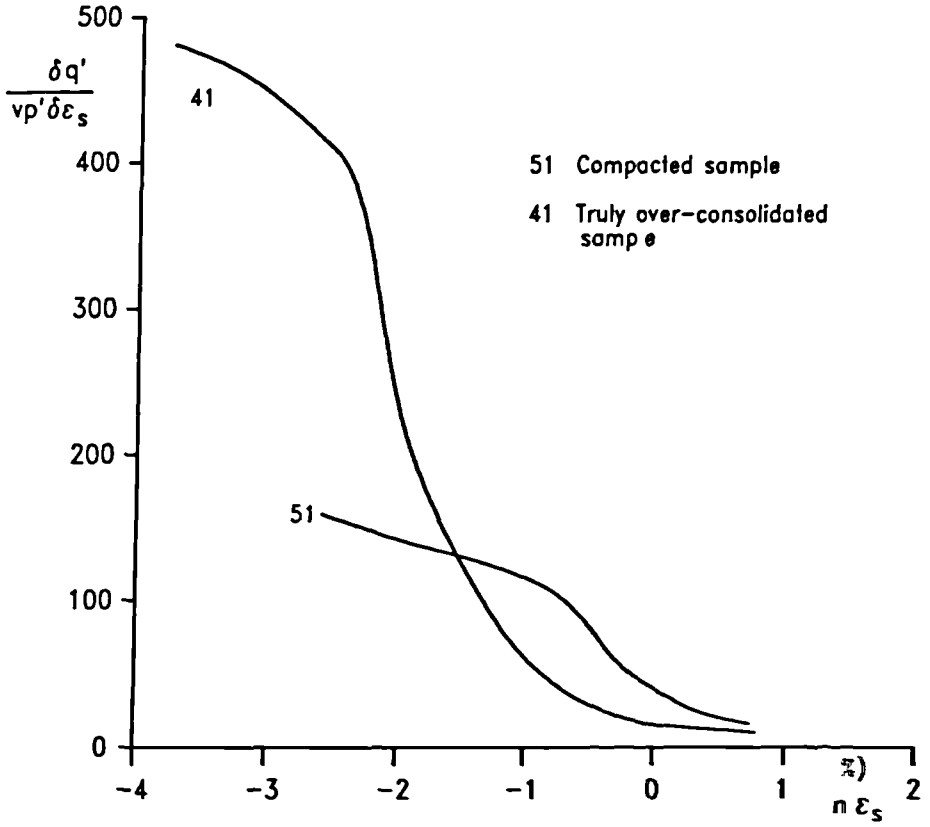

Figure 6.41 Normalised stiffnesses of compacted and truly over-consolidated samples

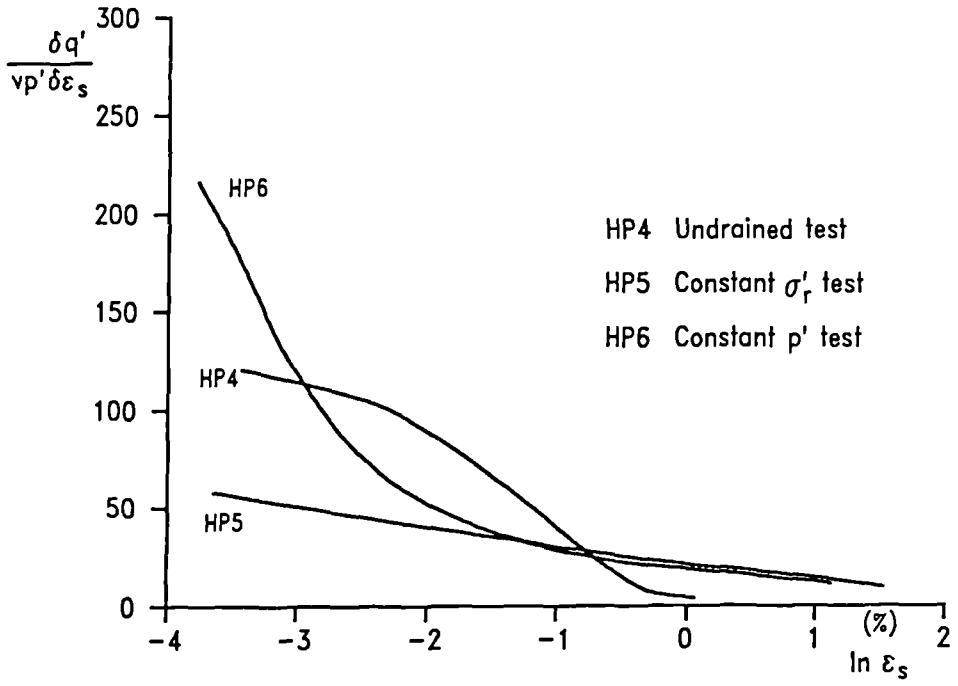

Figure 6.42 Effects of stress path on the stiffness

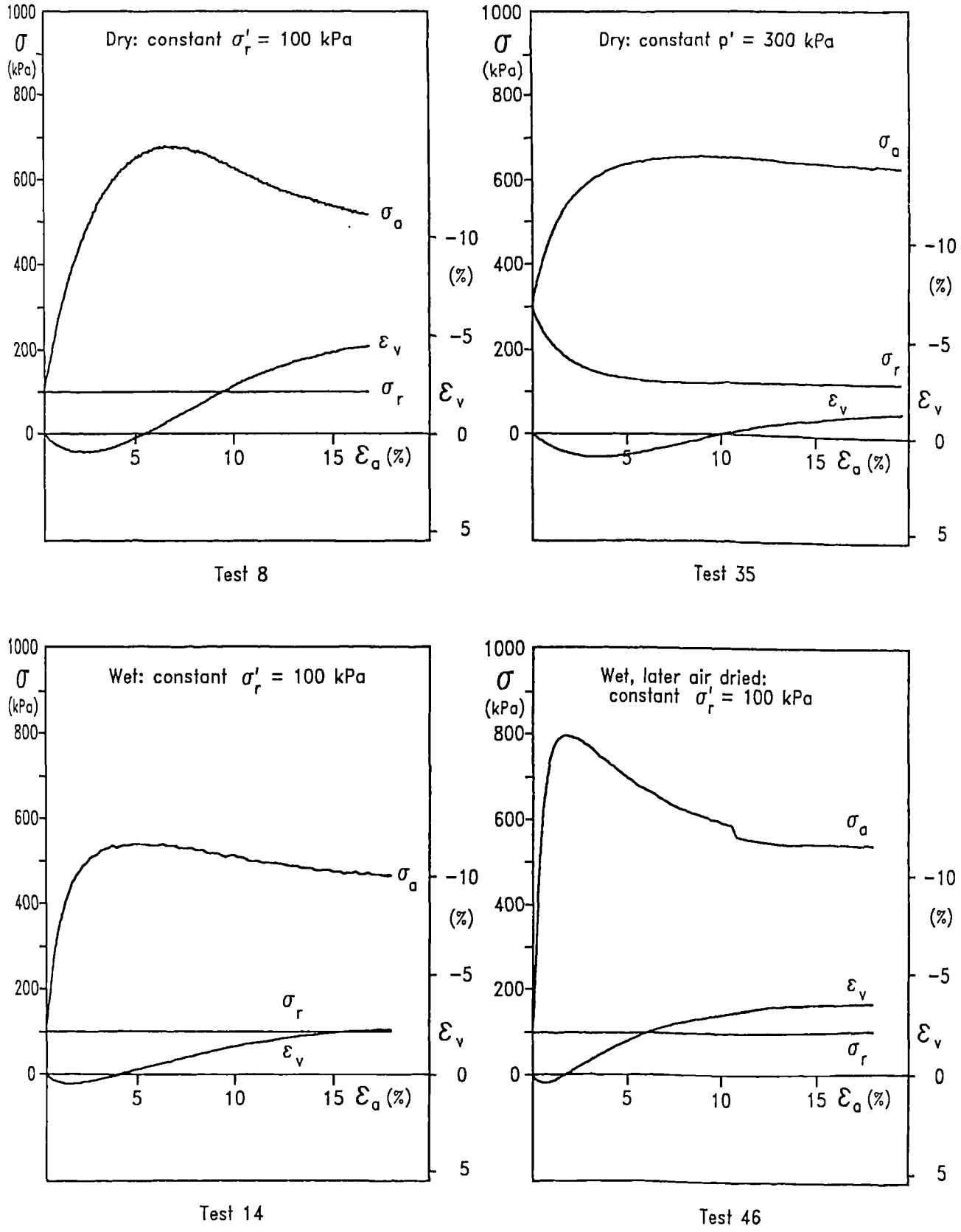

Figure 6.43 Typical test results of dry and wet samples

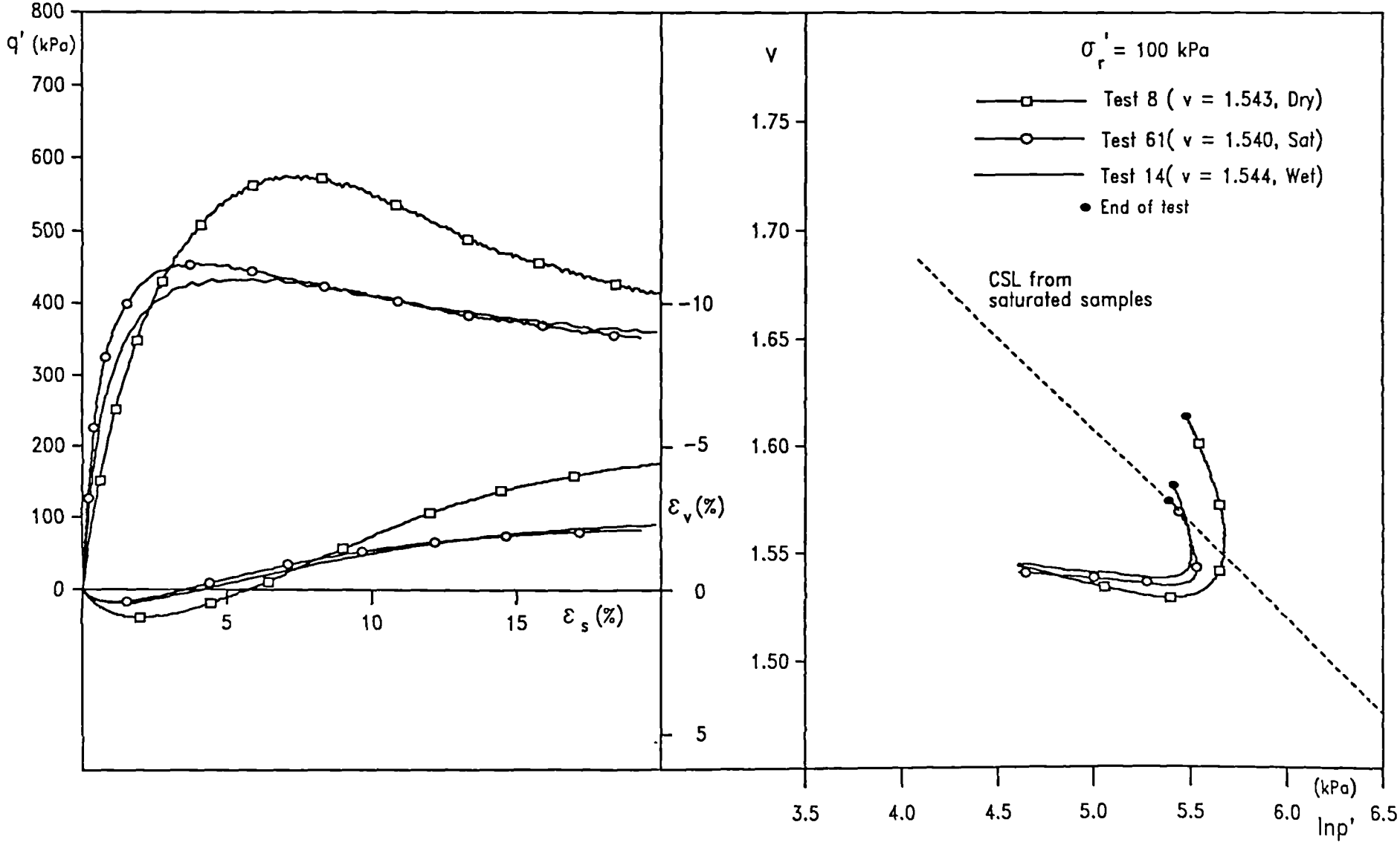

Figure 6.44 Comparison of stress–strain behaviour for dry, wet and saturated samples

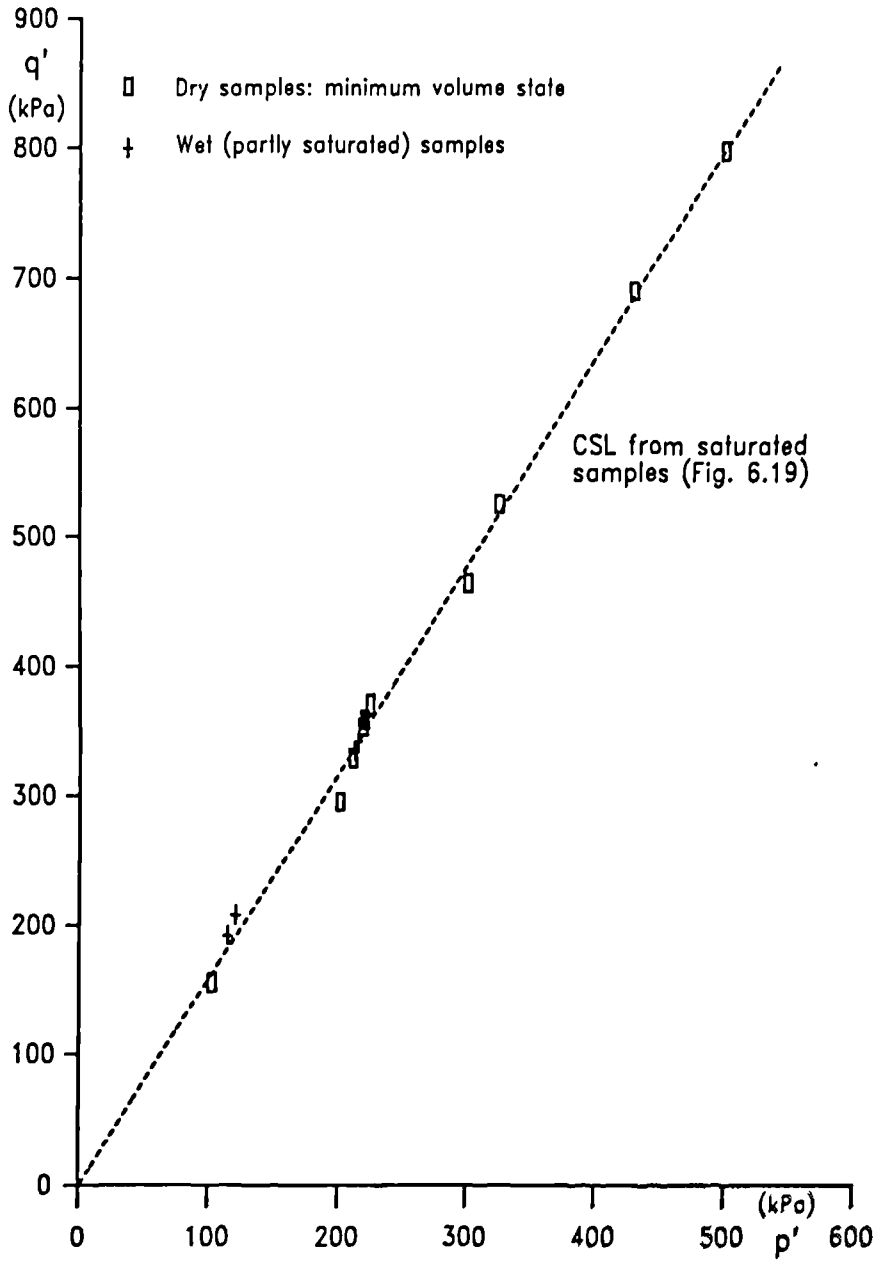

Figure 6.45 Critical states in q':p' space
(dry and wet samples)

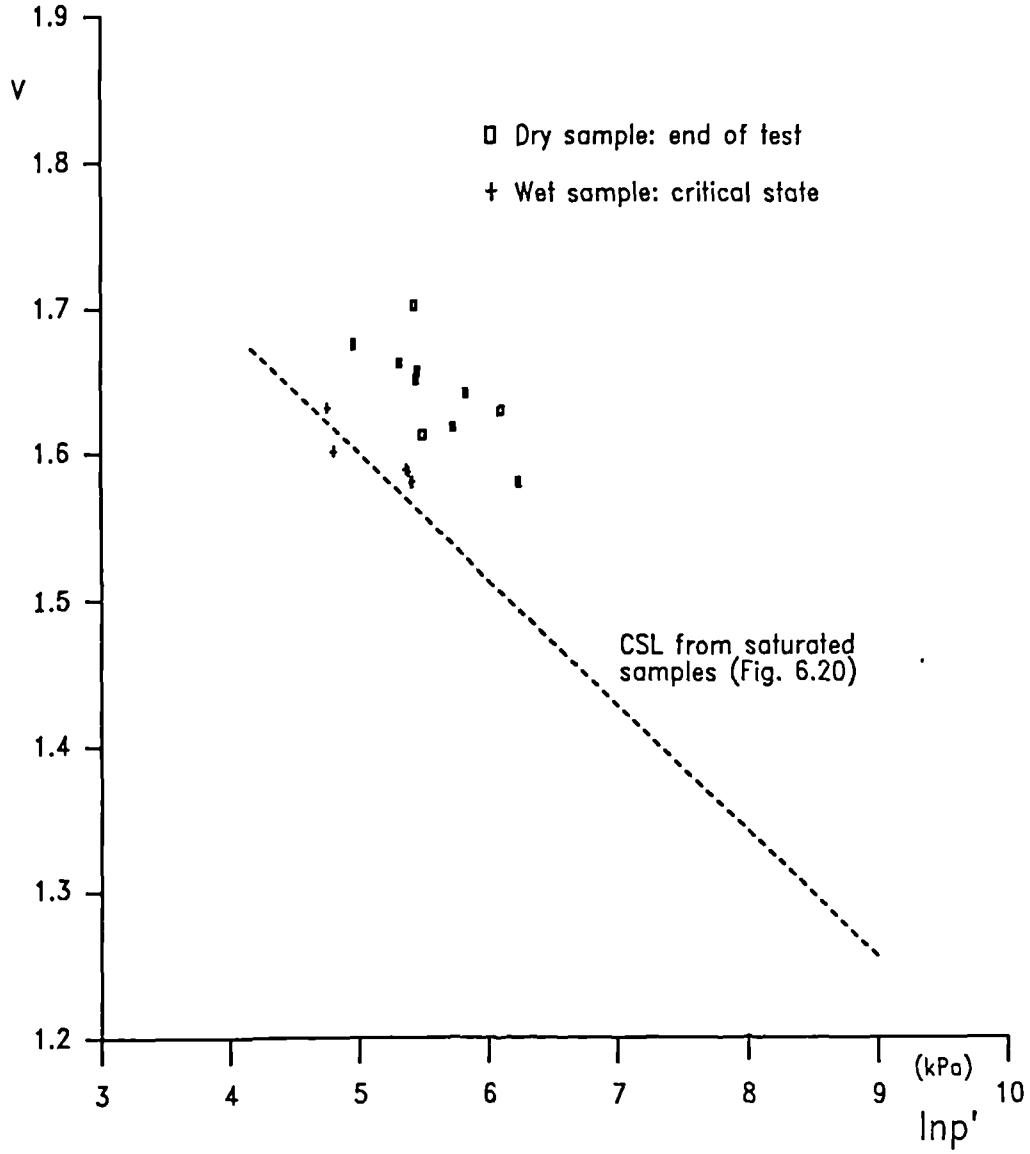

Figure 6.46 The critical and end states in v:lnp' space (Wet and dry samples)

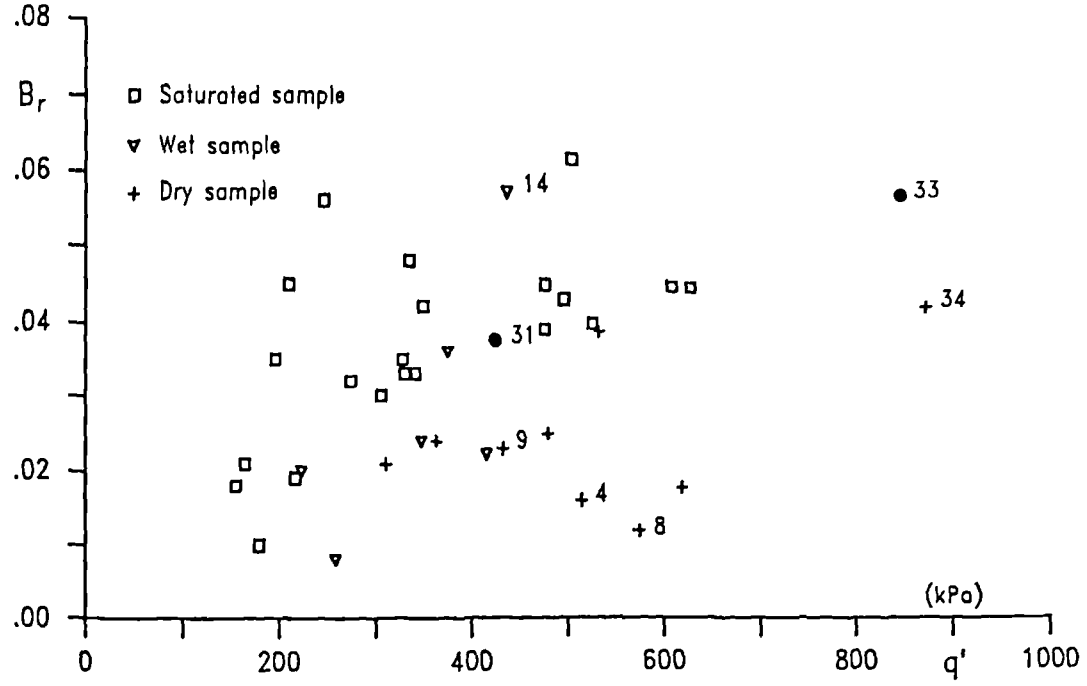

Figure 6.47 Particle crushing and the sample moisture condition

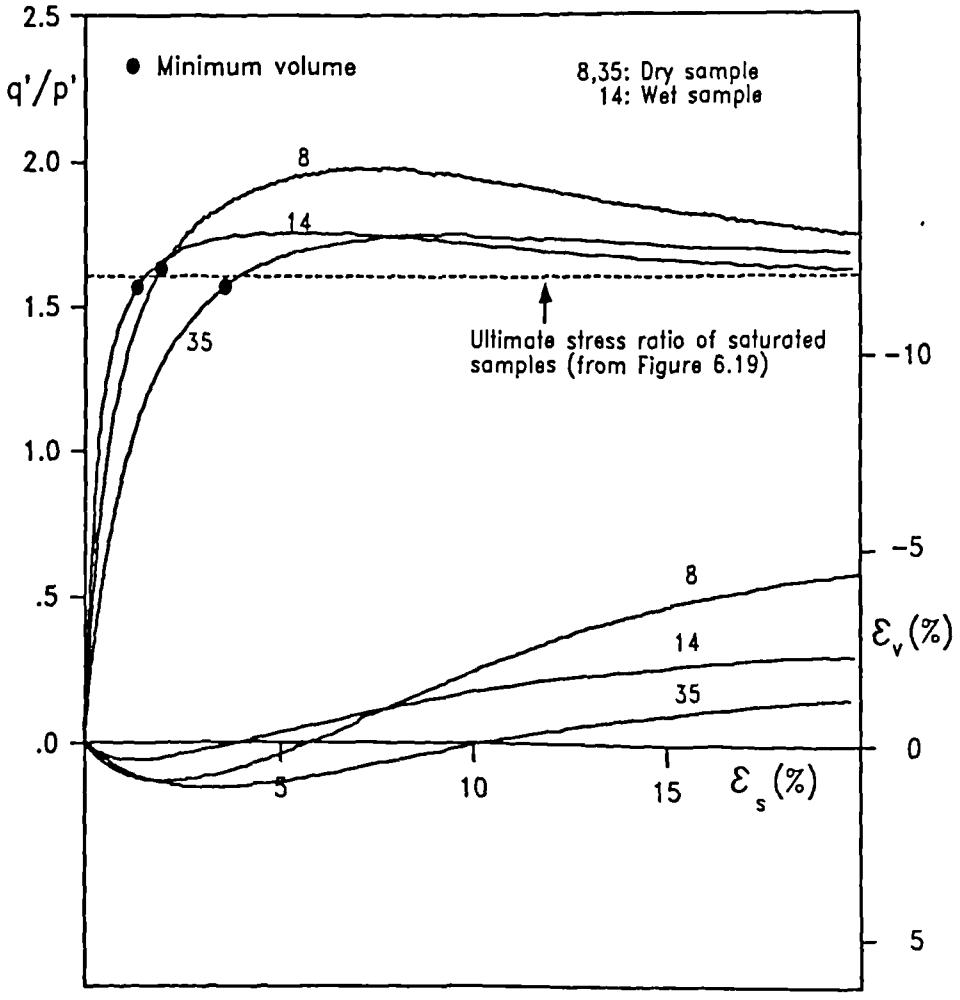

Figure 6.48 Stress ratio – shear and volumetric strains for dry and wet samples

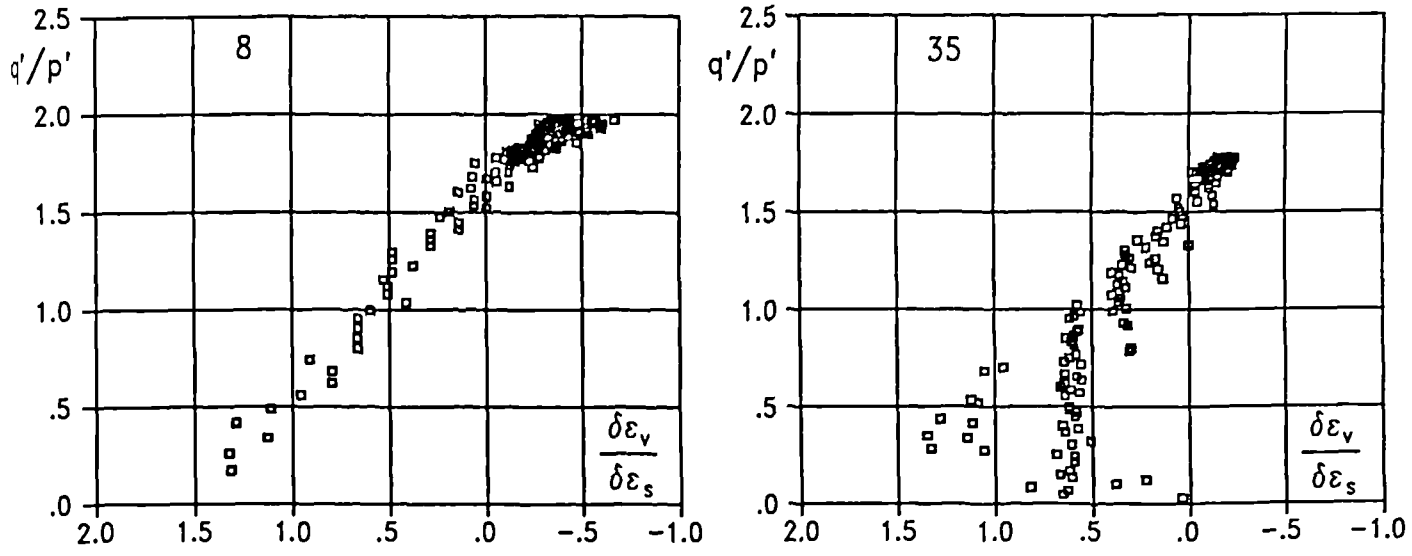

Figure 6.49 Stress –dilatancy of dry samples

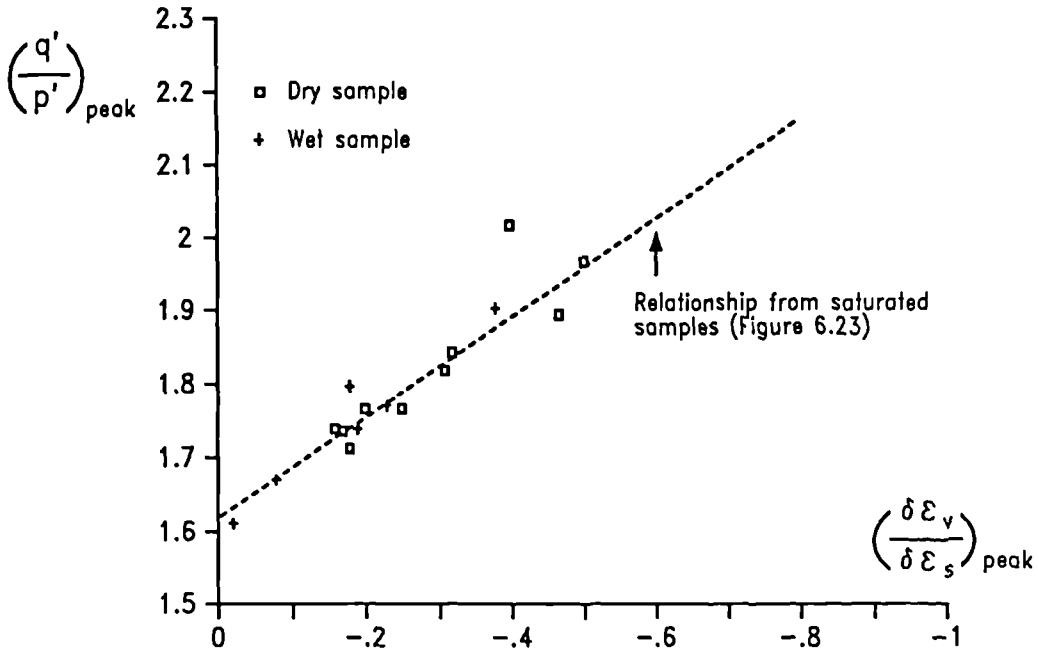

Figure 6.50 Stress –dilatancy relationship for peak states (dry and wet samples)

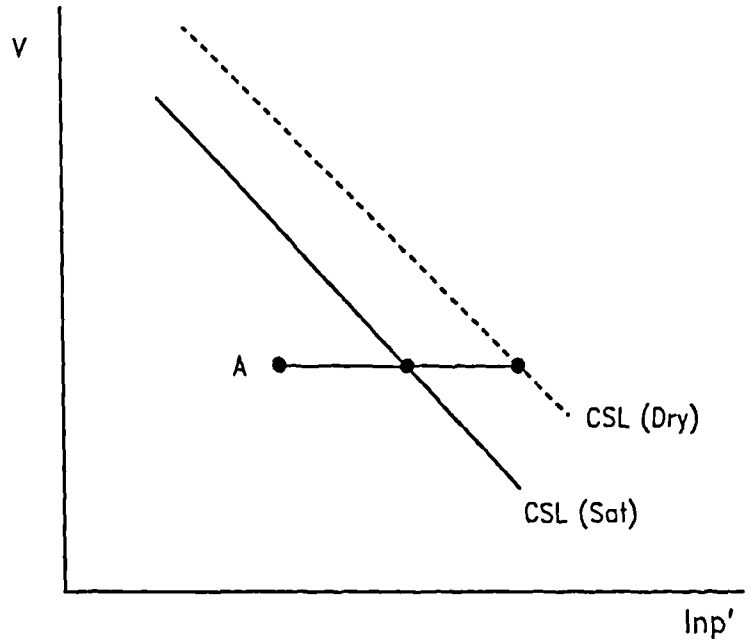

Figure 6.51 Current state in v:lnp' space

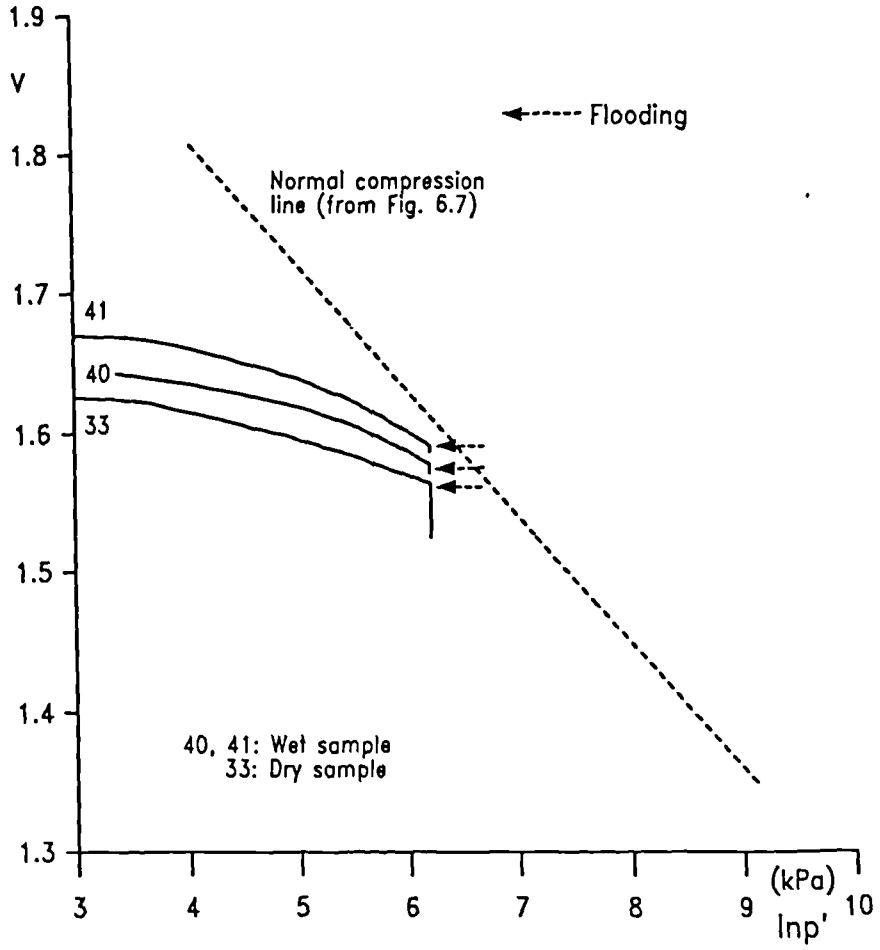

Figure 6.52 Effect of flooding on the isotropically compressed soils

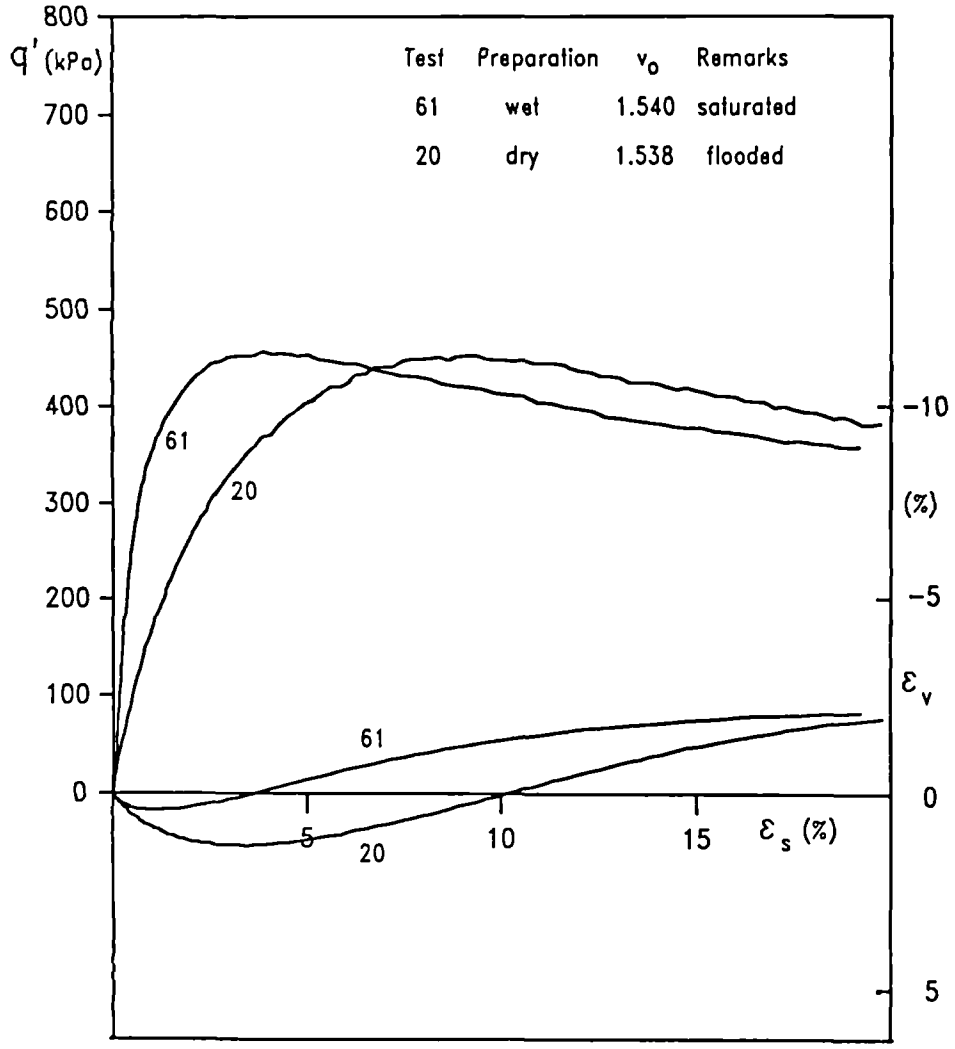

Figure 6.53 The effect of sample preparation on soil behaviour

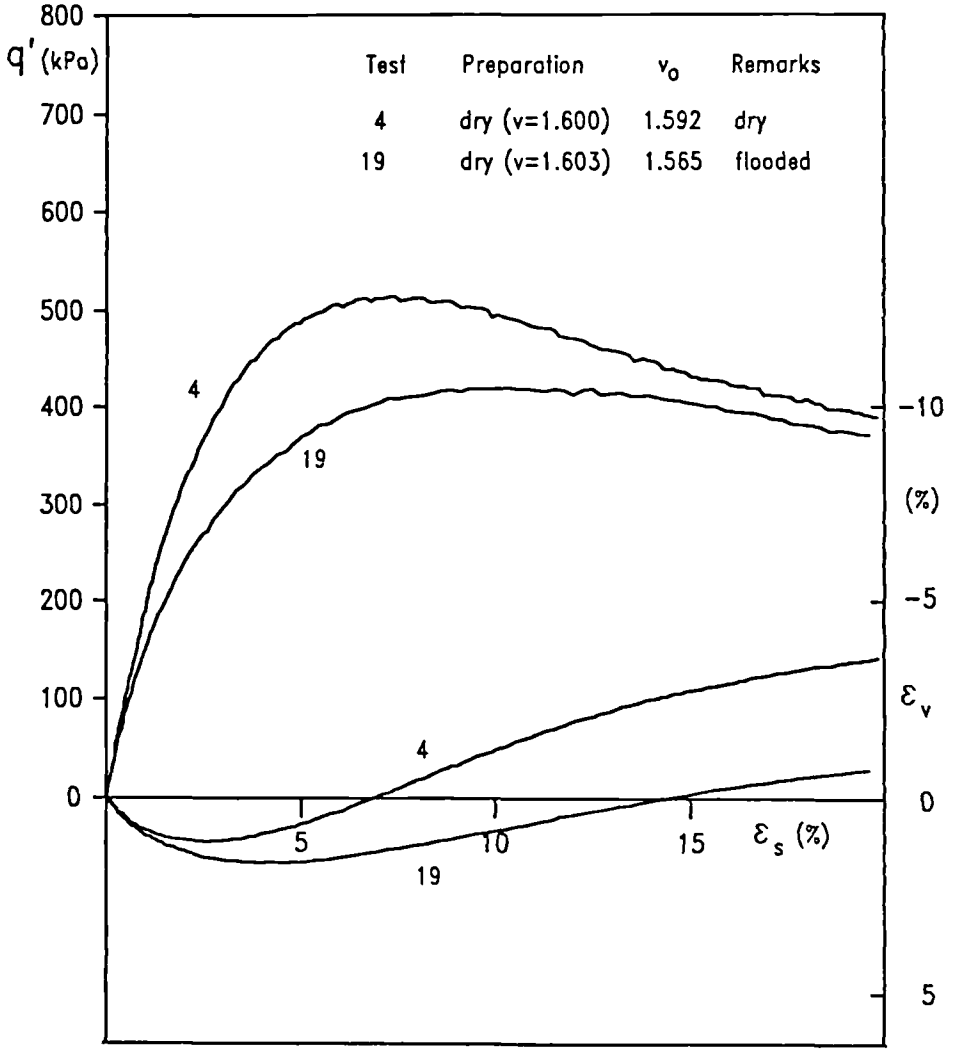

Figure 6.54 Effects of flooding on the soil stiffness

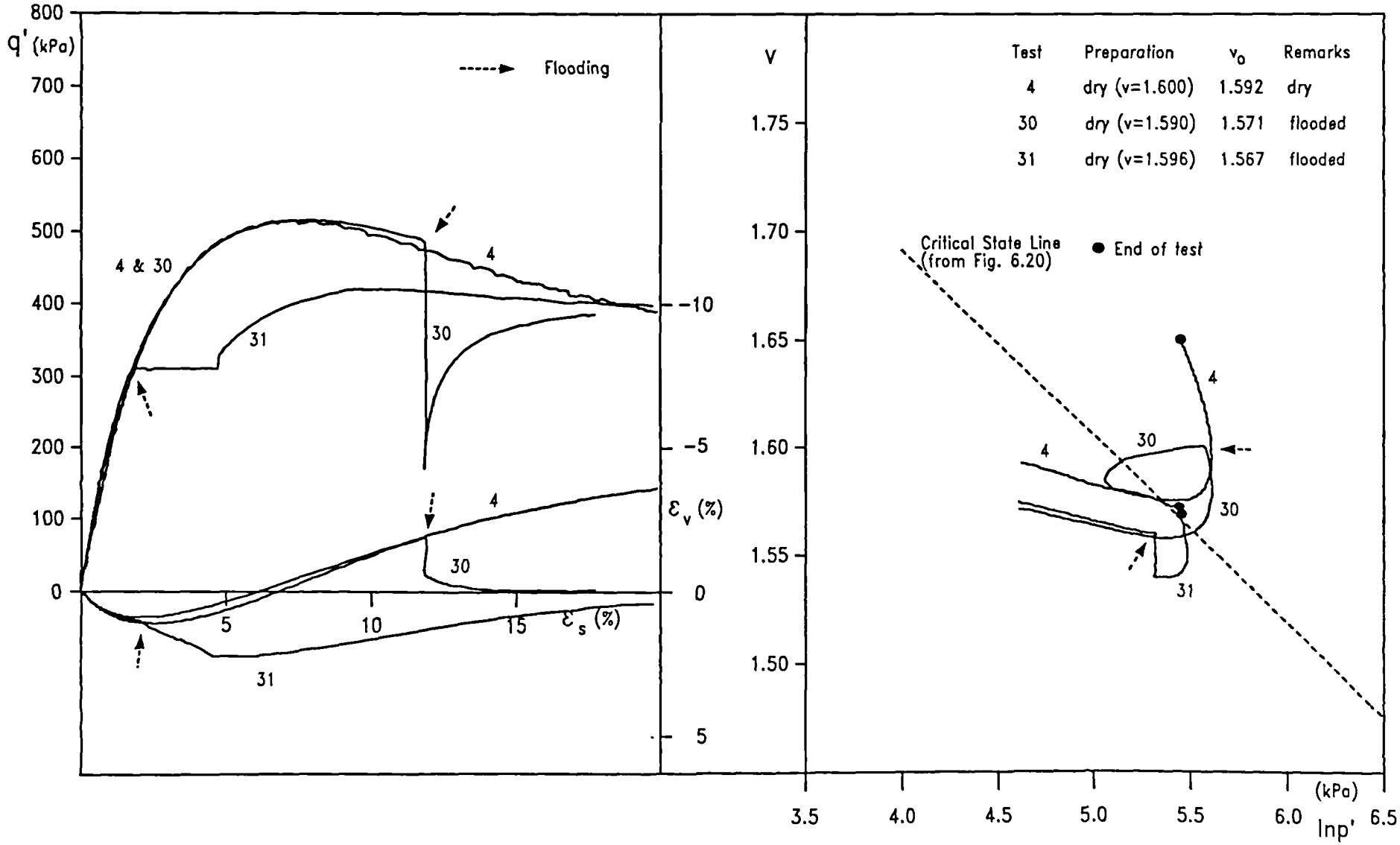

Figure 6.55 Effects of flooding on the behaviour of dry samples

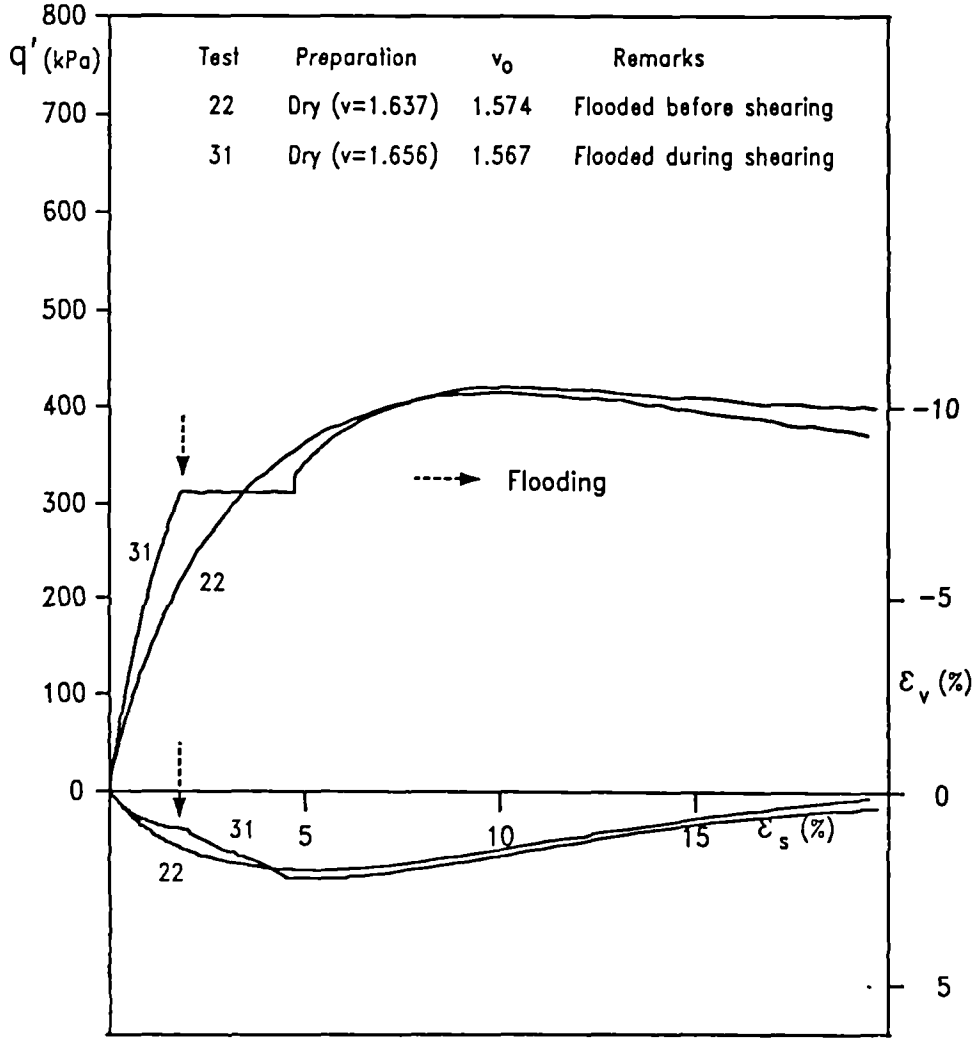

Figure 6.56 Stress–strain behaviour of flooded samples

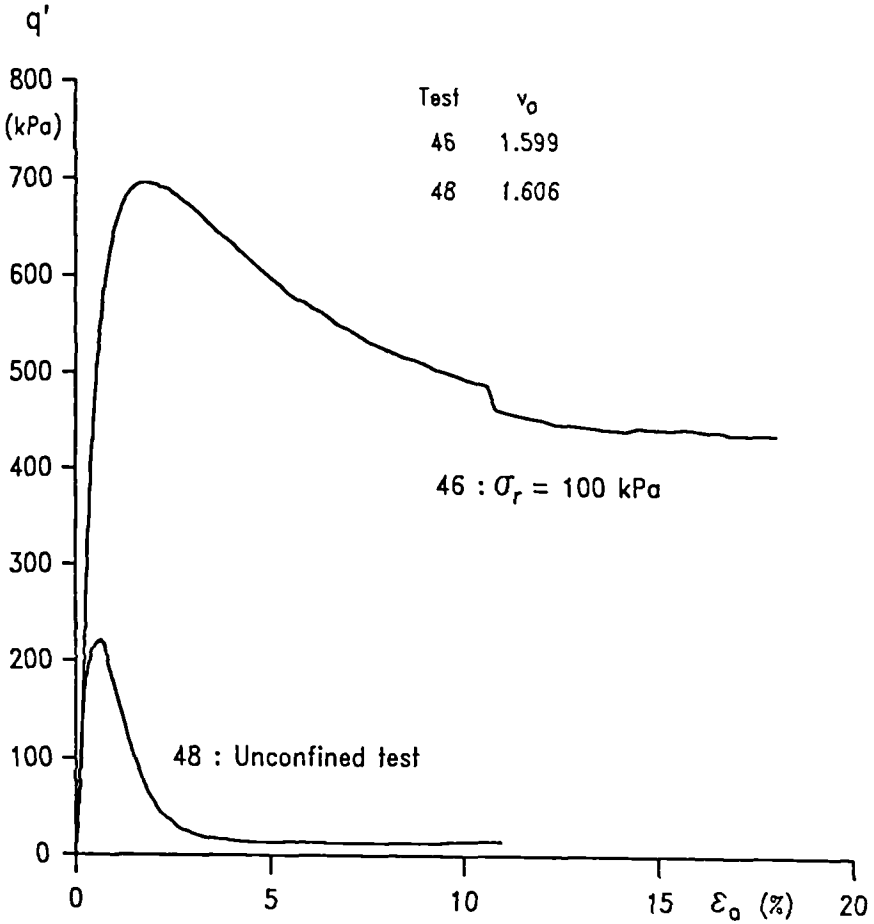

Figure 6.57 Behaviour of wet compacted and later air–dried samples

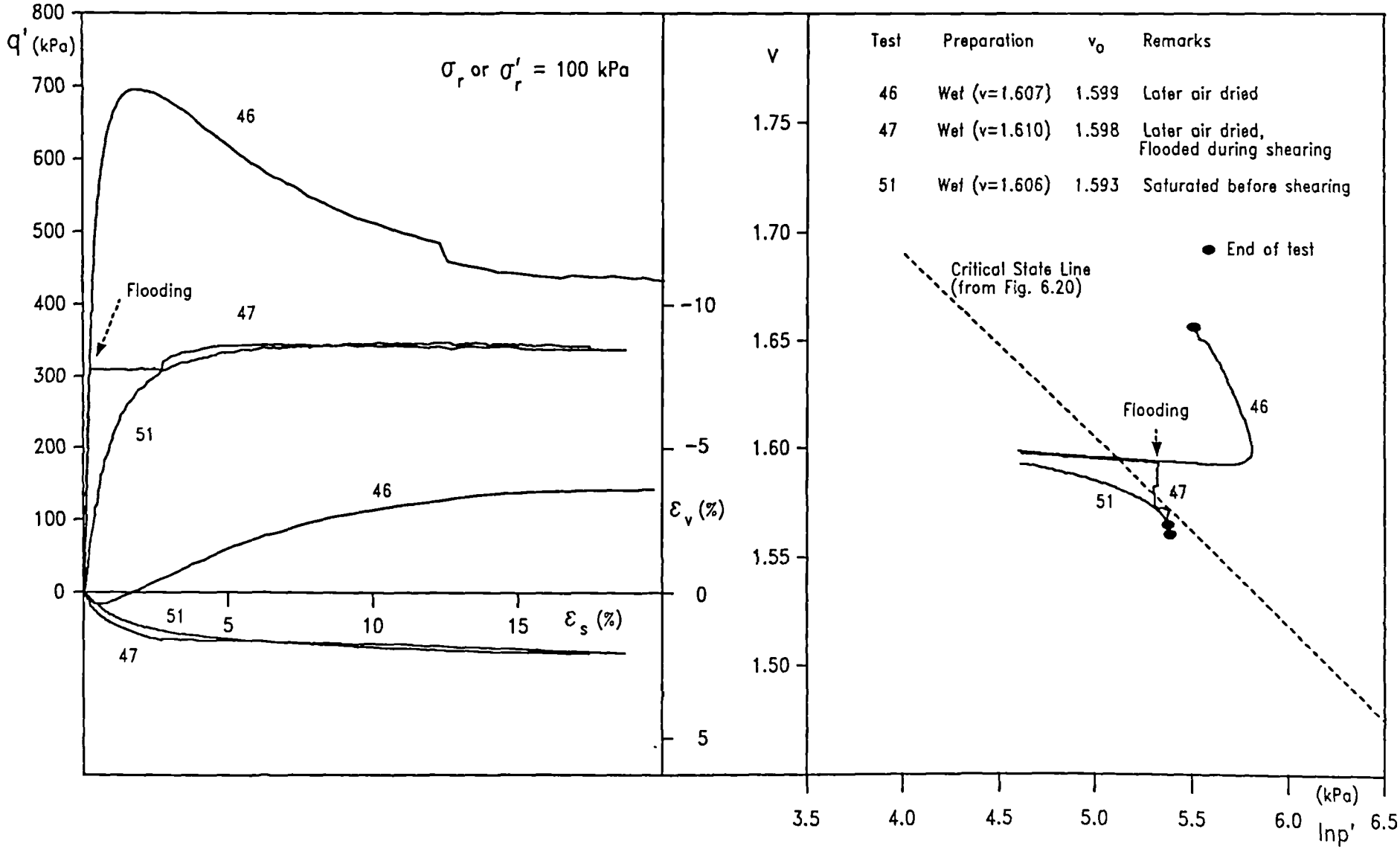

Figure 6.58 Effects of flooding on the behaviour of wet compacted and later air-dried samples